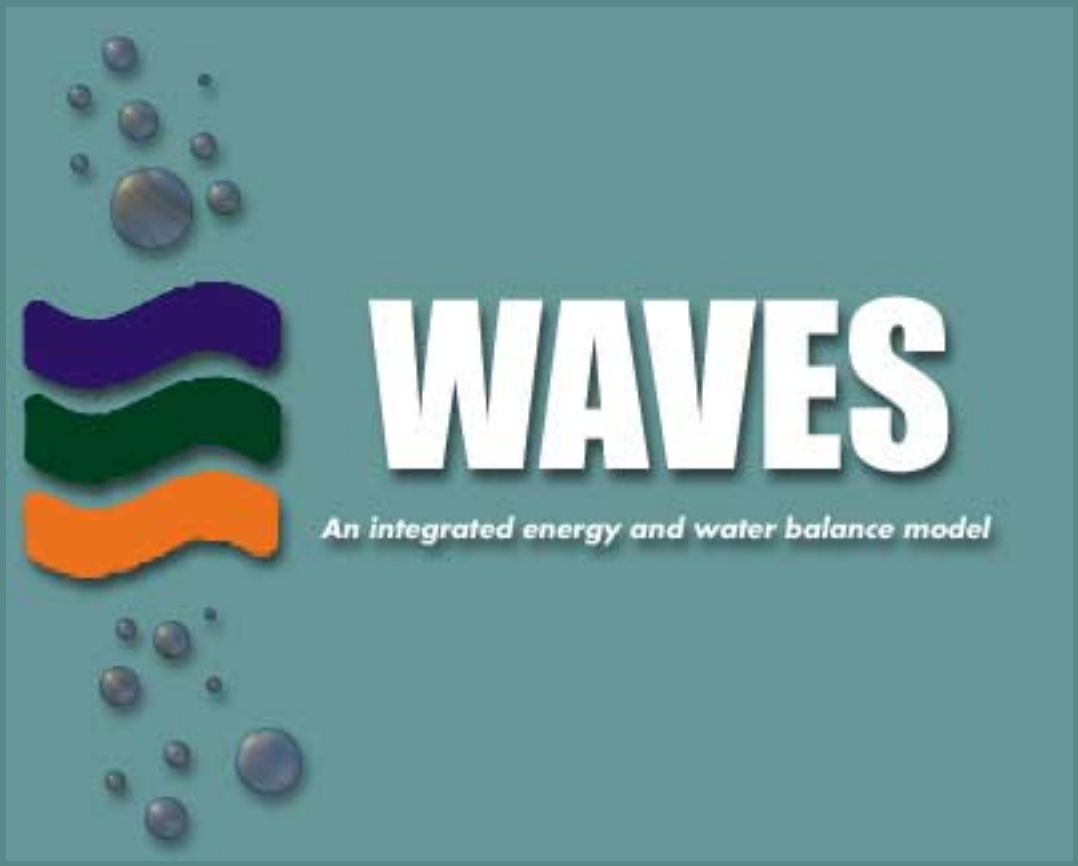

CSIRO

Editors

Lu Zhang and Warrick Dawes

CSIRO Land and Water

Technical Report No. 31/98

WAVES

An integrated energy and water balance model

Editors

Lu Zhang and Warrick Dawes

CSIRO Land and Water Technical Report No. 31/98

August 1998

CSIRO Land and Water
GPO Box 1666
Canberra ACT 2601
Australia

E-mail: lu.zhang@cbr.clw.csiro.au, warrick.dawes@cbr.clw.csiro.au

CONTENTS

PREFACE

The interactions between climate, vegetation and soil are all around us. They provide the driving forces and fluxes for the atmosphere above the ground, and the large groundwater systems below it. Understanding and quantifying these interactions has therefore long been of great interest to researchers.

In the Australian context, the main questions are: what is the current water balance, how has it changed from historical levels, and what is the optimum land management regime to satisfy a range of competing needs? Dryland salinity is a good example of a disturbed water balance with land management implications. Historically, groundwater levels were well below the soil surface, and were kept there by deep-rooted perennial native vegetation. Widespread clearing of this vegetation, and replacement with more shallow-rooted annual cropping and grazing systems, has led to an increase in groundwater recharge. This has caused groundwater levels to rise, mobilise the stored salt in the soil profile, and bring it close to the surface where evaporative concentration has resulted in dryland salinity. The question being addressed in this field is whether rising water-level trends can be halted or reversed using only vegetation management, or in combination with engineering options.

WAVES is a one-dimensional, daily time-step model that simulates the fluxes of mass and energy between the atmosphere, vegetation, and soil systems; it has been under development since 1993. It is a process-based model that couples these systems by modelling the interactions and feed-backs between them. WAVES attempts to model each sub-system with a consistent level of detail, so that no area is over emphasized or requires too many parameters, and similarly no area is treated in a trivial manner. More than this, WAVES tries to strike a balance between the complexity of the model as a whole, the usefulness of the model and its ease of use, and the accuracy of the model outputs. If these balances have been struck, then WAVES should be easy enough to use, but accurate enough to believe.

The material in this work is broken into five chapters, with the level of detail varied through each, so that everyone should be able to get the information they require. Chapter 1 is an Executive Summary that provides a broad-brush view of the WAVES model, highlighting strengths and weaknesses, to allow readers to gauge whether WAVES could be applied to any particular problem. Chapter 2 contains the conceptual model for each of the sub-systems of WAVES. This provides more detail on the assumptions used to scale processes to a daily-time-step, and some of the specific process formulations used in WAVES. Chapter 3 is a very detailed description of the equations that are solved in running WAVES and, where required, provides the solution method

for nonlinear equations and matrix solution schemes. A skilled scientist should be able to essentially reproduce the functions of WAVES from this chapter. Chapter 4 provides a sensitivity analysis of the major parameters in WAVES, and testing of the quality of the mass and energy balances as simulated for test cases. It also provides an extensive treatise on use of Richards' equation for solving soil-water dynamics; without a robust solution method for this sub-system, WAVES would not be possible. Chapter 5 is a compilation of case studies that have used WAVES, showing the range of application of WAVES as well as the excellent results that can be obtained with it. These studies test the full capabilities of WAVES in many varied environments; it is not an exhaustive list of all the applications that have been made and published by all workers using WAVES. At the end are two appendices. Appendix A details some of the mathematics that underpin the longwave radiation equations used in WAVES. Appendix B details the equations and solution of the analytic model used to test the Richards' equation with a particular soil hydraulic model.

The material presented represents a working document for WAVES v3.5. It is anticipated that further changes will be made to WAVES in the future, as new processes call to be modelled, and new techniques and physical descriptions are developed.

WAVES has been developed and used as part of work funded by the Murray–Darling Basin Commission, Natural Resource Management Strategy, the Land and Water Resources Research and Development Corporation, the National Dryland Salinity Program, Australian Water Resources Advisory Council, Landcare Australia, and the Australian Centre for International Agricultural Research. Collaborating parties have been the Commonwealth Scientific and Industrial Research Organisation, Cooperative Research Centre for Catchment Hydrology, NSW Department of Agriculture, Victorian Department of Agriculture, Victorian Department of Natural Resources and Environment, and the Chinese Academy of Sciences.

Warrick Dawes

Lu Zhang

August 1998

CHAPTER 1. EXECUTIVE SUMMARY

L. Zhang and W.R. Dawes

1.1. Introduction

The movement of water through the whole continuum of the soil, vegetation, and atmosphere is an important process that we must learn to understand, and this process is central to the energy, carbon, and solute balances of the system. The total system is integrated and changes in one part of the system will affect the others. Therefore, it needs to be dealt with in an integrated way by considering the dynamic interactions and feedbacks between the processes.

Most of our current environmental problems arise from tampering with one or a few aspects of the system without any understanding of whole-system function. For example, in Australia much environmental degradation, including salinisation, is associated with changes in the near-surface water balance induced by massive clearing of native vegetation. These changes have led to significant increases in groundwater recharge, which in turn have led to rising watertables and salinisation. The temporal and spatial scales over which these changes evince themselves precludes field experimentation as a wholly sufficient or practical tool for identifying optimal or appropriate land use. The main emphasis of current salinity control strategies generally involves either improving the growth of existing annual crops and pastures or replacing these land systems with perennial vegetation. The idea here is to have larger leaf area and deeper roots so that plants can use the evapotranspirative capacity to remove more excess soil water and hence reduce recharge to groundwater. This is called biological drainage (Fig. 1.1) as opposed to engineering ones such as a ditch or well.

However, increased water use by plants could lead to larger upward flux of water and in the case of shallow saline groundwater tables this could cause salt to build up in the root zone. It is expected that the plant roots would die back and it would become more difficult for the plants to extract water. What would happen to the plants in the long run? Are these management options

sustainable? The investment and uncertain ecohydrological returns demand a means to predict the expected effectiveness and sustainability of such schemes.

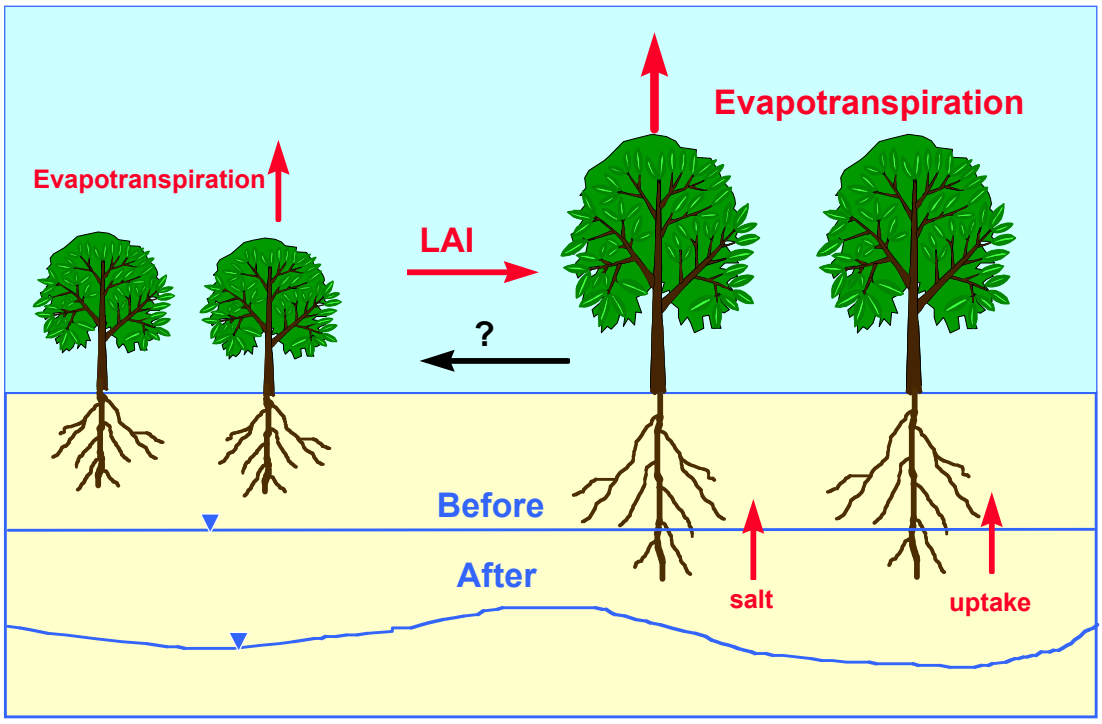

Fig. 1.1: Impact of salinity on plant growth and water use over shallow groundwater tables.

The hydrological cycle along with several other processes is influenced by vegetation through the exchange of energy, water, carbon and other substances. As a result, they are critical for many hydrological processes, in particular transpiration, infiltration, and runoff. The physiological response of vegetation when exposed to an increase in atmospheric carbon dioxide (CO_2) concentration could result in closure of stomata. Consequently, this could decrease evapotranspiration and affect surface water balance (See Fig. 1.2). The study of the biological controls of the hydrological cycle, and their ecological and environmental significance also requires an integrated approach that builds upon process understanding. This is essential for developing management strategies.

Models of the soil–vegetation–atmosphere system can be formulated at almost any level of complexity. All these models represent approximations of reality and include simplifications of the real process behaviour. Historically, process-based models have been developed to represent the system with increasing detail. When combined with appropriate data sources, such models have a great potential for exploring the interactions and feedbacks between processes and responses of the system under different management and/or climatic regimes.

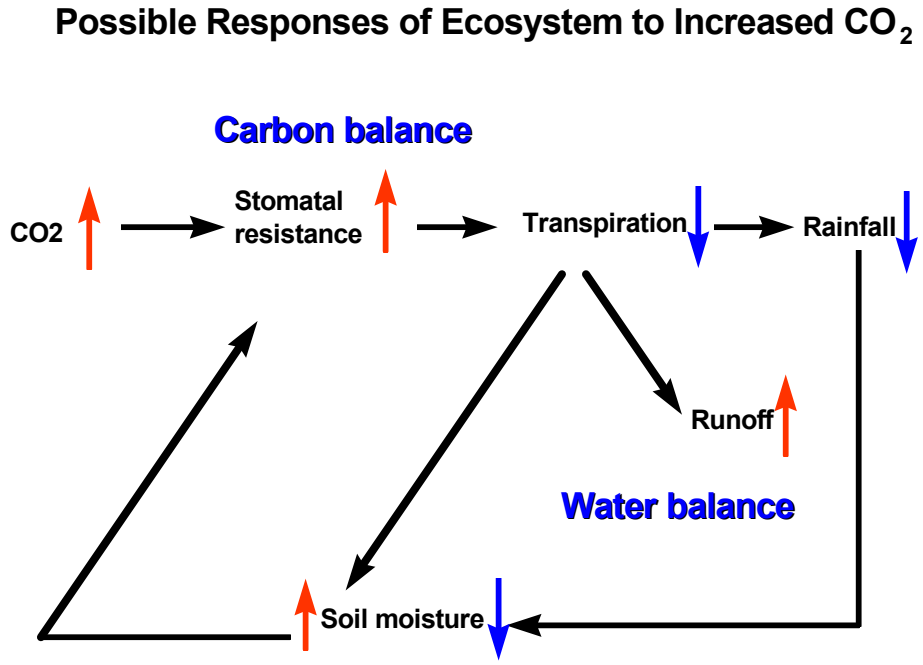

Fig. 1.2: Impact of climate change on the hydrological cycle and ecosystem.

1.2. Model Overview

WAVES is designed to simulate energy, water, carbon, and solute balances of a one-dimensional soil–canopy–atmosphere system (Dawes and Short, 1993, Zhang *et al.*, 1996). It is a process-based model and it integrates soil, canopy–atmosphere with a consistent level of process detail. WAVES predicts the dynamic interactions and feedbacks between the processes. Thus, the model is well-suited to investigations of hydrological and ecological responses to changes in land management and climatic variation, such as those discussed above.

WAVES models the following processes on a daily time-step:

- interception of rainfall and light by canopy
- surface energy balance
- carbon balance and plant growth
- soil evaporation and canopy evapotranspiration
- surface runoff and infiltration
- saturated/unsaturated soil moisture dynamics (soil water content with depth)
- drainage (recharge)
- solute transport of salt (NaCl)
- watertable interactions.

A diagram of the components of WAVES is shown in Fig. 1.3. The model is based on five balances:

- ***Energy Balance:*** partitions available energy into canopy and soil for plant growth and evapotranspiration (Beer's law);
- ***Water Balance:*** handles infiltration, runoff, evapotranspiration (Penman–Monteith equation), soil moisture redistribution (Richards equation), drainage, and water table interactions;
- ***Carbon Balance:*** calculates carbon assimilation using IRM and dynamically allocates carbon to leaves, stems, and roots, and to estimate canopy resistance for plant transpiration;
- ***Solute Balance***: estimates conservative solute transport within the soil column and the impact of salinity on plants (osmotic effect only);
- ***Balance*** of complexity, usefulness, and accuracy.

The energy balance module calculates net radiation from incoming solar radiation, air temperature, and humidity, then partitions it into canopy and soil available energy using Beer's law. Evapotranspiration is calculated using the Penman–Monteith equation (Monteith, 1981) with available energy, vapour pressure deficit, and air temperature as inputs. The Penman–Monteith equation is a 'big leaf' model based on the combination of energy balance and aerodynamic principles. It requires estimation of aerodynamic and canopy resistances. The aerodynamic resistance is estimated from wind speed and surface roughness, while canopy resistance is calculated as a function of net assimilation rate, vapour pressure deficit, and CO_2 concentration. WAVES couples canopy and atmosphere using the omega approach proposed by Jarvis and McNaughton (1986) and handles multi-layer canopy explicitly.

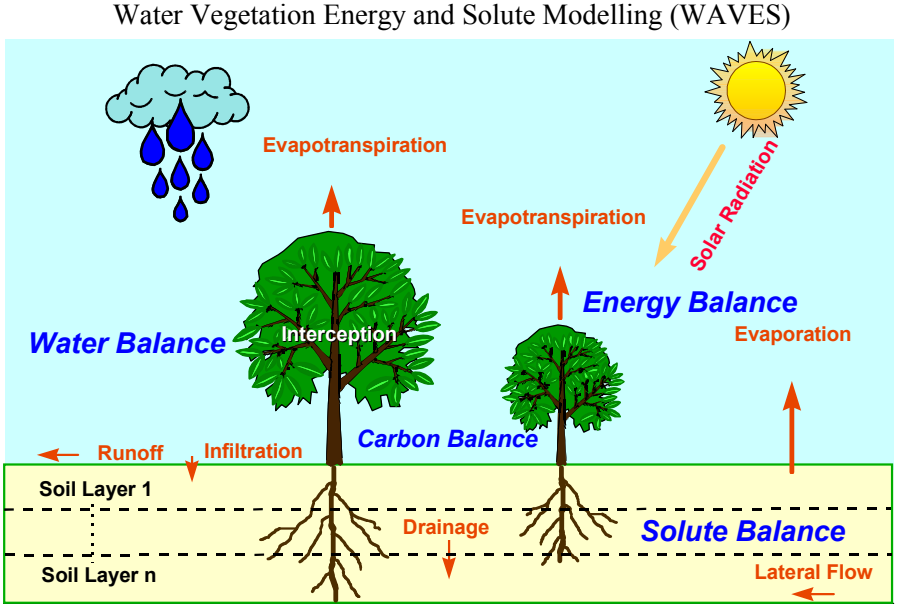

Fig. 1.3: Conceptual diagram showing the major processes modelled by WAVES.

WAVES is a daily time-step model, and it is assumed that the canopy and ground surface temperatures are equal to the average daily air temperature. This assumption does not introduce much error in the energy balance for relatively dense plant stands with non-limiting water supply (Zhang *et al.*, 1996). The ground heat flux is neglected in the energy balance equation because over land surfaces the daily mean value of the ground heat flux is one or more orders of magnitude smaller than the net radiation.

The carbon balance and plant growth module is based primarily on calculating actual daily carbon assimilation from a maximum value, and the relative availability of light, water, and nutrients; the limiting effects of temperature and salt in the soil water on assimilation are modelled explicitly. It is assumed that the actual growth rate is dependent on the potential growth rate and the level of the available resources. To combine the three limiting factors on plant growth into a single scalar we use the integrated rate methodology (IRM) of Wu *et al*. (1994), which allows other limiting factors, such as atmospheric CO_2 concentration, to be easily included. Once actual carbon assimilation is calculated, it is used as input to dynamic allocation of carbon to leaves, stems, and roots, and into the calculation of canopy resistance for transpiration (Slavich *et al.*, 1998).

The soil water balance module handles rainfall infiltration, overland flow, soil and plant water extraction, moisture redistribution, drainage (recharge), and water table interactions. Soil water movement in both the unsaturated and saturated zones is simulated using a fully implicit finite-difference numerical solution of a mixed form of the Richards' equation (Richards 1931, Dawes and Short 1993, Short *et al*. 1995). A full description of Richards' equation solution can be found in Dawes and Short (1993). Overland flow can be generated when the rainfall rate exceeds the infiltration rate of the soil, and when rain falls on a saturated surface. Both of the mechanisms are considered explicitly in WAVES. A watertable may develop anywhere within the soil profile. If non-zero slope is specified as input, then lateral subsurface flow occurs via any saturated water table at a soil layer boundary, and is described by Darcy's law. A regional groundwater depth may be specified, and changed on a daily basis with weather, and interacts with the WAVES soil column. Evaporation and transpiration draw water out of the soil, and when the internal saturated water level is below the regional watertable, leakage into the column occurs and may bring salt with it. Conversely, when the internal water level is above the regional watertable, due to plant inactivity or large amounts of infiltration, water may leak out of the column and leach salts.

To solve Richards' equation, the analytical soil model of Broadbridge and White (1988) is used to describe the relationships among water potential, volumetric water content and hydraulic conductivity. This soil model has five parameters: saturated hydraulic conductivity, volumetric soil moisture content at saturation, air-dry volumetric water content, the soil capillary length

scale, and a soil structure parameter. The Broadbridge and White (1988) soil model can realistically represent a comprehensive range of soil moisture characteristics, from highly nonlinear associated with a well-developed capillary fringe, to weakly nonlinear associated with highly structured soil and macropores.

The assumptions of the Richards equation is that the soil is incompressible, non-hysteretic and isothermal, and that moisture moves in a single phase only. It also assumes that flow is via the soil matrix only, and not via macropores and larger preferred pathways. The soil is assumed to isotropic for the formulation of Darcy's equation for lateral movement. Any water ponded on the surface can either be left to pond, or appear as runoff within the time-step. Soil air flow is ignored.

Solute transport within the soil column is solved with a convection-dispersion equation, in the same way as soil moisture dynamics (Dawes and Short, 1993). It is assumed that the solute concentration does not interact with soil hydraulic properties, so water fluxes and contents are constants with respect to the solutes, and that salt never crystallises out of solution. This makes the solution of solute dynamics an explicit solution. The feedback to plants of salinity is through the reduction in apparent available water due to the osmotic potential induced by dissolved salt (sodium chloride) alone.

WAVES emphasises the physical aspects of soil water fluxes and the physiological control of water loss through transpiration. It can be used to simulate the hydrological and ecological effects of scenario management options (e.g. for recharge control). The model strikes a good balance between generality, realism and accuracy, and provides a powerful tool for recharge study.

1.3. Strengths and Weaknesses

The strengths of WAVES are:

- WAVES is a generic model not specifically designed for any particular climatic region, soil types, or vegetation systems. WAVES represents a wide range of dynamic processes, with appropriate feedbacks, at a consistent level of complexity. It strikes a good balance between complexity, usefulness, and accuracy.
- Weather data requirements are readily available. The minimum dataset comprises daily maximum and minimum air temperatures, and daily rainfall.
- The soil parameters used in WAVES are physical quantities that can be readily measured or estimated.
- WAVES can perform long-term simulations for as much weather data as is available or can be generated.

- WAVES is a DOS-based program not requiring Windows, and all output is in standard ASCII files that can be read into any commercial graphing software. It is quick to run, requiring about 2–3 seconds per year of simulation on a Pentium, regardless of which combination of processes is being simulated.
- WAVES has been extensively tested and the results have been published in international journals. Test sites include HAPEX-MOBILHY in France and FIFE in USA (Zhang *et al.*, 1996), Hillston in New South Wales and Walpeup in Victoria (Zhang *et al.*, 1999*a*), Loddon–Campaspe catchments in Victoria (Salama *et al*., 1999), Griffith in New South Wales (Zhang *et al*., 1999*b*), the North China Plain in China (Wang *et al*., 1997), Chowilla in South Australia (Slavich *et al.*, 1998), North Stradbroke Island in Queensland (Green *et al.*, 1997*a*), and the Swan Coastal Plain in Western Australia (Green *et al.*, 1997*b*).

The weaknesses are:

- WAVES is a one-dimensional model, although the effects of slope and aspect on intercepted radiation and local lateral movement in water tables are incorporated.
- The form of Richards' equation used in WAVES assumes that there are no thermal effects on water flow, that the soil does not shrink or swell, and that the soil is non-hysteretic. Macropores, preferred pathways, and cracking soils cannot be modelled explicitly with WAVES, unless these effects can be represented within the soil hydraulic model.
- WAVES is a daily time-step model, and process representations are simplified to match this, and smaller time scale phenomena are not modelled.
- The generic plant growth model in WAVES is designed for looking at the hydrological impact of plants and does not model plant phenology, or dynamically fill grain. Estimation of grain yield from crops is through use of two forms of the Harvest Index. WAVES does not allow dynamic selection of vegetation type.
- WAVES uses an abstraction of relative nutrition, and does not perform nutrient cycling and leaching.

1.4. Data Requirements

WAVES requires three types of data: (i) meteorological data; (ii) soil parameters; and (iii) vegetation parameters. The meteorological data required are maximum and minimum daily air temperature, daily average vapour pressure deficit, rainfall, rainfall duration, daily solar radiation. Some or all of these data are available from weather stations, and with only the temperatures and rainfall, realistic estimates of the other data can be made. The soil data required is knowledge of the soil layering, and the parameters that describe the relationships between ψ (soil water potential), θ (volumetric water content), and K (hydraulic conductivity). Use of the Broadbridge–White soil model allows WAVES to guarantee accuracy and convergence of the water dynamics. For plant

growth and the calculation of the energy balance, WAVES requires 22 vegetation parameters. Most of these can be measured directly or taken from plant physiological literature, with only a few remaining for fitting, or adapting to local conditions. Hodges (1992), Vertessy *et al.* (1996), Hatton *et al*. (1995), Salama *et al*. (1999), and Zhang *et al*. (1999*a,b*) have published the sources and values of the parameters used in the WAVES vegetation growth module.

1.5. Model Availability

The WAVES model software (including source code) plus documentation is supplied free of charge through collaboration or direct application to CSIRO Land and Water. The documentation and executables (Version 3.5) will be available on the WWW in 2000.

CHAPTER 2. MODEL DESCRIPTION

L. Zhang and W. R. Dawes

2.1 Introduction

The physical and biological processes describing the surface water, energy and solute balances of the plant–soil–atmosphere system are, in general, well understood. Models of that system can be formulated at almost any level of complexity with as many or as few processes as required. The level of model complexity is usually determined by the application.

Historically, physically based models have been developed to represent the real world with increasing detail. The place and use of such models, and the information contained in the data required to run them, have been debated in hydrology literature for over 20 years, most recently by Beven (1989, 1993), Hauhs (1990), Wheater and Jakeman (1993) and Barnes (1993). These authors argue that physically based models are most appropriately used in exploring the interactions between processes and fluxes under different management and/or climatic regimes, given clearly stated assumptions about which small-scale processes are relevant.

In Australia, most environmental degradation is associated with changes in the surface water balance induced by changes in land cover. The temporal and spatial scales over which these changes evince themselves precludes field experimentation as a wholly sufficient or practical investigative tool for identifying optimal or appropriate land use. Decision-makers are therefore reliant on models, especially physical process models, for predicting expected changes in the landscape; the diversity of recent hydrological modelling tools in use in Australia (see Grayson and Chiew 1994 and Hatton *et al*. 1994 for recent reviews) is testament to this need.

The WAVES model was designed to enable the simulation of soil–vegetation–atmosphere system behaviour under alternative management and climatic variation. The aim is to represent the interactions and feedbacks of the system in the simplest possible way, yet with adequate description of the key processes. The model predicts the dynamic interactions, and fluxes of energy, water, carbon, and solute within soil–vegetation–atmosphere systems.

The model adopts a one or two layer canopy representation with a soil layer underneath. The aerodynamic resistance at the top of the canopy is determined based on Monin–Obukhov surface layer similarity theory and the within canopy aerodynamic resistances are estimated using the

mixing-length approach (Raupach and Thom, 1981). The boundary layer resistances are neglected for simplicity. The model formulates the physiological control on transpiration using the canopy resistance calculated as a function of the net assimilation rate, and the vapour pressure deficit and CO_2 concentration at the canopy surface. The soil hydrology is described by the Richards equation. A distinguishing feature of the model is to couple the soil–vegetation–atmosphere system by changing the value of the saturation vapour pressure deficit of air in the canopy. The model can be used to predict plant growth using a saturation rate kinetics formulation and to simulate solute transport in the soil (Hatton *et al.* 1992, Dawes and Short, 1993, Wu *et al.* 1994, Zhang *et al.* 1996, Dawes *et al.* 1997).

This section provides a detailed technical description the conceptual framework, theoretical background, and process representation. It also describes the governing equations, parameter estimation, and assumptions within WAVES. The document is adapted from existing publications on WAVES.

2.2 General Principles

A realistic formulation of the interaction between soil–vegetation–atmosphere must represent the following physical or biological processes:

- radiation balance: to determine the available energy at the surfaces of each canopy layer and the underlying soil, to estimate sensible and latent heat fluxes;
- interception: to determine the amount of water intercepted on the canopy surface;
- atmospheric turbulence: to determine the atmospheric and boundary layer resistances for momentum, heat and mass transfer;
- canopy physiology: to determine the physiological control of transpiration;
- runoff generation: to determine surface runoff based on precipitation, evaporation and infiltration;
- soil dynamics: to determine heat and water transport in the soil, recharge to groundwater, and the available soil moisture;
- solute transport and impact on plant growth: to estimate conservative solute transport within the soil column and the impact of salinity on plants.

This list is not comprehensive, but highlights the major processes and interactions. The complexity of a model should be constrained by the questions being answered, critical interactions, probable data availability, and the need to represent the processes consistently. Any model of the soil–vegetation–atmosphere should be designed with a clear objective and used appropriately. WAVES is composed of four modules, which solve energy, water, carbon, and solute balances on a daily time step. The schematic diagram of WAVES is shown in Fig. 2.1.

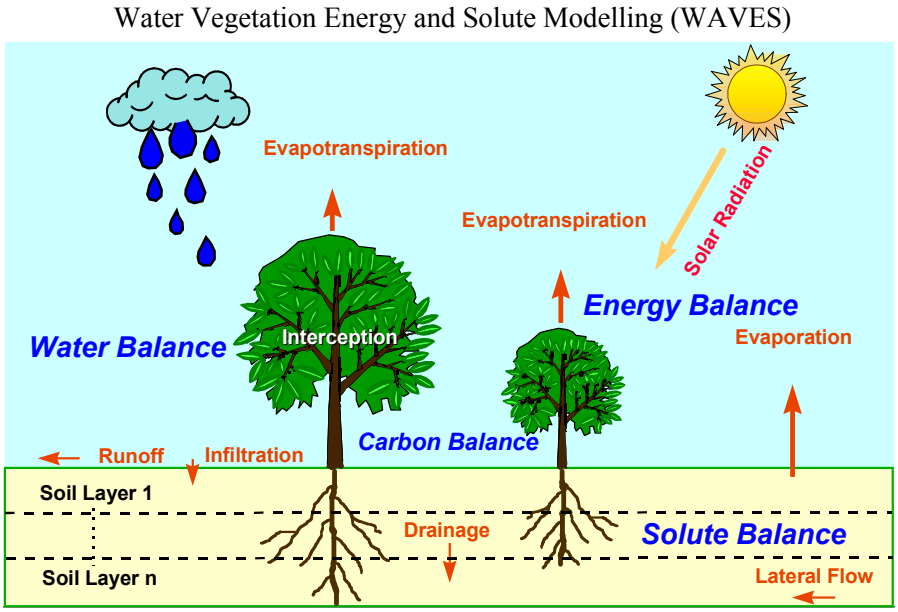

Fig. 2.1. Conceptual diagram showing the major processes modelled by WAVES.

The energy balance module calculates net radiation from incoming solar radiation, air temperature, and humidity, then partitions it into canopy and soil available energy using Beer's law. The carbon balance and plant growth module is based primarily on calculating actual daily carbon assimilation from a maximum value, and the relative availability of light, water, and nutrients; the limiting effects of temperature on light, and salt in the soil water are modelled explicitly. The soil water balance module handles rainfall infiltration, overland flow, soil and plant water extraction, moisture redistribution, drainage (recharge), and water table interactions. The solute balance module solves a convection-dispersion equation, in the same way as soil moisture dynamics (Dawes and Short, 1993). It is assumed that the solute concentration does not interact with soil hydraulic properties, so water fluxes and contents are constants with respect to the solutes. The feedback to plants of salinity is through the reduction in apparent available water due to the osmotic potential induced by dissolved common salt (sodium chloride, NaCl) alone.

These four modules are linked in the following way. At the beginning of each day time-step, the climatic forcing variables are set. The next step is to use the current values for leaf area to perform the surface energy balance, and set limits on the availability of water to plants for this day. The plant growth routines are required next to calculate gross carbon assimilation, plant respiration, and root growth. The actual assimilation rate is used to calculate canopy conductance, and plant transpiration. The soil evaporation is also calculated using the surface conditions from the start of the day. These fluxes set the surface boundary condition, and internal sinks, for solution of Richards' equation, which partitions rainfall into runoff, infiltration, drainage or uptake from a

watertable, and stored water. After this solution, the internal water fluxes are set, and conservative solute transport of common salt can be determined.

2.3 Rainfall interception

Rainfall interception for each canopy layer and the litter layer is scaled as a linear function of leaf area index as in Running and Coughlan (1988) and Hatton *et al*. (1992). When no rain occurs on a given day, evaporation is allowed to take place at the rate calculated from the Penman–Monteith equation. Where rain does occur, a sub-daily time step equal to the rainfall duration is performed with the intensity calculated from the rainfall amount and duration, and then evaporation from the surface occurs for the remainder of the day. When rain falls, any existing vegetation canopies can intercept water according to a linear relationship between leaf area and maximum interception:

$$I_{max} = K_r LAI \tag{2.1}$$

where K_r is the rainfall interception coefficient (m LAI^{-1}), and LAI is the leaf area index of the canopy layer. Any intercepted water must be evaporated before transpiration can occur, and all precipitation in excess of the interception capacity, reaches the next lowest canopy, or the ground surface. Vertessy *et al.* (1993) showed that this rainfall interception model worked well over a wide range of rainfall rates, and with a growing forest cover.

2.4 Energy balance and evapotranspiration

2.4.1 Energy balance

Evapotranspiration and sensible heat flux into the atmosphere are constrained by the available energy at the soil–vegetation–atmosphere interface. Depending on the nature of the surface, this interface may consist of water, bare soil, vegetation, or of some other substrate. For practical purposes, the energy balance equation can be written as:

$$R_n - P_s - G - A_h - \lambda E - H = S \tag{2.2}$$

where R_n is net radiation, P_s the energy flux for photosynthesis, G is the ground heat flux, A_h is the advection of energy from the surrounding, λE is evapotranspiration, H is the sensible heat flux, and S is the rate of energy storage.

The importance of the terms in the energy balance equation depends on the nature of layer for which the energy balance is written. In general, net radiation is the dominant term in the energy balance equation not only in the absolute sense, but also because the magnitudes of all the other

terms depend to some extent, directly or indirectly, on the size of net radiation. The net radiation flux can be determined from meteorological data, and the method is described in the next section. The energy absorbed for photosynthesis in day-time ranges from 6 to 16 W m^{-2}, depending on species (Monteith and Unsworth, 1990). Thus, it is usually negligible in comparison with net radiation and often be ignored in the energy balance equation, except when the objective is to determine the rate of energy absorption by photosynthesis itself. The ground heat flux is positive during the day, ranging from 2 to 20 per cent of net radiation, and negative at night with more or less the same magnitude. However, the daily mean values of the ground heat flux are often one or more order of magnitude smaller than the major terms in the energy balance equation (Brutsaert, 1982, Zhang *et al.,* 1996). The energy advection term is often neglected in the energy balance equation because it is difficult to estimate (Thom, 1975). Evapotranspiration and sensible heat flux are the most important terms in the energy balance equation. There are a number of methods for estimating these fluxes. In the next section, we will describe the combination method for calculating evapotranspiration. The rate of change in energy storage is often omitted from the energy balance equation in the case of a thin layer of water, soil or canopy, especially on a daily basis. However, this term may have to be considered in the case of a tall vegetation such as forest.

2.4.2 Radiation budget

The surface radiation balance can be written as:

$$R_n = R_{sd} - R_{su} + R_{ld} - R_{lu} \tag{2.3}$$

where R_n is the net radiation, R_{sd} is the shortwave downward radiation, R_{su} is the shortwave upward radiation, shortwave or solar radiation consists of direct and diffuse radiation, R_{ld} is the longwave downward radiation, and R_{lu} is the longwave upward radiation.

The shortwave downward radiation is the radiant flux resulting directly from the solar radiation. It is considerably modified by passage through the atmosphere. The measurement of the short-wave downward radiation can easily be made by using a calibrated pyranometer. In the event that suitable radiation data are not available, the shortwave downward radiation can be estimated from the actual number of bright sunshine hours and the number of daylight hours (Brutsaert, 1982). The shortwave upward radiation or reflected shortwave radiation is a significant term in the radiation balance and is mostly affected by the albedo of the surface. The longwave downward radiation from the atmosphere can be measured radiometrically, or calculated from knowledge of the vertical profiles of temperature and humidity, or estimated from empirical formulae. Due to the fact that necessary data of temperature and humidity profiles are not always available, it is

often convenient to express the longwave downward radiation as a function of meteorological data at screen height and the longwave upward radiation is estimated in a similar way (Brutsaert, 1982):

$$R_{ld} = \varepsilon_a \sigma T_a^4 \tag{2.4}$$

$$R_{lu} = \varepsilon_s \sigma T_a^4 \tag{2.5}$$

with $\varepsilon_a = 1.24(e_a/T_a)^{1/7}$ (2.6)

in which T_a is the air temperature at screen height in K, ε_a is the atmospheric emissivity, e_a is the vapor pressure in hPa, ε_s is the surface emissivity (equal to 0.97), and σ is the Stefan–Boltzman constant.

To calculate net radiation fluxes for different canopy layers and ground surface, we must determine longwave radiation of the atmosphere and that emitted from the canopy layers and ground surface *a priori*. WAVES is a daily time step model and at this level of complexity, it is not unreasonable to assume that the temperatures of the overstorey, understorey and ground surface are equal to air temperature (Ross, 1981). The differences in their longwave radiations are due to the emissivity. This is a good approximation for relatively dense plant stands with non-limiting water supply. WAVES is not a leaf level model and it integrates over whole canopies. The emphasis of WAVES is on water balance not leaf photosynthesis. Therefore, there is no need to separate sunlit and shaded leaves, which will complicate the model and increase the number of parameters. Attempts have been made in WAVES to represent different processes with a consistent level of complexity and this treatment can also be justified against these objectives.

When the radiation balance equation is applied to a plant canopy, the interception, reflection, transmission and absorption of radiation by vegetation have to be dealt with. Ross (1981) has shown that the theoretical equations for direct and diffuse radiation transfer in a plant canopy are complicated and cumbersome. These equations offer a theoretical treatment of the problem, but are of limited use in practice. For this reason, attempts have been made to simplify the theoretical formulae and replaced some of the functions with empirical constants. As a result, some comparatively simple equations have been derived namely semi-empirical formulae. These equations retain the key physical processes governing radiation transfer and contain bulk constants. It has been shown that these equations generally agree well with experimental data (Ross, 1981). Shortwave radiation transfer equations used in WAVES are, in a strict sense, not theoretically derived but semi-empirical. WAVES makes no distinction between direct and diffuse radiation and this can be seen as an approximation. As shown by Ross (1981, 1975) and Monsi and Saeki (1953) that the total solar radiation (direct + diffuse) can be described by a

(1953) that the total solar radiation (direct + diffuse) can be described by a simple exponential equation (Beer's Law).

In WAVES no distinctions are carried between different wave bands visible (PAR) and near-infrared (NIR). The attenuation of shortwave radiation, PAR, and NIR with depth is shown in Fig. 2.2. It can be seen that PAR decreases more rapidly than NIR and the attenuation of short-wave radiation lying between them. This suggests that using a single attenuation coefficient for shortwave radiation does not lead to any errors in irradiance for energy balance purposes. For calculating PAR for plant growth, however, it is important. WAVES currently uses 50% as a fixed PAR ratio.

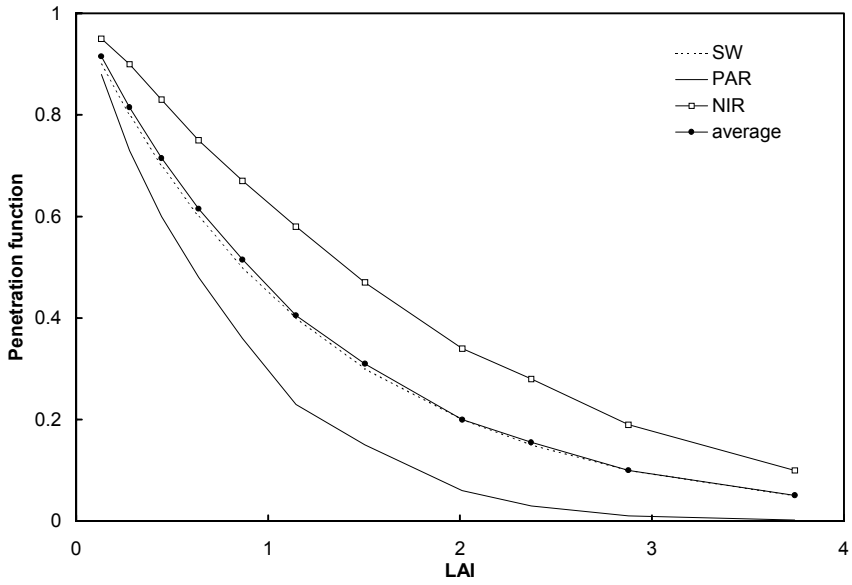

Fig. 2.2. Penetration function for shortwave (SW), visible (PAR), and near-infrared (NIS)

The longwave radiation calculations in WAVES are simplified on the basis of having daily time step, the canopy is a turbid medium, and in isothermal conditions. Ross (1981) has shown that net longwave radiation in a canopy can be dealt with in a similar way as for shortwave radiation (see Appendix A).

We assume all leaves are randomly distributed with horizontal inclination. For a two-layer canopy, the partial coverage of the individual layers can be determined by (Monteith and Unsworth, 1990; Van De Griend and Van Boxel, 1989):

$$\Lambda_1 = 1 - exp(-kLAI_1) = 1 - \tau\ (LAI_1) \qquad (2.7)$$

$$\begin{aligned}\Lambda_2 &= \left[exp(-kLAI_1) - exp(-k(LAI_1 + LAI_2))\right] / exp(-kLAI_1) \\ &= \left[\tau\ (LAI_1) - \tau(LAI_1 + LAI_2)\right] / \tau(LAI_1)\end{aligned} \tag{2.8}$$

and the total coverage of the ground surface follows from equations (2.7) and (2.8) as:

$$\Lambda = 1 - (1 - \Lambda_1)(1 - \Lambda_2) \tag{2.9}$$

where k is the attenuation coefficient for light, and LAI_1 and LAI_2 are the leaf area indices of the overstorey and understorey canopy respectively.

Following Ross (1981), the radiation transfer equations for the soil–vegetation system are given by:

Overstorey

$$R_{sv1}\downarrow = R_{sd}\Lambda_1 \tag{2.10}$$

$$R_{sv1}\uparrow = R_{sd}\alpha_1\Lambda_1 \tag{2.11}$$

$$R_{sn1} = R_{sd}(1 - \alpha_1)\,\Lambda_1 \tag{2.12}$$

$$R_{ln1} = (R_{ld} - R_{lu1})\,\Lambda_1 \tag{2.13}$$

$$R_{n1} = \{R_{sd}(1 - \alpha_1) + (R_{ld} - R_{lu})\}\Lambda_1 \tag{2.14}$$

Understorey

$$R_{sv2}\downarrow = R_{sd}\exp(-KLAz_1)\Lambda_2 \tag{2.15}$$

$$R_{sv2}\uparrow = R_{sd}\alpha_2\exp(-KLAz_1)\Lambda_2 \tag{2.16}$$

$$R_{sn2} = R_{sd}(1 - \alpha_2)\exp(-kLAI_1)\Lambda_2 \tag{2.17}$$

$$R_{ln2} = (R_{ld} - R_{lu2})\,exp(-kLAI_1)\Lambda_2 \tag{2.18}$$

$$R_{n2} = \{R_{sd}(1 - \alpha_2) + (R_{ld} - R_{lu2})\}\exp(-kLAI_1)\Lambda_2 \tag{2.19}$$

Ground surface

$$R_{sg}\downarrow = R_{sd}\exp(-KLAI_t) \tag{2.20}$$

$$R_{sg}\uparrow = R_{sd}\alpha_g\exp(-KLAI_t) \tag{2.21}$$

$$R_{sng} = R_{sd}(1 - \alpha_g)\exp(-kLAI_t) \tag{2.22}$$

$$R_{ln2} = (R_{ld} - R_{lug})\,exp(-kLAI_t) \tag{2.23}$$

$$R_{ng} = \{R_{sd}(1 - \alpha_g) + (R_{ld} - R_{lug})\}\exp(-kLAI_t) \tag{2.24}$$

where the subscripts *d* and *u* indicate downward and upward radiations; *s* and *l* indicate shortwave and longwave radiations; *1, 2*, and *g* represent overstorey, understorey, and ground surface respectively; *n* indicates net shortwave or longwave radiation; α_i is the albedo of a particular surface; and LAI_t is the cumulative leaf area index (LAI_1+LAI_2).

2.4.3 Initial and atmospheric boundary conditions

The initial conditions are generally set up the users. The atmospheric boundary conditions necessary to run WAVES include maximum and minimum daily air temperature, vapour pressure, rainfall, and solar radiation. These data are normally measured at most meteorological stations. If the complete set of data is not available, missing data can be generated using a program called GENCLIM, which is a modification of the program MTCLIM by Running *et al.* (1987). In irrigation areas, information on amount of water applied and frequency can be considered as boundary conditions as well.

Assumptions in energy balance and radiation budget

- It is assumed that all leaves in the canopy are randomly distributed with horizontal inclination. The partitioning of radiation between the canopy layers can be described by Beer's law.
- WAVES makes no distinction between direct and diffuse radiation. No separation is made for different wave bands such as visible (PAR) and near-infrared (NIR).
- The canopy temperatures of the overstorey, understorey, and ground temperature are equal to the air temperature. It is a reasonable approximation for a daily time step model.
- The differences in longwave radiation from different surfaces are due to the emissivity.
- Net radiation, evapotranspiration, and sensible heat flux are the dominant terms in the energy balance equation.

2.4.4 Combination methods

Estimation of evapotranspiration can be based either on aerodynamic approaches or on principles of energy balance. However, both of the methods require information at two or more levels above the surface. In practice, this information is difficult to obtain. To facilitate calculation of evapotranspiration using measurements made at one level only, Penman (1948) first introduced the combination equation by combining aerodynamic and energy balance principles for open water surface or short green vegetation with adequate moisture at all times. The method was further developed by Monteith (1965) who combined aerodynamic and surface (canopy) parameters, and energy balance in an evapotranspiration equation known as the Penman–Monteith

equation for a surface of any type in any state of water supply. In what follows, the derivation of this equation is described.

Fig. 2.3 illustrates schematically the structure of a single-layer model for the partition of available energy into latent heat (evapotranspiration) and sensible heat fluxes. The resistances shown in Fig. 2.3 are stomatal resistance (r_{st}), boundary resistance (r_B), 'eddy diffusive' resistance for heat (r_H), and for water vapour (r_V). The boundary resistance is usually combined with eddy diffusive resistance to form the aerodynamic resistance (r_a).

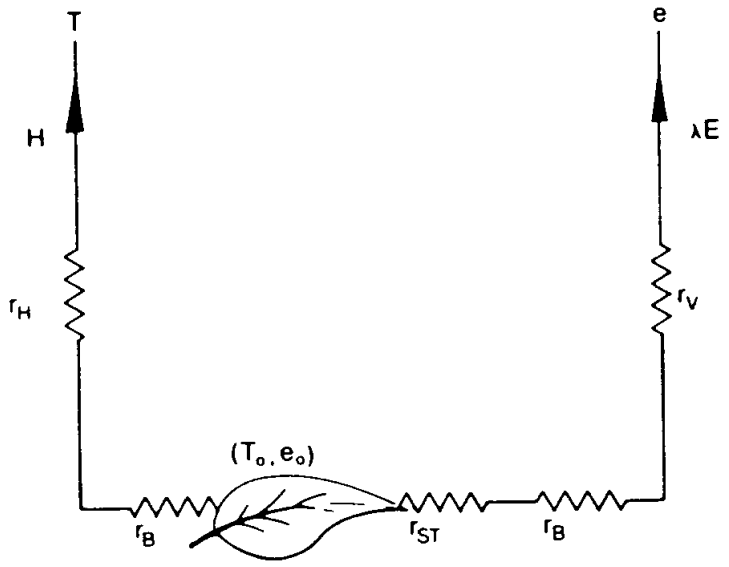

Fig. 2.3. The resistance network used in 'big leaf' model of the vegetation/atmosphere interaction (from Shuttleworth, 1979).

The transfer of sensible heat is given by

$$H = \rho\, c_p \frac{T_s - T_a}{r_a} \tag{2.25}$$

where ρ and c_p are respectively the density and the specific heat of the air at constant pressure, T_s is the surface temperature of the vegetation canopy, r_a is the aerodynamic resistance for sensible heat.

While subject to additional resistance (canopy resistance), the transfer of latent heat flux (evapotranspiration) can be expressed as

$$\lambda E = \frac{\rho\, c_p}{\gamma} \frac{e_s - e_a}{r_a + r_s} \tag{2.26}$$

where γ is the psychrometric constant, e_s is the saturated vapour pressure, e_a is the actual vapour, and r_s is the canopy resistance.

Using an average gradient (Δ) of the saturated vapour pressure versus temperature, one obtains the following expression by combining equations

$$\lambda E = \frac{\Delta(R_n - G) + \frac{\rho c_p}{r_a}(e_s - e_a)}{\Delta + \gamma(r_a + r_s)/r_a} \tag{2.27}$$

Equation (2.27) has a two-term structure suggesting that evapotranspiration has both energy and aerodynamic contributions. This equation is generally known as the Penman–Monteith equation and it is obtained by treating the entire canopy as one 'big leaf' with a bulk stomatal resistance (or canopy resistance) and a bulk aerodynamic resistance. As mentioned, the main feature of the combination equation is that it requires measurements of meteorological variables at one level only.

2.4.5 Evapotranspiration

Fig. 2.4 shows the schematic resistance network for WAVES. The transpiration from the overstorey and understorey canopy layers, and evaporation from the soil can be separately calculated using equations of the Penman–Monteith type

$$\lambda E_1 = \frac{sR_{nv1} + \rho c_p D_a/(r_{a1} + r_{b1})}{s + \gamma\left[1 + r_{c1}/\left(r_{a1} + r_{b1}\right)\right]} \tag{2.28}$$

$$\lambda E_2 = \frac{sR_{nv2} + \rho c_p D_{c1}/(r_{a2} + r_{b2})}{s + \gamma\left[1 + r_{c2}/\left(r_{a2} + r_{b2}\right)\right]} \tag{2.29}$$

$$\lambda E_s = \frac{sR_{ng} + \rho c_p D_{c2}/r_{as}}{s + \gamma\left(1 + r_s/r_{as}\right)} \tag{2.30}$$

where s is the slope of the saturation vapor pressure versus temperature curve, ρ is the air density, c_p is the specific heat of air at constant pressure, D_a is the vapor pressure deficit at reference height, D_{c1} and D_{c2} are the vapor pressure deficit at canopy source height for the overstorey and understorey respectively, r_{a1}, r_{a2} and r_{as} are the aerodynamic resistances between the overstorey canopy source height and a reference level, between the understorey source height and the overstorey canopy source height, and between the soil surface and the air within the understorey canopy, respectively; r_{b1}, r_{b2} are bulk boundary layer resistances of the vegetation elements in the

overstorey and understorey canopies, r_{c1}, r_{c2} are the canopy resistances for overstorey and understorey canopies, r_s is the soil resistance, γ is the psychrometric constant.

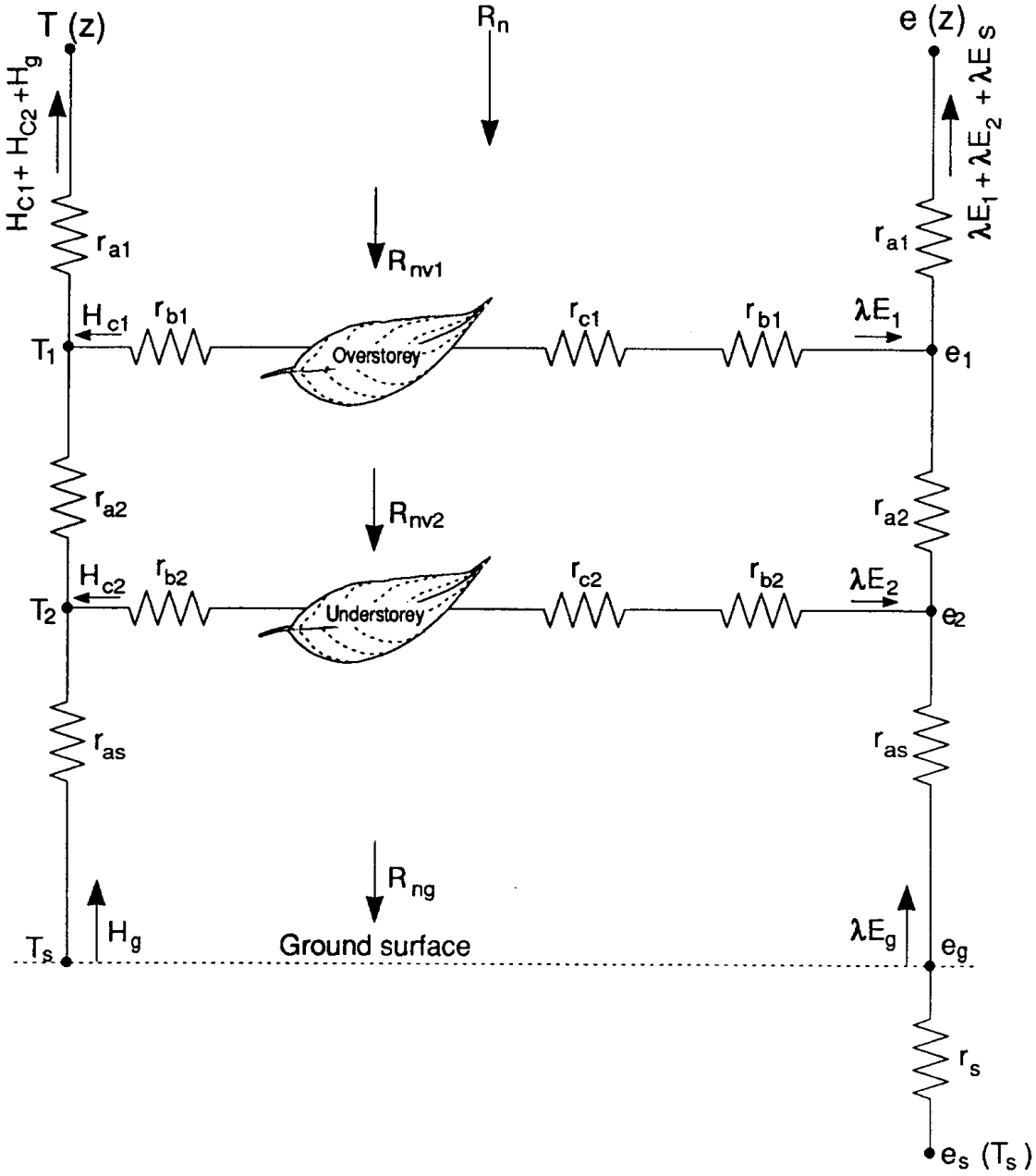

Fig. 2.4. A schematic resistance network for the WAVES model. The symbols are defined in the text.

The ground heat flux is neglected in equation (2.30) because over land surfaces the daily mean value of the ground heat flux is one or more orders of magnitude smaller than the net radiation (Brutsaert, 1982). The boundary layer resistances are generally much smaller than the corresponding aerodynamic resistances, especially if the leaf area index is large (Shuttleworth and Wallace, 1985; Choudhury and Monteith, 1988). As well, the Penman–Monteith equation is found to be rather insensitive to the values of the boundary layer resistance (Shuttleworth and

Wallace, 1985). Based on these observations, the boundary layer resistances are neglected and equations (2.24) and (2.25) can now be expressed as:

$$\lambda E_1 = \frac{sR_{nv1} + \rho c_p D_a / r_{a1}}{s + \gamma(1 + r_{c1} / r_{a1})} \tag{2.31}$$

$$\lambda E_2 = \frac{sR_{nv2} + \rho c_p D_{c1} / r_{a1}}{s + \gamma(1 + r_{c1} / r_{a1})} \tag{2.32}$$

Assumptions in evapotranspiration sub-model

- The canopy can be represented as a 'big leaf' using bulk aerodynamic resistance and bulk canopy resistance.
- Ground heat flux can be neglected over land surface on a daily time step.
- The boundary resistances are much smaller than the corresponding aerodynamic resistances, especially when the leaf area index is large.

2.4.6 Feedback processes between canopy and atmosphere

There exist feedback responses between canopy transpiration, vapour pressure deficit at the canopy surface, and canopy resistance (Jarvis and McNaughton, 1986). For example, an increase in the canopy vapour pressure deficit can affect the canopy resistance, transpiration, and photosynthesis. These primary responses can result in secondary responses. As transpiration increases, the water potential of the mesophyll cells will increase, which has a feedback on canopy resistance. On the other hand, increases in transpiration will also affect canopy vapour pressure deficit. The vegetation canopy and the atmosphere are coupled and the feedback between the processes can be explained using the omega coefficient proposed by Jarvis and McNaughton (1986):

$$D_{ci} = \Omega_{ci} D_{eqi} + (1 - \Omega_{ci}) D_a \tag{2.33}$$

with

$$D_{eqi} = \gamma \varepsilon R_{nvi} \left(\frac{r_{ci}}{c_p} \right) / (\varepsilon + 1) \tag{2.34}$$

$$\Omega_{ci} = (\varepsilon + 1) / (\varepsilon + 1 + r_{ci} / r_{ai}) \tag{2.35}$$

where the subscript i is equal to 1 for the overstorey and 2 for the understorey, Ω_{ci} is the decoupling coefficient, D_{eqi} is the equilibrium saturation deficit, ε is s/γ. Tall vegetation canopies, such as coniferous and deciduous forest, have small omega values and they are well coupled to their environment. As a result, transpiration rate is sensitive to changes in the vapour pressure deficit and canopy resistance. On the other hand, short vegetation canopies, such as crops and pasture, have high omega values and are decoupled from their external environment. The vapour pressure deficit at the canopy surface tends to a equilibrium value and the transpiration is controlled strongly by net radiation.

2.4.7 Aerodynamic resistances

In describing transfer of latent heat and sensible heat fluxes, it is convenient to use the so-called aerodynamic resistance approach. By analogy to Ohm's law in electricity, the aerodynamic resistance can be defined as:

$$aerodynamic\ resistance\ = \frac{concentration\ difference\ of\ an\ entity}{flux\ density\ of\ the\ entity} \tag{2.36}$$

This definition is arrived at by replacing in Ohm's law 'potential difference' by concentration difference and 'current' by flux density. The aerodynamic resistance represents the time in which a unit volume of air exchanges energy with a unit area of surface. It can be calculated from wind speed and surface roughness by assuming a logarithmic wind profile (Thom, 1975). The dimension of aerodynamic resistance is (velocity)$^{-1}$.

In WAVES, separate aerodynamic resistances are calculated for the overstorey, understorey, and ground surface. These resistances vary with wind speed and roughness length. Above the overstorey, the wind speed profile is assumed to be logarithmic and mean wind speed decreases exponentially through the overstorey and understorey. The aerodynamic resistance between overstorey canopy source height and reference level is determined by Monin–Obukhov surface layer similarity theory:

$$r_{a1} = \left\{\ln\left[\left(z-d\right)/z_{01}\right]-\psi\right\}^2/\left(k^2u\right) \tag{2.37}$$

where u is the wind speed at the reference height z, k is the von Karman constant, z_{01} is the roughness length of the overstorey canopy, d is the zero plane displacement, ψ is the atmospheric stability function. It is reasonable to approximate the roughness length and the zero plane displacement as fractions of the canopy height (Brutsaert, 1982; Monteith and Unsworth, 1990). The effect of atmospheric stability on the aerodynamic resistance is not considered in WAVES.

The aerodynamic resistance between understorey source height (z_2) and overstorey canopy source height (z_1+z_2) is defined as:

$$r_{a2} = \int_{z_2/2}^{(z_1+z_2)/2} dz / K(z) \tag{2.38}$$

The increase of the diffusivity $K(z)$ with height is approximately exponential and the relation may be expressed by (Thom, 1975):

$$K(z) = K(H)\, exp[-\alpha(1 - z/H)] \tag{2.39}$$

where H is the height of the overstorey canopy, α is an attenuation coefficient, and

$$K(H) = k^2 (H - d)u / \ln[(z - d)/ z_{01}] \tag{2.40}$$

The following expression can be obtained from equations (2.38) and (2.39):

$$r_{a2} = \frac{H \exp(\alpha)}{\alpha K(H)} [\exp(-\alpha z_2/2H) - \exp[-\alpha (z_1 + z_2)/2H]] \tag{2.41}$$

The aerodynamic resistance between the soil surface and the air within the understorey canopy is defined in a similar way as for r_{a2}:

$$r_{as} = \frac{H \exp(\alpha)}{\alpha K(H)} [\exp(-\alpha z_{02}/2H) - \exp[-\alpha z_2/2H]] \tag{2.42}$$

where z_{02} is the roughness length for the understorey canopy.

2.4.8 Surface resistance to soil evaporation

The surface resistance r_s in WAVES is assumed to be zero until the water content in the first node depth drops below the air dry soil moisture content; commonly called stage 1 soil evaporation (Ritchie, 1972). The soil resistance during stage 2 evaporation is determined by the method of Choudhury and Monteith (1988):

$$r_s = \tau l / (p D_m) \tag{2.43}$$

where p is the porosity of the soil, D_m is the molecular diffusion coefficient for water vapour, τ is a tortuosity factor and l is the depth of the air-dry soil layer. The depth of the soil layer is determined dynamically by the finite difference Richards' equation of water content, by finding how deep below the surface the soil is at air-dry potential.

Assumptions in aerodynamic resistances

- The conventional log-linear wind profile is assumed to be valid above the canopy.
- It is assumed that on a daily time-step the effect of atmospheric stability on the aerodynamic resistance is not significant.
- The vertical profile of wind speed within a plant canopy is assumed to be similar to that of eddy diffusivity, which tends to decrease exponentially with depth.

2.5 Soil water dynamics and runoff

2.5.1 Richards' equation

Movement of water through a soil matrix is governed Darcy's law:

$$q = -k\frac{dH}{dz} = -k\left(1 - \frac{\partial \psi}{\partial z}\right) \tag{2.44}$$

where q is water flux density, H is the total hydraulic head, which is the sum of the gravitational potential, and the matric potential ψ, z is the vertical distance from the soil surface downward, and k is the hydraulic conductivity. Darcy's law states that water flux density is proportional to the hydraulic gradient, which is the driving force. The proportionality factor k is generally known as the hydraulic conductivity.

Darcy's law assumes that the soil is homogeneous and isotropic so that the hydraulic conductivity is uniform and has no dependence on the direction of water movement. It further assumes that the soil is isothermal, isotropic, incompressible. Darcy's law is valid for most range of flow velocities observed in soil.

The continuity equation of water flow can be expressed as:

$$\frac{\partial \theta}{\partial t} = -\frac{\partial q}{\partial z} + S \tag{2.45}$$

where θ is volumetric water content, t is time, and S is a source/sink term.

Combining equations (2.44) and (2.45) gives the general flow equation:

$$\frac{\partial \theta}{\partial t} = -\frac{\partial q}{\partial z} + S = -\frac{\partial}{\partial z}\left(k - k\frac{\partial \psi}{\partial z}\right) + S \tag{2.46}$$

Equation (2.46) is the fundamental mixed form of the Richards equation.

For analytic solutions and common numerical solution techniques, equation (2.46) is often cast with a single dependent variable. The ψ-based form was used by Richards and has traditionally been seen as mandatory to treat soils that may become saturated. A criterion for choosing a form of the equation is the need to minimise nonlinearity in time and space. Redinger *et al.* (1984) and Ross and Bristow (1990) minimised nonlinearity in time by using θ on the left hand side of the equation, and reduced nonlinearity in space by using the Kirchhoff transform in the flux term:

$$\frac{\partial \theta}{\partial t} = -\frac{\partial}{\partial z}\left[K - \frac{\partial U}{\partial z}\right] + S \tag{2.47}$$

where θ is the soil water content, t is time, K is the hydraulic conductivity and U is the Kirchhoff transform variable defined as:

$$U = \int_{-\infty}^{\psi} K d\Psi \tag{2.48}$$

where Ψ is the matric potential of the soil water.

The sink term S which accounts for the rate of water extraction from the soil is modelled as follows. For evapotranspiration, the water is extracted from the entire root zone according to a weighting function which depends on the rooting density and availability of soil moisture. The model first calculates total root water uptake potential (*RWUP*):

$$RWUP = \sum_{i=1}^{n} r_i(\psi_{l\,max} - \psi_i)\Delta z_i \tag{2.49}$$

where r_i is the root biomass, ψ_{lmax} is the most negative water potential under which roots can still extract water (its value can be estimated from the minimum leaf water potential), ψ_i is the total potential (matric and osmotic), Δz_i is the depth of the discretised soil layer, and subscript i represents the soil layer. Then water uptake from each discretised soil layer is determined by

$$S_i = \frac{r_i(\psi_{l\,max} - \psi_i)\Delta z_i}{RWUP}\lambda E \tag{2.50}$$

The calculated water uptake from equation (2.50) is balanced with the available water which can be obtained by

$$S'_i = (\theta_i - \theta_d)\Delta z_i \tag{2.51}$$

The actual water uptake from each discretised soil layer is determined by

$$S_i = min\{S_i, S'_i\} \quad (2.52)$$

This method does not require a functional form of the equation for root water extraction and is suitable for investigating the impact of salinity on water extraction and plant growth.

2.5.2 Initial and boundary conditions

The initial conditions can be specified by the user as matric potential at specified depths. The lower boundary condition in equation (2.47) is defined as a fraction (β) of hydraulic conductivity: β is set to 1 when the lower boundary condition is free drainage, and β is set equal to zero for an impermeable boundary. For the upper boundary condition, three conditions may exist. Firstly, all rainfall or evaporation can be transmitted through the soil surface; in this case the flux of rain or evaporation is set. Rainfall may exceed the capacity of the soil either because the rate is too high (Hortonian runoff), or the soil becomes saturated (Hewlett or Dunne runoff); in this case the surface is set to a constant saturated potential, and all rainfall in excess becomes runoff. Finally evaporation may be limited by dry soil; in this case the soil surface is set to a constant air-dry potential and the flux passing the surface node is returned as the daily evaporation.

To solve Richards' equation, an analytical soil model of Broadbridge and White (1988) is used to describe the relationships among water potential, volumetric water content and hydraulic conductivity. This soil model has five parameters, including the saturated hydraulic conductivity, the volumetric soil moisture content at saturation, air-dry volumetric water content, the soil capillary length scale which is a function of sorptivity, and a soil structure parameter. The Broadbridge and White soil model can realistically represent a comprehensive range of soil moisture characteristics, from the highly nonlinear associated with a well developed capillary fringe, to the weakly nonlinear associated with highly structured soils and macropores. The model is subject to two levels of dimensionless scaling that lead to simple rules for guaranteed numerical performance (Short *et al*., 1995).

Assumptions in the Richards' equation

- The soil is rigid, incompressible, non-hysteretic, and isothermal.
- Water flow is via the soil matrix only, and not via macropores and larger preferred pathways.
- The soil is isotropic so that the saturated hydraulic conductivity of the soil is used in the formulation of Darcy's law for lateral movement.
- Vapour flow within the soil is not modelled explicitly, but included in the soil hydraulic model if possible.

2.5.3 Runoff generation

Overland flow can be generated from the excess of rainfall intensity over soil infiltrability, and the occurrence of precipitation over saturated surfaces. Both of the mechanisms are considered explicitly in WAVES. Water tables may develop anywhere within the soil profile. If non zero topographic slope is specified as input, then lateral subsurface flow occurs via the saturated water table and is described by Darcy's law.

2.6 Solute Transport

2.6.1 Theory

Soil water contains dissolved salts which may range from 5 mg per litre in rainwater to as high as 10 000 mg per litre in drainage from saline soil (Hillel, 1980). Solute transport in the soil is governed by three mechanisms, namely convection, diffusion, and hydrodynamic dispersion.

The convection of soil water carries with it a convective flux of solutes q_{sc} , which is proportional to their concentration c:

$$q_{sc} = qc = -c(k\, dH/dz) \tag{2.53}$$

The average apparent velocity $\bar{v}$ of the flowing solution can be calculated as:

$$\bar{v} = q/\theta \tag{2.54}$$

where θ is volumetric water content. Combining eq. (2.53) and (2.54) yields:

$$q_{sc} = qc = \bar{v}\,\theta\, c \tag{2.55}$$

Diffusion processes commonly occur within gaseous and liquid phases. The net effect is a tendency to equalise the spatial distribution of diffusible components in any mixed or multicomponent fluid. As such, diffusion processes are extremely important in the soil. If solutes do not happen to be distributed uniformly throughout a solution, concentration gradients will exist and solutes will tend to diffuse from high concentration to low concentration. In bulk water at rest, the rate of diffusion q_{sd} is related by Fick's law to the gradient of the concentration c:

$$q_{sd} = -D_s(\theta)dc/dz \tag{2.56}$$

in which D_s is the diffusion coefficient in the soil and dc/dz is the concentration gradient.

Equation (2.56) can only describe steady-state diffusion processes. For transient-state processes, we must invoke the mass conservation law, as formulated in the continuity equation. Let us assume that there are no sources or sinks for the diffusing solute in the soil and consider a rectangular volume element of soil which contains a liquid phase and which is bounded by two parallel square planes, of area A, separated by a distance Δz. The amount of solute diffusing through one of these planes into the volume element per unit time is Aq_{sd}, and the amount diffusing out the volume element through the second plane is $A[q_{sd} + (\partial q_{sd}/\partial z)\Delta z]$. The rate of accumulation of the solute in the volume elements is $-A(\partial c/\partial t)\Delta z$, where $\partial c/\partial t$ is the time rate of change of concentration. Thus,

$$A\left(\partial c \big/ \partial t\right)\Delta z = A\left[q_{sd} + \left(\partial q_{sd} \big/ \partial z\right)\Delta z\right] - Aq_{sd} \tag{2.57}$$

Combining this equation with eq. (2.56), we obtain a second-order equation as follows:

$$\frac{\partial c}{\partial t} = \partial\left(D_s \, \partial c \big/ \partial z\right) \big/ \partial z \tag{2.58}$$

The motion of any inhomogeneous solution in a porous body brings another process which differs from diffusion in its mechanism but which tends to produce an analogous or synergetic effect, which is to mix and eventually even out the concentration or composition difference between different portions of the flowing solution. This process is called *hydrodynamic dispersion*. It results from the microscopic nonuniformity of flow velocity in the soil's conducting pores. Mathematically, hydrodynamic dispersion is formulated in a manner analogous to the formulation of diffusion as give by eq. (2.56) and (2.58), except that, instead of a diffusion coefficient a *dispersion coefficient* is introduced. This coefficient, which we will designate D_h, has been found to depend more or less linearly on the average velocity:

$$D_h = a\bar{v} \tag{2.59}$$

with a an empirical parameter.

Because of the similarity in effect (though not in mechanism) between diffusion and dispersion, it is tempting to assume the two effects to be additive. Accordingly, the diffusion and dispersion coefficients are often combined into a single term, namely *the diffusion-dispersion coefficient* D_{sh}, which is a function of both the fractional water content and the average velocity:

$$D_{sh}(\theta, \bar{v}) = D_s(\theta) + D_h(\bar{v}) \tag{2.60}$$

To take into account the three mechanisms of solute movement, we can combine these equations to obtain:

$$q_s = \bar{v}\,\theta\,c - [D_s(\theta)\,dc/dz + D_h(\theta)\,dc/dz] \tag{2.61}$$

Since in practice the diffusion and dispersion phenomena can not be separated, the foregoing equation is usually written in the form:

$$q_s = \bar{v}\,\theta\,c - D_{sh}(\theta)\,dc/dz \tag{2.62}$$

Here q_s is the total mass of a solute transport across a unit cross-sectional area for soil per unit time.

For transient-state processes, we once again invoke the continuity condition, which for combined convective-diffusive-dispersive transport can be written:

$$\partial(c\theta)/\partial t = -\partial q_s / \partial z \tag{2.63}$$

For the rate of change of the solute mass present in a volume element of soil equal to the difference between the incoming and outgoing fluxes of the solute for that volume element.

Combining eq. (2.61) and (2.62), one obtains:

$$\partial(c\theta)/\partial t = -\partial(\bar{v}\theta c)/\partial z + \partial\left(D_{sh}(\theta)dc/dz\right)/\partial z \tag{2.64}$$

or

$$\partial(c\theta)/\partial t = -\partial\left(qc\right)/\partial z + \partial\left(\theta\,D_s(\theta)dc/dz\right)/\partial z \tag{2.65}$$

where q is the flux of water and $D_s(\theta)$ is the diffusion-dispersion coefficient of solute in the soil.

2.6.2 Initial and boundary conditions

The initial solute concentration in the profile is specified in an input file, in units of kg/ℓ. There are two other concentrations required: the solute concentration in the rain (and flood) water, and in the groundwater. When there is leakage from the soil column, the concentration of solute at the bottom node is used to calculate the amount of solute leached, and if there is uptake from the groundwater, then the solute concentration in the groundwater is used to calculate the amount of solute accumulated.

Assumptions in solute transport

- The solute is conservative, i.e. the solute is non-volatile, does not adsorb to, or desorb from, the soil matrix, and that solute concentration does not affect soil hydraulic properties.
- The soil water solution is perfectly mixed, is completely mobile, and is at concentrations that do not cause a precipitate.
- The solute is not taken up by root water extraction, or lost by soil evaporation.

2.7 Carbon allocation and plant growth

2.7.1 Integrated rate methodology

Plant growth is a complex process and dependent on a number of factors such as light, water, and nutrients. Attempts have been made to develop models that incorporate detailed biochemical and biophysical processes (Farquhar *et al.*, 1980, Collatz *et al*., 1991). An important aspect of such models is their value in helping to improve our process understanding, but they have limited application in practice because of the model complexity and data requirements. On the other hand, purely empirical plant growth models have been developed by statistical means (Hunt, 1982) and they contain few physically based functions to relate input to output. Within the range of data analysed, such a model may be highly successful. However, these models can not be used to make any predictions beyond the range of actual experience.

In WAVES, an intermediate position between the above two approaches was taken. The method defines a potential growth rate and modifies it by the availability of resources using an integrated rate methodology (IRM). The assimilation rate A_i is expressed as:

$$A_i = A_{\max} r_i \tag{2.66}$$

where A_{max} is the maximum carbon assimilation rate (see Table 2.1) and r_i is the relative carbon assimilation rate given by Wu *et al.* 1994 as:

$$r = \frac{1 + w_H + w_N}{1/\eta_T \chi_L + w_H / \chi_H + w_N / \chi_N} \tag{2.67}$$

where w_W is the weighting of water relative to light, w_N is the weighting of nutrients relative to light, χ_H, χ_N, and χ_L are the relative resource availabilities for water, nutrient, and light respectively, and η_T is the modifier of light availability due to temperature. The availability of light is

determined from intercepted radiation and air temperature, the availability of nutrients is an explicit constant for a growing season. The availability of water is a depth-weighted integral of the soil matric and osmotic potentials in the root zone. This value is made relative by dividing by the maximum soil water potential at which the plants can extract water, and subtracting from 1.

A normalised index of light availability (χ_L) is calculated as the ratio of the average PAR per unit leaf area to the light saturation value of a unit leaf:

$$\chi_L = \frac{R_P}{R_{max}} \tag{2.68}$$

where R_p is the average PAR per unit leaf area of the canopy calculated from available energy, R_{max} is the light availability at which maximum growth is obtained. The temperature modifier (η_T) is set to 1 at the optimum growth rate temperature (T_{opt}) and 0.5 at the half optimum temperature (T_h):

$$\eta_T = \exp\left(\frac{(T_a - T_{opt})^2}{(T_{opt} - T_h)^2} * \ln(0.5)\right) \tag{2.69}$$

where T_a is the average daily temperature. The availability of soil water for transpiration is estimated from the total soil water potential, *i.e.* the sum of the matric (ψ) and osmotic (π) potential of the soil water. The matric potential is calculated directly from the moisture characteristic function, whilst the osmotic potential is estimated from the sodium chloride concentration of the soil water. This assumes that the soil water is chloride dominated. The total soil water potential of each soil layer is normalised using the lowest soil water matric potential (ψ_{wilt}) against which the plant can transpire. A weighting factor adjusts for different effects of osmotic and matric potential on water availability. For the *i*-th soil layer:

$$\chi_{wi} = 1 - \frac{\psi_i + w_{osm}\pi_i}{\psi_{wilt}} \tag{2.70}$$

where w_{osm} is an osmotic potential weighting factor representing the ratio of the lowest matric potential to the lowest osmotic potential against which transpiration can occur. The osmotic potential of the soil water is calculated by

$$\pi_i = -2C_{NaCl}RT \tag{2.71}$$

where C_{NaCl} is the molarity of sodium chloride in the soil water, R is the universal gas constant, T is temperature. The index of water availability to the plant is estimated as the water uptake weighted average soil water availability:

$$\chi_w = \frac{\sum_{i=1}^{n} W_{ri}\chi_{wi}}{\sum_{i=1}^{n} W_{ri}} \tag{2.72}$$

where W_{ri} is a layer weighting factor and assumed to be related to the relative amount of root carbon in each soil layer, n is the number of soil layers in the potentially active root zone. The relative availability of nutrients (χ_N) is an input parameter (0–1).

The zero to one scalar r multiplied by the vegetation's maximum carbon assimilation rate gives the daily gross assimilation. After meeting growth respiration, any remaining carbon is dynamically allocated between leaf, stem and root carbon pools. If the plant has a net deficit during a day, the carbon is removed from these pools. Because WAVES concentrates only on the hydrological aspects of plants growth, e.g., leaf area index, the model does not fill grain or otherwise account for reproductive material of crops, grass, or trees.

The IRM framework provides an explicit means of integrating the net effect of multiple limiting factors. It also provides a means of taking into account not only the relative availability of resources, but also other possible factors such as salinity. IRM retains a mechanistic representation of relative plant growth response to resources availability in the form of its enzyme kinetics origins. A fully detailed description of the plant growth model in WAVES, and how to calculate the weighting factors for (2.67), can be found in Hatton *et al.* (1992) and Wu *et al.* (1994).

2.7.2 Carbon allocation and plant growth

The simulated carbon is partitioned to leaves, stems, and roots on a daily basis. The partitioning coefficients depend on both genotype and environment. The amount of leaf, stem, and root carbon allocated is reduced by growth and maintenance respiration and mortality rates. The daily carbon increment is given by:

$$\Delta C_L = n_L Y_L (A_i - C_L R_L) - C_L M_L \tag{2.73}$$

$$\Delta C_{S,R} = n_{S,R} Y_{S,R} \{(A_i - C_L R_L) - C_{S,L} R_{S,R}\} - C_{S,R} M_{S,R} \tag{2.74}$$

where subscripts L, S, and R refer to leaves, stems, and roots respectively, C is the carbon content of the biomass, n_L is the proportion of net canopy assimilation allocated to the leaves, n_S, and n_R

are the proportions allocated to stem and root growth of the remaining carbon assimilation, Y are respiration coefficients which account for conversion of assimilated carbon to biomass, R are maintenance respiration coefficients and M are mortality coefficients. Note that leaf maintenance respiration is subtracted before carbon is allocated to stems or the roots and maintenance respiration is deducted before assimilation is used for growth.

Carbon allocated to leaves is assumed to increase leaf area by an amount determined by the specific leaf area and the carbon allocated to roots is distributed amongst soil layers using the same weight function used for the soil water availability (2.72).

2.7.3 Canopy resistance

The canopy resistance of vegetation plays a major role in partitioning the available energy into evapotranspiration. It is governed by stomatal function and is primarily dependent on the photosynthetic rate and environmental factors, such as light interception, temperature, and vapour pressure deficit. For vegetation transpiration, the canopy resistance for the overstorey and the understorey is calculated using the empirical model of Ball *et al*. (1987) as modified by Leuning (1995):

$$r_{si} = (g_{si})^{-1} = \{g_0 + g_1 A_i / [(c_{si} - \Gamma)(1 + D_{ci} / D_{co)}]\}^{-1} \tag{2.75}$$

where the subscript i equals to 1 for the overstorey and 2 for the understorey, g_{si} is the leaf stomatal conductance, g_0 is a residual stomatal conductance, g_1 is an empirical coefficient, C_{si} is CO_2 mole fraction of the air at the canopy surface, Γ is the CO_2 compensation point, D_{ci} is the vapor pressure deficit at the canopy surface, D_{co} is an empirical coefficient. The values of these coefficients are given in Table 2.1.

The leaf stomatal conductance model (2.75) can be integrated to yield canopy conductance model (Sellers *et al.*, 1992a):

$$r_{ci} = (g_{ci})^{-1} = \{g_0 LAI + g_1 A_i / [(c_{si} - \Gamma)(1 + D_{ci} / D_{co)}]\Pi\}^{-1} \tag{2.76}$$

with

$$\Pi = (1 - exp(-kLAI))/k \tag{2.77}$$

The canopy resistance for water vapour can be estimated from (2.76) by considering the gaseous pathway and adjusting for the diffusivity of CO_2 and water vapor:

$$r_{wi} = r_{ci} / [1.6(1 + \chi_w / w\chi_L\chi_T)] \tag{2.78}$$

Assumptions in carbon balance and plant growth

- It is assumed that plants are greedy, constantly germinate, and attempt to fully stock an area if possible, i.e., when conditions are good, the vegetation attempts to close the canopy and develop a maximum leaf area.
- Carbon assimilation rate is controlled mainly by the availability of light, water, and nutrients.
- It is assumed that temperature and CO_2 concentration are invariant with depth in the canopy.

2.8 Parameter Estimation

As a physically based model, WAVES involves a number of parameters to describe processes occurring in the soil–vegetation–atmosphere system. Generally, two types of model parameters can be identified: *physical parameters* and *process parameters*. Physical parameters are well-defined and physically measurable properties such as albedo, saturation water content, hydraulic conductivity, saturation light intensity, etc. Process parameters are used to represent processes that are not well-defined; these parameters are not directly measurable properties such as capillary length, root mortality coefficient, relaxation coefficient, etc. A necessary step in applying the model is to determine the values of these model parameters or constants for the site under consideration. Parameter estimation may have at least as great an effect on the accuracy of the model results as the intrinsic accuracy of the model itself, e.g. even a model that perfectly describes a system will produce the wrong answers if the parameters are wrong. Three techniques are employed for estimating parameter values: *direct estimation, knowledge-based estimation,* and *model calibration*. Direct estimation or measurement of parameter values from field observation is logically the best approach, but it requires well-defined parameters which have a physical meaning and relate to the biophysical processes. Parameter values can also be estimated on the basis of published data, knowledge of likely values, and previous experience. The third technique is to calibrate the model against experimental data, or to fit model parameters. This is usually necessary in the use of any model, but must be treated with caution and the number of fitted parameters should be kept to a minimum. Calibrated parameters are often affected by deficiencies in the model structure and conceptualisation, as well as by measurement errors. In what follows, a detailed description of parameter estimation for WAVES is given.

The input variables and principal parameters used in WAVES are summarised in Table 2.1. WAVES requires three types of data: a) meteorological data; b) soil parameters; and c) vegetation parameters.

2.8.1 Meteorological variables

The meteorological data provide the atmospheric boundary conditions necessary to drive WAVES. They include maximum and minimum daily air temperature, daily average vapour pressure deficit, rainfall, rainfall duration, daily solar radiation, and wind speed. Some or all of these data are available from weather stations, and with only the temperatures and rainfall, realistic estimates of the other data can be made.

2.8.2 Soil parameters

The soil data required is knowledge of the soil layering, and the parameters that describe the relationships between ψ (soil water potential), θ (volumetric water content), and K (hydraulic conductivity). Before WAVES can be used, users need to estimate the parameter values of the soil water retention and hydraulic conductivity functions. In idea cases, these parameter values can be obtained by fitting experimental data to specified functions (*e.g*. Cresswell and Paydar, 1996). When no such data are available, the parameter values can be estimated based on particle size distribution and textural description Salama *et al.,* 1999). In some cases, inverse modelling techniques can also be used (Ross, 1993, Hume *et al.,* 1996). WAVES reads soil hydraulic properties from a table generated by an external program and thus allows the users to choose which soil water retention and hydraulic conductivity functions they want to use.

2.8.3 Vegetation parameters

WAVES requires 22 vegetation parameters to describe canopy energy and carbon balance, and interactions between soil and vegetation. Most of these parameters can be measured directly or taken from plant physiological literature, with only a few remaining for fitting, or adaptating to local conditions. Canopy albedo (α_v) is considered as a constant for a given vegetation and can be obtained from literature (Monteith and Unsworth, 1990). Roughness length (z_{ov}) affects the turbulence transport of water between canopy and the atmosphere. It is generally estimated from the height of vegetation canopy (Brutsaert, 1982). Light extinction coefficient (K) depends on the geometry of radiation with respect to the architecture of canopy. In practice, values of light extinction coefficient can be determined by measuring the attenuation of radiation in a plant canopy or taken from literature (Monteith and Unsworth, 1990). Rainfall interception coefficient (K_r) defines the maximum rainfall interception for a given vegetation canopy. Dunin *et al*.(1988) and Leuning *et al.* (1994) reported values for Eucalyptus and wheat crops. Specific leaf area (SLA) is used to convert leaf carbon to leaf area and its value can be found in Charles-Edwards (1982) for crop species and Raison *et al.* (1992) and Read and Busby (1990) for forests. Maximum assimilation rate of carbon (A_{max}) is a species dependent parameter and Collatz *et al.* (1991)

and (1992) reported values for C_3 and C_4 plants. It should be mentioned that the unit for A_{max} has changed from μmol m^{-2} s^{-1} to kg C m^{-2} d^{-1}. The availability of water for plant transpiration decreases as the matric potential of the soil water decreases. The maximum plant available water potential (LWP_{max}) is 100–150 m for most plants (Hillel, 1971, Marshall *et al.*, 1996). Drought-tolerant plants can use soil water at a lower matric potential over long periods. Saturation light intensity (L_{max}) defines the irradiance beyond which photosynthesis is not limited by light and its value varies between 1000 to 2000 μmol m^{-2} d^{-1}(Monteith, 1979, Wu *et al*., 1994). Maximum rooting depth (RD_{max}) depends on plant species and soil properties. It can be measured directly in the field (Incerti and O'Leary, 1990) or obtained from literature (Canadell *et al.,* 1996, Jackson *et al.,* 1996). Temperatures when growth is optimum and half-optimum were estimated for a range of plant species by Slavich et al (1998) based on Verteeg and Keulen (1986) and Larcher (1980). Respiration coefficients for crops vary from 0.0036 to 0.0095 kg C kg^{-1} C d^{-1} and are approximately 0.00084 kg C kg^{-1} C d^{-1} for evergreen trees (Larcher, 1980). Most of the parameters listed in Table 2.1 may be considered constants and set at representative values. When specific information is available, these parameters can be adjusted, and this is part of model calibration exercise. It should be emphasised that most of the parameters used in WAVES are well defined and can be measured directly. However, others are less well defined and have to be determined or inferred indirectly from field measurements or other source of information.

Table 2.1. List of input meteorological variables and principal model parameters of WAVES

Definition	Symbol	Unit	Parameter estimation
a. Meteorological inputs			
Total solar radiation	R_s	kJ m^2 day^{-1}	field measurements
Maximum daily temperature	T_{max}	°C	field measurements
Minimum daily temperature	T_{min}	°C	field measurements
Mean daily vapour pressure deficit	D_a	hPa	field measurements
Total daily precipitation	P	mm	field measurements
b. Soil parameters			
Soil albedo	α_s	—	Brutsaert (1982)
Soil roughness length	z_{0s}	m	Brutsaert (1982)
Saturated hydraulic conductivity	K_s	m day^{-1}	Clapp and Hornberger (1978)
Volumetric water content at saturation	θ_s	cm^3 cm^{-3}	Clapp and Hornberger (1978)
Air-dry soil moisture content	θ_d	cm^3 cm^{-3}	Clapp and Hornberger (1978)
Capillary length scale	λ_c	m	Estimated based on soil texture
Shape parameter	C	—	Estimated based on soil texture
c. Vegetation parameters			
Canopy albedo	α_v	—	Brutsaert (1982)
Rainfall interception coefficient	K_r	m day^{-1} LAI^{-1}	Vertessy *et al*. (1996)
Light extinction coefficient	K	—	Monteith and Unsworth (1990)
Specific leaf area	SLA	—	Measured
Maximum assimilation rate of carbon	A_{max}	μmol m^{-2} s^{-1}	Collatz *et al*. (1992)
Maximum plant available water potential	LWP_{max}	m	Hillel (1971)
Saturation light intensity	L_{max}	μmol m^{-2} day^{-1}	Wu *et al* (1994)
Maximum rooting depth	RD_{max}	m	Measured (soil depth limited)
Canopy roughness length	z_{ov}	m	Brutsaert (1982)
Residual stomatal conductance	g_0	mol m^{-2} s^{-1}	Leuning (1995)
Slope parameter of the conductance model	a_1	—	Leuning (1995)
CO_2 mole fraction of the air	C_s	μmol mol^{-1}	Measured
CO_2 compensation point	Γ	μPa Pa^{-1}	Leuning (1995)
Temperature when growth is optimum	T_{opt}	°C	
Temperature when growth is half optimum	T_h	°C	
Leaf maintenance respiration coefficient	R_l	kg C kg^{-1} C d^{-1}	Running and Coughlan (1988)
Stem maintenance respiration coefficient	R_s	kg C kg^{-1} C d^{-1}	
Root maintenance respiration coefficient	R_r	kg C kg^{-1} C d^{-1}	
Leaf Mortality coefficient	M_l	kg C kg^{-1} C d^{-1}	
Stem Mortality coefficient	M_s	kg C kg^{-1} C d^{-1}	
Root Mortality coefficient	M_r	kg C kg^{-1} C d^{-1}	
Vapour pressure coefficient	D_{co}	hPa	Leuning (1995)

CHAPTER 3. PROGRAM STRUCTURE AND NUMERICAL SOLUTIONS

W. R. Dawes

3.1 Introduction

This section details the logical flow, and numerical solution methods for the four balances solved in WAVES: water, energy, carbon, and solute. All models that perform balances of quantities follow the same pattern: the amount present at the end of a time-step is equal to the amount present at the beginning of the time-step, plus the amount added, minus the amount removed; WAVES is no different in this regard. The water, carbon, and solute balances use the method mentioned, while the energy balance only partitions the amount of energy received, and we assume there is no carry-over from one day to the next. The amount at the start and end of the time-step is effectively zero.

3.2 Energy Balance

The energy balance equations and theory are discussed in Chapter 2, but the important steps, theories, and assumptions are repeated here for completeness with the three other balance descriptions.

3.2.1 Radiation

The energy balance of any point can be described by:

$$R_n = P_s + \lambda E + H + A_h + G + S \tag{3.1}$$

where R_n is net radiation, P_s is energy absorbed for photosynthesis, λE is energy used for evapotranspiration, H is sensible heat, A_h is advected energy from or to the surroundings, G is energy that heats the soil, and S is energy that is stored. All these terms are in units of W m^{-2}. The variable R_n can also be expressed as:

$$R_n = R_{sd} - R_{su} + R_{ld} - R_{lu} \tag{3.2}$$

where R_{sd} is the downward shortwave radiation, R_{su} is the upward shortwave radiation, R_{ld} is the downward longwave radiation, and R_{lu} is the upward longwave radiation. All these terms are in units of W m^{-2}.

The energy balance assumptions in WAVES are that:

- the temperature of the soil, canopy, and air is the same, and equal to the average of the maximum and minimum daily temperature,
- differences in upward longwave radiation from the different surfaces is a function of emissivity alone,
- on the daily time-step, all storage and heating terms are negligible,
- in a one-dimensional model, lateral energy transfers cannot be estimated or used,
- leaf angles are randomly distributed and do not reflect energy within the canopy, so that the canopy may be treated as translucent absorbing layer (the so-called 'big leaf model').

Applying the appropriate assumptions to (3.1) leaves us with:

$$R_n = \lambda E + H \tag{3.3}$$

Such an equation looks relatively easy to work with. However, in general the two largest terms are R_n and λE (Monteith and Unsworth 1990), so H can be estimated by difference. In practice within WAVES, H has no significance to the water, carbon, or solute balance, so only R_n and λE are modelled explicitly.

WAVES expects as input daily downward shortwave radiation, which is easy to measure or estimate. To complete the terms in Equation (3.2) we need estimates of longwave radiation. Following Brutsaert (1982), we have:

$$R_{ld} = \varepsilon_a \sigma T_a^4 \tag{3.4}$$

$$R_{lu} = \varepsilon_s \sigma T_a^4 \tag{3.5}$$

$$\varepsilon_a = 1.24 \left(\frac{e_a}{T_a} \right)^{1/7} \tag{3.6}$$

where ε_a is the atmospheric emissivity, ε_s is the surface emissivity (this ranges from 0.95 to 0.99 for surfaces like snow, open water, soil, and plant canopies, so in WAVES it is a constant set at

0.97), σ is the Stefan–Boltzman constant (5.67×10^{-8} W m^{-2} K^{-4}), T_a is the average of daily maximum and minimum air temperature (Kelvin), and e_a is vapour pressure (millibars) based on T_a.

Net longwave radiation, that is $R_{ld} - R_{lu}$, is in general a negative quantity. In the cascading energy balance WAVES performs, *i.e*. one layer at a time, longwave losses must be subtracted from each layer, not as a bulk cost to the total available energy. For a vegetation layer, the energy balance components are:

$$R_{sin} = R_{sd}(1 - exp(k\ LAI)) \tag{3.7}$$

$$R_{snet} = R_{sin}(1 - \alpha) \tag{3.8}$$

$$R_{lnet} = (R_{ld} - R_{lu})\frac{R_{sin}}{R_{sd}} \tag{3.9}$$

$$R_{net} = R_{snet} + R_{lnet} \tag{3.10}$$

where R_{sd} is the downward shortwave radiation that reaches the soil or canopy surface (for the first canopy it is incoming solar radiation, for the next canopy it is the shortwave radiation that passes through the first canopy, *etc*), k is the light extinction coefficient of the canopy, *LAI* is the leaf area index of the vegetation canopy (m^2 leaf m^{-2} ground), α is surface albedo, R_{sin} is the shortwave radiation that is potentially available to the canopy, R_{snet} is the net shortwave radiation after reflection from the canopy, R_{lnet} is the net longwave radiation of the canopy (these wavelengths are not affected by albedo), and R_{net} is the net available total radiation to the canopy.

These equations can be cascaded through a series of canopies, by repeating the calculations with that radiation passing through the canopy as R_{sd} for the next lower canopy. At the soil surface there is no canopy to filter and absorb radiation, so in (3.7) $R_{sin} = R_{sd}$. Other than that, these equations hold for the soil energy balance also.

3.2.2 Vapour Pressure Deficit

Just as the amount of radiation cascades down through a series of canopies, so the vapour pressure deficit under a canopy is, in general, less than above the canopy. Jarvis and McNaughton (1986) proposed a method of estimating how to quantify this decrease, through use of a coefficient describing how well coupled the atmosphere is to the air within and below the canopy. The method for the omega coefficient is as follows:

$$D_i = \Omega_c D_{eq} + (1 - \Omega_c) D_a \tag{3.11}$$

where D_i is the within and below canopy vapour pressure deficit (millibars), D_a is the above canopy vapour pressure deficit (millibars), D_{eq} is the equilibrium vapour pressure deficit (millibars), and Ω_c is the atmospheric coupling coefficient, defined by:

$$D_{eq} = \frac{\gamma \varepsilon R_{nv} r_c}{c_p(\varepsilon + 1)} \tag{3.12}$$

$$\Omega_c = \frac{\varepsilon + 1}{\varepsilon + 1 + r_c/r_a} \tag{3.13}$$

where $\varepsilon = \Delta/\gamma$, Δ is the slope of the saturated vapour pressure *v.* temperature curve (millibar K^{-1}), γ is the psychrometric constant, r_c is bulk canopy resistance (s m^{-1}), c_p is the specific heat of air at constant pressure (W kg^{-1} K^{-1} s), and r_a is bulk aerodynamic resistance (s m^{-1}).

Just as radiation cascades downward, using the amount of radiation passing through the next highest canopy as the starting energy, the vapour pressure deficit is progressively reduced moving down toward the ground. The vapour pressure deficit in the climate file will affect the upper canopy, the lower canopy will use a reduced vapour pressure deficit, and the soil below will use yet another vapour pressure deficit.

3.2.3 Aerodynamic and Canopy Resistance

The Soil Surface

For the soil, aerodynamic and canopy (read as surface) resistance for evaporation are extremely simplified. The aerodynamic resistance (r_a) is set to a constant of 100 s m^{-1}. The values of roughness length for soil reported in Brutsaert (1982) are from 0.001 to 0.01 m, and assuming a constant wind speed of 2 m s^{-1} at 2 m this translates to a resistance of 85 to 172 s m^{-1}.

The surface resistance is a function of four possible variables; (1) the wetness of the surface soil, (2) the depth of any drying front, (3) the amount of litter, and (4) whether the site is flooded. When the soil is not air-dry at the surface, r_s is set to zero. When the soil is air-dry at the surface, then the depth of drying front is calculated from the soil water potentials solved by the water-balance module (see section 3.3). The surface resistance is then set according to Choudhury and Monteith (1988):

$$r_s = \frac{\tau \ell}{\rho D_v} \tag{3.14}$$

where τ is the tortuosity factor (constant set to 2), ℓ is tortuous path-length equal to the depth of drying front (m), ρ is soil porosity, and D_m is the molecular diffusion coefficient for water vapour in air (constant set to 2.5 x 10^{-5} m^2 s^{-1}). If there is plant litter on the soil surface, then the path-length ℓ is increased by:

$$\ell = \ell + \frac{C_{lit}}{20} \tag{3.15}$$

where C_{lit} is the weight of litter (kg m^{-2}).

If the soil is flooded, *i.e.* has standing water with a positive soil water potential at the surface node, $r_s = 0$ and $r_a = 80$ s m^{-1}.

The Plant Canopy

The aerodynamic resistance of each plant canopy in WAVES is treated as a constant. This is for several reasons related to the exposition in section 2 from (2.36) to (2.42). The first is that we do not always have windspeed available as input data. Second, and more importantly, we do not know the roughness length of the vegetation, or how that varies in time. For example, it may be adequate to express the height of a grass or crop as a fraction of the leaf area index, but this would clearly not work for trees. In that case, a relationship based on accumulated stem mass might be good, but only up to certain ages. In any event, these data and relationships are so rarely available, that a constant value for r_a is the only practical alternative. For very rough canopies, such as closed canopy forests, the surface is very rough and a small constant resistance is a good approximation, $r_a = 10$ s m^{-1} (Monteith 1981). For smoother surfaces, such as grass and crops, a higher resistance is required, but the value is likely to be less constant over the whole growing season, $r_a = 30$ s m^{-1}.

Canopy or surface resistance is the mechanism for coupling environmental stresses back to transpiration. In Ball *et al.* (1987) type conductance models, canopy conductance (the reciprocal of canopy resistance) is a function of the assimilation of carbon. In section 3.5 there is a detailed description of how daily assimilation is calculated, and so here we will assume this value is available, and proceed with the estimation of canopy conductance. First the conductance to CO_2 is calculated by:

$$g_c = 0.0005 LAI\, k + \frac{g_1 A}{0.9[CO_2]DL(1 + D_a / 3.5)} \tag{3.16}$$

where g_c is the conductance to CO_2 (m s^{-1}), g_1 is the slope of the assimilation versus conductance line, A is the actual assimilation (kg C m^{-2}), [CO_2] is the atmospheric CO_2 concentration (constant set to 1.8324 x 10^{-4} kg C m^{-3}), and DL is the day length (in seconds). Next, the conductance to water vapour is estimated by:

$$g_w = g_c\left(1 + \frac{\chi_w}{sm_c \chi_l \chi_t}\right)1.6 \tag{3.17}$$

where g_w is the conductance to water vapour (m s^{-1}), χ_w is the relative availability of water, χ_l is the relative availability of light, χ_t is the relative favourability of temperature, sm_c is the ratio of stomatal to mesophyll conductance (constant equal to 0.2 for C_3 vegetation and 0.8 for C_4 vegetation), and 1.6 is the ratio of the diffusion rates of CO_2 and H_2O vapour.

The result from (3.17) is limited to the maximum value obtained when A is at the maximum assimilation rate, and the three availability scalars χ_w, χ_l, and χ_t are equal to 1.0. Canopy resistance for estimating transpiration is the reciprocal of conductance from (3.17).

3.2.4 Transpiration and Evaporation

With all the necessary quantities defined and calculated, we can estimate the daily transpiration and evaporation rates. WAVES uses the Penman–Monteith combination equation:

$$\lambda E = \frac{\Delta R_n + \rho c_p \Delta_a / r_a}{\Delta + \gamma(1 + r_c / r_a)} \tag{3.18}$$

where E could be for any vegetation layer or the soil surface (m d^{-1}), using the appropriate value for R_n, D_a, r_c, and r_a. The constant c_p is set to 1010, and constants are applied to (3.18) give the estimated rate in m d^{-1}. The following empirical functions are used to determine the parameters for equations (3.1) to (3.18). Saturation vapour pressure e_a, psychrometric constant γ, slope of saturation vapour pressure curve Δ, density of air ρ, and latent heat of vapourisation λ, are calculated by:

$$e_a = 6.1078 \exp\left(\frac{17.269 T_a}{T_a + 237.16}\right) \tag{3.19}$$

$$\gamma = 0.646 + 0.0006 T_a \tag{3.20}$$

$$\Delta = e_a(T_a + 0.5) - e_a(T_a - 0.5) \tag{3.21}$$

$$\rho = 1.292 - 0.00428 T_a \tag{3.22}$$

$$\lambda = 2501000 - 2400 T_a \tag{3.23}$$

where T_a is the average of daily maximum and minimum air temperature in degrees Celsius, and in (3.21) a value of saturation vapour pressure at more than, and less than, daily air temperature by one-half of a degree is determined from (3.19).

The transpiration from (3.18) is then distributed within the root zone according to the following function:

$$rw_i = E \frac{rp_i \left(1 - \frac{\Psi_i + \eta \Pi_i}{\Psi_{wilt}} \right)}{SRP} \tag{3.24}$$

where rw_i is the root-water demand at depth *node i* (m d^{-1}), rp_i is the proportion of total root mass at *node i*, Ψ_i is the water matric potential (m) at *node i*, Π_i is the osmotic potential (m) due to solutes at *node i*, η is the salt sensitivity factor of the vegetation, Ψ_{wilt} is the wilting point of the vegetation (m), and SRP is the sum of the numerator over all nodes. The result from (3.24) can be further reduced if there is not enough water at any particular node while solving the water movement equations.

3.2.5 Computational Flow

The sequence of steps to run a single day time-step is as follows:

- adjust incoming shortwave direct and diffuse radiation for slope and aspect
- calculate downward and upward longwave radiation
- calculate root-water experience by adding matric and osmotic potential at each depth node with roots; sum this for whole profile for water availability, and sum this multiplied by proportion of roots at each node for distributing transpiration
- calculate net radiation of each vegetation canopy layer
- calculate net radiation of soil surface
- calculate rainfall interception for each canopy layer (see section 3.5) and reduce available radiation by the amount of energy required to vapourise that water
- CALL plant growth routine, which calculates actual assimilation
- calculate constants required for estimating evapotranspiration, including soil surface resistance and plant canopy conductance

- calculate transpiration from each vegetation canopy layer, reducing vapour pressure deficit below each one
- calculate soil surface evaporation
- distribute transpiration down profile; where roots compete for water at a node with less water available than required, reduce demand at that node proportionally.

3.3 Water Balance

WAVES does the water balance in a specific order, with relevant assumptions for use of a one-day time-step, and the rate of change of processes. The different types of fluxes, and order in which they are calculated in, are shown in Fig. 3.1.

The solution for soil water movement, water sources, and sinks, is all handled within the solution of Richards' equation (Richards 1931). The soil-water gradients provide the internal driving forces, while ponded and free infiltration, evaporation, plant transpiration, lateral fluxes, drainage, and groundwater exchange are all simple sources and sinks within the soil profile. Some of these are coupled into the iterative solution, such as the depth of a watertable, and some rates are constant, such as plant extraction rates over the day.

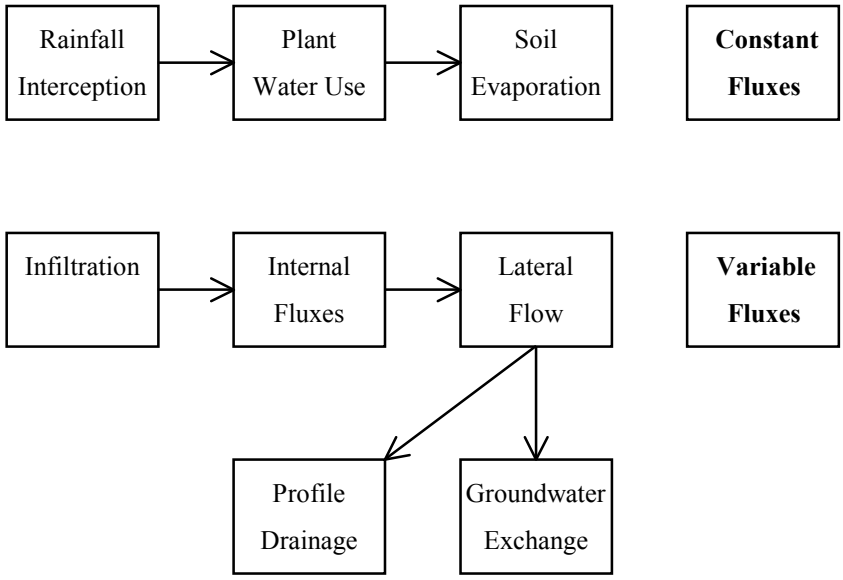

Fig. 3.1: WAVES Water Balance Flux Components. *Constant Fluxes* are calculated once at the beginning of the time-step and do not change during solution. *Variable Fluxes* are updated each iteration of the water movement solution until they are consistent with the calculated water contents.

3.3.1 Theory

The assumptions used in WAVES for water-balance modelling are that:

- the soil is rigid, *i.e.* it does not shrink or swell
- the soil is isothermal, *i.e.* the air temperature is the same as the soil temperature and this has no feedback onto the soil properties
- the soil is non-hysteretic, *i.e.* single-valued functions describe the relationships between water content and potential, and water content and hydraulic conductivity
- all soil-water flow is through the matrix, *i.e.* macropores, pipes, preferred pathways, and bypass flows are not modelled explicitly
- soil air flow is ignored
- solute in the water is conservative, *i.e.* it is not adsorbed by the matrix, and does not feed back onto the soil properties
- soil properties do not change with time or climate, *i.e.* the surface does not form a seal (reducing hydraulic conductivity) or compact (reducing hydraulic conductivity and water holding capacity), or possess other features that change soil properties, *e.g.* sodicity or acidity
- rainfall intensity is constant for the duration of the event, and similarly, soil evaporation and plant transpiration rates are constant for the non-raining duration of the time-step.

The last point requires some explanation. WAVES will use a one-day time-step for days when there is no rain, or when the rain lasts for the entire day. When only part of the day experiences rain, the duration of the rainfall will infer an intensity. Since high rainfall intensity can cause surface saturation and runoff, this is an important process to represent. Thus, on a day when rain lasts for only part of the day, a time-step is processed for the duration of the rain, then a second time-step is processed for the remainder of the day. During any of these time-steps, with rainfall or evaporation, the flux crossing the surface soil boundary and the leaf boundary, is assumed to be constant for the entire time-step. Diurnal fluctuations in rates are not modelled, only the average rate for the time-step. This is an appropriate compromise to maintain the largest time-step, *i.e.* a full day, while modelling the most important short-duration processes, *i.e.* runoff and saturation from high-intensity rainfall.

To solve a soil water mass balance, we must provide a framework that allows the important fluxes and feedbacks to be incorporated directly, and without special conditions. Because WAVES is a one-dimensional model concerned with the interactions between water, plant roots,

and salt, it is desirable to keep track of the vertical distribution the these quantities within the soil. Accordingly, the WAVES water balance is based around solution of Richards' equation (Richards 1931). This starts with a statement of mass balance:

$$\frac{\partial \theta}{\partial t} = -\frac{\partial q}{\partial z} \tag{3.25}$$

where θ is water content ($L^3\ L^{-3}$), q is water flux ($L\ T^{-1}$), t is time (T), and z is depth positive downwards (L). Looking at the left-hand side (LHS) of (3.25), we see the change in water content with time (water storage at the end of the time-step minus water storage at the start of the time-step), and the right-hand side (RHS) of (3.25) says the change in flux with depth (water flux out of the bottom of the soil column minus water flux into the top of the soil column). The negative sign on RHS is because depth is positive downwards, and so the sign of flux matters. This is a direct statement of mass balance that matches exactly with the description in the Introduction.

Richards combined (3.25) with Darcy's Law for unsaturated conditions:

$$q = K\left(1 - \frac{\partial \psi}{\partial z}\right) \tag{3.26}$$

where K is hydraulic conductivity ($L\ T^{-1}$), and ψ is water potential (L), and derived:

$$\frac{\partial \theta}{\partial t} = -\frac{\partial}{\partial z}\left(K\left(1 - \frac{\partial \psi}{\partial z}\right)\right) \tag{3.27}$$

This is the classical 'mixed form' of Richards' equation. It is called a 'mixed form' because the dependent variable on the LHS is θ and on the RHS is ψ. Equation (3.26) has three equivalent forms that have been used in the RHS of (3.25):

$$q = K - K\frac{\partial \psi}{\partial z} = K - D\frac{\partial \theta}{\partial z} = K - \frac{\partial U}{\partial z} \tag{3.28}$$

where D is soil water diffusivity ($L^2\ T^{-1}$), and U is the Kirchhoff transform variable ($L^2\ T^{-1}$) (see for example Gardner 1958) defined by:

$$U = \int_{-\infty}^{\psi} K\, d\psi = \int_{0}^{q} D\, d\theta \tag{3.29}$$

The LHS of (3.25) has similar equivalent forms to (3.28):

$$\frac{\partial \theta}{\partial t} = C \frac{\partial \psi}{\partial t} = \frac{1}{D} \frac{\partial U}{\partial t} \tag{3.30}$$

where C is differential moisture capacity (L^{-1}) defined as $\partial\theta/\partial\psi$.

Richards (1931) stated that the solution of (3.27) was unique while the functions between variables, *i.e.* K and ψ as functions of θ, or K and θ as functions of ψ, remained monotonic throughout the entire range of application, and he placed no restrictions of the variables used in (3.28). Using different combinations of (3.28) and (3.30), Richards' equation can be described in one or more dependent variables. While each of the forms in (3.30) is analytically equivalent, when described in difference form for numerical solutions, they are not equivalent, and cause mass balance errors. Only the θ-based form of the LHS can explicitly conserve mass. Given that our primary concern here is to accurately keep track of all water, we must use θ on the LHS.

Analytic solutions of (3.27) up to the point of saturation and in uniform soils have traditionally used the θ-based form, commonly known as the Fokker–Planck equation, with θ in the LHS and RHS (*e.g.* Broadbridge and White 1988). Traditionally the ψ-based form has been used where the soil becomes saturated, or layers are required, but this form cannot conserve mass except with very small time and space steps. Haverkamp *et al.* (1977) used the U-based form of (3.27) for their numerical experiments, but this form is cumbersome and also cannot conserve mass.

Brutsaert (1971) used (3.27) for saturated and layered soils, thus proving that the traditional ψ-based form was not required for these purposes. The major step forward was to not use a Picard-type solution methods requiring a single dependent variable in the equation, but a Newton–Raphson solution scheme (see for example Shoop 1979). This allowed the equation to be formulated in any way, as long as a derivative with respect to a single dependent variable existed for each independent variable. In the general case of saturated and layered (or gradational) soils, the only continuous variable is ψ, and Brutsaert used this as the dependent variable of the solution.

Redinger *et al.* (1984) and Ross and Bristow (1990) used U on the RHS to reduce the apparent non-linearity of the flux term, while using a Newton–Raphson solution. Ross (1990) compared different transforms of ψ on the RHS, and found that a speed difference up to a factor of 200 could be achieved by using the different forms. Further, he found that different forms yielded different accuracy, compared to a detailed solution, for the same spatial discretisation. Given all forms of (3.28) are analytically equivalent and do not cause mass balance errors, the results of Ross (1990) were a function of the soil hydraulic properties used in the experiment.

In WAVES the form of Richards' equation used is:

$$\frac{\partial \theta}{\partial t} = -\frac{\partial}{\partial z}\left(K - \frac{\partial U}{\partial z} \right) + S(\psi) \tag{3.31}$$

where S represents all source and sink terms, *e.g.* root water extraction, and may be a function of the water potential at a node, *e.g.* water potential on a soil boundary specifies the depth of a water table that may be a lateral flowing sink term.

There are several reasons for using (3.31). Firstly, we do not know what soil hydraulic model the user will use. Equation (3.31) is the form that Ross (1990) found was fastest to run with a particular soil model. Since WAVES does not impose any particular soil model on the user, this will be the best equation for the soil model used by Ross. Secondly, the Newton–Raphson solution scheme requires derivatives of each term with respect to the dependent variable, in this case ψ. The derivative of U is K, and therefore we will not need extra information for derivatives of other variables. Finally, we want to minimise the number of arithmetic operations involved. With fewer variables in the equation we must reduce the absolute number of operations required.

3.3.2 Numerical Solution

Differential Equations

Equation (1) can be represented in finite-difference form at a depth node i, over time-step j to $j+1$, with arbitrary temporal weighting and central spatial weighting as:

$$F_i = \alpha(q_{i+0.5}^{j+1} - q_{i-0.5}^{j+1}) + (1-\alpha)(q_{i+0.5}^{j} - q_{i-0.5}^{j}) + e_i + S_i = 0 \tag{3.32}$$

where

$$q_{i+0.5}^{j} = K_{i+0.5}^{j} - \frac{U_{i+1}^{j} - U_{i}^{j}}{Dz_{fi}} \tag{3.33}$$

$$K_{i+0.5}^{j} = \sqrt{K_i^j K_{i+1}^j} \tag{3.34}$$

$$e_i = \left(\theta_i^{j+1} - \theta_i^j\right)\frac{Dz_{ci}}{Dt_j} \tag{3.35}$$

z_c refers to a central difference, z_f refers to a forward difference, and S_i is any combination or source and sink terms that may or may not be functions of soil water potential. Equation (3.34) is a geometric mean of the conductivity. In finite-element solution schemes, linear or arithmetic

averages are required due to the solution formulation. Using a finite-difference solution, there is no restriction on the form of flux, or even how the average is taken or the variables used to describe it. As long as they are consistent between iterations there is no numerical problems created. The geometric mean causes 'average' values to be lower, which we think is more physically realistic than the arithmetic average, or an upstream or downstream weighting.

At the top and bottom boundary, the equations are modified because a central difference does not exist at these points. At the surface node, nominally *node zero*, we have:

$$F_0 = \alpha\left(q_{0.5}^{j+1} - q_0^{j+1}\right) + (1-\alpha)\left(q_{0.5}^{j} - q_0^{j}\right) + e_0 = 0 \tag{3.36}$$

$$e_0 = \left(\theta_0^{j+1} - \theta_0^{j}\right)\frac{\Delta z_{f0}}{2\Delta t_0} \tag{3.37}$$

Note that there are no extra source or sink terms at *node zero*. At the bottom node, nominally *node n*, we have

$$F_0 = \alpha\left(q_n^{j+1} - q_{n-0.5}^{j+1}\right) + (1-\alpha)\left(q_n^{j} - q_{n-0.5}^{j}\right) + e_n + S_n = 0 \tag{3.38}$$

$$e_0 = \left(\theta_n^{j+1} - \theta_n^{j}\right)\frac{\Delta z_{fn-1}}{2\Delta t_j} \tag{3.39}$$

Let us consider the value of α, which sets the temporal weighting of the solution. When $\alpha = 1$ it is a fully implicit equation that requires an iterative solution, does not use information from the previous time-step to get solution fluxes, and has few restrictions on time and space step size. When $\alpha = 0.5$ it is a Crank–Nicolson type, or central weighted, equation that requires an iterative solution, uses the last time-steps results as well as current estimates of the solution to proceed to an answer, and has some restrictions on time and space step size. When $\alpha = 0$ it is a fully explicit equation that does not require iteration, uses only the result from the current time-step to get a solution, makes guesses at the fluxes and boundary conditions (since you can't go back!), but has great restrictions on the allowable size of space and time-steps.

WAVES is designed to be a daily time-step hydrologic model, running with arbitrary soil types and climate, and practical to run on a PC, so we therefore cannot be restricted by using $\alpha = 0$. Using $\alpha = 0.5$ presents some conceptual problems, especially with boundary fluxes. The flux passing the surface node from time *j* to *j+1* is, from (3.36):

$$q_s = \alpha q^{j+1} + (1-\alpha) q^j \tag{3.40}$$

so with $\alpha = 0.5$ we have the flux at the end of the last time-step contributing to flux for this time-step. Consider a daily evaporation flux of 10 mm day^{-1}, dropping at a rate of 1 mm day^{-1} until it reaches 1 mm day^{-1}. The actual flux, q_s, passing the surface is 10, 9, 8, 7, 6, 5, 4, 3, 2, 1, 1, 1 mm day^{-1}, etc. The q^j on the other hand would be 10, 10, 8, 8, 6, 6, 4, 4, 2, 2, 0, 2, 0 mm day^{-1}, etc. With a less smooth drop off, such as the q_s halving each day, e.g. 16, 8, 4, 2, 1, 1, 1 mm day^{-1}, you can generate absurd values of q^j such as 16, 16, 0, 8, –4, 6, –4 mm day^{-1}, etc. The values of q^j generated for alternating days of rain and evaporation are similarly absurd. This leaves $\alpha = 1$ as the most useful compromise. From (3.40) we have the daily surface flux as a constant for the whole time-step, and perfectly defined. The number of terms, and therefore the number of operations, amount of storage, and derivatives required, in (3.36) and (3.38), will be minimised.

There are similar conceptual concerns with inferring the flux across a boundary with a constant potential. When there is a constant potential at the surface node, there is no change in water content at that node. From (3.38), with $S_0 = e_0 = 0$, we have:

$$F_0 = \alpha\left(q_{0.5}^{j+1} - q_0^{j+1}\right) + (1-\alpha)\left(q_{0.5}^{j} - q_0^{j}\right) = 0 \tag{3.41}$$

If $\alpha = 1$, then the solution to (3.41) is that $q_0 = q_{0.5}$, with $\alpha = 0$ we have a guessed solution based on last time-steps conditions, and with any other weighting we have a mixture of terms that will contain the surface fluxes described with flux boundary conditions. These arguments clearly point out that $\alpha = 1$ is the only practical temporal weighting. The other benefits in terms of maximising the solution convergence space, minimising the amount of storage and operations required, and reducing code size and scope for coding errors, are bonuses on this pragmatic decision.

The spatial weighting is much less important than the temporal weighting, since we must retain all the detail in the vertical regardless of the solution. Ross (1990) and Ross and Bristow (1990) did make some comments on the use of upstream weighting, but this may have had more to do with the soil hydraulic functions than the actual solution technique. In any event, WAVES uses a central spatial weighting in solution of (3.31).

Matrix Solution

The Newton–Raphson solution solves a matrix of the form:

$$-[F]=\left[\frac{\partial F}{\partial \psi}\right][\Delta\psi] \tag{3.42}$$

where $[F]$ is a 1 × N matrix describing how well mass is balanced at each depth node based on current estimates of $[\psi]$ (see Equations (3.32) – (3.39)), $[\partial F/\partial\psi]$ is a tridiagonal N × N matrix of the derivatives of Equations (3.32), (3.36), and (3.38), and $[\Delta\psi]$ is a 1 × N matrix to be solved for that are the corrections to $[\psi]$ to make all $[F]$ approach zero. Estimates of $[\psi]$ are updated by:

$$[\psi_{new}]=[\psi_{old}]-[\Delta\psi] \tag{3.43}$$

This procedure allows re-calculation of $[F]$ with $[\psi_{new}]$ and iteration until the solution converges. This criterion for convergence can be done on the basis of either mass balance (the $[F]$ matrix), or required changes to the dependent variable (the $[\psi]$ matrix). Given that we may have a range in ψ from millimetres to hundreds of metres and both positive and negative values, a consistent criterion for a change in ψ is difficult. However, being primarily concerned with mass balance, $[F]$ gives a direct estimate of how well balance is achieved at each node, and provides a very convenient convergence criterion. In WAVES, the solution is deemed to have converged when:

$$|F_i| \le 10^{-10} \tag{3.44}$$

Theoretically, and in practice, this allows mass to be balanced to within 10^{-10} of the largest water balance component, usually rainfall or evaporation. Other important considerations are the size of changes to $[\psi]$, and an oscillating solution. Using a tangent method, such as Newton–Raphson, where very small gradients exist, a very large change in the value of ψ at a node can result. To prevent this from causing further problems, a bi-directional limit is set:

$$\Delta\psi_i < 0.8|\psi_i| + k, \ \ for\ all\ \psi_i < 0 \tag{3.45}$$

where k is a suitable finite number, set to 0.1 m. Points to note about this limit are as follows.

Ross and Bristow (1990) used a limit that only stopped a node becoming wetter too quickly, *i.e.* essentially (3.45) without taking absolute values and if the change is to make the node wetter, but numerical experiments quickly found this to be unsuitable for the continual wetting and drying cycles modelled with WAVES.

A finite offset value is required in (3.45) to allow a node to reach saturation, otherwise it would asymptotically approach saturation and never reach it, and converge the solution.

The factor 0.8 is apparently arbitrary, but stops a node from becoming saturated in a single iteration. Again numerical experiments quickly showed the worth of this.

The value of ψ_i only needs to be negative, since above saturation the behaviour of ψ is linear and therefore does not require constraint with a gradient method, even when the node is becoming drier, i.e. $\Delta\psi_i$ is towards the unsaturated.

The second criterion for changes in $[\psi]$ is to minimise the effects of an oscillating solution. Where successive iterations indicate a change in the sign of the correction to ψ_i, the size of the correction is halved. This avoids the classical oscillation a constant amount above and below the actual solution.

Solution of the matrix equation (3.42) requires assemblage of $[\partial F/\partial\psi]$. The contents of this matrix are the derivatives of (3.32), (3.36), and (3.38) with respect to ψ at each depth *node i*. As stated, this is a tridiagonal matrix and is subject to extremely efficient solution. The components of $[\partial F/\partial\psi]$ at *node zero* are:

$$\frac{\partial F_0}{\partial \psi_0} = \frac{K'_0}{2}\sqrt{\frac{K_1}{K_0}} + \frac{K_0}{\Delta z_{f0}} + \frac{\theta'_0\,\Delta z_{f0}}{2\Delta t_j} \tag{3.46}$$

$$\frac{\partial F_0}{\partial \psi_1} = \frac{K'_1}{2}\sqrt{\frac{K_1}{K_0}} - \frac{K_1}{\Delta z_{f0}} \tag{3.47}$$

where K_i is unsaturated hydraulic conductivity, K' is the derivative of K with respect to ψ, and θ' is the derivative of θ with respect to ψ. The components of $[\partial F/\partial\psi]$ at *node i* are:

$$\frac{\partial F_i}{\partial \psi_{i-1}} = \frac{K'_{i-1}}{2}\sqrt{\frac{K_i}{K_{i-1}}} - \frac{K_{i-1}}{\Delta z_{fi-1}} \tag{3.48}$$

$$\frac{\partial F_i}{\partial \psi_i} = \frac{K'}{2}\left(\sqrt{\frac{K_{i+1}}{K_i}} - \sqrt{\frac{K_{i-1}}{K_i}}\right) + K_i\left(\frac{1}{\Delta z_{fi-1}} - \frac{1}{\Delta z_{fi}}\right) + \frac{\theta_i'\Delta z_{ci}}{\Delta t_j} \tag{3.49}$$

$$\frac{\partial F_i}{\partial \psi_{i+1}} = \frac{K'_{i+1}}{2}\sqrt{\frac{K_i}{K_{i+1}}} - \frac{K_{i+1}}{\Delta z_{fi}} \tag{3.50}$$

The components of $[\partial F/\partial\psi]$ at *node n* are:

$$\frac{\partial F_n}{\partial \psi_{n-1}} = \frac{K'_{n-1}}{2}\sqrt{\frac{K_n}{K_{n-1}}} - \frac{K_{n-1}}{\Delta z_{fn-1}} \tag{3.51}$$

$$\frac{\partial F_n}{\partial \psi_n} = \frac{K'_n}{2}\sqrt{\frac{K_{n-1}}{K_n}} + \frac{K_n}{\Delta z_{fn-1}} + \frac{\theta'_n \Delta z_{fn-1}}{2\Delta t_j} \tag{3.52}$$

Source and Sink Terms

All sink terms are added or subtracted from (3.32), (3.36), or (3.38) as required. If these terms are constant, such as evaporation or rainfall rate, or root water extraction rate, then they have a zero derivative with respect to ψ, and therefore do not appear in any of the derivative terms. An example of a sink term that is a function of ψ at a node is lateral flux. A watertable that develops on a soil layer boundary *node i* will generate a lateral flux, defined by Darcy's law for saturated conditions:

$$q_\ell = \psi_i K_s m \tag{3.53}$$

where q_ℓ is the lateral flux (m^3 d^{-1}), ψ_i is the positive water potential at *node i* (m), K_s is the saturated hydraulic conductivity of the soil layer (m d^{-1}), and m is the slope of the land surface (m m^{-1})*. Equation (3.53) would be added to (3.32) or (3.38) as required. The derivative term is:

$$\frac{dq_\ell}{d\psi_i} = K_s m \tag{3.54}$$

This term is added to (3.49) or (3.52) as appropriate. Equation (3.53) is recalculated each iteration with an updated value of ψ_i.

Soil Layers

With layered soils, there are special considerations. At a soil layer boundary, the only continuous quantities are soil water potential and soil water flux. We plan to calculate water content changes using variables other than ψ, so we must take into account that two values of these variables exist at the layer boundary. Since flux terms are defined between nodes, they require no special treat-

* Darcy's law of saturated flux consists of a conductivity, depth, slope, and width. Conductivity is taken from the soil hydraulic properties, depth of flow is the soil water potential at the layer boundary, slope is a constant for the soil profile specified by the user, and for dimensional consistency, the lateral flux flows across a unit width of soil.

ment. However, the e_i terms in (3.36) and (3.38) are defined at nodes, and do require special formulation and derivatives. At a *node i* straddling a boundary, e_i is defined by:

$$e_i = ((\theta_{up}^{j+1} - \theta_{up}^{j})\Delta z_{fi-1} + (\theta_{lo}^{j+1} - \theta_{lo}^{j})\Delta z_{fi})\frac{1}{2\Delta t_f} \qquad (3.55)$$

where θ_{up} refers to the soil layer above the boundary, and θ_{lo} refers to the soil layer below the boundary. Similarly, the derivative term in (3.49) and (3.52) will contain a mixture of derivatives.

Boundary Conditions

There are two possible boundary conditions at the top and bottom of the soil column: constant flux and constant water potential. At the surface, a constant flux condition would occur with non-ponded infiltration or energy-limited (stage 1) evaporation, and a constant potential condition would occur with ponded infiltration or soil-limited (stage 2) evaporation. WAVES allows a range of different options for surface ponded water: all ponded water becomes runoff, water is allowed to pond as if the area were flooded, or a flood depth is imposed. All of these options are handled transparently.

A constant flux boundary condition is set when rainfall or evaporation occurs with an unsaturated surface soil. This is done by prescribing the rate of rainfall or evaporation as q_0^{j+1} in Equation (3.36). If evaporation causes the surface node to become drier than the air-dry water potential of the soil, or rainfall causes the surface node to become saturated, then the time-step is re-run with a potential boundary condition. This will cause a mass balance problem, because the potential at the surface is imposed for the entire time-step. To avoid this, a triangle of water equal to the difference between the current water content and that at the constant potential for the top depth node must be added or removed, and placed in the accounting for water passing the surface node, *i.e.* $(\theta_{pot} - \theta_{old}) / 2 \times \Delta z_{f0}$.

If the surface dries out due to evaporation, the time-step is re-run and the flux passing the surface boundary is $q_{0.5}^{j+1}$, from (3.41) with $\alpha = 1$, plus the triangle of mass removed. When the surface node becomes saturated, forcing a constant flux would cause compression of water in the soil profile, and very large water potentials. The apparent rainfall flux is therefore reduced by the amount of water that is ponded, thus:

$$q_0 = q_{rain} - \frac{\psi_0}{\Delta t_{rain}} \qquad (3.56)$$

where q_0 is the flux that appears in (3.36), q_{rain} is the rainfall rate, and ψ_0 is the estimated water potential at *node zero* equivalent to the depth of ponded water, and Δt_{rain} is the duration of the rainfall. Because (3.56) is a function of the potential at *node zero*, a derivative equal to $-1/\Delta t_{rain}$ will appear in (3.46). If water is allowed to pond, then after convergence the program continues. If ponded water is runoff, then the time-step is re-run using a constant potential condition of $\psi_0 = 0$, and the runoff becomes the rainfall minus the infiltration ($q_{0.5}^{j+1}$) minus the triangle of mass added.

At the base of the soil column there is only a single boundary condition: constant flux. This flux however, may interact with a user imposed groundwater level. In the simplest case, the soil column is allowed to drain at a rate determined by the conductivity of the boundary node and a throttle value β ranging from 0 to 1. If $\beta = 0$, there is no drainage out of the soil column, and a watertable may develop. If $\beta = 1$ there is gravity drainage assuming a unit gradient, at a rate equal to the unsaturated hydraulic conductivity of the boundary node. When $0 < \beta < 1$, we have a throttled condition which assumes a gradient less than free drainage, due conceptually to a semi-infinite block of lower conductivity material below the modelled soil profile. In general the drainage flux is:

$$q_d = \beta K_n \tag{3.57}$$

where q_d is the drainage rate, and K_n is the unsaturated hydraulic conductivity at *node n*. This term appears in (3.38), and it has a derivative term:

$$\frac{dq_d}{d\psi_n} = \beta K'_n \tag{3.58}$$

which appears in (3.52). This flux is always a sink term, *i.e.* it is water lost to the soil column, and is always recalculated between iterations.

The other condition that may exist at the base of the soil column is a groundwater interaction term. In this coupling, the user specifies the depth of an external regional groundwater table, and this level may be changed daily through the weather file. This regional level interacts with any local water table through the following flux:

$$q_g = \varepsilon (d_{gw} - z_n + \psi_n) \tag{3.59}$$

where q_g is the rate of drainage from the local to regional groundwater table, d_{gw} is the depth to regional groundwater, z_n is the depth of the soil column, ψ_n is the water potential at *node n*,

equivalent to the depth of water table in the soil column, and ε is a coupling coefficient related to the rate of bore recession after a rise. Again, this term appears in (3.38) and has a derivative term:

$$\frac{dq_g}{d\psi_n} = \varepsilon \tag{3.60}$$

which appears in (3.52). When the regional groundwater table is deeper than the local water table, q_g is positive and can be thought of as drainage from the soil column. When the local water table is deeper than the regional water table, q_g is negative and represents filling of the soil depleted by evapotranspiration. The value of q_g from (3.59) is restricted so that its magnitude, whether positive or negative, never exceeds the saturated hydraulic conductivity of the bottom soil layer. Under these conditions, no derivative exists because the value is no longer a function of potential, and (3.60) is not required.

The quantity ε deserves some description. In a system where the regional groundwater table strongly controls local levels, because of high conductivity and good hydraulic connection, or in a lysimeter where groundwater levels are controlled externally, ε has a value close to 1.0, meaning that for every millimetre of water extracted, the regional groundwater can supply one in return. In this system the local water table is at the same depth as the regional groundwater table. As water table recessions become slower, the value of ε decreases. If $\varepsilon = 0.001$, for example, then for every 1.0 metre of head difference between the local and regional water table, 1.0 millimetre of water per day would be able to be exchanged, conductivity restrictions notwithstanding. So if vegetation were able to evaporate 1 mm day^{-1} more than rainfall, then the local water table would be 1.0 m below the regional groundwater table on average. The value of ε should theoretically be based on the ratio of the hydraulic conductivities of the soil and aquifer systems.

3.3.3 Computational Flow

The sequence of steps to run a single day time-step is as follows:

- determine whether all rainfall can be intercepted → no rainfall time-step required
- calculate available water and total osmotic plus matric potential at each depth node
- if first call for this time-step, CALL energy-balance, which calculates net rainfall
- determine surface boundary condition

**** re-entry point for failed solution, or need to set new boundary condition ****

- get values of soil water functions for state of last time-step
- set first estimate of solution to state of last time-step
- LOOP
    - get values of soil water functions for current solution estimate

- calculate coefficients and derivatives for matrix solution
- incorporate source and sink terms into matrices, i.e. transpiration, watertables, groundwater interaction or drainage.
- solve matrix equation
- check for solution convergence
- modify estimates of solution, restricting large changes and oscillation
- check for failed solution, and re-enter if necessary
- check for change in boundary conditions, and re-enter if necessary
- accumulate all solved mass balance components.

This sequence is repeated if both rainfall and surface evaporation occur on the same day. Evaporation and transpiration fluxes, and stresses, are not recalculated in this case.

3.3.4 Soil Hydraulic Functions

As stated at the end of section 3.3.1, we do not know what soil hydraulic model the user will want to use, so we place no restrictions on this. However, Short *et al.* (1995) provide a treatise on the use of the Broadbridge–White (BW) soil model in practical daily time-step modelling (Broadbridge and White 1988, White and Broadbridge 1988). They presented spaces where convergence was guaranteed with constant rate infiltration into very dry soil; one of the most numerically difficult problems. The strength of the BW soil model is that it links water potential, water content, and hydraulic conductivity by starting with a physically realistic representation of soil water diffusivity. Other important properties are that the functions between ψ, θ, and K are monotonic. With a solution scheme that depends on the gradients of these functions, not having zero or infinite slope is a great benefit; this is also physically realistic. It has been suggested that slope discontinuities are a problem for the Newton–Raphson solution scheme. However, a slope discontinuity apparently exists at every point on the soil tables used by WAVES without causing numerical problems. Brutsaert (1971) successfully used the Newton–Raphson solution scheme with only 10 points to describe the soil hydraulic curves. The issue of zero and infinite slopes in the curves is critical to the convergence of the solution, whereas slope discontinuities are almost irrelevant.

The BW soil model has five physically meaningful and measurable parameters, and can represent a wide range of soil moisture characteristics ranging from highly nonlinear, associated with uniform sands, to weakly non-linear, associated with well-structure forest soils. The space in which convergence of the solution is guaranteed for all rainfall rates into all soils described by the BW model, shown in Short *et al.* (1995), is where the spacing between depth nodes is no

greater than the characteristic length scale of the BW soil model. This condition is very practical, and for a model that must run for long times with dynamic climatic and vegetation stresses, the existence of this space is mandatory. Such spaces may exist for other soil hydraulic models but they are not available in general, so while another soil model, or a set of empirical equations fitting observations, may be used with WAVES, the stability and convergence of Richards' equation cannot be guaranteed.

3.4 Solute Balance

3.4.1 Generalised Equations

Solute Mass Balance

The solute balance in WAVES is concerned with conservative solutes only, and in particular common salt, sodium chloride (NaCl). This solute is assumed to not attach to the soil matrix, or affect soil hydraulic properties, or to removed by the plant roots or surface evaporation. Further we assume that the saturation concentration in water is never exceeded, thus avoiding problems with different solubilities of salts, precipitation of salt, and re-dissolving of salt. Under these conditions, we may write a mass balance equation for solute that is similar to that for water (3.31):

$$\frac{\partial (\theta \quad \varsigma)}{\partial t} = -\frac{\partial q_s}{dz} \quad + S(\varsigma) \tag{3.61}$$

where c_s is the concentration of salt (kg ℓ^{-1}), q_s is the flux of salt (m d^{-1} kg ℓ^{-1}, sometimes reduced to kg d^{-1}), and S is a source or sink term that may be a function of the salt concentration. With the salt transport in WAVES, we assume that the salt concentration does not affect the soil hydraulic properties, does not adsorb to the soil and transfer between the soil matrix and soil water, and is not removed from the soil by plants or evaporation. Under these conditions, the sink/source term can be omitted, and the soil property values and fluxes are constant for any concentration of solute.

In a similar way to water, we can write equations (3.32) to (3.35) for (3.61), thus:

$$G_i = q_{s,i+0.5}^{j+1} - q_{s,i-0.5}^{j+1} + h_i = 0 \tag{3.62}$$

where

$$q_{s,i+0.5} = q_{i+0.5} c_{s,i+0.5} - \theta_{i+0.5} D_{s,i+0.5} \frac{c_{s,i+1} - c_{s,i}}{\Delta z_{fi}} \tag{3.63}$$

$$h_i = (c_{s,i}^{j+1}\theta_i^{j+1} - c_{s,i}^{j}\theta_{s,i}^{j})\frac{\Delta z_{ci}}{\Delta t_f} \tag{3.64}$$

$$c_{s,i+0.5} = \frac{c_{s,i}\theta_i + c_{s,i+1}\theta_{i+1}}{\theta_i + \theta_{i+1}} \tag{3.65}$$

$$D_{s,i+0.5} = D_1\theta_{i+0.5}\tau + D_2\frac{|q_{i+0.5}|}{\theta_{i+0.5}} \tag{3.66}$$

where D_s is solute diffusivity ($m^2\ d^{-1}$), D_1 is diffusion coefficient in free water (constant set to 0.001 $m^2\ d^{-1}$), τ is an impedance factor (constant set to 0.5), and D_2 is dispersivity (constant set to 0.02 m). Equations (3.63) to (3.66) are formulated at *time j+1*, and this index has been omitted where possible for clarity.

Equations (3.62) and (3.64) are modified at the upper and lower boundary. At the surface *node 0*, we have:

$$G_0 = q_{s,0.5}^{j+1} - q_{s,0}^{j+1} + h_0 = 0 \tag{3.67}$$

$$h_0 = (c_{s,0}^{j+1}\theta_{s,0}^{j+1} - c_{s,0}^{j}\theta_0^{j})\frac{\Delta z_{f0}}{2\Delta t_j} \tag{3.68}$$

and at the bottom *node n*, we have:

$$G_n = q_{s,n}^{j+1} - q_{s,n-0.5}^{j+1} + h_n = 0 \tag{3.69}$$

$$h_n = (c_{s,n}^{j+1}\theta_n^{j+1} - c_{s,n}^{j}\theta_n^{j})\frac{\Delta z_{fn-1}}{2\Delta t_j} \tag{3.70}$$

With the water fluxes solved for, $q_{s,0}$ and $q_{s,n}$ are easily determined. If rainfall or irrigation has occurred, with or without a potential boundary condition, the surface flux of salt is the volume of water that infiltrated multiplied by the salt concentration in the rain or irrigation water. If evaporation has occurred, then there is no salt flux from the surface node. When a potential boundary condition is imposed at the surface however, the surface salt concentration must be adjusted to account for the change in water content at the surface; see section 3.3.2 *Boundary Conditions*. If there is drainage from the bottom node, then the flux out of the soil column is the drainage flux multiplied by the concentration of salt at the bottom node. Similarly if there is upflow from a

groundwater table then the flux of salt into the soil column is the inflow flux multiplied by the concentration of salt in the groundwater.

Matrix Derivative Terms

Equations (3.62) to (3.70) can be expressed in finite difference form, and have derivatives taken with respect to c_s at each node. At the surface *node 0* we have:

$$\frac{\partial G_0}{\partial c_{s,0}} = q_{0.5}\frac{\theta_0}{\theta_0 + \theta_1} + \frac{\theta_0 D_{s,0.5}}{\Delta z_{f0}} + \frac{\theta_0 \Delta z_{f0}}{2\Delta t_j} \tag{3.71}$$

$$\frac{\partial G_0}{\partial c_{s,1}} = q_{0.5}\frac{\theta_0}{\theta_0 + \theta_1} - \frac{\theta_{0.5} D_{s,0.5}}{\Delta z_{f0}} \tag{3.72}$$

At a general intermediate *node i* we have:

$$\frac{\partial G_i}{\partial c_{s,i-1}} = q_{i-0.5}\frac{\theta_{i-1}}{\theta_{i-1} + \theta_i} - \frac{\theta_{i-1} D_{s,i-0.5}}{\Delta z_{fi-1.0}} \tag{3.73}$$

$$\frac{\partial G_i}{\partial c_{s,i}} = q_{i+0.5}\frac{\theta_i}{\theta_i + \theta_{i+1}} + \frac{\theta_{i+0.5} D_{s,i+0.5}}{\Delta z_{fi}} - q_{i-0.5}\frac{\theta_i}{\theta_{i-1} + \theta_i} + \frac{\theta_{i-0.5} D_{s,i-0.5}}{\Delta z_{fi-1}} + \frac{\theta_i \Delta z_{ci}}{\Delta t_j} \tag{3.74}$$

$$\frac{\partial G_i}{\partial c_{s,i+1}} = q_{i+0.5}\frac{\theta_{i+1}}{\theta_i + \theta_{i+1}} - \frac{\theta_{i+1} D_{s,i+0.5}}{\Delta z_{fi}} \tag{3.75}$$

At the bottom *node n* we have:

$$\frac{\partial G_n}{\partial c_{s,n-1}} = q_{n-0.5}\frac{\theta_{n-1}}{\theta_{n-1} + \theta_n} - \frac{\theta_{n-0.5} D_{s,n-0.5}}{\Delta z_{fn-1}} \tag{3.76a}$$

$$\frac{\partial G_n}{\partial c_{s,n}} = q_{n-0.5}\frac{\theta_n}{\theta_{n-1} + \theta_n} + \frac{\theta_{n-0.5} D_{s,n-0.5}}{\Delta z_{fn-1}} + \frac{\theta_n \Delta z_{fn-1}}{2\Delta t_j} \tag{3.76b}$$

Inspection of the derivative terms (3.71) to (3.76b) reveals that c_s does not appear on the RHS of any of the equations. The system of equations is linear, and may therefore be solved in a single iteration with the Newton–Raphson gradient method. Even with other water-based processes included, the solution remains linear in salt concentration. Take for example lateral flows. Equation (3.53) describes a lateral flux q_ℓ as a function of water potential, conductivity and gradient.

When salt is also involved, some mass will be lost from the column via lateral transfers. Specifically, the flux is:

$$q_{\ell,s} = q_\ell \, c_{s,i} \tag{3.77}$$

where $q_{\ell,s}$ is the lateral salt flux at a node, q_ℓ is the lateral water flux from (3.53), and $c_{s,i}$ is the salt concentration at *node i* with a perched watertable. The derivative of (3.77) is:

$$\frac{\partial q_{\ell,s}}{\partial c_{s,i}} = q_\ell \tag{3.78}$$

which is not a function of salt concentration, and leaves the solution linear in c_s. Equation (3.77) is added to (3.62) or (3.69), and (3.78) is added to (3.74) or (3.76b).

Soil Layers

At soil layer boundaries, special consideration must be given to (3.64) and its derivative equation (3.74). At a soil layer boundary there are two parts to each of the mass components, yielding the following, where *node k* is the soil boundary, and the superscript 'a' is for the layer above and 'b' is for the layer below:

$$h_k = (c_{s,k}^{j+1}\theta_k^{a,j+1} - c_{s,k}^{j}\theta_k^{a,j})\frac{\Delta z_{fk-1}}{2\Delta t_j} + \left(c_{s,k}^{j+1}\theta_k^{b,j+1} - c_{s,k}^{j}\theta_k^{b,j}\right)\frac{\Delta z_{fk}}{2\Delta t_j} \tag{3.79}$$

$$\frac{\partial G_k}{\partial c_{s,k}} = \frac{\theta_k^{a,j+1}\Delta z_{fk-1} + \theta_k^{b,j+1}\Delta z_{fk}}{2\,\Delta t_j} \tag{3.80}$$

Calculation of (3.65) requires careful algebra also to ensure the integrity of the formulation and solution. If the solution fails to converge in a single iteration, then it is most likely that the equations have been derived or coded incorrectly.

3.4.2 Computational Flow

The sequence of steps to run a single day time-step is as follows:

*** allow soil water solution to converge to get state values and fluxes ***

- estimate values of soil hydraulic properties between nodes
- estimate values of solute diffusion and boundary solute fluxes
- set first estimate of solution to state of last time-step
- LOOP (once only!)

- calculate coefficients and derivatives for matrix solution
- incorporate source and sink terms into matrices, i.e. water tables, groundwater interaction or drainage.
- solve matrix equation
- check for solution convergence
- modify estimates of solution

- check for failed solution, indicating bad solution
- accumulate all solute mass balance components.

This sequence is repeated if both rainfall and surface evaporation occur on the same day. Because the solution is explicit (*i.e.* fixed coefficients requiring no iterations, there are theoretical restrictions on the size of time-steps given) we have fixed the depth nodes. These warnings are ignored in WAVES and, as a result, small negative values for solute concentration can occur with full solute transport but without a saline watertable. The presence of a watertable tends to smooth out fluxes, water contents, and sink terms, and provides a generally larger amount of solute that eliminates the negative values sometimes obtained.

3.5 Carbon Balance

3.5.1 Generalised Equations

The carbon balance is performed as part of calculation of evaporation and transpiration demand for a given day. These fluxes are calculated based on the soil conditions at the start of the day, and are not updated during the solution of the water flow equation. A portion of the energy balance, all of section 3.2.1, is first used to estimate the stresses on the vegetation, the carbon balance routine is called to calculate assimilation based on those stresses, and then evaporative demand is calculated using a conductance based on that assimilation rate. In this way a complete feedback between the atmosphere, soil and salt, and vegetation is made.

The WAVES plant growth model is a generic algorithm with rate-based equations and sound physical principles, however empiricism is used where appropriate. WAVES does not attempt to model discrete phenological growth stages, and does not fill grain in crops for a prediction of yield. WAVES further treats the plant as three buckets of carbon representing leaves, stems, and roots. Each of these is assumed to occupy the conceptual site fully. The leaves are evenly spread across each square metre, stem numbers are not determined but assumed to be again uniformly spread, and the roots totally explore the depths to which root carbon is allocated. This approach to plant growth modelling is a result of designing WAVES to be primarily a hydrological model

and leaf area index and root distribution are the primary variables interacting with the hydrologic cycle.

Gross Photosynthesis

The first step in growing our plant is to calculate the stresses on the plant. Within the transpiration subroutine the availability of water to the plant is calculated, in a similar way to (3.24).

$$\chi_w = \sum_{i=1}^{N} \frac{\left(1 - \frac{\psi_i + \eta \Pi_i}{\psi_{wilt}}\right) \Delta z_i}{z_{max}} \tag{3.81}$$

where χ_w is the relative availability of water, z_{max} is the depth of the deepest roots within the soil, and the sum is taken only over those depth nodes with roots present.

The osmotic potential due to salt is given by Metten (1966) as:

$$\Pi_i = 2 C_{s,i} R T_a \tag{3.82}$$

where $C_{s,i}$ is the molar concentration of salt at the depth *node i* (mol ℓ^{-1}) given by dividing $c_{s,i}$ (kg ℓ^{-1}) by the molar weight of salt in kilograms (0.0585 kg mol^{-1}), R is the universal gas constant (0.832 m ℓ K^{-1} mol^{-1}), and T_a is average daily temperature expressed in Kelvin. A factor of two appears because two ions contribute to osmotic potential, both Na^+ and Cl^-, and they are assumed to contribute equally.

Next the availability of light is calculated, along with the modifying effect of air temperature, thus:

$$\chi_l = \frac{R_n \, 4600}{2 \, DL \, L_{sat}} \tag{3.83}$$

$$\chi_t = exp[-\alpha_t (T_a - T_{opt})^2] \tag{3.84}$$

where R_n is the net radiation for the canopy of interest (kJ m^{-2} d^{-1}), 4600 is a units conversion factor, L_{sat} is the saturation light intensity (μmoles m^{-2} s^{-1}), the factor of two assumes that half of sunlight is photosynthetically active radiation, T_{opt} is the temperature at which maximum assimilation occurs, α_t is a factor so that $\chi_t = 0.5$ at the temperature when half of maximum assimilation occurs. The value of χ_ℓ is limited to lie between 0 and 1.

At this stage, the actual relative growth rate can be estimated using the integrated rate methodology of Wu *et al.* (1994) by:

$$g = \frac{1 + w_w + w_N}{\frac{1}{\chi_\ell \chi_t} + \frac{w_w}{\chi_w} + \frac{w_n}{\chi_N}} \tag{3.85}$$

where g is the actual relative growth rate, w_w is the weighting of water relative to light, w_N is the weighting of nutrients relative to light, and χ_N is the relative availability of nutrients. In WAVES full nutrient cycling and leaching calculations are not performed so χ_N is a constant set by the user.

Next gross production is calculated from Slavich *et al.* (1998):

$$A = A_{max} g(1 - exp(k\, LAI\,)) \frac{DL}{43200} \tag{3.86}$$

where A_{max} is the maximum production rate (kg C m^{-2} 12 hr^{-1}), and the scalar on the RHS is a correction for day lengths greater or less than 12 hours.

Respiration and Losses

There are two methods for estimating plant respiration. The first is to assume that it is some fixed or dynamic proportion of gross production (see, for example, Landsberg and Waring 1997), or to calculate it independently by invoking a rate equation based on the amount of material present; in WAVES we do the latter. The maintenance respiration loads for leaves, stems, and roots are calculated as follows:

$$L_{resp} = L_{rate}\, exp(0.085\, T_{min}) \left(1 - \frac{DL}{86400}\right) L_{car} \tag{3.87}$$

where L_{resp} is the dark respiration of the leaves (in units of kg C), L_{rate} is the leaf respiration rate (kg C kg C^{-1} d^{-1}), T_{min} is the minimum daily temperature, and L_{car} is the total amount of leaf carbon (kg C). The factor 0.085 in the exponential term doubles the respiration load for an 8 degree increase in temperature. This is termed dark respiration because the leaf is assumed to get all the sustenance it requires during the day as part of normal photosynthesis, and the maximum net production parameter A_{max} already accounts for this loss. This is also why the minimum

temperature, assumed to occur during the night, and the proportion of the day that is night is used in the calculation.

$$S_{resp} = S_{rate}\, exp(\, 0.085\, T_a\,)\, S_{car} \tag{3.88}$$

$$R_{resp} = R_{rate}\, exp(0.085 T_a\,)\, R_{car} \tag{3.89}$$

where S_{rate} is the stem respiration rate (kg C kg C^{-1} d^{-1}), S_{car} is the total amount of stem carbon (kg C, which may be zero if the plant has no woody stem), R_{rate} is the root respiration rate (kg C kg C^{-1} d^{-1}), and R_{car} is the total amount of root carbon (kg C). For all intents and purposes L_{resp}, S_{resp}, and R_{resp} are unknown, and are empirical fitting parameters.

Leaves and roots are subject to turnover also, where a fixed proportion of the carbon is lost each day, thus:

$$L_{loss} = M_{rate}\, L_{car} \tag{3.90}$$

$$R_{loss} = M_{rate}\, R_{car} \tag{3.91}$$

where M_{rate} is the mortality rate of leaves and roots, or fraction lost each day (d^{-1}).

Dynamic Partitioning

The losses in (3.87) to (3.91) are reconciled against the gross production after that production is partitioned to the available carbon pools. This is done on the basis of determining first how much is assigned to above-ground and below-ground. This is dictated by water availability and a maximum partitioning factor:

$$L_f = S_f = 0.1 + \beta\, \chi_w \tag{3.92}$$

$$R_f = 1 - L_f - S_f \tag{3.93}$$

where L_f is the fraction of production partitioned to leaves, S_f is the fraction of production partitioned to stems, β is the partitioning factor (between 0 and 0.4), and R_f is the fraction of production partitioned to roots. This model suggests that when water is not easily available, *i.e.* a low value of χ_w, more resources are placed below ground to find water, and when water is plentiful resources are put into growing canopy and above ground structures.

Now an updated value of the three carbon pools can be calculated by:

$$L_{car}^{new} = L_{car} + 0.65 L_f A - L_{resp} - L_{loss} \tag{3.94}$$

$$S_{car}^{new} = S_{car} + 0.65 S_f A - S_{resp} \tag{3.95}$$

$$R_{car}^{new} = R_{car} + 0.65 R_f A - R_{resp} - R_{loss} \tag{3.96}$$

where the 0.65 factor is a fixing efficiency of assimilate to actual material.

There are certain limits placed on the accumulation of carbon pools relative to one another, and in total. Leaf carbon will not be accumulated after 99% of light can be intercepted by the canopy, due to the marginal cost of maintaining extra leaf resources relative to the extra assimilation gained. If the plant has stems, then the stem carbon must be at least equal to the leaf carbon, to provide mechanical and hydraulic support to the leaf mass. Root carbon can only be accumulated to a maximum of twice the leaf carbon if no stems exist, and four times the leaf carbon if stems are present.

Considerations for Annual Vegetation

WAVES is simplistic with regard to perennial vegetation, so that when either leaf or root carbon is reduced to zero, the vegetation dies and does not regrow. Annual vegetation has a more predictable cycle of germination, growth, and death, and must be accounted for by the generic growth model. This is done by the addition of two parameters: the year-day of germination (1 to 365), and the lifespan of the plant in degree daylight hours.

WAVES must check for the day when the plant germinates, and initialise the leaf, stem, and root carbon pools. Annuals are assigned an amount of carbon such that the leaf area index is 0.1, a matching amount of carbon is given to stems (if they are present), and twice that amount to roots. The root carbon profile is assumed to be linear with depth at a density of 0.1 kg C m^{-3}.

On the day of germination, all resource availabilities are assumed to be at maximum for numerical purposes, and the counter for degree daylight hours is initialised to zero. The degree day hours are accumulated for each growing day by multiplying the average of maximum and minimum daily temperature by the number of sunlit hours in the day, with a minimum of 1 degree day hour for any one-day time-step. After an annual has been growing for its full lifetime, all production rates are assumed to be zero, and the respiration load is multiplied by 20 to cause the carbon pools to senesce. This last process representation is totally arbitrary, but avoids introducing extra parameters to better describe this part of the life cycle.

Estimates of yield can be made from knowledge of above-ground biomass and actual and potential transpiration, based on empirical curves (Charles-Edwards 1982). The simplest equation uses the Harvest Index:

$$Y = HI \cdot DM \tag{3.97}$$

where Y is grain yield (kg m^{-2}), HI is the harvest index, and DM is the total above ground dry matter produced (kg m^{-2}, in WAVES this is $2 \times L_{car}$). Values of HI can be found in literature, and commonly range from 0.2 to 0.5. Alternative yield estimates can be made by adding knowledge of transpiration (de Wit 1958), thus:

$$Y = Y_{max} m \cdot \frac{ET_{act}}{ET_{pot}} \tag{3.98}$$

where Y_{max} is maximum grain yield, m is an empirical constant, ET_{act} is actual transpiration (m), and ET_{pot} is average potential transpiration rate over the growing season (m). Within WAVES, the values of ET_{act} and ET_{pot} are stored and can be used for these calculations with a user-specified Y_{max} and m parameter.

Litter and Grazing

WAVES keeps track of a fourth carbon pool for ground litter. The effects of litter have already been described, for example in equation (3.15) for surface resistance to evaporation. The above-ground loss term in (3.90) is added to the ground litter pool, and is allowed to decompose over time. The decomposition rate is an empirical function of temperature and moisture at the soil surface:

$$d_\ell = \frac{\Theta_0 \chi_t}{10} \tag{3.99}$$

where d_ℓ is the proportion of litter decomposed, Θ_0 is the relative water content at the surface (0 is air-dry, and 1 is saturated), and the factor 10 indicates that 10% of the total litter may decompose each day under optimal rotting conditions.

Grazing can be imposed if plants are to be grown. Grazing pressure is indicated by specifying the number of stock equivalents (ewe and lamb pairs) per hectare, and the year-day that they are let on, and taken off. Each stock equivalent is assumed to consume 0.5 kg C d^{-1} ha^{-1}, and this amount is removed from the overstorey, understorey, and litter carbon pools in proportion to their sizes.

3.5.2 Root Growth

Roots are growth by a chaotic algorithm, with three very simple rules. The root zone is broken into the same node spacings as for the soil water dynamics modelling with Richards' equation (see section 3.3 *Water Balance*) and root carbon is assigned to each node. This root activity is assumed to occur in the region half-way to the next node up, and half-way to the next node down. Because of this, no root carbon is assigned to either the surface node at 0 m, or the bottom most node, at the base of the soil column.

The rules that cover root growth are as follows. Firstly, we must maintain a connected root system to the deepest node with roots; any net root carbon growth must first satisfy this need. Secondly, root growth occurs where there is the most water and oxygen available and an existing root mass. This is determined by a method similar to (3.81), thus:

$$FAV_i = \left(1 - \frac{\psi_i + \eta\Pi_i}{\psi_{wilt}}\right)\left(1 - \frac{z_i}{z_{max}}\right)\frac{R_{ci}}{R_{car}} \qquad (3.100)$$

where FAV_i is the favourability for root growth at *node i*, z_i is the depth of *node i*, and R_{ci} is the amount of root carbon at *node i*. The first term of the RHS represents the water availability, taking salt into account, the second term represents oxygen availability, *i.e*. the deeper below the ground the less oxygen diffuses down there, and the final term means that a greater investment will be made where roots already exist. The value of (3.100) is calculated at each node, summed, made into a relative value, and carbon is assigned to nodes on the basis of the favourability as a proportion of the root carbon to be assigned.

The final rule for root growth is that the plant wants to explore new areas. In practice, if the deepest roots are shallower than the maximum rooting depth of the plant, then the favourability of the next node is calculated as available for assignment of carbon.

The other housekeeping issues involved are (1) to maintain a maximum level of root carbon accumulation, (2) that root carbon respiration is subtracted on the basis of the proportion of total root carbon at each depth node, and (3) that roots will not grow in saturated soil.

3.5.3 Computational Flow

The sequence of steps to run a single day time-step is as follows:

(General Plant Growth)

- gather availability of water and root growth favourability from other routines
- calculate availability of light and modifying effect of temperature

- determine maximum allowable carbon accumulation levels
- calculate growth rate and gross assimilation
- check status of annual plants

  IF GERMINATION

  - set growth rate and assimilation to maximum
  - assign minimum carbon to plant carbon pools
  - distribute roots down soil profile

  ELSE

  - accumulate degree day hours of growing season
- calculate respiration loads

  IF PLANT IS SENESCING

  - set growth rate and assimilation to zero
  - increase respiration loads by factor of 20
- calculate dynamic allocation amounts
- calculate carbon pool mortality amounts
- update carbon pools for assimilation, respiration, and mortality
- update litter pool for leaf drop
- check status of grazing
  - calculate amount of carbon grazed
  - reduce leaf carbon and litter pools

(Dynamic Root Growth)

- gather favourability index and carbon allocation and respiration from other routines
- calculate distribution of potential losses due to respiration or saturated soil
- calculate distribution of potential growth according to general favourability
- update root carbon for all losses
- update root carbon at each depth to maintain minimum root carbon for connected root system
- update root carbon from remaining assimilation
- recalculate relative amount of carbon at each depth node.

CHAPTER 4. SENSITIVITY ANALYSIS AND TESTING

L. Zhang, W. R. Dawes, T. J. Hatton,
and P. Dyce

4.1 Introduction

WAVES is a complex process-based model and it attempts to represent the key processes with a fair degree of physical fidelity. As a result, a sensitivity analysis of all inputs over their potential range and complexity is not feasible. Thus we take a more pragmatic and constrained approach to model sensitivity analysis in this study. We are aided in setting constraints by the physical nature of the parameterisation. Further, with an understanding of model structure and the underlying physics and physiology, it is possible to identify *a priori* a set of key parameters to which the model is most sensitive. This section presents such an analysis and discussion of the behaviour of the WAVES model to perturbation of selected set of input parameters.

4.2 Site Description and Data Collection

The sensitivity analysis was conducted using data from an experimental area in a 109-ha mixed cropping catchment named ‘Tambea’, at Wagga Wagga, N.S.W. (35°10' S and 147°18' E). In the 1992 and 1993 seasons, the crops sown were canola, oats and wheat. The soils of the experimental area formed on granite parent material. The dominant soil type, Red Earth (haplic eutrophic red kandasol), comprises weakly structured clay loam to light clay, red in colour and free of stone and coarse sand. The upper slopes and low rounded crests have *in situ* red podzolics (haplic mesotrophic red chromosol) which grade into weathered granite at less than 1 m. On the main drainage line, the soils are formed of colluvium overlying a clay that appears to have developed *in situ* on the granite.

Various data relating to climate, soil water content, and plant growth were collected over two winter growing seasons from June 1992 to January 1994, separated by fallow. The growing season and fallow period from June 1992 to June 1993 was used to calibrate the free parameters. The subsequent growing season until January 1994 was used as a validation period, where no parameters were changed, only water balance and plant growth estimates examined.

One year is a short time to calibrate a complex physical model. However, at this latitude there is a large variation in the climatic inputs over a year. Given that the annual crops grew in winter with an abundance of resources, we needed only to fit four critical plant growth parameters. During the summer months when the area was fallow, we could fit the soil moisture profiles with a single parameter without the need to fit plant growth in parallel. The results presented in Section 4 will show that the calibration obtained from the first year produced good results in the second year.

Soil hydraulic properties

Soil hydraulic conductivity was estimated at various depths using a well permeameter, or Gleuph type infiltrometer, at 12 sites in the catchment that included the three main soil groups. Total soil depth was estimated from the depth at which conductivity reduced to near zero. Saturated and air-dry volumetric water contents were estimated from the range of water contents reported from the soil moisture monitoring, and from soil descriptions reported in Forrest *et al.* (1985). Values of the capillary length scale, l_C, and the soil structure parameter, C, were estimated from moisture characteristics reported by Forrest *et al.* (1985) and soil texture and structure descriptions from Fogarty (1992). Hydraulic conductivity was adjusted downwards during calibration to match observed soil moisture profiles.

Climatic data

Climatic data collected on site at Tambea was measured with an automatic weather station. Wet and dry bulb temperatures were measured using temperature sensors with a standard muslin and wick changed fortnightly. A Rimik tipping bucket rain gauge recorded rainfall amount and intensity. A three cup anemometer with 64mm diameter cups mounted 2m above ground level was used to record windrun. Radiation sensors with a spectrum response < –3dB from 500 to 1000 nm were used to record total global radiation and reflected solar radiation. Additional climatic data was collected at ‘Shanagh’, approximately 1 km northeast of ‘Tambea’, with a similar range of sensors.

Soil moisture measurement

During the period 1992 to 1993, soil moisture contents were measured fortnightly at 11 sites across the area using a modified Tektronix Time Domain Reflectometry (PYELAB TDR SYSTEM) and CSIRO Software. Probes were inserted horizontally at up to five depths below the surface; due to considerations of the experimental budget, placing more probes at regular depths was not done. Individual calibrated probes were read manually in the field every 2 to 4 weeks, and stored traces were reanalyzed and compared with volumetric soil moisture estimates to check the accuracy of the measurements.

Leaf area index

The leaf area index (LAI) was measured on monthly intervals throughout the growing season. In each of the paddocks at Tambea, three randomly placed 1-m^2 quadrats were clipped to ground level. The one-sided green leaf area was measured using an electronic planimeter. The leaf areas for each of the three quadrats was averaged to give a single value for each paddock. Frequent checking, and if necessary, fine adjustment of the planimeter was carried out using known standards to maintain accuracy to at least 5%.

Total evaporation

Poss *et al*. (1995) made measurements of evaporation using lysimeters in an adjacent catchment. Data from June 1992 to December 1993 was collected at 1- to 4-week intervals; a total of 23 data points. The total evaporation modelled by WAVES was aggregated over the same periods, averaged for the number of days in each measurement period and compared directly.

Streamflow measurement

Total catchment runoff was measured using a modified V-notch weir. Flow heights were measured at two stilling wells using 'Wesdata' capacitance probes and 390 series data loggers. A low flow rate calibration curve was derived by measurements taken using a 'Hydrological Services' OSS PC1 current meter. Due to the extremely small amount of runoff and stream flow, only low flows occurred, and were recorded, during the simulated period.

4.3 Method

The model was first calibrated for Site D, over a period of 15 months (27 April 1992 to June 1994). Model inputs were adjusted to achieve the best agreement between predicted and measured LAI for the wheat crop. The parameters adjusted were: plant maximum assimilation of carbon; the IRM weightings of water and nutrients relative to light, and the plant respiration coefficients. We recognised that resultant parameter set is not unique but it does present a plausible model of wheat growth for the Tambea catchment. This calibrated base set of parameters was used to test the sensitivity WAVES in this analysis. These parameters are essentially those used in part by Dawes *et al*. (1997) in simulations of this catchment.

We recognise that with the use of this simulation alone it isn't possible to produce a completely comprehensive analysis of all variables, especially for other vegetation types and soils. The sensitivity analysis was conducted in a standard manner in which the model was run with the value of single parameter altered by plus and minus 10%, holding all other variables constant. The climatic inputs to the model were constant for all iterations.

The soil parameters were handled as a special case. As it often the case, the soil as described for Site D was modelled as a set of layers with distinct hydraulic properties. In those simulations testing the sensitivity of any one soil parameter, the values of that parameter were altered by the same amount in each layer throughout the profile. The rationale behind this scheme is purely pragmatic; model sensitivity to a change in a soil hydraulic parameter in any single, arbitrary layer will be chaotic with respect to the position this layer holds in relation to the rest of the profile.

4.4 Results and Discussion

The selected parameters were compared with a set of model outputs. These outputs were used as indicators of performance and are commonly used in comparing modelling scenarios. The outputs are: evaporation from vegetation (transpiration, E_v) and soil (E_s) to indicate changes in energy flux; deep drainage (DD) to indicate effect on the soil water balance; and maximum leaf area index for the growing season (LAI_{max}) to indicate effects on plant growth. The results are summarised in Table 4.1.

The calculated transpiration is sensitive to the maximum assimilation rate of carbon (A_{max}), the slope of the stomatal conductance model (g_1), canopy albedo (α_v), and the soil shape parameter (C). The actual assimilation rate of carbon is closely related to its maximum value; equation (21) shows that the canopy resistance is inversely proportional to the actual assimilation rate. As a result, changes associated with A_{max} affects canopy transpiration; g_1 influences transpiration in a similar way. The parameters A_{max} and g_1 are related to canopy resistance and the discussions are valid for canopies with similar aerodynamic characteristics (*e.g.* roughness length). Changes in canopy resistance caused by these parameters may have different degrees of effects on transpiration depending upon the roughness length of the canopy. The predicted value of transpiration is sensitive to the canopy resistance when the aerodynamic resistance is relatively small (*e.g.* tall crops and forests). At large values of the aerodynamic resistance (*e.g.* short crops and grass), and especially under non-water limited conditions such as were experienced in the two winter growing seasons, the transpiration is much less sensitive to the canopy resistance, and the partitioning of the available energy into sensible and latent heat fluxes is significantly controlled by the aerodynamic resistance. Increased α_v reduces the available energy reaching the canopy surface, hence decreases the transpiration. The shape parameter C, which is related to soil structure, affects transpiration significantly because of its effect on plant available water at a given potential. The next most sensitive parameters are leaf area index and the weightings for water and nutrients, which have reduced effects on canopy transpiration because of the nonlinearity of the relationships between the canopy resistance and these parameters.

Table 4.1. Summary of sensitivity analysis performed on site D for growing season 1992–93. E_v, E_s refer to transpiration from vegetation and evaporation from soil in mm, *Q* is the total drainage in mm, LAI_{max} is the maximum leaf area index. The columns labelled '%' refer to percentage changes from 'control' values. LBC refers to 'lower boundary condition' defined as fraction of saturated hydraulic conductivity. Other symbols are defined in Table 2.1.

Parameter	Change	E_v	$\%E_v$	E_s	$\%E_s$	Q	%Q	LAI_{max}	$\%LAI_{max}$
				Standard					
		196.3	----	406.0	----	30.6	----	3.2	----
α_S	+	198.4	+1.1	393.6	–3.0	30.8	+0.7	3.2	0.0
	–	193.8	–1.3	418.2	+3.0	30.3	–0.8	3.2	0.0
α_V	+	178.3	–9.2	418.9	+3.2	30.7	+0.3	2.9	–9.6
	–	210.0	+7.0	396.4	–2.3	30.5	–0.3	3.5	+9.2
A_{max}	+	224.2	+14.2	378.2	–6.9	30.4	–0.5	4.2	+29.4
	–	159.7	–18.6	439.1	+8.1	30.7	+0.4	2.4	–24.3
LAI	+	190.1	+5.8	423.7	–2.4	30.5	–0.5	3.5	----
	–	167.2	–7.0	445.2	+2.6	30.9	+0.4	2.9	----
K_e	+	196.7	+0.2	402.8	–0.8	30.6	0.0	3.1	–2.9
	–	194.9	–0.7	410.1	+1.0	30.6	0.0	3.3	+3.2
g_1	+	230.2	+17.3	402.7	–0.8	30.5	–0.2	3.2	0.0
	–	188.1	–4.2	409.8	+0.9	30.6	0.0	3.2	0.0
χ_H	+	206.4	+5.1	396.1	–2.4	30.5	–0.5	3.5	+9.9
	–	184.8	–5.8	416.9	+2.6	30.6	0.0	2.9	–9.6
χ_N	+	188.7	–3.8	413.2	+1.8	30.6	0.0	2.9	–6.2
	–	203.9	+3.8	398.6	–1.8	30.5	–0.5	3.4	+7.1
F_l	+	190.5	–3.0	411.9	+1.5	30.6	0.0	3.2	0.0
	–	202.9	+3.4	399.1	–1.7	30.6	0.0	3.2	0.0
LBC	+	196.3	0.0	405.9	0.0	33.4	+9.3	3.2	0.0
	–	196.3	0.0	405.9	0.0	27.7	–9.4	3.2	0.0
K_S	+	196.3	0.0	404.7	–0.3	34.2	+11.7	3.2	0.0
	–	196.2	0.0	407.4	+0.4	26.9	–11.7	3.2	0.0
θ_S	+	199.1	+1.5	417.1	+2.7	29.8	–2.5	3.2	0.0
	–	192.5	–1.9	394.8	–2.7	31.3	+2.4	3.2	0.0
θ_d	+	197.1	+0.4	401.8	–1.0	30.7	+0.3	3.2	0.0
	–	197.4	+0.5	410.1	+0.7	30.5	–0.5	3.2	0.0
λ_c	+	197.4	+0.5	408.7	–0.7	32.0	+4.7	3.2	0.0
	–	194.9	–0.7	403.3	+2.2	28.5	–6.8	3.2	0.0
C	+	178.2	–9.2	415.2	+2.2	29.5	–3.6	3.2	0.0
	–	196.1	–0.1	414.2	+2.0	31.7	+3.6	3.2	0.0

The predicted soil evaporation was relatively sensitive to A_{max}, which affects the soil evaporation indirectly through its effects on canopy transpiration and canopy development (*i.e.* soil shading). The soil hydraulic properties have little influence on the cumulative soil evaporation and this may have the implication that the uncertainties associated with the soil properties will not cause large errors in predicted soil evaporation from TOPOG_IRM. However, other factors such as the formulation of soil surface resistance (*e.g.* equation 2.56) may play a significant role in controlling the soil evaporation.

The total drainage was affected significantly by the lower boundary conditions and the saturated hydraulic conductivity. In WAVES, the lower boundary conditions are defined as a fraction of the saturated hydraulic conductivity ranging from free drainage, where the fraction is one, to no drainage, where the fraction is zero. The lower boundary conditions determine the amount of water potentially drained from the bottom of the soil layer. The results in Table 4.1 showed that a 10% change in either the lower boundary conditions or the saturated hydraulic conductivity could lead to an equivalent change in the total drainage. When the model is applied to study the effects of land-use management on groundwater recharge, these two parameters become critical.

Because of the nonlinear dependence of leaf area index and A_{max}, changes of 10% in the maximum assimilation rate produced changes in the maximum leaf area index of about 25%. The maximum leaf area index was also sensitive to α_v, and the weightings of water and nutrients.

4.5 Summary

The plant growth model in WAVES is particularly sensitive to the maximum assimilation rate, and under certain conditions, to the IRM weighting factors. The potential feedback, direct and indirect, on the surface water balance are significant. Of the soil parameters, conductivity appears to most drastically affect deep drainage. Although not demonstrated in this series of simulation, the other hydraulic parameters do have significant effect on the shape of the soil moisture profile. The conductivity of the lower boundary of the numerical soil water redistribution model was of paramount importance to the magnitude of deep drainage; the extreme sensitivity to this condition has serious implications to any soil water balance model predicated on a continuity equation for moisture redistribution.

4.6 Testing energy balance components

The following experiment was designed to test the energy balance component of WAVES under controlled conditions. The meteorological inputs have the following characteristics:

$R_{sd} = 312\ W/m^2$ (shortwave downward radiation)

$T_a = 20\ ^{\circ}C$ (average air temperature)

$e_a = 12.0\ hPa$ (average vapour pressure)

$K_s = 0.60$ (light extinction coefficient)

$L_1 = 3.0$ (leaf area index)

$\alpha_1 = 0.22$ (canopy albedo)

$\alpha_s = 0.22$ (surface albedo)

We assumed one vegetation layer plus one soil layer. The soil was loam with the total depth of 100 cm. For simplicity, precipitation, runoff and drainage were assumed to be zero and the simulation started with saturated soil moisture content throughout the soil profile. Therefore, the maximum annual evapotranspiration should equal to the total available water in the soil layer. In what follows, we will first calculate radiation budget and its partitioning between the vegetation canopy and the soil surface. Then we will show the simulated energy balance from WAVES for the vegetation and soil layers. This will provide a diagnostic check on the energy balance component of the model.

The radiation budget is calculated as:

$$e_a = 1.24(12/(273.15+20))^{1/7} = 0.79$$

$$R_{ld} = 0.79 * 5.6697 * 10^{-8} * (273.15 + 20.0)^4 = 330.0\,W/m^2$$

$$R_{lu} = 1.0 * 5.6697 * 10^{-8} * (273.15 + 20.0)^4 = 418.0\,W/m^2$$

For the vegetation layer

$$R_{sv1}\downarrow = 312(1 - exp(-0.60 * 3.0)) = 260.0 W/m^2$$

$$R_{sv1}\uparrow = 312 * 0.22(1 - exp(-0.60 * 3.0)) = 57.2 W/m^2$$

$$R_{lv1}\downarrow = 330.0(1 - exp(-0.66 * 3.0)) = 275.0 W/m^2$$

$$R_{lv1}\uparrow = 418(1 - exp(-0.6 * 3.0)) = 349.0 W/m^2$$

The net radiation for the vegetation layer is

$$R_{nv1} = 260 - 57 + 275 - 349 = 129.0\ W/m^2$$

For the soil layer

$$R_{sg}\downarrow = 312\,exp(-0.6*3.0) = 52\ W/m^2$$

$$R_{sg}\uparrow = 312*0.22\,exp(-0.6*3.0) = 11.0\ W/m^2$$

$$R_{lg}\downarrow = 330\,exp(-0.6*3.0) = 54.0\ W/m^2$$

$$R_{lg}\uparrow = 418\,exp(-0.6*3.0) = 69.0\ W/m^2$$

The net radiation for the soil layer is

$$R_{ng} = 52 - 1.0 + 54.0 - 69.0 = 26.0\ W/m^2$$

Therefore, the total net radiation received by the system (vegetation + soil) is

$$R_n = R_{nvl} + R_{ng} = 129.0 + 26.0 = 155\ W/m^2$$

The simulated net radiation from WAVES are 129.0 and 26.0 W/m^2 for the vegetation and soil layers respectively. It is clear that the radiation and its partitioning in WAVES is as expected. The energy balance components during the period of simulation are shown in Fig. 4.1. The total evapotranspiration was 315.9 mm, which is almost identical to the available water in the soil layer (*i.e*. 316.0 mm). Although this is not a complete test for the energy balance, it provided a diagnostic check on the energy balance and indicated that energy is neither created nor destroyed in the system.

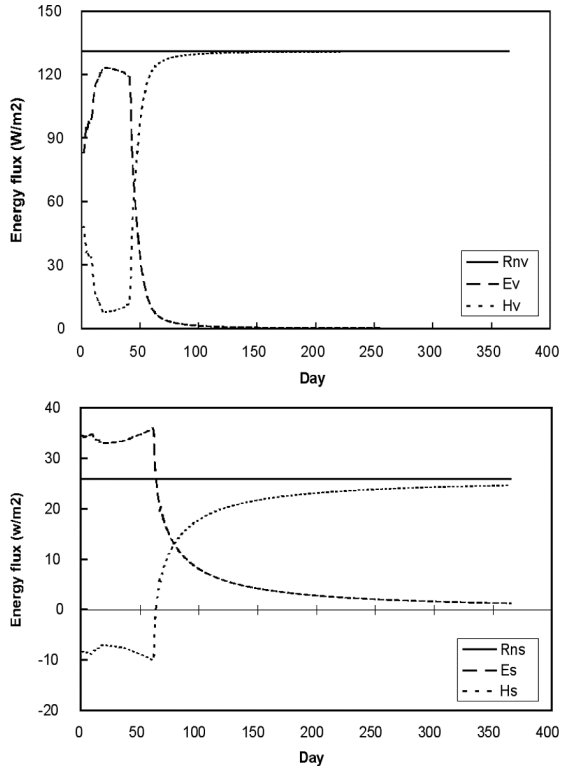

Fig. 4.1. Time course of net radiation, evapotranspiration, and sensible heat flux simulated by WAVES. R_n, E, H represent net radiation, evaporation, and sensible heat flux, respectively. Subscripts v and s represent vegetation canopy and soil.

4.7 Testing water balance component

A summary table is reported at the end of each simulation to ensure a perfect mass balance for water. In most cases, the model will achieve good mass balance. When errors occur in mass balance, users will be notified and should check their input files for possible errors. Following table is an example of mass balance for water. The results are obtained from a simulation using data from Griffith, NSW. It is clear that model achieved a perfect mass balance for water.

Table 4.2. Check for Mass Balance of Water

Initial Storage (mm)	505.50
Final Storage (mm)	407.81
Change in Storage (mm)	–97.69
Total Gross Rainfall (mm)	1500.00
Total Overstorey Interception (mm)	193.06
Total Understorey Interception (mm)	0.00
Total Net Rainfall (mm)	1306.94
Total Evaporation from soil (mm)	454.08
Total Overstorey Transpiration (mm)	986.20
Total Understorey Transpiration (mm)	0.00
Total Evapotranspiration (mm)	1440.29
Total Lateral Fluxes (mm)	0.00
Total Overland Flow (mm)	125.46
Total Deep Drainage (mm)	0.00
Total Flood Extra (mm)	0.00
Total Groundwater Extra (mm)	161.13
Total Groundwater Changes (mm)	0.00
Mass Balance Error (mm)	0.000000

4.8 Testing solute balance component

Similar to the mass balance for water, a summary table for solute is also reported at the end of each simulation when involving solute transport. The following summary table was obtained from WAVES simulation for lucerne grown in a lysimeter in Griffith, NSW. A nonsaline watertable (EC 0.1 dS m^{-1}) at 60 cm below the soil surface was established before sowing and was later dropped to 100 cm using the Mariotte tanks. When the lucerne fully established, a saline watertable was introduced (EC 16 dS m^{-1}) and maintained at 100 cm depth until the end of the experiment. It is clear that most of the solute came from the saline watertable as a result of upward flux of water and transpiration. Rain and irrigation water contributed a little to the total solute in the soil profile. It is obvious that WAVES obtained a perfect mass balance for solute.

Table 4.3. Check for Mass Balance of Solute

Initial Solute Mass (kg)	0.00
Final Solute Mass (kg)	3.10
Solute from Surface (kg)	0.08
Solute from Basement (kg)	3.02
Solute from Lateral Flows (kg)	0.00
Mass Balance Error (kg)	0.000000

4.9 Guaranteeing Numerical Convergence and Stability of Finite Difference Solutions of Richards' Equation

D. L. Short*, W. R. Dawes
CSIRO Land and Water, Canberra, Australian Capital Territory

I. White
Centre for Resource and Environmental Studies, ANU, Canberra, Australian Capital Territory

Abstract

Two distinctive features of the soil hydraulic model of *Broadbridge and White* (1988) permit guaranteeing *a priori* the numerical performance of finite difference solutions of Richards' soil-water flow equation, for a wide range of nonlinearity of soil hydraulic properties. Firstly, soil-water diffusivity remains (realistically) finite as soil becomes either very dry or 'saturated'. Thus solutions of the differential and finite difference equations remain determinate under all conditions. Secondly, hydraulic functions may be scaled across all soils described by the model, and finite difference solutions scaled in terms of space-step, time-step and transformed rainfall rate. The critically difficult case of constant-rate infiltration into semi-infinite dry soil permits numerical performance to be investigated comprehensively, using only a three-dimensional parameter space. A particularly efficient numerical scheme is identified. Scaled solutions for cases of coarse fixed space-time mesh correspond closely to analytical solutions, without propagation of short-time errors, for both semi-infinite and finite depth soils. Criteria are developed for guaranteed numerical convergence and stability, for Crank–Nicolson and backward difference schemes. Scaling and determinacy are proposed for comprehensively testing alternative numerical schemes.

---

* Now an independent scientific consultant.

4.9.1 Introduction

Because of advances in numerical techniques, numerical solutions of the soil-water flow equation of *Richards* (1931) are now available for a wide range of practical situations (e.g. *Brutsaert*, 1971; *Ross*, 1990). However, general use of numerical solutions is restricted by our inability to robustly predict numerical convergence and stability.

There appear to be no reports of making such predictions *a priori* for arbitrary space and time steps and rainfall rates, for a wide range of soil hydraulic properties. Sometimes it is stated that convergence and stability can be 'guaranteed' (e.g. *Celia et al.*, 1990; *Li*, 1993). However, these guarantees are not *a priori* in that time-steps are controlled dynamically, and space steps appear to be based on knowledge of a limited range of soil hydraulic properties and boundary conditions.

For linear convective-diffusive equations (CDE), criteria for numerical stability are readily derived (e.g. *Noye*, 1990) by scaling four parameters, space-step, time-step, velocity and diffusion coefficient, in terms of two free parameters, the dimensionless Courant and Péclet numbers. Some performance criteria may be derived theoretically, and any criteria may be derived experimentally by searching the two-dimensional space comprising the ranges of these parameters. The nonlinearity of the CDE reported by *Richards* (1931) necessarily requires scaling in terms of at least three parameters, and comprehensively searching a space with corresponding dimensions.

There are two requirements for providing *a priori* guarantees of numerical performance for a nonlinear CDE. Firstly, the equation must be scalable in terms of a small number of parameters, so that it is practical to search the entire parameter space. Secondly, the properties of the nonlinear functions must allow the solution of the differential and finite difference equations to be determinate under all initial and boundary conditions.

With most soil hydraulic models, solutions must be represented in terms of numerous parameters: space-step, time-step, various soil hydraulic parameters and rainfall. The dimensionality of the parameter space may be reduced to three, using the soil hydraulic model (BW) of *Broadbridge and White* (1988). They pointed out that their model permitted scaling of soil hydraulic functions, Richards' equation, and initial and boundary conditions for rainfall infiltration, in terms of linear transformations of space, time and rainfall rate. Thus solutions could be scaled in terms of three parameters across all soils represented by the model. Another feature of this model is incorporation of *Fujita's* (1952) diffusivity function, which ensures that diffusivity remains finite as soil becomes very dry. This ensures that solutions of Richards' equation remain physically meaningful and determinate under all unsaturated conditions.

The BW soil hydraulic model has five parameters, each field measurable and having physical meaning. Four of these are related linear scaling factors, and the fifth embodies the nonlinearity of the hydraulic properties. This model appears to span a wide range of the known behaviour of field soils, ranging from highly to weakly nonlinear.

The range of nonlinearity of the BW soil model, combined with the ability to scale solutions in terms of three parameters, offers the prospect of guaranteed numerical performance in modelling a wide range of soils. We will demonstrate this using a particularly efficient numerical scheme, which can be readily incorporated into routine models of vertical soil-water dynamics. In the search for a suitable numerical scheme, a prime criterion is *Philip's* (1957a) principle of using exact global mass balance, which helps to constrain errors in approximate solutions, and also balances mass for simple water balance models having low accuracy requirements.

In this work we first discuss formulations of Richards' equation, then discuss requirements for determinacy of solutions. The BW soil model is examined and the range of analytical solutions (*Broadbridge and White*, 1988; *Broadbridge et al.*, 1988) is presented in a readily usable form. We present precise requirements for exact mass balance, and modify a particularly efficient mass-conserving numerical scheme investigated by *Ross* (1990). We compare analytical and numerical solutions for infiltration into extremely dry soil, using unusually large and fixed depth and time steps. For these conditions we develop criteria for guaranteed numerical convergence and stability.

4.9.2 Formulation of the flow equation

We restrict our attention to one-dimensional vertical soil-water flow, and assume that the soil is homogeneous, structurally stable, incompressible, isothermal and nonhysteretic. We will not consider here sources and sinks of water within the soil profile.

The term 'saturation' is somewhat misleading compared with 'satiation' (*Miller and Bresler*, 1977). For $\psi > 0$ some air is normally trapped within the soil pore space, so that even after the development of surface ponding or a watertable, θ increases slightly as ψ increases further.

Forms of the flow equation

The starting point in deriving the flow equation is conservation of mass for water flow in soil (*Gardner*, 1919):

$$\frac{\partial \theta}{\partial t} = -\frac{\partial q}{\partial z} \tag{4.1}$$

Nomenclature

z	depth below soil surface, +ve downwards [L]
t	time [T]
θ	volumetric soil-water content [$L^3\ L^{-3}$]
ψ	matric potential (pressure head) [L]
$K(\psi)$	hydraulic conductivity [$L\ T^{-1}$]
	soil-water diffusivity [$L^2\ T^{-1}$]
$D(\theta)$	$D = K\,\partial\psi/\partial\theta$
	D is also used in reference to linear CDEs
θ'	differential moisture capacity [L^{-1}] $\theta' = \partial\theta/\partial\psi$
K'	$\partial K/\partial\psi\ [T^{-1}]$
U	Kirchhoff transform, or matric flux potential [$L^2\ T^{-1}$] $U = \int_{-\infty}^{\psi} K\,d\psi = \int_{0}^{\theta} D\,d\theta$
q	soil-water flux in z-direction [$L^3\ L^{-2}\ T^{-1}$]
v	convective component of soil-water or solute flux [$L\ T^{-1}$]
P_e	Péclet number [dimensionless] $P_e = v\,\Delta z / D$
C_o	Courant number [dimensionless] $C_o = v\,\Delta t / \Delta z$

Subscripts and superscripts:

b	backward difference
f	forward difference
c	central difference
i	initial value
j	beginning of time-step for numerical solution
$j + 1$	end of time-step
0	soil surface
m	lower boundary
$*$	dimensionless form of variable, except that Θ is used for the dimensionless form of θ
$\ddagger$	form of variable with soil-independent scaling (see section 4.9.4)
s	the point at which soil becomes ‘saturated’, $\psi = 0$
r	residual moisture, using simplification $\theta \to \theta_r$ as $\psi \to -\infty$

Gardner derived a flow equation by substituting into (4.1) an expression for q developed for an 'ideal' soil. *Gardner* (1920) and *Gardner and Widtsoe* (1921) also clarified the meaning of *Buckingham's* (1907) potentials (matric and total), giving Buckingham's expressions for q the meaning:

$$q = K\left(1 - \frac{\partial \psi}{\partial z}\right) = K - D\frac{\partial \theta}{\partial z} \tag{4.2}$$

Richards (1931) substituted the first form of (4.2) into (4.1) and used differential moisture capacity $\theta' = \partial\theta/\partial\psi$, to obtain (in one-dimensional form) the flow equations:

$$\frac{\partial \theta}{\partial t} = -\frac{\partial}{\partial z}\left(K - K\frac{\partial \psi}{\partial z}\right) \tag{4.3}$$

$$\theta'\frac{\partial \psi}{\partial t} = -\frac{\partial}{\partial z}\left(K - K\frac{\partial \psi}{\partial z}\right) \tag{4.4}$$

These equations have great generality for describing non-hysteretic flow in soils, as the only constraint on soil properties proposed by Richards was that the hydraulic function $\psi(\theta)$ should be strictly monotonic.

Richards used equation (4.4) with ψ as the sole dependent variable, to derive an analytical solution, but proposed that one was free to choose either θ or ψ as the dependent variable. Richards suggested that 'mathematical expediency' should be the criterion for choosing the dependent variable. In the case of θ, the flow equation is derived very simply by substituting the second form of (4.2) into (4.1), giving:

$$\frac{\partial \theta}{\partial t} = -\frac{\partial}{\partial z}\left(K - D\frac{\partial \theta}{\partial z}\right) \tag{4.5}$$

Equation (4.5) was used by *Childs and Collis-George* (1950) and solved numerically by *Klute* (1952). Equations (4.4) and (4.5) are both highly nonlinear, since K, θ' and D are normally highly nonlinear functions of ψ.

Brutsaert (1971) extended the freedom to choose formulations as proposed by Richards, by solving (4.3), which has mixed dependent variables, using a finite difference technique. The use of a mixture of dependent variables means also that there is no fundamental distinction between dependent variables and nonlinear soil hydraulic functions such as θ', K, and D. Brutsaert used coarse node spacings Δz and Δt for a fairly general case involving satiated and layered soils, and highly nonlinear soil properties.

Other forms of the flow equation have been investigated with a view to dealing with its nonlinearity. *Haverkamp et al.* (1977) formulated the equation with Kirchhoff transform U as the sole dependent variable, giving:

$$\frac{\theta'}{K}\frac{\partial U}{\partial t} = -\frac{\partial}{\partial z}\left(K - \frac{\partial U}{\partial z}\right) \tag{4.6}$$

This linearises the diffusive term of the nonlinear convective-diffusive equation. However, the time derivative and the convective term $-\partial K/\partial z$ in (4.6) remain highly nonlinear. In fact, lower numerical efficiency was found than when solving (4.4). Others, (e.g. *Redinger et. al.*, 1984; *Campbell*, 1985), have applied the transform (*Gardner*, 1958) to just the diffusive term of (4.3), so that it becomes:

$$\frac{\partial \theta}{\partial t} = -\frac{\partial}{\partial z}\left(K - \frac{\partial U}{\partial z}\right) \tag{4.7}$$

with linear diffusive term and temporal derivative. *Ross* (1990) and *Ross and Bristow* (1990), using a finite difference scheme, found that solving (4.7) increased computational speed by an order of magnitude over solving (4.3), for a test case, and more than a further order of magnitude over solving (4.4). However, linearising individual terms of the differential equation for soil-water flow in no way changes the non-linearity of the soil functions or the flow problem. Because of this, and the success of *Brutsaert* (1971) in solving (4.3), it cannot be assumed that (4.7) will yield greater numerical efficiency than (4.3) for all rainfalls and the forms of the functions used in all soil hydraulic models.

Formulation as a convective-diffusive equation (CDE)

CDEs are generally used to model transport of solutes moving with liquids. For one-dimensional flows the form is:

$$\frac{\partial C}{\partial t} = -\frac{\partial}{\partial z}\left(vC - D\frac{\partial C}{\partial z}\right) \tag{4.8}$$

where C is solute concentration and v fluid velocity. Equation (4.5) has this form with: θ interpreted as concentration of water in the soil by volume, diffusivity interpreted in the usual way, and velocity v interpreted as K/θ.

Recognising that residual soil-water ($\psi \to -\infty$) is immobile, an appropriate refinement is the definition $v = K / (\theta - \theta_r)$. This has two advantages. Firstly, the increase in velocity makes claims

later in this work conservative, regarding dominance of diffusion over convection in soil-water flows. Secondly, this definition is consistent with use of the dimensionless forms of K and θ, *viz.* K^* and Θ, defined in Table 4.4 and used in various soil hydraulic models. The dimensionless Péclet and Courant numbers, P_e and C_o, have been used widely to investigate the performance of numerical schemes for solving linear CDEs; the definitions are given earlier. *Noye* (1990) discussed various finite difference representations of a linear CDE, having four parameters: v, D, Δz and Δt. The equations were scaled in terms of two independent parameters using C_o and a dimensionless diffusion number, with P_e implicit. Numerical stability was unconditional for $C_o = 1$ and $P_e = 2$ for a range of difference schemes. The parameter C_o is the magnitude of v relative to the length and time scales Δz and Δt, with values >> 1 requiring specialised numerical techniques. P_e represents relative dominance of convective components of flux over diffusive components relative to the length scale.

For soils and with dimensionless variables, which do not affect the meanings of these numbers (see Table 4.4), the definitions earlier yield:

$$P_e = \frac{1}{\Theta}\frac{\Delta\Theta}{\Delta\psi^*}\Delta z^* \tag{4.9}$$

$$C_o = \frac{K^*}{\Theta}\frac{\Delta t^*}{\Delta z^*} \tag{4.10}$$

It should be noted that effectively using a dimensionless form of (4.5) to formulate P_e and C_o does not constrain the choice of form of Richards' equation for numerical solution.

Recent studies (*El-Kadi and Ling*, 1993; *Huang et al.*, 1994) have considered P_e and C_o, at least implicitly, in studying numerical solutions of the nonlinear CDE for soil-water flow. It was assumed that at each point in space and time, P_e and C_o criteria based on local soil-water content could be developed for infiltration into semi-infinite soil profiles. In the special case of a region with relatively uniform θ-values, criteria developed for linear CDEs could be expected to apply directly.

We disagree with the last mentioned authors regarding the form of Richards' equation that may be interpreted as a CDE. *El-Kadi and Ling* (1993) transformed (4.6) into a CDE with dependent variable U. Convective term v was defined using the incorrect assumption $\partial/\partial z\ (vU) = v\ \partial U/\partial z$. It appears that Richards' equation cannot be formulated consistently as a mathematical CDE in U. Perhaps more importantly, it is inappropriate to formulate P_e and C_o using mathematical convection and diffusion of an intensive (intensity or potential) variable such as U (*El-Kadi and Ling*, 1993) or ψ (*Huang et al.*, 1994), rather than extensive (content) variables like θ or Θ. Specifi-

cally, intensive variables give no physical meaning to the concepts of convection and diffusion. Therefore they cannot yield direct insight into the relative roles of convection and diffusion of soil water content. Further, with such variables, we cannot meaningfully compare numerical performance criteria with those for linear CDEs.

Finally, we pose the question as to whether P_e and C_o values ever need to be high enough to cause numerical problems for rainfall infiltration, or other unconfined aquifer soil-water dynamics. For the traditionally difficult case of infiltration into extremely dry soil ($\psi \rightarrow -\infty$), we found essentially zero values of P_e and C_o as represented by the soil hydraulic models of *Campbell* (1974) and *Broadbridge and White* (1988). With these models, numerical infiltration should be extremely easy at the leading edge of the wetting front, as far as P_e and C_o values are concerned, as the problem is completely diffusion-dominated. This situation is to be expected for any soil model that is physically realistic for very dry conditions, because water movement is primarily in the vapour phase, for which convection due to gravity is irrelevant.

In the case of satiated soil, $K^* \cong \Theta \cong 1$, so that $C_o = \Delta t^* / \Delta z^*$, permitting large node spacings. Further $\partial\Theta / \partial\psi^* \cong 0$, so $P_e \cong 0$; again the problem is nearly completely diffusion dominated if the soil hydraulic model is physically realistic. In this case Richards' equation approximates a linear CDE, so that numerical convergence and stability are obtained very easily. For intermediate soil-water contents, *Philip* (1993) justified the assumption of diffusion-dominated flow in deriving an approximate solution.

4.9.3 Determinacy of solutions of the flow equation

Performance of numerical solution techniques cannot be guaranteed unless solutions of both the differential and finite difference equations are always determinate, that is, exact and unique solutions must exist under all conditions. Further, the finite difference equations must be solvable using practical techniques. In part, these requirements impose constraints on the forms of the soil hydraulic functions. We will examine the adequacy of *Richards'* (1931) constraint that $\psi(\theta)$ is strictly monotonic.

Existence of solutions in very dry soil

Philip (1957b) recognised that vapour diffusion makes D finite in extremely dry soil, but proposed the simplification that $D = K\partial\psi/\partial\theta \rightarrow 0$ as $\psi \rightarrow -\infty$, in developing quasi-analytical solutions. *Philip* (1992) and *Philip and Knight* (1991) obtained analytical solutions using the same simplification for cases where $D(\theta)$ and $\partial K/\partial\theta$ were represented by power law functions. Exact solutions of the flow equation exist for $D = 0$ with arbitrary 'well behaved' soil functions, for

prescribed flux boundary conditions. Zero D makes gradients $\partial\theta/\partial z, \partial\theta/\partial t$, $\partial D/\partial z$, etc, infinite. The solution has these physically implausible properties at the soil surface, for an infinitesimal value of *t*, and over an infinitesimal region at the leading edge of the wetting front for all finite *t*.

Because these singular regions are infinitesimal, analytical solutions are determinate, but problems arise in finding numerical solutions. Firstly, solutions of the finite difference equations do not exist, in general, if the initial estimate of Θ is zero at any space node. Numerical difficulty must be expected when this condition is approached closely. Secondly, it is impractical to change the modelled region continually to avoid dry regions. Thirdly, if strategies are devised to obtain solutions for specific numerical schemes, no finite degree of reduction of depth node spacing Δz can cause numerical solutions to converge toward exact solutions. Finally, the infinite gradients in the singular regions will be approximated in finite difference solutions by very large gradients. These, combined with finite fluxes, may cause the numerical problems normally associated with convection-dominated flows.

Richards' (1931) requirement, that $\psi(\theta)$ should be strictly monotonic, is sufficient to prevent $\partial\psi/\partial\theta$ from becoming infinite at finite values of ψ. This is physically reasonable, and assures non-zero values of $\partial\theta/\partial\psi$ as required, for example, by Newton–Raphson numerical solution schemes (see section 4.9.6). However, for numerical schemes a weak additional constraint should be imposed on *K* or *D*, so that $D = K\partial\psi/\partial\theta$ remains finite; this requirement is met by the hydraulic model of *Broadbridge and White* (1988).

Widely used soil models such as those of *Campbell* (1974) and *van Genuchten* (1980) do not meet this requirement. For water balance modelling purposes the formulation of *D* in dry soils is irrelevant, as the quantities of water that may be distributed inaccurately by a solution are very small. However, numerical models require strategies for coping with zero *D*, otherwise numerical performance cannot be guaranteed.

Uniqueness of solutions in satiated soils

In satiated soils, *Richards'* (1931) requirement of strictly monotonic $\psi(\theta)$ yields unique solutions. This is because $\partial\theta/\partial\psi$ remains non-zero, in keeping with air entrapment and compression in 'saturated' soils. This ensures that *D* remains finite, regardless of whether $\partial K/\partial\psi$ is assumed to be small, or zero in accordance with common practice. A unique exact solution of (4.5) therefore exists.

Most soil hydraulic models set $\partial\theta/\partial\psi = 0$ in the satiated range of ψ. This range may be $\psi = 0$, or $\psi = \psi_a$, where ψ_a (negative) is the 'air-entry' potential. A moisture characteristic, $\psi(\theta)$, for the

latter case is shown in Fig. 4.2, for the soil model of *Campbell* (1974). For this model $\partial\theta/\partial\psi = 0$ in the satiated range makes D infinite. A very high D does not pose numerical problems, but infinite D makes the solution indeterminate, and numerical problems may arise. These problems may be overcome by extending $\psi(\theta)$ monotonically through the satiated range. This is very simple for the model of *Broadbridge and White* (1988), as $\partial\theta/\partial\psi$ is finite at $\psi = 0$. This condition does not hold for most other models, so that additional parameters may be needed.

The problem of determinacy in satiated soil has been partly addressed previously. It has been recognised (e.g. *Philip* 1958; *Haverkamp et al.*, 1977) that the usual practice of setting $\partial\theta/\partial\psi = 0$ in satiated soil makes the fluxes on the right hand side of (4.5) indeterminate. The proposed solution was to solve only (4.4). However, in (4.3) and (4.7) the fluxes are equally indeterminate with this assumption, although other workers (e.g. Brutsaert, 1971; *Ross and Bristow*, 1990) have solved these equations for satiated soil.

Nevertheless, the time course of solutions may be indeterminate. This can be illustrated by considering the redistribution of water in a soil profile with depth less than $-\psi_a$ and an impermeable lower boundary. When the whole system is satiated, the spatially uniform zero flux and the variation of ψ with depth are determinate. But because we also have $\partial\theta/\partial t = 0$, there is no way for a solution of the flow equation to determine actual values of ψ, or changes with time. In this situation the depth of the watertable ($\psi = 0$) may assume any value within the soil profile.

We investigated this case numerically for the Campbell soil model using the computer code provided by *Ross and Bristow* (P. J. Ross, personal communication, 1991). Fig. 4.3 shows simulated 'watertable' depth, expressed as $z/(-\psi_a)$, after one day's redistribution following a spatially uniform initial condition $\psi = \psi_a$. Each point represents a simulation with the soil profile discretised into the given number of depth nodes. The 'watertable' depth is chaotic, ranging over the whole soil depth. The gaps represent convergence failures, which are mostly associated with decimal values of Δz that have exact binary representations (e.g. 0.25). This is because, when the soil profile is full, the indeterminate problem posed by the differential equation, when using the Campbell soil model, requires solution of a mathematically singular matrix in the numerical scheme. Where the convergence occurred, computational round-off error obscured the singularity of the matrix.

This example was, of course, carefully chosen to demonstrate numerical failure. Two points must be stressed here. Firstly, this situation is likely to be encountered frequently by soil-water dynamics models used in a routine way; the soil profile or a soil layer will often be filled. Secondly, the overall numerical strategy of Ross and Bristow is very efficient, and indeterminacy arises from the properties of the soil hydraulic functions used.

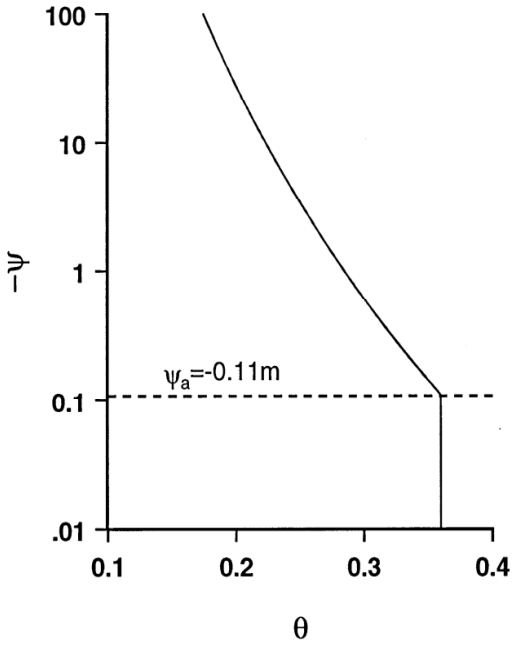

Fig. 4.2 : Example of a moisture characteristic, using the soil hydraulic model of Campbell (1974), showing $\partial\theta/\partial\psi=0$ for $\psi \geq \psi_a$, where ψ_a is the air-entry potential.

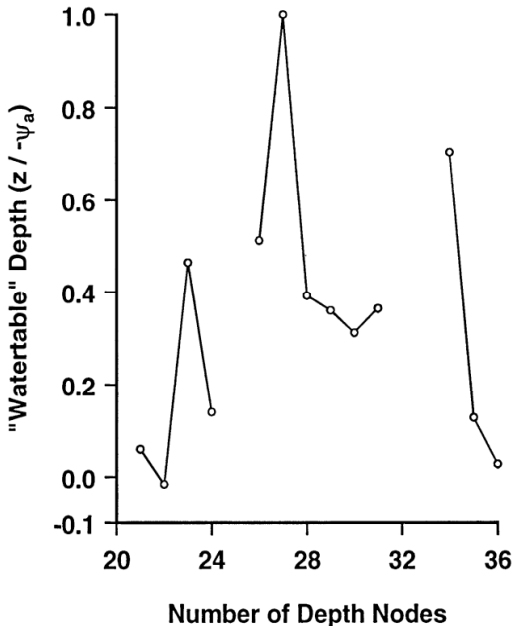

Fig. 4.3: Simulated watertable depths in 'tension-saturated' soil, plotted against the number of depth nodes into which a soil with depth $-\psi_a$ was discretised, using the Campbell soil hydraulic model. Gaps represent convergence failures.

There are precedents for adapting soil hydraulic models for finite $\partial\theta/\partial\psi$ in the satiated ψ-range. For example, *Paniconi et al.* (1991) used such a modification of the van Genuchten soil model, to prevent Richards' equation from becoming elliptical in multidimensional cases, and to overcome numerical problems found with two of the six numerical schemes they investigated for one-dimensional infiltration. We propose general use of this strategy, to permit guaranteeing numerical performance without imposing unnecessary constraints on the choice of numerical scheme.

4.9.4 Soil hydraulic model and analytical solutions

Broadbridge–White Soil Hydraulic Model

The model represents soil-water content up to the point of soil satiation (i.e. for $\psi \leq 0$). It encompasses a realistic range of moisture characteristics and $K(\psi)$, and is conceptually simple with physically identifiable parameters. There are five parameters:

θ_s volumetric soil-water content at satiation

θ_r residual soil-water content ($\psi \to -\infty$) we write $\Delta\theta = \theta_s - \theta_r$

K_s $K(\theta_s) = K(\psi_{=0})$, satiated hydraulic conductivity

$K_r = K(\theta_r)$, is normally assumed to be zero

λ_c macroscopic capillary length scale, a scaling length for space and soil moisture potential [L]

C a soil structure parameter, describing the degree of nonlinearity of the soil properties, and related to the slope of $\psi(\theta)$ as $\theta \to \theta_s$. As $C \to \infty$ the soil is weakly nonlinear, as $C \to 1$ the soil is highly nonlinear.

The first four parameters can be measured in the field or laboratory (*White and Broadbridge*, 1988). The parameter λ_c arises in many different contexts in soil-water flow (see e.g. *Raats and Gardner*, 1971; *White and Sully*, 1987). It is inversely proportional to a flow-weighted mean pore size and is also related to the matric flux potential, *U*. It is an appropriate scaling quantity for matric potential and for distance. The parameter *C* is related to the slope of the moisture characteristic at satiation. That is, it is related to the size distribution of the larger pores. The parameters θ_s, θ_r, K_s and λ_c are factors used to scale the fundamental variables θ, ψ, K into dimensionless variables Θ, Ψ^*, K^*. This yields linear scaling of all other hydraulic variables, flux (e.g. rainfall rate), space and time. The dimensionless variables are given in Table 4.4, with their relation to familiar dimensioned parameters, and the corresponding functional dependence assumed by the model, where appropriate. As well, the non-dimensional flux and rainfall are also shown.

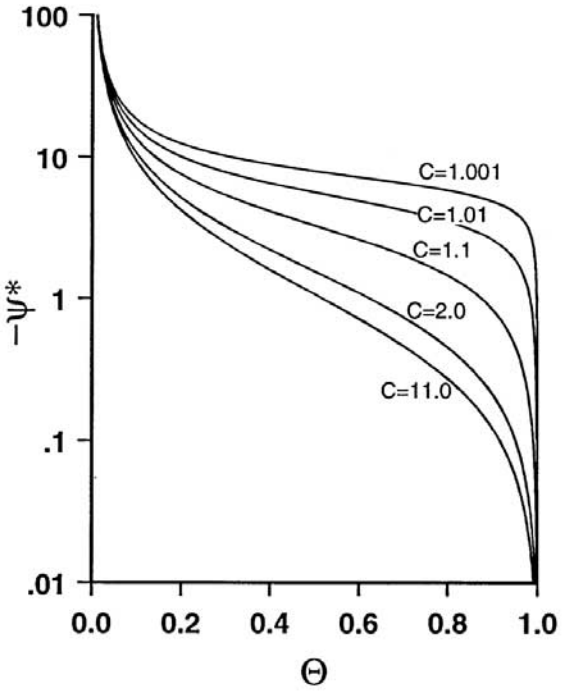

Fig. 4.4: Dimensionless moisture characteristics used in the BW soil hydraulic model, parameterized by the single soil parameter *C*.

Dimensionless functions assist in visualising the relationships between the hydraulic properties of all soils having the same nonlinearity. Dimensionless soil functions, and solutions of the flow equation, for a particular value of *C* are applicable to all soils with that value of *C* but possessing different K_s, λ_c, θ_s and θ_r. Fig. 4.4 shows dimensionless moisture characteristics, $\psi^*(\Theta)$, for selected values of *C*; the family of curves may be scaled to all soils represented by the model.

Table 4.4: Dimensionless variables for scaling BW soil hydraulic model

Scaling of Variable	Function
$\Theta = \frac{\theta - \theta_r}{\theta_s - \theta_r}$	
$\psi^* = \frac{\psi}{\lambda_c}$	$\psi^* = 1 - \frac{1}{\Theta} - \frac{1}{C} ln \frac{C - \Theta}{(C-1)\Theta}$
$K^* = \frac{K}{K_s}$	$K^* = \Theta^2 \frac{C-1}{C-\Theta}$
$D^* = \frac{D\, t_c}{\lambda_c^{\,2}}$	$D^* = \frac{C(C-1)}{(C-\Theta)^2}$
$U^* = \frac{U}{K_s\, \lambda_c}$	$U^* = \Theta \frac{C-1}{C-\Theta} = \frac{K^*}{\Theta}$
$\frac{\partial \Theta}{\partial \psi^*} = \frac{\partial \theta}{\partial \psi} \frac{\lambda_c}{\Delta \theta}$	$\frac{\partial \Theta}{\partial \psi^*} = \Theta^2 \frac{C-\Theta}{C}$
$\frac{\partial K^*}{\partial \psi^*} = \frac{\partial K}{\partial \psi} \frac{\lambda_c}{K_s}$	$\frac{\partial K}{\partial \psi^*} = \Theta^3 \frac{(C-1)(2C-\Theta)}{C(C-\Theta)}$
$t^* = \frac{t}{t_c}$	$t_c = \frac{\Delta\theta\, \lambda_c}{K_s}$
$z^* = \frac{z}{\lambda_c}$	
$R^* = \frac{R}{K_s}$	
$q^* = \frac{q}{K_s}$	
$v^* = \frac{v \Delta\theta}{K_s}$	$v^* = \frac{K^*}{\Theta} = U^*$
	$P_e = \frac{\Theta(C-\Theta)}{C} \Delta z^*$
	$C_o = \frac{\Theta(C-1)}{C-\Theta} \frac{\Delta t^*}{\Delta z^*} = U^* \frac{\Delta t^*}{\Delta z^*}$

Note that C is the only parameter in the model, and variables are functions of dimensionless water content Θ only. The functions are suitable for most practical modelling applications, providing reasonable approximations to known soil properties, along with a comprehensive range of non-linearity of soil behaviour.

To assist in relating the model to actual soils, we consider surface soils having two values of the soil structure parameter, C = 1.02 and C = 1.5. These values correspond to approximately the range found in the field (White and Broadbridge, 1988). The first soil is a rather unstructured sand, with highly nonlinear moisture characteristic: C = 1.02, θ_s = 0.4, θ_r = 0.05, K_s = 2.0 m d^{-1}, λ_c = 0.3 m, and $t_c = \lambda_c \Delta\theta / K_s$ = 0.052 d. The second, a structured surface soil, with weakly non-linear moisture characteristic, is represented by: C = 1.5, θ_s = 0.5, θ_r = 0.1, K_s = 1.0 m d^{-1}, λ_c = 0.1 m, and t_c = 0.04 d. A final example is a clay subsoil. Because of its fine texture, variability of soil particles yields a high value of the structure parameter, C = 2.0, in spite of the absence of macropores, and also a high length/potential scale parameter, λ_c = 2.0 m, and low hydraulic conductivity scale parameter, K_s = 0.01 m d^{-1}. With soil-water content scaled by θ_s = 0.4 and θ_r = 0.15, the time scale becomes t_c = 50 d.

Functional forms of P_e and C_o given in Table 4.4 were derived by substituting soil model functions into (4.9) and (4.10). $C_o \le \Theta \, \Delta t^*/\Delta z^*$ for all $\Theta \le 1$, so that the condition $C_o \le 1$ is always met if $\Delta z^* > \Delta t^*$. $P_e \le \Theta \, \Delta z^*$ for all $\Theta \le 1$, so that the condition $P_e \le 2$ is always met if $\Delta z^* \le 2$. Translating these criteria to dimensioned variables, we have $\Delta z \le 2 \, \lambda_c$ with $\Delta t \le 2 \, t_c$. Referring back to the three soil examples, we see that direct application of P_e and C_o criteria for linear CDEs to soil-water flows would permit unusually large node spacings, that is, Δz at least a large fraction of a metre with Δt over 1 hour, for numerical stability, even for the surface soils.

Numerical solutions remain determinate as $\Theta \to 0$, as D^* has the small but finite value $(C–1)/C$. As $\Theta \to 1$, D^* approaches the large but finite value $C/(C–1)$. To retain determinacy for $\psi \to 0$, it is necessary to extend $\Theta(\psi)$, $D(\psi)$ and $K(\psi)$ monotonically from $\psi = 0$. Two things follow from the BW soil model's feature that $\partial\theta/\partial\psi$ is finite for $\psi = 0$. It allows monotonicity to be achieved very simply, without modification within the model's original unsatiated range. However, it also makes monotonicity mandatory, because if $\partial\theta/\partial\psi = 0$ for $\psi > 0$, numerical convergence is normally unobtainable, whereas when $\partial\theta/\partial\psi = 0$ for $\psi > \psi_a$, convergence is obtained in many cases.

In this work, dimensionless numerical simulations will solve a dimensionless form of (4.7):

$$\frac{\partial \Theta}{\partial t^*} = -\frac{\partial}{\partial z^*}\left(K^* - \frac{\partial U^*}{\partial z^*} \right) \tag{4.11}$$

Scaling the soil model and flow equation across all soils

Broadbridge and White (1988) pointed out that further scaling of their model made variables and solutions of the flow equation independent of C, that is, scaling could be performed across all soils represented by the model. This is achieved by using Θ/C, $C\psi^*$ and $K^*/(4C(C-1))$, to transform soil-water content, potential and hydraulic conductivity, respectively, to 'universally scaled' variables, which we shall represent by the superscript '‡'.

Table 4.5 shows the universally scaled functions, variables and fluxes, analogous to Table 4.4. The functions, which represent all soils, involve no parameters. All the information in Table 4.4 is embodied here, however, apart from an arbitrary constant in the expression for $\psi^{\ddagger}$. To scale functions to a particular soil, we require the condition $\Theta^{\ddagger} = 1/C$, so that the model is still used only up to the point of satiation. For satiated cases, it is not feasible to scale across all soils, although the quasi-linearity of satiated soil hydraulics makes this case simple numerically.

Comparing the forms of P_e and C_o with those of Table 4.4, we see that for given dimensioned parameter values, these numbers are not changed by the further scaling. However since the form of P_e in Table 4.5 is independent of C, we can avoid the global inequality used earlier. Then the condition $P_e \le 2$ yields a less conservative upper limit for Δz, *viz.* $8\,\lambda_c/C$.

Table 4.5: Universal dimensionless variables for scaling BW soil hydraulic model

Universal Function	Universal Function
$\Theta^{\ddagger} = \dfrac{\Theta}{C}$	$\psi^{\ddagger} = \psi^* C$
$m = 4C(C-1)$	$K^{\ddagger} = \dfrac{K^*}{m}$
$D^{\ddagger} = D^* \dfrac{C^2}{m}$	$U^{\ddagger} = U^* \dfrac{C}{m}$
$\dfrac{\partial \Theta^{\ddagger}}{\partial \psi^{\ddagger}} = \dfrac{\partial \Theta}{\partial \psi^*} \dfrac{1}{C}$	$\dfrac{\partial K^{\ddagger}}{\partial \psi^{\ddagger}} = \dfrac{\partial K}{\partial \psi^*} \dfrac{1}{C\,m}$
$z^{\ddagger} = z^* C$	$\tau = t^* m$
$\rho = \dfrac{R^*}{m}$	$q^{\ddagger} = \dfrac{q^*}{m}$
$P_e^{\ddagger} = \Theta^{\ddagger}\left(1-\Theta^{\ddagger}\right)\Delta z^{\ddagger}$	$C_o^{\ddagger} = \dfrac{\Theta^{\ddagger}}{4\left(1-\Theta^{\ddagger}\right)} \dfrac{\Delta\tau}{\Delta z^{\ddagger}}$

The universally scaled hydraulic functions are even more powerful than those of the original form of the soil model, for expressing physical relationships between cases. They meet our requirement for a tool for comprehensively investigating and predicting numerical performance. In terms of the universally scaled variables, flow equation (4.7) becomes:

$$\frac{\partial \Theta^{\ddagger}}{\partial \tau} = -\frac{\partial}{\partial z^{\ddagger}}\left(K^{\ddagger} - \frac{\partial U^{\ddagger}}{\partial z^{\ddagger}} \right) \tag{4.12}$$

Analytical solutions

For comparison with numerical solutions we consider analytical solutions for constant vertical flux into semi-infinite and finite depth columns of uniform soil, with both zero and finite initial soil-water content, whose hydraulic properties are described by the BW model. The dimensionless analytical solutions corresponding to the original form of the soil model for constant flux infiltration up to the point of surface satiation are:

$$\frac{\Theta}{C} = 1 - \frac{1}{2\rho + 1 - (\partial u/\partial \zeta)/u} \tag{4.13}$$

$$C\, z^{*} = \rho(\rho + 1)\tau + (2\rho + 1)\zeta - \ln u \tag{4.14}$$

where u is a function of initial and boundary conditions and is given in Appendix B. It can be seen from the structure of (4.13) and (4.14) that these solutions may be transformed to universally scaled exact solutions of the flow equation, using the universally scaled variables Θ/C, Cz^{*} and ρ.

For a semi-infinite profile with zero initial soil-water content, u is a function of ζ, τ and ρ, which are space, time and rainfall variables resulting from transformations that linearise the flow equation (*Broadbridge and White*, 1988). For a finite-depth profile with zero initial soil-water content, $u = u(\zeta, \tau, \rho, C\, l^{*})$, where $l^{*} = l / \lambda_c$ is the dimensionless depth of the soil profile (*Broadbridge et al.*, 1988). For finite initial soil-water content Θ_i, in either semi-infinite or finite depth soils, u becomes a function of Θ_i also (*Broadbridge*, 1990). Expressions for u and $\partial u/\partial \zeta$ for these cases are presented in Appendix B. Numerical problems can be encountered in computing the analytical solutions. Precautions to ensure the accuracy of analytical solutions presented in this paper are explained in Appendix B.

Universal scaling does not depend on the existence of analytical solutions. The latter are used because of the soil model's considerable degree of realism (*White and Broadbridge*, 1988), and to illustrate the accuracy obtainable with universally scaled numerical solutions with large practical node spacing. Universal scaling may not depend on the particular functional forms of the BW soil

model. However, it is desirable for any future approach to universal scaling to ensure determinacy of solutions of Richards' equation, and to address the question of diffusion-dominance of soil-water flow.

4.9.5 Exact mass balance in finite difference solutions

The immediate aim of this work is to show that an approach to soil hydraulic modelling, which gives determinacy and scaling of solutions, achieves the completely predictable numerical performance required for routine use in practical models. Predictability could be demonstrated using any numerical scheme, using in particular, any form of the flow equation. However, we propose to demonstrate predictable performance using the numerical advantages of exactly mass-conserving schemes.

It must be stressed that all forms of the differential equation are analytically equivalent, and incorporate the mass conservation of (4.1), so that exact solutions must balance mass exactly. We are concerned here with retaining this feature in spite of the approximations involved in using finite difference solution techniques. We do not distinguish in this context between 'finite difference' and 'finite element' methods for devising the finite difference representation of the differential flow equation.

In practical modelling applications mass should be conserved accurately, even when there are low accuracy requirements for determining soil-water distribution. Further, for more demanding applications, exact global mass balance necessarily imposes constraints on errors. In particular, this constrains propagation of the substantial errors that necessarily occur shortly after infiltration begins, if using relatively large uniform Δz and Δt. Likewise, numerical instabilities are constrained.

Philip (1957a) proposed exact global mass balance to constrain errors in quasi-analytical solutions, using the divergence theorem of vector calculus. This theorem says that the surface integral of flux of into a region across its boundaries, equals the volume integral of the rate of increase in content over the region, provided that it contains no sources or sinks. Exact mass balance has been long used in finite difference solutions in fluid mechanics (see e.g. *Roache*, 1976), by generalising the divergence theorem to arbitrary finite space and time steps.

Exact mass balance has been reported also in finite difference solutions of Richards' equation or the related nonlinear diffusive equation for horizontal soil-water flow (see e.g. *Hornung and Messing*, 1981; *Ross*, 1990; *Celia et al.*, 1990). In these works two fundamental requirements are clear, (a) the flow equation must be a form using $\partial\theta/\partial t$ as the temporal derivative, for example, equations (4.3), (4.5) and (4.7), and (b) exact mass accounting requires linear interpolation of θ

between space nodes, i.e. trapezoidal integration of mass. Further, this result may be obtained for all boundary conditions, as recognised by *Celia et al.* (1990), and demonstrated in the computer code of *Ross and Bristow* (P. J. Ross, personal communication).

We now set out precise requirements for mass-conservative finite differencing, using the short-hand notation of a finite difference representation of continuity equation (4.1). It is important not to impose any unnecessary constraints on the choice of numerical scheme.

Equation (4.1) in finite difference form is, at an internal depth node:

$$F_i = \alpha\left(q_{i+0.5}^{j+1} - q_{i-0.5}^{j+1}\right) + (1-\alpha)\left(q_{i+0.5}^{j} - q_{i-0.5}^{j}\right) + e_i = 0 \tag{4.15}$$

with $$e_i = \left(\theta_i^{j+1} - \theta_i^{j}\right)\Delta z_{ci} / \Delta t_{fj} \tag{4.16}$$

Here $q_{i+0.5}$ is soil-water flux at the midpoint between depth nodes i and $i+1$, $\Delta z_{ci} = (\Delta z_{fi} + \Delta z_{fi-1})/2$, Δt_{fj} is size of the time-step beginning at time j, and α is the temporal weighting of the spatial differential. At the upper and lower boundaries, we use simple non-centred differences in space over the top and bottom half node spacings. The difference equations at the upper and lower boundaries are respectively:

$$F_0 = \alpha\left(q_{0.5}^{j+1} - q_0^{j+1}\right) + (1-\alpha)\left(q_{0.5}^{j} - q_0^{j}\right) + e_0 = 0 \tag{4.17}$$

$$F_m = \alpha\left(q_m^{j+1} - q_{m-0.5}^{j+1}\right) + (1-\alpha)\left(q_m^{j} - q_{m-0.5}^{j}\right) + e_m = 0 \tag{4.18}$$

where the boundary e-values are calculated using $\Delta z_0 = \Delta z_{f0}/2$ and $\Delta z_m = \Delta z_{bm}/2 = \Delta z_{fm-1}/2$. Summing F_i over all depth nodes, all internal q's cancel, leaving boundary fluxes. Multiplying by Δt and rearranging, we have:

$$\begin{aligned}\sum_{i=0}^{m} F\,\Delta t = {} & \Delta t\left(\alpha q_m^{j+1} + (1-\alpha) q_m^{j}\right) - \Delta t\left(\alpha q_0^{j+1} + (1-\alpha) q_0^{j}\right) + \\ & \sum_{i=0}^{m-1}\left(\theta_{i+1}^{j+1} + \theta_i^{j+1}\right)\Delta z_{fi}/2 - \sum_{i=0}^{m-1}\left(\theta_{i+1}^{j} + \theta_i^{j}\right)\Delta z_{fi}/2 = 0\end{aligned} \tag{4.19}$$

The four terms on the right hand side of (4.19) for a single time-step are, in order: cumulative flux of water at the lower boundary; cumulative flux at the upper boundary; final soil-water content in the profile; and initial soil-water content in the profile. Equation (4.19) expresses mass balance over the time-step Δt, provided that soil-water content in the profile is obtained by trapezoidal integration of θ. Also, when fluxes vary in time, the cumulative boundary fluxes are computed by integration of q using the same temporal weighting as in the difference equation.

If mass balances exactly over one time-step, it also balances exactly over an arbitrary number of time-steps. Summing (4.19) over N time-steps from $j = 0$ to $j = N$, and cancelling profile contents at intermediate times, we obtain the corresponding exact mass balance for the duration of a simulation:

$$\sum_{j=0}^{N-1}\sum_{i=0}^{m} F_i \Delta t^j = \sum_{j=0}^{N-1} \Delta t^j \left(\alpha q_m^{j+1} + (1-\alpha) q_m^j\right) - \sum_{j=0}^{N-1} \Delta t^j \left(\alpha q_0^{j+1} + (1-\alpha) q_0^j\right) + \sum_{i=0}^{m-1} \left(\theta_{i+1}^N + \theta_i^N\right) \Delta z_{fi} / 2 - \sum_{i=0}^{m-1} \left(\theta_{i+1}^0 + \theta_i^0\right) \Delta z_{fi} / 2 = 0 \tag{4.20}$$

The above result holds, irrespective of whether boundary fluxes are prescribed in advance, or are determined by gravity drainage with $\partial\psi/\partial z = 0$ at the lower boundary. It also holds for potential boundary conditions, since (4.17) and (4.18) still contribute to mass balance, although they are no longer used in obtaining the solution.

Potential boundary conditions, however, do cause two complications. For a prescribed condition at the surface, the first complication is that in order to preserve mass balance, it is necessary to set $q_0 = q_{0.5}$, at time j or $j+1$. This is because fixed surface potential ψ_0 sets $e_0 = 0$ in (4.17). While this may be intuitively unsatisfying, the cost of a more sophisticated relationship between q_0 and $q_{0.5}$ is a loss of mass balance. The second complication is that, in general, there is a transient contradiction between a given moisture profile at time j and a potential boundary condition introduced at the same time. Imposing ψ_0 entails an instantaneous change in θ_0, and requires a corresponding change in profile moisture content of $0.5\,(\theta_{0,new} - \theta_{0,old})\,\Delta z_{f0}$, for exact mass accounting.

The cancellation of all internal fluxes and intermediate profile soil-water contents, implicit in (4.20), achieves exact mass balance for a wide range of situations. The first is arbitrary spatial arrangement of depth nodes and arbitrary variation of time node spacing. The second is any method of estimating midpoint hydraulic conductivity (e.g. arithmetic, geometric or harmonic mean). The third is any representation of θ, for example, in terms of θ, ψ or U. The fourth condition is arbitrary spatial and temporal variation in the formulation of q. Even completely arbitrary internal fluxes must cancel, provided only that flux at a given point in space and time is the same for the two times it is computed.

The generality of (4.20) may be extended further, to spatial weighting of temporal differentials, provided that precisely the sum of the e-values of (4.16) is distributed among all the depth nodes. For example, the Douglas finite difference scheme (e.g. *Mitchell*, 1969) meets this condition.

There are constraints on direct use of finite element techniques in mass-conservative schemes. For example, a finite element scheme with piecewise linear basis functions and a consistent time

matrix, which was investigated by *Celia et al.* (1990), does not conserve mass exactly for spatially variable Δz, although this is nearly the same as the Douglas finite difference scheme. Also, direct use of finite element techniques with higher-order differencing in space is inconsistent with the requirement for linear spatial interpolation of θ for mass accounting. If this requirement is met, higher-order finite difference equations, which have been used in pursuit of more accurate solutions (e.g. *Chaudhari*, 1971; *Bresler*, 1973), will conserve mass.

Mass will not be conserved for flux boundary conditions if the flux is represented in finite difference form, instead of simply being prescribed (see e.g. *Whisler and Klute*, 1967; *Haverkamp and Vauclin*, 1981; *Wallach and Shabtai*, 1992). A finite difference representation of surface flux q_0, involves setting up unknown potential ψ_{-1} at a conceptual node just outside the boundary, expressing q_0 in terms of central differences at $i = 0$, and using the prescribed value of θ_0 to eliminate ψ_{-1}. This causes mass balance error in two ways, when the F_i are summed. Firstly, e_0 in equation (4.17) uses double the correct Δz value, so that spurious soil-water outside the boundary is included in the summation. Secondly, the flux not cancelled by the summation is $\theta_{-0.5}$ instead of the boundary flux θ_0.

In this work we have found that this treatment of the boundary flux imposed very severe Δz and Δt constraints in numerical solutions of (4.4) for any reasonable mass balance. It required, for example, $\Delta z_0 << 1$ mm, to achieve cumulative surface flux errors in mass balance of 1 part in 100 for rainfall and 1 part in 5 for evaporation.

The final requirement for mass conservation is a mass-conserving criterion for convergence of the solution at the end of each time-step. This criterion is the convergence of the vector $[F_i]$ to nearly zero (*Ross*, 1990). With a complete mass-conservative numerical scheme, mass accounting requires only trivial computational effort. The change in global mass balance over the time-step is simply the sum of F_i over all depth nodes. If a potential boundary condition has been introduced at the beginning of the current time-step, then the correction described above must be used as well.

In this work, we use a convergence criterion of $|F_i| < 10^{-10}$, and mass balance errors in cumulative infiltration are less than one part in 10^{11} for all simulations reported.

4.9.6 Numerical scheme

Choosing the numerical scheme

A flow problem that is generally regarded as numerically difficult is high-rate infiltration into very dry soil. Depending on choice of numerical scheme and soil hydraulic functions, computa-

tional effort for a single infiltration event of this type may range from hundreds of seconds on a highly configured supercomputer (e.g. *Paniconi et al.*, 1991), to a few seconds on a personal computer (IBM PC-AT) having low performance by current standards (e.g. *Ross*, 1990).

We seek a numerical strategy that is known to be computationally efficient and conserves mass exactly, and this will be used with the hydraulic functions that permit guaranteed numerical performance. A literature search suggested the following features: use of (4.7) as the form of the flow equation, the simple finite differencing described in section 4.9.5, a Newton–Raphson iterative scheme for solving the finite difference equations, and the simplest possible initial estimate of the solution for the current time-step, *viz.* the solution for the previous time-step. We note that all these features are to be found in the work of *Ross and Bristow* (1990). Our numerical solutions of (4.3), (4.4) and (4.7), including comparisons of Newton–Raphson and Picard solution schemes and comparisons of the BW and Campbell soil models, confirmed this choice as appropriate for the range of infiltration events studied. However, we found advantages in changing some details of the numerical strategy of Ross and Bristow.

We found some convergence problems with the computer code of *Ross and Bristow* (1990), occurring unexpectedly within parameter ranges that generally seemed reliable. For example, for infiltration into their 'sand' with initial condition $\psi = -351$ m, and node spacing $\Delta z = 0.0625$ m and $\Delta t = 0.015625$ d, the procedure converged for rainfall $R = 0.239$ m d^{-1}and $R = 0.241$ m d^{-1}, but not for $R = 0.240$ m d^{-1}. A previously successful case for $R = 0.23$ m d^{-1} failed if either Δz or Δt was halved. In such cases we found that the iterative procedure for one time-step failed after estimated ψ approached $-\infty$ at a depth node just below the wetting front. The problem was rectified, for the cases we found, by modifying the authors' constraints on the magnitude of $\Delta\psi$ between iterations. Their constraint, limiting positive changes to estimated ψ-values over most of the negative range, was changed to a bi-directional version applied to all ψ-values, combined with absolute upper and lower limits. Thus we use $|\Delta\psi| \leq 0.8\,|\psi| + k$, and $\psi_{min} \leq \psi \leq \psi_{max}$, where k is a constant, ψ_{min} is at the negative end of a table of hydraulic properties, and ψ_{max} is computed assuming less than 1 m depth of surface ponding. None of the values of constants in this constraint are critical, using either soil model.

We found that a further modification of the numerical scheme of Ross and Bristow, to use geometric mean hydraulic conductivity instead of their arithmetic mean, increased the upper limit of Δz for numerical convergence and stability (using the Campbell soil model). With this change, equations (4.15) to (4.18) yield a complete difference scheme using:

$$q^{l}_{k+0.5} = K^{l}_{k+0.5} - \frac{U^{l}_{k+1} - U^{l}_{k}}{\Delta z_{ck}} \qquad (4.21)$$

$$K^{l}_{k+0.5} = \sqrt{K^{l}_{k}\ K^{l}_{k+1}} \qquad (4.22)$$

where k is depth i or $i+1$, and l is time j or $j+1$.

The geometric mean causes some numerical sharpening of the wetting front (*Warrick*, 1991; *Li*, 1993) with any soil model, and partially compensates for numerical diffusion caused by using a 'fully implicit' or backward difference scheme ($\alpha = 1$) when using large time-steps.

Our final change to the details of the numerical strategy of Ross and Bristow was to evaluate soil hydraulic functions using lookup tables. This increased the efficiency of computing the required soil hydraulic properties from vector [ψ], the estimate of the solution computed during the previous iteration. High-resolution tables of all functions are linked, with exponential spacing of ψ-values. Thus for each element of [ψ], a simple calculation is used instead of a search to determine position on the table, and another simple calculation determines an interpolation factor used to evaluate all other soil hydraulic properties for the precise ψ-value. Use of tables, with 300 points in the range $\psi_a \geq \psi \geq -1000$ m required about 1 more iteration per time-step, but achieved faster computation per iteration. Overall computation was slightly faster, even with the very simple functions of the Campbell soil hydraulic model.

There is necessarily a slope discontinuity for each variable at every point on a lookup table used with linear interpolation. Numerical problems associated with $\partial\theta/\partial\psi = 0$ are commonly attributed to slope discontinuities (e.g. *Ross and Bristow*, 1990). But these, *per se*, cause no difficulties for Newton–Raphson solution schemes or for the numerical procedure as a whole. Discontinuous functions, non-monotonic functions, and zero slopes, however, will all cause numerical failures.

There is no speed penalty in tabulating the slightly more complicated functions and derivatives of the BW soil model to achieve determinacy and scaling, as computational speed is independent of the forms of the hydraulic functions. Further, use of tables makes the algorithm for solving the flow equation independent of the soil model, making comparison of soil models particularly easy.

For the purposes of this work, there is no time-step control during a simulation, so that if convergence fails, the procedure stops. The only control on the solution procedure, the above mentioned $\Delta\psi$ constraint, remains unchanged for all simulations. The numerical scheme described above will be used with two temporal weightings of the spatial differential, $\alpha = 0.5$ and 1.0, to determine the parameter space for numerical convergence and stability for Crank–Nicolson and backward difference schemes, respectively.

Alternative iterative schemes for solving the finite difference equation

We recognise that our choices of various numerical features, including the Newton–Raphson iterative scheme, are by no means absolute, being based on spot checks of performance. The scheme of Ross and Bristow is undoubtedly near the fast end of the computational speed spectrum. This appears to be due largely to three factors: exact mass conservation, reduction of the consequences of indeterminacy of solutions in very dry soil due to solving (4.7), and using a Newton–Raphson scheme to permit direct solution of forms of the flow equation having mixed dependent variables. However, the numerical scheme of *Celia at al.* (1990), with a modified Picard solution scheme, also conserves mass exactly. At present there appear to be no direct performance comparisons with schemes related to that of *Ross and Bristow* (1990). We therefore consider the differences between these solution schemes.

The Picard solution scheme may be used to directly solve forms of the flow equation using a single dependent variable. Thus to solve (4.4) for $[\psi]$, terms in F_i are rearranged so that the set of equations becomes the matrix equation:

$$[A]\left[\psi^{j+1}\right] = [b] \tag{4.23}$$

where the vector $[\psi^{j+1}]$ represents potentials at the end of the current time-step, the vector $[b]$ incorporates all terms involving the beginning of the time-step, time j, and element A^i_k in matrix $[A]$ is the coefficient of ψ_k^{j+1} in row i.

The Newton–Raphson solution scheme may be used to solve directly any form of the flow equation. The matrix equation is:

$$-[F] = \left[\frac{\partial F}{\partial \psi^{j+1}}\right][\Delta\psi] \tag{4.24}$$

where $[\partial F/\partial\psi^{j+1}]$ is a tridiagonal matrix of the derivatives of (4.15) – (4.18) with respect to ψ (sometimes referred to as a Jacobian matrix), and vector $[\Delta\psi]$ yields a correction to the existing estimate of $[\psi^{j+1}]$.

The complete algorithm has nearly identical structure with either Picard or Newton–Raphson solution scheme. Firstly, matrix $[A]$ is tridiagonal, and is solved very rapidly and accurately using the Thomas algorithm (e.g. *Press et al.*, 1986). Secondly, the matrix equation is solved iteratively, each time using the previous estimate of $[\psi^{j+1}]$.

Apart from the algorithm, major differences do exist between these schemes. The conceptual difference is that the Newton–Raphson scheme applies directly to all forms of the flow equation. Further, *Paniconi et al.* (1991) showed that the Newton–Raphson scheme converged more

quickly, and over a wider Δt range, yielding slightly faster computation for infiltration into relatively dry soil. They argued that the Newton–Raphson scheme is more difficult to implement, on the grounds of greater complexity. But we found that despite having slightly more complex algebra, individual matrix and vector elements are mathematically and physically more intelligible. Because of this, and the ease of determining whether errors are in the vector or the matrix, we found that it was easier to implement the Newton–Raphson scheme.

Various workers have investigated or used modified Picard schemes (e.g. *Huyakorn et al.*, 1984; *Milly*, 1985; *Celia et al.*, 1990; *Kirkland et al.*, 1992) or modified Newton–Raphson schemes (*Cooley*, 1983; *Huyakorn et al.*, 1984; *Allen and Murphy*, 1985, 1986; *Li*, 1993). In each case, a scheme for solving (4.4) was modified to obtain indirect solutions of (4.3), which has mixed dependent variables. In each case the concept is to split a finite difference representation of the temporal derivative of (4.4) into two parts. The major part is approximated, during each iteration, by directly using $\Delta\theta/\Delta t$ from the immediately preceding iteration. The difference between these two iterations is used in the procedure for solving for $[\psi]$, the vector comprising matric potentials at all depth nodes.

Both modified schemes are significantly more complex than *Brutsaert's* (1971) direct Newton–Raphson solution of (4.3). The above-mentioned works indicate the need for very small Δt values near the start of a simulation, whereas *Brutsaert* (1971) and *Ross* (1990) used relatively large fixed time-steps. *Huyakorn et al.* (1984) found that a modified Picard scheme converged much more slowly, and over a smaller range of conditions, compared with a modified Newton–Raphson scheme. These facts suggest that modified Picard schemes, which are becoming well known, are less efficient than modified Newton–Raphson schemes, and that both are considerably less efficient than direct solution of (4.3).

Having said this, it seems that *Celia et al.* (1990) are unnecessarily conservative, claiming only that their modified Picard scheme is not slower than the traditional Picard solution of (4.4). Their explanation of matching Δt constraints seems to be applicable only to a single time-step, with matching initial conditions. By contrast, *Huyakorn et al.* (1984) found modifications were required to improve the numerical efficiency of Picard schemes.

In the absence of direct performance comparisons, we shall assume that the efficiency of the modified schemes is intermediate between that of direct solutions of (4.3) and (4.4).

4.9.7 Scaled solutions

We now present scaled numerical solutions and compare them with analytical solutions, to demonstrate the accuracy achieved by our numerical scheme with moderate to very large fixed node

spacing. The examples are for the numerically demanding problem of constant-flux infiltration into extremely dry soil, using a Crank–Nicolson finite difference scheme ($\alpha = 0.5$), unless stated otherwise.

Fig. 4.5 shows a case of constant-flux infiltration into a semi-infinite dry soil, using the ordinary dimensionless variables of the BW soil hydraulic model (*qv.* Table 4.4). The dry initial condition is represented by $\psi^* = -10\,000$, corresponding to matric potentials more negative than –1000 m for most soils. Rainfall, given by $R^* = 0.5$, is relatively high, and the dimensionless soils in Fig. 4.5 are represented by $C = 1.02$ and $C = 1.5$. The fixed node spacings are $\Delta z^* = \Delta t^* = 0.25$. Analytical solutions are shown for comparison.

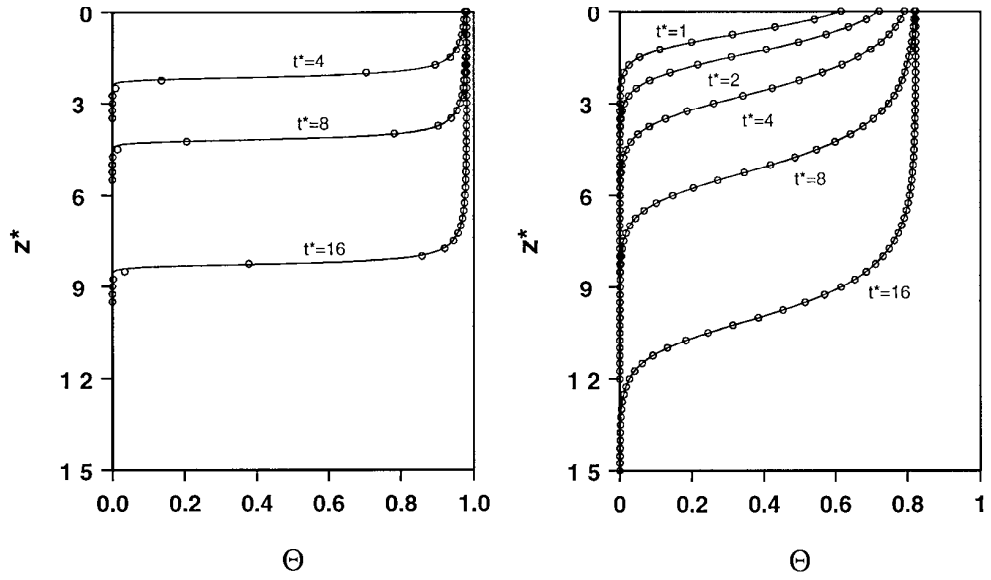

Fig. 4.5. Comparison of dimensionless numerical and analytical solutions for constant-flux infiltration, $R^* = 0.5$, into a semi-infinite 'dry' soil profile, represented by $\psi^* = -10^4$ for (a) highly nonlinear soil, $C = 1.02$, (b) weakly nonlinear soil, $C = 1.5$.

The numerical solutions of Fig. 4.5a, for the case of a highly nonlinear soil represented by $C = 1.02$, exhibit the theoretically expected 'travelling wave' (*Philip*, 1958), a wetting front of constant shape. Over most of the Θ-range, agreement between the analytical and numerical solutions is very close. Each numerical wetting front is more diffuse than the analytical solution at the leading edge ($\Theta < 0.05$). In this region the depth node spacing is too large to permit good piecewise linear representation of the moisture profile. At the end of the first time-step we found that the analytical wetting front occupied about one depth node spacing, and the numerical solution had errors in Θ of about 0.05 at the top and bottom of this range. These errors are not propagated; in fact they are greatly reduced. There is some numerical instability, manifested as spatial oscillation in near-surface Θ of the order of 10^{-4}, but it is much too small to appear on the scale the figure.

The case of a weakly nonlinear moisture characteristic (C = 1.5) in Fig. 4.b shows more diffuse wetting fronts. Here the numerical solutions correspond closely to analytical solutions throughout, even at times prior to the development of the travelling wave. We found complete freedom from numerical instability in this case. For both soils, errors in surface soil-water content Θ_0 were less than 0.1%, and far too small to appear on the figure. Mass balance errors were of the order of 1 part in 10^{12} of cumulative infiltration. With both Crank–Nicolson and backward difference schemes, we found that extreme precision is easily achieved with small node spacings.

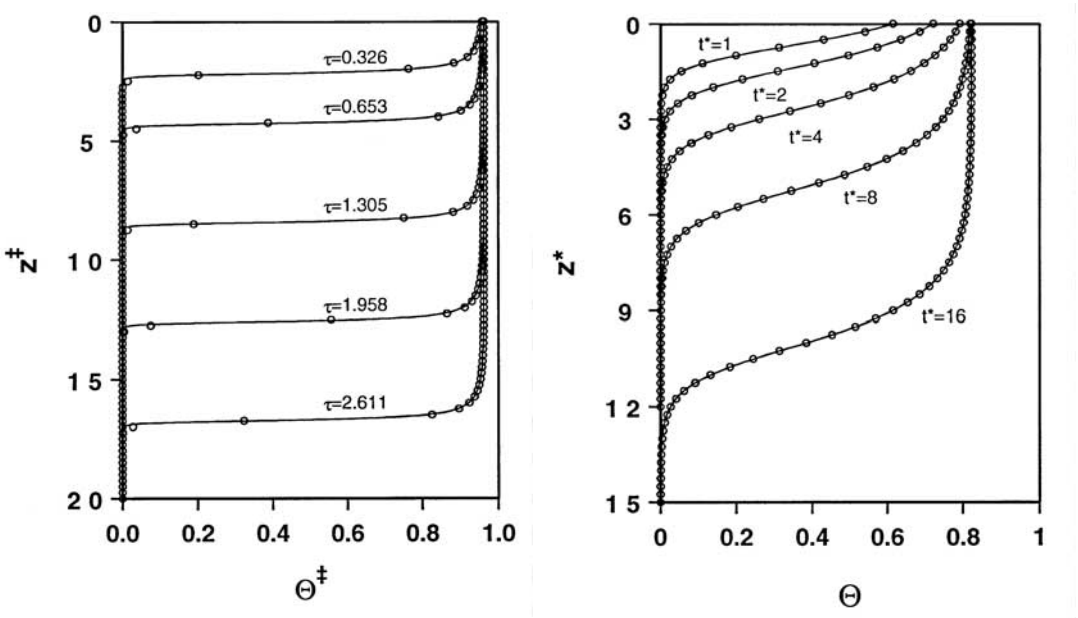

Fig. 4.6: Comparison of universally scaled (independent of soil type) numerical and analytical solutions for constant-rate infiltration into a semi-infinite 'dry' soil profile, for scaled rainfall rates (a) ρ = 6.127, and (b) ρ = 0.1667. Note that each solution scales to an infinity of cases.

Fig. 4.6 shows universally scaled solutions for constant-flux infiltration into dry soil, represented by the scaled initial condition $\psi^{\ddagger} = -10\,000$. Fig. 4.6a shows solutions for a high scaled rainfall rate ρ = 6.127. The sharp wetting fronts at scaled times τ = 0.326, 0.653, and 1.305 scale exactly to the cases of Fig. 4.5a, except for the extremely small discrepancy between the initial conditions $\psi^{\ddagger} = -10\,000$ and $\psi^* = -10\,000$. The solutions scale also to an infinity of cases with the same value of ρ, but different values of rainfall R^* and soil structure C. Physically, this says that the sharp wetting fronts shown may be due to cases ranging from that of Fig. 4.5a, with moderate rainfall into the highly nonlinear soil, to extremely high rainfall into weakly nonlinear soil. Fig. 4.6b, with the lower scaled rainfall rate given by ρ = 0.1667, likewise scales to an infinity of cases, including those for t^* = 4, 8 and 16 in Fig. 4.5b, and to very low rainfall into a highly nonlinear soil.

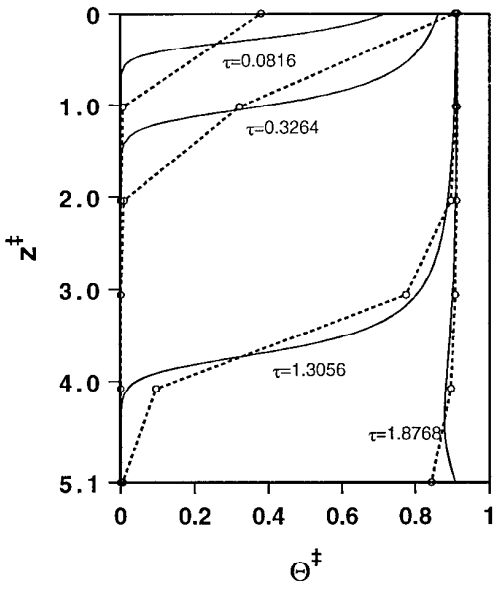

Fig. 4.7: Comparison of universally scaled numerically calculated moisture profiles with very coarse node spacings, and scaled analytical solutions for infiltration into a finite depth 'dry' soil, for ρ = 2.451. Note the lack of propagation of the severe short-time errors occurring shortly after infiltration begins.

For finite-depth soil profiles, there appear to be no numerical difficulties associated with the wetting front interacting with the lower boundary, possibly due in part to gravitational and matric potential gradients partially cancelling. Fig. 4.7 compares scaled numerical solutions, using very coarse node spacings $\Delta z^{\ddagger} = 1.0$ and $\Delta\tau = 0.0816$, with analytical solutions for a finite-depth soil profile with scaled depth $l^{\ddagger} = 5.1$, scaled rainfall rate $\rho = 2.451$, and the same extremely dry initial condition as used in Fig. 4.6. The analytical solution at the shortest time, $\tau = 0.0816$, shows that the wetting front has reached only about half way to the first subsurface depth node used for the numerical solution, which here uses a single time-step. This means that node spacings are much greater than the spatial and temporal scales of the early stages of infiltration, and numerical errors at this time are necessarily large, regardless of what numerical scheme might be used. For example, the error in computed surface soil-water content, which is only about half of the correct value, is required for trapezoidal integration of $\Theta^{\ddagger}$ (indicated by the dashed lines) to conserve mass. However, this severe short-time error does not propagate; by time $\tau = 1.3056$ some numerical self-correction has been achieved, and by time $\tau = 1.8768$ errors in $\Theta^{\ddagger}$ are relatively small.

Fig. 4.8 shows self-correction of short-time errors for another case of constant-flux infiltration into a finite-depth dry soil profile, using a backward difference scheme (α = 1.0). The initial condition is unchanged, scaled soil depth is $l^{\ddagger} = 5.85$ and rainfall is $\rho = 0.796$. In this case $\Delta z^{\ddagger} = 0.585$, which is small enough to permit accuracy in a piece-wise linear representation of an analytical solution, and $\Delta\tau = 0.1$. The Crank–Nicolson difference scheme yielded close correspon-

dence with analytical solutions at all times. Backward differencing necessarily causes some numerical diffusion, which is evident in the wetting front at time $\tau = 0.2$. Errors associated with numerical diffusion progressively self-correct with time, as the initially high spatial and temporal gradients in $\Theta^{\ddagger}$ decrease. Once the travelling wave has developed, by about time $\tau = 2$, errors in the numerical wetting front remain stable, until the front begins to interact with the lower boundary. Then gradients again decrease, and the numerical solution at time $\tau = 4.67$ is quite accurate.

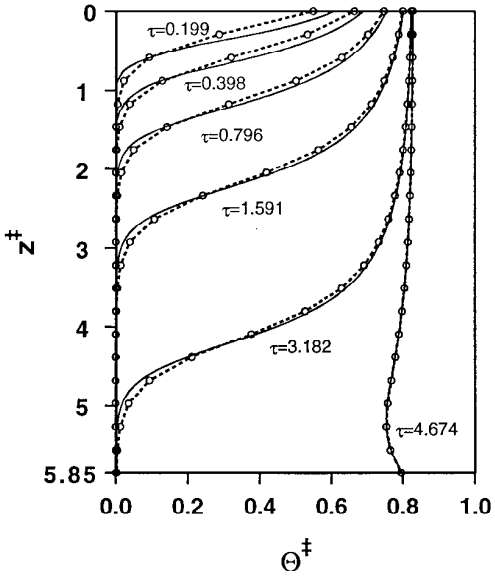

Fig. 4.8: Comparison of scaled analytical and numerical solutions for backward differencing in time, for scaled constant-flux infiltration given by $\rho = 1.05$. Note the freedom from propagation of errors, and self-correction of errors where spatial and temporal gradients decrease with time.

Numerical diffusion is determined by time-step $\Delta\tau$, as well as the gradients noted. For a linear CDE, *Noye* (1990) gives $v^2\Delta t/2$ as the numerical diffusion coefficient. For the nonlinear Richards' equation with universally scaled variables, the numerical diffusion coefficient then becomes $U^{\ddagger 2}\Delta\tau/2$; the functional form may be derived from Table 4.5.

In practice, numerical solutions for field situations will not used scaled variables. Fig. 4.9 illustrates the accurate numerical equivalence between numerical solutions obtained with and without scaling. The initial condition is $\psi^* = -10\,000$, and we have selected $C = 1.5$, $R^* = 0.2$, $l^* = 5.0$, $\Delta z^* = 1.67$ and $\Delta t^* = 4$. Solutions represented by dashed lines were obtained by transforming the initial and boundary conditions to universally scaled variables ($\rho = 0.0667$, $\psi^{\ddagger} = -10\,000$, $l^{\ddagger} = 7.5$, $\Delta z^{\ddagger} = 2.5$, $\Delta\tau = 12$), solving the flow equation with these variables, and scaling back. Here the circles represent solutions obtained without scaling. Discrepancies in Θ between scaled and unscaled solutions are less than 10^{-5} in each case. These could be reduced to computational round-

off error by scaling the initial condition and all details of the numerical procedure, for example, soil hydraulic property tables and the convergence criterion.

Using the hydraulic properties of the structured surface soil example in section 4.9.4, Fig. 4.9 could apply to a structured soil having depth 0.5 m, with a high rainfall rate R = 1.0 m d^{-1}. Exact solutions are approximated well using space step Δz = 0.167 m, and time-step Δt = 0.16 d. The spatial discretisation here is about as coarse as that used in less physically rigorous models that generalise the Green–Ampt infiltration model to multiple sharp wetting fronts as an alternative to solving Richards' equation (e.g. *Markar and Mein*, 1985). *Short et al.* (1995) demonstrated that Richards' equation based models are competitive with these, even on the basis of CPU time.

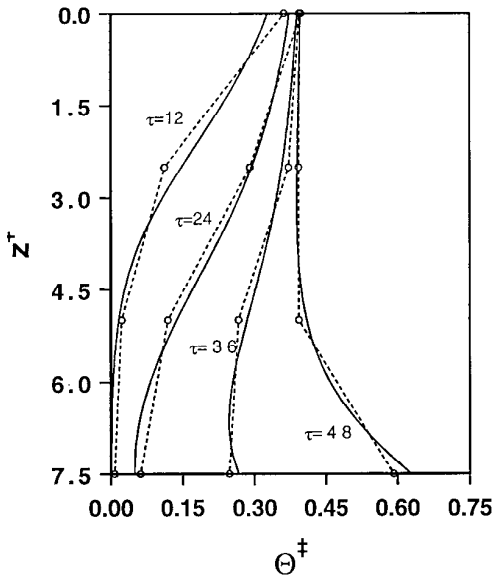

Fig. 4.9: Comparison of numerical and analytical solutions for constant-rate infiltration into a semi-infinite 'dry' soil for ρ = 0.0667, using extremely coarse node spacings. Dashed lines and symbols represent respectively numerical solutions obtained with and without solving the flow equation with scaled variables, illustrating easy attainment of accurate equivalence between scaled and unscaled solutions.

As mentioned earlier, universal scaling is not applicable to satiated conditions. However, the resulting quasi-linear CDE yields much simpler scaling and numerical performance prediction, the flow problem is highly diffusion dominated (in unconfined aquifers), and numerical solution is straightforward. Extension to 3-dimensional flows should also be easy, since horizontal flux has no convective (gravitational) component, and horizontal flows are fully diffusion dominated.

4.9.8 Criteria for guaranteed numerical convergence and stability

Numerical convergence was obtained without difficulty for all cases in section 4.9.7. With coarse discretisation, the extremely dry initial conditions required about 20 iterations per time-step, compared with 5–7 iterations for moderate discretisation and relatively moist initial conditions. No oscillation of estimated solutions was observed during the iterative process, and solutions approached their final values asymptotically. There was usually complete freedom from numeri-

cal instability, except for the very low-amplitude oscillation noted for the demanding case of Figs. 4.5a and 4.6a.

We now use scaling to search the parameter space $(\Delta z^{\ddagger}, \Delta\tau, \rho)$, in order to develop criteria for complete freedom from numerical instability and convergence failure. This is a practical alternative to searching the 4-dimensional space $(\Delta z^*, \Delta t^*, R^*, C)$ required using the BW soil hydraulic model without universal scaling, or the still higher dimensioned space required when dimensioned variables, such as in other soil models, are used.

von Neumann instability

Instability in the von Neumann sense is the propagation of perturbations as the solution proceeds in space and time (e.g. *Noye*, 1990). Linear CDEs are unconditionally stable in this sense, for both Crank–Nicolson and backward difference schemes (*Narasimhan*, 1976; *Noye*, 1990).

In this work we did not encounter this type of instability under any conditions with scaled solutions of Richards' equation. This is to be expected because the flow problem is diffusion dominated with $P_e < 2$ and $C_o < 1$ for all $\Theta^{\ddagger}$, with depth node spacing much coarser than those used in section 4.9.7. In particular, because $P_e^{\ddagger} \rightarrow 0$ as $\Theta^{\ddagger} \rightarrow 0$, numerical instability cannot be expected at the leading edge of the wetting front, as the problem is completely diffusion dominated. Diffusion dominance should assure freedom from von Neumann instability, but this does not necessarily guarantee freedom from other numerical problems.

'Wiggles'

Another numerical problem encountered with linear CDEs is the spatial oscillation that sometimes occurs at and near boundaries, but which need not propagate as the solution proceeds. This type of perturbation of the solution, described as 'wiggles' by *Roache* (1976), is caused by discretising the flow equation at the boundaries. It is most prominent with prescribed concentration boundary conditions, but occurs also with flux boundary conditions and in steady-state solutions (*Roache*, 1976), so that it cannot be eliminated over the whole parameter space using backward difference schemes.

We encountered 'wiggles' in some scaled solutions of Richards' equation, and for the purposes of this work, we include both von Neumann instability and wiggles in the term 'numerical instability'. This is because the small spatial scales of many soil-water flow problems relative to *D*- and *K*-values make 'wiggles' undesirable.

Guaranteed convergence

To guarantee obtaining solutions using the very fast Thomas algorithm for the tridiagonal solution matrix (see section 4.9.6), the matrix must be diagonally dominant. This imposes an upper limit of a little over 2 on P_e (*Noye*, 1990), and we have seen from section 4.9.4 that this imposes an upper limit on the space step of $\Delta z^{\ddagger} \cong 8$, or $\Delta z \cong 8\ \lambda_c / C$.

It should be noted that solvability of the solution matrix is necessary, but not sufficient, to guarantee that the iterative solution procedure required for a nonlinear CDE will converge. With coarse node spacings, for example, initial estimates of solutions may be inadequate for this purpose. We found convergence failures for $\Delta z^{\ddagger} = 8$, in some cases when ρ was high. The parameter space must be searched to find the region of convergence.

We searched the parameter space $(\Delta z^{\ddagger}, \Delta\tau, \rho)$ to determine the region in which solutions were both convergent and stable for constant-flux infiltration into extremely dry soil, with initial condition $\psi^{\ddagger} = -10\ 000$. The criterion for freedom from numerical instability was that any spatial or temporal oscillation in $\Theta^{\ddagger}$ should have amplitude less than 10^{-6}. The space was searched over a grid with successive values of each parameter differing by a factor of $\sqrt{2}$. This gives performance maps without smooth boundaries between numerical success and failure, but provides practical criteria for guaranteed numerical performance.

Using the Crank–Nicolson difference scheme, we found constraints on both $\Delta z^{\ddagger}$ and $\Delta\tau$, for convergence and stability for given ρ. It is practical to map the time-step limit $\Delta\tau_{max}$ as a function of ρ, for given $\Delta z^{\ddagger}$. However, we found that $\rho\,\Delta\tau_{max}$, the scaled cumulative infiltration during the time-step, shows only weak dependence on ρ. This is shown in Fig. 4.10a, for $\Delta z^{\ddagger} = 1$. Similar maps could be produced for different space steps, to show the resulting weak constraints on time-step. It can be seen that a simple practical criterion for guaranteed numerical convergence and stability with relatively large node spacing is: $\rho\Delta\tau < 0.1$, for $\Delta z^{\ddagger} \leq 1$. This criterion is quite conservative, as is shown by the examples in Figs. 4.5a and 4.6a. There $\rho\,\Delta\tau = 0.125$ and the solution just fails our stability criterion, due to wiggles in near-surface $\Theta^{\ddagger}$ having amplitude about 10^{-5}; although for most purposes stability would be regarded as very good.

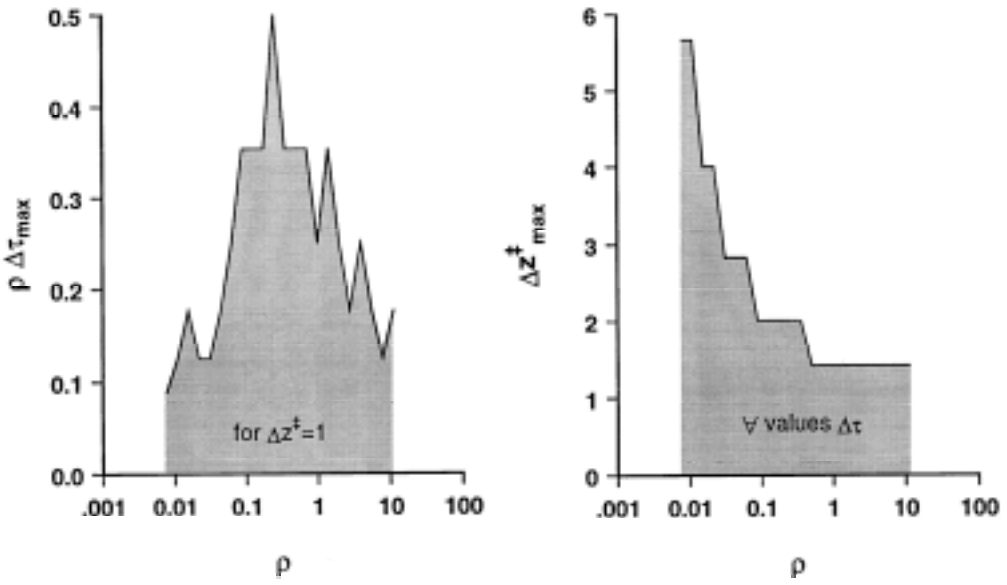

Fig. 4.10: Maps of domains of allowable step sizes which give complete freedom from numerical instability in terms of universal parameters (a) upper bound of $\rho\Delta\tau$ for the Crank–Nicolson difference scheme, (b) upper bound of $\Delta z^{\ddagger}$ for the backward difference scheme, which may be approximated by $1.4/\Theta_e^{\ddagger}$.

When a backward difference scheme (α = 1) is used, we find that numerical convergence and stability are independent of $\Delta\tau$ over an extremely wide range. This permits mapping performance in a two-dimensional plot, using the space $(\Delta z^{\ddagger}, \rho)$. Fig. 4.10b shows $\Delta z^{\ddagger}_{max}$ as a function of ρ. While this difference scheme yields a larger region for guaranteed convergence and stability, it yields slightly less accurate solutions. This can be seen, for example, in Fig. 4.8, where scaled parameters lie in the guaranteed performance space of both schemes.

We see in Fig. 4.10b that the upper bound for $\Delta z^{\ddagger}$ for numerical stability is approximately $\Delta z^{\ddagger}_{max} \leq 1.4/\Theta_e^{\ddagger}$, where $\Theta_e^{\ddagger}$ is the equilibrium surface moisture after the travelling wave is fully developed, given by $\Theta_e^{\ddagger} = 2\rho(\sqrt{1+1/\rho} - 1)$ (*Broadbridge and White*, 1988, eqn (46)). A simpler and generally conservative criterion for all soils and rainfall rates is: $\Delta z < \lambda_c$, where λ_c is the macroscopic capillary length used to scale depth and potential, as discussed in § 4.9.4. The dependence of the more precise criterion on $\Theta_e^{\ddagger}$ is consistent with our observation that numerical stability is most difficult to achieve at the surface, with a well developed travelling wave. At this point, $\Theta_0^{\ddagger}$ has its greatest value for the simulation, and wiggles are most likely to be initiated. This point cannot be explained in terms of the Péclet number, which has its maximum here only for relatively low scaled rainfall rates, *viz.* $\rho < 0.125$ ($\Theta_e^{\ddagger} < 0.5$). While a simple justification for the numerical performance criterion for higher values of ρ does not seem possible, it is tempting to speculate that a basis will be found for the convergence and stability criterion: $\Delta z^{\ddagger}_{max} \leq \sqrt{2}/\Theta_e^{\ddagger} < 8$.

Other criteria may be developed for guaranteed performance, for example, for accuracy with constant-flux infiltration, or for prescribed potential boundary conditions. Criteria for the latter case, which may be somewhat tighter, would be appropriate for modelling ponded infiltration. These are beyond the scope of this work, which is concerned with models of soil-water dynamics under natural rainfall. For such models (e.g. *Dawes and Hatton*, 1993; *Dawes and Short*, 1993), when ponding occurs during rainfall, soil is relatively moist at the beginning of the time-step, and the criterion presented here suffices. To date, we have achieved robust convergence for simulations of unsatiated/satiated soil-water dynamics for more than 100 000 soil-column years, with widely varying soil types, soil layering and weather conditions.

4.9.9 Discussion

Scaling and determinacy of solutions have been used in this work to guarantee numerical convergence and stability of solutions of the flow equation. These principles provide a technique for testing alternative numerical solution schemes more comprehensively than previously.

The ability to test numerical schemes comprehensively eliminates the need to rely on the usual *ad hoc* spot checks on numerical performance. Any choice of numerical scheme or refinements can be tested in this way. A particularly useful example would be to compare the efficiency of the modified Picard scheme of *Celia et al.* (1990) with direct methods of solving (4.3). Such testing would assist modellers to choose effectively from the plethora of available numerical schemes.

Comparisons between numerical schemes are not needed for all aspects of performance. For example, the parameter space for guaranteed convergence and stability may be examined directly. Further, accuracy may be tested by comparison with analytical solutions. However, direct comparison with an informal numerical standard is desirable, to examine computational speed comprehensively.

CPU time does not provide an ideal basis for comparison, due to rapidly changing computer technology. This situation is changing, however, with the evolution of standard measures of computer performance. Further, differences in computer architecture will have little effect on relative speeds if nearly all of the computational effort is devoted to arithmetic, which is itself a computationally efficient strategy. This may be achieved by computing hydraulic properties from $[\psi]$ during each iteration either analytically, or by using tables structured to avoiding searching, as we have done here (*qv.* section 4.9.6).

A useful alternative approach is to compare numbers of nodes and numbers of iterations required per time-step. This is because many numerical schemes have similar computational effort per iteration. In a preliminary investigation we found, for example, that for the various forms of the

flow equation discussed in section 4.9.2, with direct use of either Newton–Raphson or Picard solution schemes, and for various representations of midpoint hydraulic conductivity, computational speed per iteration did not vary by more than a factor of 2. Further, it appears from *Celia et al.* (1990) that the modified Picard scheme, in spite of additional conceptual complexity, requires very little additional computational effort per iteration.

For the algorithm reported in this work, the number of iterations per time-step varies by less than an order of magnitude over a very wide range of boundary and initial conditions, as noted in section 4.9.8. A general indication of computational speed, for the dated personal workstation used (floating point speed 1.7 MFLOPS), is 2×10^{-4} s per depth node per iteration or 10^{-3} s per depth node per time-step.

Scaling need not confine the choice of soil hydraulic model to the BW model, although there are few current alternatives. The model of *Barry et al.* (1993), for example, permits arbitrary moisture characteristics, and yields some analytical solutions. However, it appears not to permit scaling to a 3-dimensional space. It also imposes the condition $\partial^2 K^*/\partial\Theta^2 < 0$ for all Θ, so that a travelling wave solution for infiltration, which is essential for practical testing of numerical schemes, or approximating the behaviour of real soils, does not develop. One possible alternative is to recast the soil hydraulic functions and analytical solutions of the alternative approach of *Sander et al.* (1988) in terms of a practical soil hydraulic model, and to further scale to variables related to $z^{\ddagger}$, τ, and ρ. Their K and ψ functions so scaled may differ from those of *Broadbridge and White* (1988) in that K is less nonlinear, although D is common to both models.

4.9.10 Conclusions

We have shown in this work that use of the BW soil hydraulic property model provides a strategy for guaranteeing *a priori* the performance of numerical schemes for the soil-water flow equation, for prescribed flux boundary conditions. This is due to two features of the model, (a) determinacy of solutions at both the wet and dry ends of the water content range, and (b) universal scaling of solutions in terms of three parameters. The latter allows the investigation of numerical performance comprehensively over a tractable three-dimensional parameter space. This eliminates the need for *ad hoc* tests of numerical performance for each case studied, and should facilitate more general use of Richards' equation in models of soil-water dynamics.

Scaling and determinacy appear to provide powerful strategies for various purposes, including coping with numerical difficulties inherent in the non-linearity of the flow equation, and evaluating alternative numerical schemes. Preliminary work suggests that this strategy also makes numerical performance largely independent of either the choice of mass-conservative form of the

flow equation or the representation of midpoint hydraulic conductivity, using a Newton–Raphson solution scheme.

The relatively simple algorithm used here permits *a priori* choice of a coarse fixed space-time mesh, with no dynamic adjustments of the numerical procedure to deal with special cases, yet achieves high self-correction of errors that necessarily occur shortly after infiltration begins.

The allowable node spacings are so large as to suggest that they can be chosen largely on the basis of the spatial and temporal scales of the physical processes of interest. These spacings indicate the practicability of using Richards' equation as the basis for robust general purpose models of soil-water dynamics. Thus one can replace the simple two-layer models of soil-water dynamics commonly incorporated into models of crop growth (*e.g.* WAVES, *Dawes and Short* 1994, *Zhang et al.* 1996) or moisture and energy exchanges at the land surface (e.g. Shao *et al.* 1997), and even simple single-layer water balance models. Many existing models of these processes, all of which attempt to approximate solutions of equations (4.1) and (4.2), simplify solutions for numerical efficiency. However, this need not confer significant computational speed advantages over efficient use of Richards' equation (*Short et al.*, 1995), which would help to model soil-water dynamics with equivalent rigour to other parts of these models.

Acknowledgements. We thank Dr John Knight, CSIRO Centre for Environmental Mechanics, for stimulating discussions, and Dr Peter Ross, CSIRO Division of Soils, for his generosity in providing computer code for comparison with his results, and for insisting that mass balance should be exact. We thank Dr Robin Wooding of the Centre for Environmental Mechanics and Professor Wilford Gardner of the University of California at Berkeley for helpful comments. One of us, Warrick Dawes, acknowledges financial support from the Australian Water Resources Advisory Council and Land Care Australia. Another, Ian White, acknowledges support from the National Soil Conservation Program, grant 87/12 and the CSIRO Land and Water Care Program.

CHAPTER 5. APPLICATIONS OF WAVES

5.1 Modelling Hydrologic Processes Using WAVES

L. Zhang, W. R. Dawes, T. J. Hatton

Adapted from the *Journal of Hydrology*, 185 (1996), 147–169

Abstract

WAVES was tested using the energy flux and soil moisture measurements from the First ISLSCP Field Experiment (FIFE) and Hydrologic Atmospheric Pilot Experiment and Modélisation du Bilan Hydrique (HAPEX-MOBILHY). The simulated net radiation, evapotranspiration and soil moisture content agreed well with the observations and with previous studies of transpiration and soil evaporation. The success of the model was due to the reasonably realistic treatment of the soil and canopy processes. The utility and limitations of the model are discussed.

5.1.1 Introduction

The physical and biological processes describing the surface water, energy and solute balances of the plant–soil–atmosphere system are, in general, well understood. Models of that system can be formulated at almost any level of complexity with as many or as few processes as required. The level of model complexity is usually determined by the application.

Historically, physically based models have been developed to represent the real world with increasing detail. The place and use of such models, and the information contained in the data required to run them, have been debated in hydrology literature for over 20 years, most recently by Beven (1989, 1993), Hauhs (1990), Wheater and Jakeman (1993) and Barnes (1993). These authors argue that physically based models are most appropriately used in exploring the interactions between processes and fluxes under different management and/or climatic regimes, given clearly stated assumptions about which small scale processes are relevant.

In Australia, most environmental degradation is associated with changes in the surface water balance induced by changes in land cover. The temporal and spatial scales over which these changes evince themselves precludes field experimentation as a wholly sufficient or practical investigative tool for identifying optimal or appropriate land use. Decision-makers are therefore reliant on models, especially physical process models, for predicting expected changes in the

landscape; the diversity of recent hydrological modelling tools in use in Australia (see Grayson and Chiew 1994 and Hatton *et al.* 1994 for recent reviews) is testament to this need.

The soil water balance of many Australian land systems does not have to be treated with a fully three-dimensional model (*sensu* Hatton *et al.* 1992, Vertessy *et al.* 1993), but rather may be approximated with a one-dimensional treatment. For such systems, the CSIRO Division of Water Resources developed the physically based ecohydrological model WAVES to enable the simulation of land system behaviour under alternative vegetation management and climatic variation.

The WAVES model predicts the dynamic interactions, and fluxes of mass and energy, within soil–vegetation–atmosphere systems. The model adopts a one or two layer canopy representation with a soil layer underneath. The aerodynamic resistance at the top of the canopy is determined based on Monin–Obukhov surface layer similarity theory and the within canopy aerodynamic resistances are estimated using the mixing-length approach (Raupach and Thom 1981). The boundary layer resistances are neglected for simplicity. The model formulates the physiological control on transpiration using the canopy resistance calculated as a function of the net assimilation rate, and the vapour pressure deficit and CO_2 concentration at the canopy surface. The soil hydrology is described by the Richards equation. A distinguishing feature of the model is to couple the soil–vegetation–atmosphere system by changing the value of the saturation vapour pressure deficit of air in the canopy. The model can be used to predict plant growth using a saturation rate kinetics formulation and to simulate solute transport in the soil (Hatton *et al.* 1992, Wu *et al.* 1994, Salama *et al.* 1999, Dawes and Short 1993).

There is a need to test and evaluate models against data sets from well-designed field experiments so that improvements or simplifications can be made. Over the last decade, several large-scale data sets have been collected, and are useful for this purpose (Shuttleworth 1991). In this paper, we test the energy and water balance components of WAVES with data obtained from the First ISLSCP Field Experiment (FIFE) and Hydrologic Atmospheric Pilot Experiment and Modélisation du Bilan Hydrique (HAPEX-MOBILHY). The plant growth and solute transport features of the model are not included in these tests. We also compare model performance against expected behaviour as described in the literature.

The data used in the present study were obtained from the First ISLSCP Field Experiment (FIFE) (Sellers *et al.* 1988) and Hydrologic Atmospheric Pilot Experiment and Modélisation du Bilan Hydrique (HAPEX-MOBILHY) (André *et al.* 1988). We first describe the experimental sites and the type of data that were available, followed by the assignment of model parameters based on soil and plant properties.

5.1.2 Experiments and Data

FIFE was conducted during the period of May to October 1987 over a 15 km × 15 km experimental area, situated 39° 00' N 96° 30' W in northeastern Kansas (Sellers *et al*. 1988). The vegetation of the experimental area consists primarily of native tall prairie grass, the growing season of which is from mid-March to mid-October. The modelled area is the King's Creek catchment, located in the northwestern quadrant of the FIFE experimental domain. During FIFE 1987, four intensive field campaigns (IFCS 1–4) were organized to measure surface fluxes. IFC 1 (May 26 to June 6) was targeted at capturing the vegetation 'green-up' phase of late spring, IFC 2 (June 25 to July 11) was to monitor the 'peak-greenness' stage of the vegetation, IFC 3 (August 6 – 21) was intended to capture soil moisture 'dry-down' conditions in the late summer, and IFC 4 (October 5 – 16) was targeted at characterizing the fully senescent phase of the vegetation (Sellers *et al.* 1992b).

The raw meteorological data, consisting of wet and dry bulb temperatures, wind speed, downward shortwave radiation, and precipitation, were taken every 30 minutes from Super-AMS station 5 (2123-SAM). The data were filtered manually to remove bad values and to fill in missing data. The surface fluxes of sensible and latent (evapotranspiration) heat from Bowen Ratio Station 2 (1916-BRS) located near the King's Creek gauging station were used to test the model. These flux data were also filtered and edited manually. Mean daily values were calculated for vapour pressure deficit and wind speed, maximum and minimum temperatures were selected, and daily total solar radiation calculated for input into WAVES.

The HAPEX-MOBILHY experiment took place at 43° 41' N 00° 06' W in southwestern France over an area 100 km × 100 km. The area was divided into two parts, *ie.* a forest region (40%) and a mixed agricultural region (60%). The forest region was nearly homogeneous with some large clearings of up to 10 km^2. In the agricultural region the main crops were corn, oats, and soya bean (André, *et al*. 1988). During a Special Observing Period (SOP), a number of surface networks operated in the HAPEX-MOBILHY region, including a set of 12 specially designed SAMER stations. The SAMER stations measured meteorological variables and surface energy fluxes, from which evapotranspiration was calculated. A detailed description of the surface networks can be found in André *et al*. (1988) and Goutorbe (1991). In addition, soil moisture contents were measured at the SAMER sites using the neutron scattering method (Cosby *et al*. 1984). The measurements were made at intervals of 10 cm starting from the soil surface to 1.6 m on weekly basis.

The SAMER data were recorded on a 15-minute interval at 12 sites uniformly distributed over the region. The accuracy of the data has been examined by Goutorbe (1991) using different methods. It was found that over a 15-minute interval the typical error for the sensible heat flux was 12% over short vegetation and 25% over tall crops. The error in evapotranspiration over a 15-minute

interval was about 25%. In this study , the measurements made at the SAMER site 3 were used. The main crop at this site was soya bean. Daily climate data for input to WAVES were calculated as for the FIFE experiment.

5.1.3 Parameter estimation

The dominant soil in the King's Creek catchment is silty clay loam and the depth of the soil layer is 1.6 m. The soil physical properties of saturated moisture content, θ_s, air-dry moisture content, θ_d, saturated hydraulic conductivity, K_s, capillary length scale, λ_c, and a shape parameter, C, were assigned default values on the basis of the FIFE staff science soil survey work by applying Broadbridge–White model rules of thumb to the Clapp and Hornberger classification of soil types (Clapp and Hornberger1978; White and Broadbridge 1988).

Table 5.1 lists the model parameter values used for FIFE. Estimation of the soil hydraulic properties is described above. Values of soil and canopy albedo, and roughness length for bare soil were adopted from Brutsaert (1982). The canopy roughness length was determined as a fraction of the vegetation height, which was measured for each IFC. The leaf area index (LAI) was measured within the King's Creek catchment.

The main soil type at SAMER site 3 is silty clay loam. The soil hydraulic properties, albedo, and soil roughness length were estimated in a similar way as for FIFE (Table 5.1). The period for which the energy flux measurements were available corresponds to a growing season. We assume a linear relationship between leaf area index, canopy roughness and vegetation height, which was measured. The leaf area index was set to 0.5 for emerging plants and to 3.0 at the full development. This relationship is in agreement with field measurements at SAMER site 5 (Ben Mehrez *et al.* 1992). In both FIFE and HAPEX-MOBILHY simulations, vegetation parameters were set to those used by Dawes *et al.* (1997), given that in both experiments vegetation had C_3 photosynthesis pathways, and the sites were modelled without topographic slope.

As with any model which redistributes soil water *via* a continuity equation, a lower boundary condition must be specified. In WAVES, this is done by a user specified factor b varying between 0 and 1 times saturated hydraulic conductivity. No information was available in this regard for either field experiment. This boundary condition was estimated to give stable soil water profiles in the HAPEX simulations; this equated to a potential deep drainage rate of 0.1 mm day^{-1} when the lower boundary is saturated. The same value was used in the FIFE simulations.

5.1.4 Comparison with field measurements

a. Net radiation

The net radiation for ground surface and vegetation canopy was simulated by WAVES. For most applications, the downward longwave radiation is not routinely measured. As a result, it was calculated from air temperature and vapour pressure using Stefan–Boltzman's equation. The input required for estimating net radiation are the incoming solar radiation, air temperature and vapor pressure. Fig. 5.1 shows the comparison of calculated and measured net radiation for FIFE and HAPEX-MOBILHY. The correlation coefficient was 0.96 and the best fit slope through the origin was close to unity. The root mean square error (RMSE) was 20 W m^{-2} for the two experiments. It is clear that in both cases the model produced good estimates of It should be mentioned that in the calculation, the surface emissivity was set to a constant value of 0.97 and the atmospheric emissivity was calculated as a function of air temperature and vapor pressure. Brutsaert (1982) showed that equation (22) tends to yield smaller values of atmospheric emissivity compared to empirical equations when the vapor pressure is less than 12.0 hPa. As a result, by using this relationship the net radiation could be underestimated. In the calculation the atmospheric emissivity was corrected according to Brunt (1932) for vapor pressure less than 12.0 hPa.

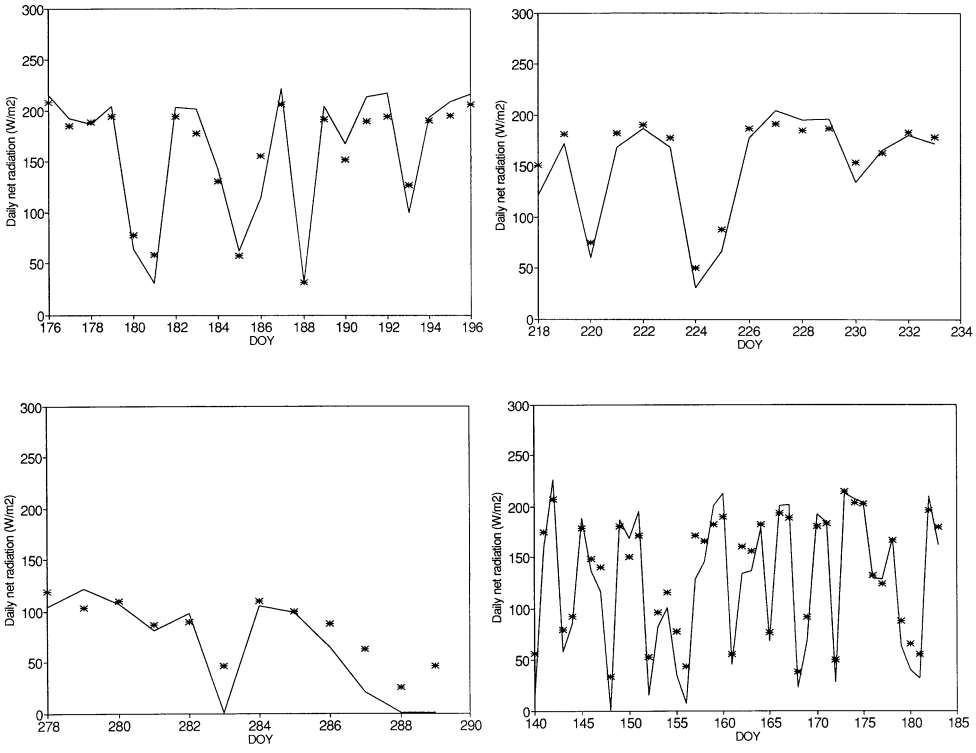

Fig. 5.1. Comparisons between simulated and observed daily net radiation during the periods of three IFCs in FIFE and SOP in HAPEX-MOBILHY. The correlation coefficient for FIFE data is 0.96 and the mean slope through the origin is 1.00. For HAPEX-MOBILHY data, the correlation coefficient is 0.96 and the mean slope through the origin is 0.97.

b. Total Evapotranspiration

Fig. 5.2 shows comparisons of the simulated and observed evapotranspiration for FIFE and HAPEX-MOBILHY for the same sites and time periods as for the net radiation in Fig. 5.1. For FIFE, the overall correlation coefficient was 0.93, the best fit slope through the origin was 1.01, and the RMSE was 0.5 mm day $^{-1}$ of average measured evapotranspiration of 3.3 mm day^{-1}. For HAPEX-MOBILHY, the correlation coefficient was 0.93, the best fit slope through the origin was 0.98, and the RMSE was 0.6 mm day^{-1} of average measured evapotranspiration of 4.0 mm day^{-1}. The total evapotranspiration estimated during the period of simulations was 159 and 172 mm for FIFE and HAPEX-MOBILHY, respectively. For the same periods, the measured total evapotranspiration was 163 and 176 mm. It is clear that the values of simulated evapotranspiration were in good agreement with the observations. It can be noted that the model performance deteriorated on day 232 and 233. Inspection of the meteorological data did not indicate why the measured evapotranspiration should be high on these two days.

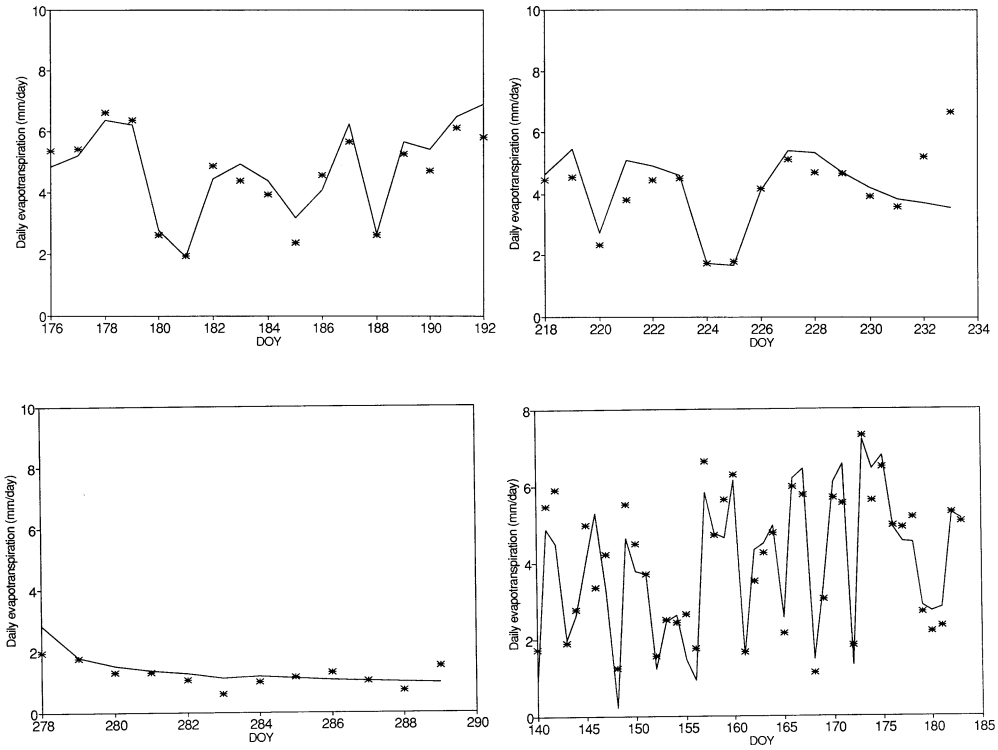

Fig. 5.2. Comparisons between simulated and observed evapotranspiration during the periods of three IFCs in FIFE and SOP in HAPEX-MOBILHY. The correlation coefficient for FIFE data is 0.93; the mean slope through the origin is 1.01. For HAPEX-MOBILHY data, the correlation coefficient is 0.93 and the mean slope through the origin is 0.98.

During the period of IFC2 and IFC3, the canopy resistance was small and the canopy was weakly coupled to the atmosphere with Ω equal to 0.7. The vapor pressure deficit of the canopy surfaces tended toward a local equilibrium value. The equilibrium value of the vapor pressure deficit

depends on the net radiation and the canopy resistance in such a way that the actual evapotranspiration approaches an equilibrium evapotranspiration rate, which was independent of canopy resistance.

Energy supply was the most important regulator of evapotranspiration. On the other hand, the values of canopy resistance for IFC4 and HAPEX-MOBILHY were relatively large and the

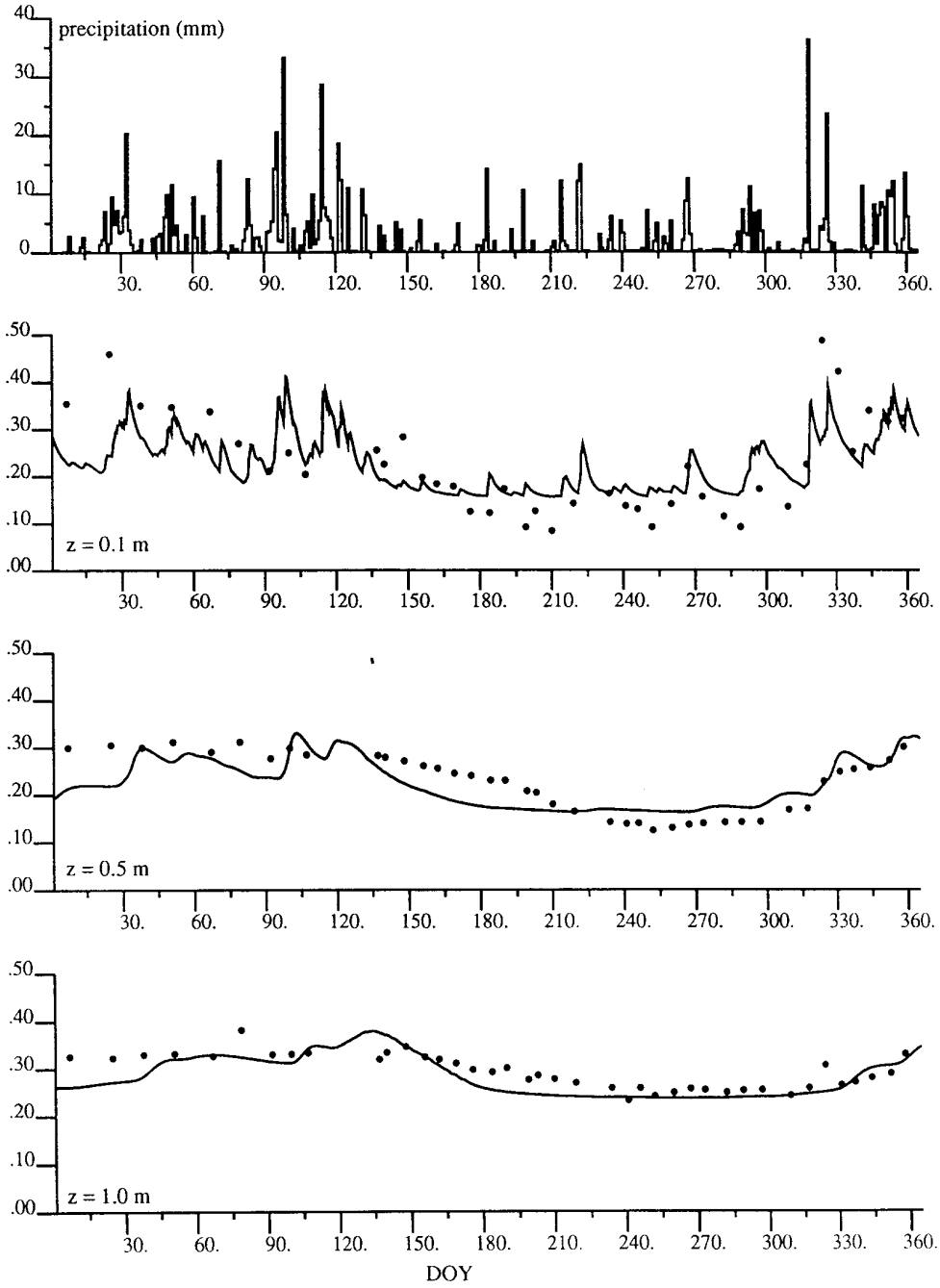

Fig. 5.3. Time course of predicted (solid line) and observed (dots) soil moisture content at SAMER site 3 for the period of January to December 1986 at three different depths.

canopies were moderately coupled to the atmosphere with W equal to 0.4. The evapotranspiration was jointly controlled by the net radiation, the vapor pressure deficit and the canopy resistance. These results showed that WAVES is capable of realistic simulation of evapotranspiration under a variety of conditions.

c. Soil moisture content

Fig. 5.3 shows the comparison between measured and simulated soil moisture content for various depths at SAMER site 3. Both the model simulations and the observations showed similar seasonal variations in the soil moisture content. In the top soil layer, the soil moisture content fluctuated strongly mainly due to precipitation. The model results showed smaller fluctuations in the soil moisture content than the measurements and the minimum soil moisture content was slightly overestimated. Model simulations of the soil moisture content at the depths of 50 cm and 100 cm were better than those near-surface simulations. In general, the calculated soil moisture agreed well with the observations considering the length of the simulation, the limited information on soil hydraulic properties, and the lack of any data regarding the lower boundary condition. The very low fitted values of b suggests that soil hydraulic properties change dramatically with depth not far below the lower boundary of the modelled region, so that there is most likely some error in assuming a homogeneous soil above this boundary.

5.1.5 Drydown process – A numerical simulation

The results in the previous sections showed that the WAVES model accurately simulated daily net radiation, evapotranspiration and soil moisture contents. Given the complexity of processes and their interactions under natural conditions, such as FIFE and HAPEX-MOBILHY, these results convey little understanding of the system behaviour and the testing of physical models, such as WAVES, *in toto* can obscure the specific behaviour associated with the processes represented. It is important to understand the roles of individual processes, and to investigate interactions between very few processes at a time. It is therefore useful to examine model performance under idealised or simplified conditions, and compare the output against expectations generalised from the literature. Specifically, it is revealing to test the model's behaviour over a period in which the soil is only drying.

The numerical simulation was designed with constant atmospheric forcing with zero precipitation. Two types of soil were considered: sandy loam and clay. The depth of the soil layer was assumed to be 1.0 m with a single C_3 vegetation layer on the top. The model was run for each soil type with initial soil moisture content set to saturation using an impermeable lower boundary condition (b = 0.0).

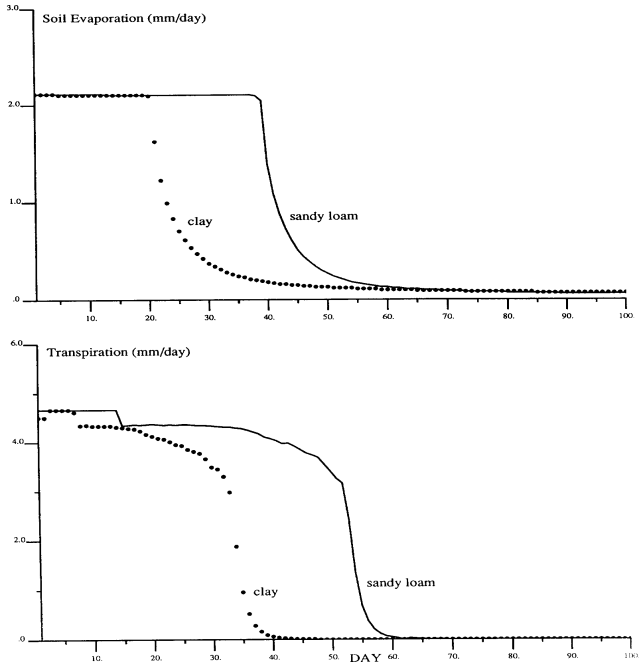

Fig. 5.4. Daily values of soil evaporation (top) and transpiration (bottom) during a 100-day simulation of the drying of initially saturated clay and sandy loam soils.

The temporal variations in the calculated soil evaporation and transpiration are shown in Fig. 5.4. It is clear that the model showed a two-stage soil evaporation process. In the first stage, the soil was wet and evaporation was controlled by the atmospheric demand. As a result, soil evaporation occurred at the potential rate (constant in this experiment). The duration of stage 1 soil evaporation depended on the hydraulic properties of the soil and lasted longer for sandy loam than for clay soils. Second-stage (soil limited) evaporation was mainly controlled by the hydraulic properties of the soil and the evaporation rate fell below the potential rate on the third day of the stage 2 drying process. The cumulative soil evaporation versus the square root of time was almost linear (Fig. 5.5).

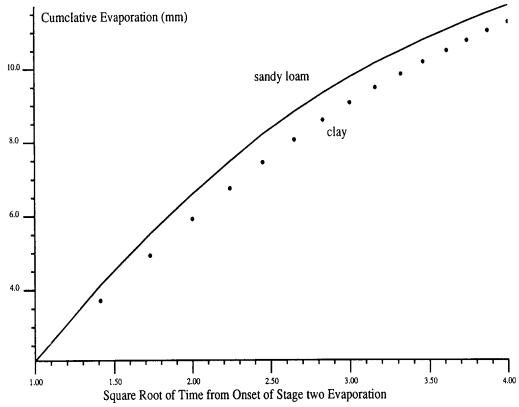

Fig. 5.5. Stage 2 cumulative soil evaporation as related the square root of time for clay and sandy loam soils.

The transpiration from WAVES showed a two-stage drying process as well: in the first stage, transpiration decreased gradually and in the second stage transpiration decreased rapidly. The stage 1 transpiration lasted longer than stage 1 soil evaporation (Fig. 5.4) since the vegetation can remove water from deeper soil. The presence of a canopy extended the period of stage 1 evaporation by several days compared with a bare soil surface and much less water was removed from the near soil surface. However, the period of the second stage of drying was significantly shortened.

As outlined in Chapter 2, the model calculates the saturation vapor pressure deficit of the canopy, which depends on degree of coupling between the canopy and the atmosphere, and the net radiation received by the canopy. For this numerical simulation, the decoupling coefficient (0.9) indicated a weak coupling between the canopy and the atmosphere. The vapor pressure deficit of the canopy was reduced by 7 hPa during the period of plant transpiration and increased to the prescribed vapor pressure deficit when the transpiration stopped.

5.1.6 Discussion

A complex, biophysically based ecohydrological model such as WAVES is a potentially useful tool for testing ideas about system behaviour as well as for generating predictions about how the surface energy and water balance might change following manipulations of the system. In Australia, the absence of field observations of landscape behaviour across the large range of physical, biological and management combinations, and the huge expense and delay in acquiring these observations, strongly argue for such a tool. While we recognise and agree with the philosophical concerns raised by ourselves (Hatton *et al*. 1994) and others (Beven 1989, Wheater and Jakeman 1993) regarding the danger of such exercises, the real and urgent need for advice on optimal land use is compelling. We also recognise the obligation to test such tools, as thoroughly as possible, against theoretical and observed behaviour. The FIFE and HAPEX-MOBILHY data offer an extraordinary opportunity to test the surface energy and water balance components of WAVES.

In general, the model closely reproduced field observations of the surface energy and water balance, and produced results consistent with theoretical expectation. Given only daily solar radiation and air temperature as climatic inputs, the model accurately predicted net radiation. This is a significant feature for models of this kind; many such treatments of the surface energy balance require net longwave as an input (e.g., Dickinson *et al*. 1986, Sellers *et al*. 1986) or use net radiation directly (Choudhury and Monteith 1988). Neither of these latter quantities is normally available across Australia.

Predicted daily total evapotranspiration compared well with observed values from the FIFE and HAPEX-MOBILHY experiments. It is significant that the daily time-step of WAVES, using mean daily values for wind speed, temperature and vapour pressure deficit, could reproduce the

summed sub-hourly measured fluxes. This is a crucial feature for any physical water balance model intended for application in Australia as standard meteorological data is limited to daily resolution. Note that the model error in evaporation is well within the stated error of measurement for the HAPEX-MOBILHY data. For the FIFE experiment in particular, the model was capable of reproducing evaporation rates ranging from 1 mm d^{-1} under conditions of senescing vegetation and limiting soil moisture to 7 mm d^{-1} under high radiation, leaf area index and soil moisture. This suggests that the calculation of surface resistance by means of the modified Ball *et al*. (1987) model (Leuning 1995), using the IRM assimilation model (Wu *et al.* 1994), can account for multiple factors limiting conductance.

In the formulation of evapotranspiration, the effect of boundary layer resistance is neglected. Shuttleworth and Wallace (1985) showed that measurements of mean boundary layer resistance generally have significant scatter and the bulk boundary layer resistance is much smaller than the corresponding aerodynamic resistance; in addition the combination equation is rather insensitive to the boundary layer resistance. The good agreement between calculated and measured evapotranspiration seem to support this assumption. Another approximation made in the WAVES model is to ignore the effect of atmospheric stability on the aerodynamic resistance. This assumption leads to underestimation (overestimation) of the aerodynamic resistance when the atmosphere is in unstable (stable) conditions. Moreover, it has been found that the Penman–Monteith equation is relatively insensitive to the aerodynamic resistance when the surface roughness length is small (Zhang and Dawes, 1995). As a result, the effect of atmospheric stability correction can be neglected. For the surface conditions in FIFE sites and the agricultural part of HAPEX-MOBILHY, the results indicated that the effect of the atmospheric stability is negligible. However, for rough surfaces (e.g., forest) ignoring the atmospheric stability may cause large errors in the calculated evapotranspiration.

There was insufficient information available from either experiment to allow direct comparisons of the contribution of transpiration and soil evaporation. The numerical results from the dry-down simulations, indicating a two-stage soil evaporation process with fluxes limited initially by energy, is consistent with field measurements (Ritchie 1972). During the second stage of soil evaporation, the hydraulic properties of the soil play a more significant role than the atmospheric demand. Black *et al*. (1969) showed that cumulative evaporation is linearly related to square root of the time from the start of the second stage evaporation. The relationship has been supported by field measurements of evaporation (LaRue *et al*. 1968; Ritchie 1972). The model shows this behaviour.

In terms of plant transpiration, the WAVES model determines the relative carbon assimilation rate which is related to the canopy resistance based on the matric potential of the soil water rather than the water content. This treatment allows plant to transpire freely until all the water in root

zone is extracted. The simulated transpiration also showed a two stage process. The stage 1 transpiration lasted longer than the stage 1 soil evaporation, while the stage 2 transpiration decreased more rapidly. These results indicated that transpiration is maintained by deep soil water through plant roots.

During the period of FIFE IFC2 to IFC3, simulated transpiration accounted for about 85% of the total evapotranspiration, while for IFC4 the transpiration component decreased to 60%. Fractional vegetation cover determined from LAI and canopy height using the method of Smith *et al*. (1993) was 0.94, 0.86 and 0.45 respectively for the three FIFE periods and it seems that the transpiration ratios maybe related to the fractional vegetation covers; this is consistent with the findings of Smith *et al*. (1993). For HAPEX-MOBILHY, the transpiration ratio increased from 60% to 86% as the fractional vegetation cover changed from 0.5 to 0.9.

The simulated soil moisture profiles for the HAPEX-MOBILHY experiment were consistent with observations. However, water content at the shallowest soil depth shows large temporal variation and is inherently difficult to model; the seasonal trends are reproduced, but the predicted value on any particular day may be in significant error. The two deeper times series of moisture are modelled better, but show less temporal variation to challenge the model. Therefore, we cannot consider this aspect of the model to be adequately tested in this study. It must be noted that the model results for the HAPEX-MOBILHY experiment were sensitive to the soil hydraulic properties and the lower boundary condition. This finding confirms the sensitivity analysis of the model (Hatton *et al*. 1995). These quantities are, in any practical sense, unknowable across a landscape. This is a serious limitation to wide geographic application of models requiring this information, but this is a feature common to any soil water balance model.

5.1.7 Summary

The WAVES model was tested using the data obtained from FIFE and HAPEX-MOBILHY experiments. Generally, it was found that the model is capable of accurately simulating daily total net radiation, evapotranspiration, and soil moisture content under different weather and canopy conditions with a reasonable degree of realism. A numerical experiment was carried out to investigate the model's performance under soil drying conditions. The model produced a two stage soil evaporation process as has been previously observed. Stage one soil evaporation proceeds at the potential rate. In the second stage, the soil evaporation falls below the potential rate and the cumulative evaporation versus the square root of time is almost linear. These results are consistent with theoretical expectation. For practical purposes, the model does not consider the effect of atmospheric stability on the aerodynamic resistance and an equivalence between radiative surface temperature and air temperature is assumed in the model. These simplifications do not seem to have degraded model predictions

The WAVES model can be used in its present form to identify important surface characteristics and to study hydrological responses under various land management practices. Practical applications of the model to real catchments are limited by the large number of the parameters on soil and vegetation properties, some of which are difficult to obtain in practice. Nevertheless, we assert that the model strikes a reasonable balance between generality, realism and accuracy, and provides a powerful tool for the prediction of landscape behaviour.

Acknowledgments

The authors would like to thank F.G. Hall (NASA), R.E. Murphy (NASA), T.J. Schmugge (USDA), and P.J. Sellers (NASA), without whose initiative and leadership FIFE experiments would not have been possible. The contributions made to FIFE by a large number of investigators and support provided by D.E. Strebel and the FIFE Information System (FIS) for accessing FIFE data are acknowledged. The authors would also like to express their gratitude to J.C. André, J.P. Goutorbe and A.P. Perrier without whose initiative and organization, the HAPEX-MOBILHY experiment would not have been possible. The SAMER and soil moisture data were kindly provided by J.P. Goutorbe and J.F. Mahouf. This research has been supported and financed, in part, by the National Resource Management Strategy Grants N298 and M4066. We are grateful to H.A. Cleugh and D. Short for comments on a draft of this paper.

5.2 Modelling Water and Salt Movement on the Chowilla Floodplain

W. R. Dawes, P. G. Slavich, T. J. Hatton and G. R. Walker

Abstract

River level management in the lower River Murray has had a profound negative impact on native floodplain vegetation. Reduced flooding, both amount and frequency, and rising levels of naturally saline groundwater have lead to salinisation of the soil and the subsequent reduction of tree density and health. To develop management guidelines there is a need to understand the effect of different flooding and watertable conditions on vegetation growth and salinisation processes.

Field studies of vegetation water use during and after a flood were used to calibrate a physically based soil–vegetation–atmosphere transfer model (WAVES). The model parameterisation was tested using long term simulations which also give insight into the development of dieback. Observed water content and chloride profiles have been reproduced after a flood event and after a drying cycle. Soil hydraulic properties were set initially using limited field measurement and soil textural descriptions. There is confidence in this approach, since calibrated parameters show remarkable consistency across five sites, with varying leaf area, groundwater depth, and time and depth of flooding. The calibrated model can be used to explore the effect of river management scenarios on existing riparian vegetation.

5.2.1 Introduction

In dry areas of Australia, flooding can be an important source of water for riparian vegetation. Where aridity is coupled with salinity, flooding can be a critical factor in supplying fresh water and leaching accumulated salts from the root zone. The native floodplain vegetation in the lower River Murray has declined in health as a result of river level management over the last few decades. A system of reservoirs and weirs (locally known as locks) was installed along the river during the 1920s to regulate the river flow for reliable year round water supply and navigation. The decline in the number of medium-sized floods has reduced salt leaching, and the installation of locks has resulted in raised saline watertables (Walker *et al.*, 1996). Guidelines for river and

groundwater management to control soil salinisation at sites along the river are currently being developed. Margules and Partners *et al.* (1990) estimated that approximately 180 km^2 of floodplain along the River Murray is severely degraded, of which 53% has saline groundwater identified as the major cause of degradation.

The time scales for soil salinisation can be used to establish simple management guidelines and have been estimated using a steady state groundwater discharge model (Jolly *et. al.*, 1993). More complex physically based models which describe soil–vegetation–atmosphere transfers (SVAT models) can be used to increase understanding of the interactions between the vegetation growth and water use and processes affecting the movement of water and salt, and can explicitly take into account changed vegetation and river level management. Guidelines based on simple steady state models also need to be evaluated using more complex SVAT models.

This section describes the first stage in attempting to understand the interactions between vegetation and soil salinisation processes occurring on the Chowilla floodplain in the lower Murray River. Field data from a number of sites representing the range of floodplain conditions are used to calibrate the SVAT model WAVES (Dawes and Short, 1993). The hydrological responses of the sites to flooding is analysed in some detail, vegetation health is related to long-term flooding history, and is shown that it may be used to better predict the impacts of changed flood management.

5.2.2 Site Description

The study region is the Chowilla anabranch, a 200 km^2 area of semi-arid saline floodplain on the Lower River Murray, located on the South Australia–New South Wales border of Australia (Fig. 5.6). Jolly and Walker (1995) provide an excellent overview of the hydrology, hydrogeology, vegetation, and management problems of the area. Briefly, the area consists of a network of streams which flow from the River Murray upstream of Lock 6, across the floodplain before joining into Chowilla Creek, and discharging back into the River Murray downstream of Lock 6. Before the installation of the lock, these streams were ephemeral and flowed only in times of flood; they now carry up to 80% of the River Murray flow. This is an excellent study region for the following reasons: (1) there has been a significant body of data collected in the region during investigations for a proposed dam, and salt interception schemes, (2) it is the site of the second-largest natural salt load to the River Murray, approximately 50 000 t yr^{-1} (Walker *et al.* 1996), and (3) it is a wetland of international significance listed under the UNESCO Ramsar Convention (Section 14.5) (NEC 1988).

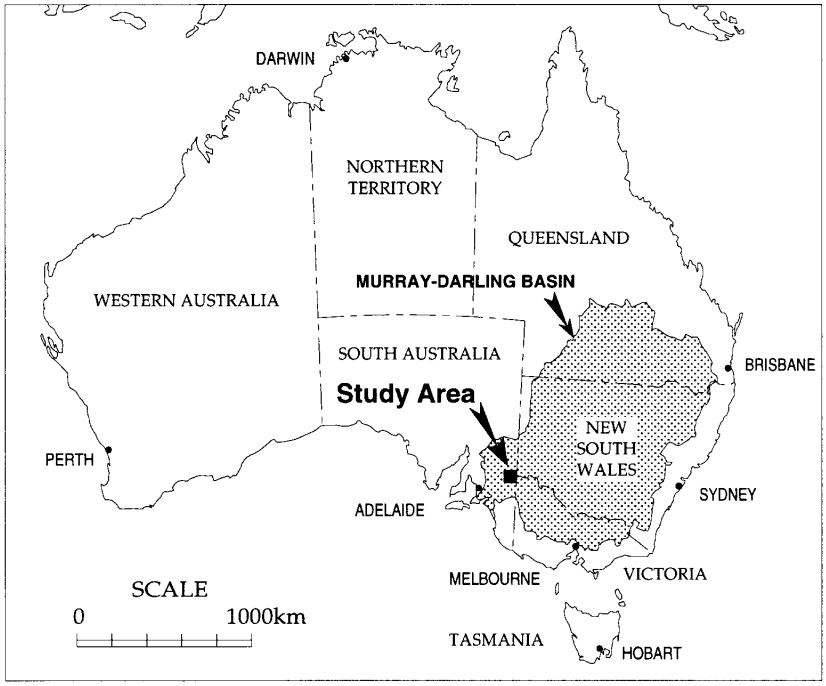

Fig. 5.6. Experimental site location map.

The Chowilla region has a semi-arid climate with annual average rainfall of approximately 250 mm yr^{-1}. This annual volume is highly variable, ranging from 100 to 500 mm yr^{-1}. Average annual potential evaporation is around 2000 mm yr^{-1} (Jolly *et al.* 1993). The composition and distribution of vegetation at Chowilla has been described by O'Malley (1990). The dominant species are the trees black box (*E. largiflorens* F. Muell.) and river red gum (*E. camaldulensis*), the shrub lignum (*Muehlenbeckia cunninghamii*), and large areas of annual grass. The distribution of these species is controlled by flood frequency, which is related to surface elevation, and groundwater salinity. Black box is located on higher areas of the floodplain, redgums occur generally along stream and creek courses, and lignum is found on clay fan features adjacent to streams. In this work we concentrate on black box, as it is the predominant species, and is known to be adversely affected by current river management (Margules and Partners *et al.*, 1990).

The soils of the Chowilla floodplain have been described by Hollingsworth *et al.* (1990). They consist generally of a layer of alluvial grey cracking clay, known as Coonambidgal Clay, up to 5 m deep, overlying an unconsolidated alluvial sand deposit, known as Monoman Sand, approximately 30 m deep. The boundary between these layers is often unclear, with transitional material of varying clay content up to 1 m thick. Groundwater levels have risen since the installation of Lock 6, from the Monoman Sand formation to between 2 and 4 m from the surface in the Coonambigdal Clay.

The hydrology of the area is described by Jolly and Walker (1995). Briefly, the frequency of medium-sized floods has decreased to about one third of natural conditions as a consequence of

development of upstream storages. Black box trees are generally found in areas where the mean return period of floods is greater than 8 years. Enhancement of floods for environmental purposes is possible by the release of water from two nearby storages, Lake Victoria and Menindie Lakes.

5.2.3 Monitoring sites

From a survey of vegetation health on the Chowilla floodplain, large scale spatial patterns of health were found to correlate with flooding frequency, groundwater depth, and groundwater salinity (O'Malley, 1990; Taylor *et al.*, 1996). Vegetation health was poorest in areas with infrequent flooding, and shallow high salinity groundwater tables. Where groundwater was fresher, or more frequently flooded, or on higher ground, vegetation health was significantly better. The variables were entered as layers into a Geographic Information System (GIS) and five broad categories were identified. Five study sites, representing each of the GIS classes, were chosen for monitoring. Soil profiles were sampled in September 1993, before a flood which occurred in November and December, just after the flood in January 1994, and in April 1994 after a three month drying period (McEwan *et al.*, 1995). Soils were analysed for gravimetric water content (kg/kg) and water-soluble chloride. This sampling gave the widest possible range of moisture and soil-water salinities for model calibration. These sites are samples only, and may not be representative of the whole of the class, and each class should not be seen as homogeneous.

Four broad soil-texture groups based on clay content (Table 5.2) were identified on the floodplain and were used to characterise soil horizons both across and within the sites. The depth of each soil horizon was estimated from field sampling, and examination of the gravimetric water content profiles.

Table 5.2. Four soil textural classes observed as soil horizons at calibration sites.

Texture Code	Clay %
T1	< 15
T2	15 – 30
T3	31 – 45
T4	> 45

5.2.4 Recorded data

The monitoring period for data analysed in this paper was the six months from October 1993 to April 1994. Soil profiles were sampled from each site in October before a flood, in January immediately after the flood, and in April after a long dry period. Water content was determined gravimetrically, matric potential was determined by the filter paper method, and chloride content was determined by 1: 5 soil paste extracts.

Daily values of maximum and minimum temperature, average vapour pressure deficit, rainfall and total radiation were obtained from an automatic weather station at the site and one at Loxton. These data were used in WAVES to estimate evaporation and transpiration demand at each site. The watertable was logged for the duration of the monitoring period using capacitance probes at each site. Transpiration was measured using the heat pulse method (Swanson and Whitfield, 1981; Green and Clothier, 1988) for several weeks at a time over the larger monitoring period. The complete dataset description can be found in McEwan *et al.* (1995).

Four of the five sites, sites S1, S3, S4, and S6, had saline groundwater. The salinity of the groundwater used in WAVES was set to that measured in soil-water extracts from just above the watertable. Site S5, however, showed significant leaching of salt below the groundwater surface, and so fresh water, with salinity of 0.004 dS m^{-1} (equal to rainfall), was used at this site. This site is closer to a creek than the other sites, and we hypothesise that fresh creek water is flushing from below during and after the flood.

Table 5.3 Values and units of vegetation growth and response parameters for Black box.

Description	Value	Units
Canopy albedo	0.1	–
Soil albedo	0.15	–
Rainfall interception coefficient	0.001	m LAI^{-1} d^{-1}
Light interception coefficient	–0.42	–
Maximum carbon assimilation rate	0.01	kg C m^{-2} d^{-1}
Canopy conductance model slope value	0.7	–
Maximum plant available soil water potential	–350	m
IRM weighting of water relative to light	1.13	–
IRM weighting of nutrients relative to light	0.3	–
Temperature when growth rate is half optimum	10	°C
Temperature when growth rate is optimum	20	°C
Saturation light intensity	1200	μmoles m^{-2} d^{-1}
Specific leaf area	12	m^2 kg^{-1}
Salt sensitivity factor	1.0	–
Aerodynamic resistance	20	s m^{-1}

The vegetation parameters required by WAVES were set using a combination of literature (Hodges, 1992; Hatton and Dawes, 1993) and measured values (Table 5.3). The maximum plant-available soil-water potential was set from seasonal observations of predawn leaf-water potentials (Eldrige *et al.*, 1993). Predawn leaf-water potentials were measured using a pressure bomb and

diurnal changes in stomatal conductance by porometry. WAVES does not calculate canopy aerodynamic resistance (r_a) dynamically, and the constant value in Table 5.3 corresponds to a wind speed of 1–2 m s^{-1} at 2 m above a canopy height of 6–12 m. The static leaf area index was estimated by Taylor (1993) as 0.23, 0.29, 0.28, 0.42, and 0.19 for sites S1, S3, S4, S5, and S6 respectively.

The flood depth and duration were measured using the depth of water in the river at Lock 6. The five monitored sites are at different elevations and were flooded for 17, 30, 78, 61, and 14 days respectively.

5.2.5 Model Calibration

All calibration was done manually, *i.e.* software that optimizes parameters for a least squares or other error criteria was not used. The calibration approach required a compromise between the degree a parameter could be adjusted for an individual site, and the degree of parameter variation across sites. Parsimony was also exercised when estimating the number of distinct soil layers within each soil profile.

For λ and C, a simulation was run and their values were adjusted until the modelled water content profiles showed the correct shape before and after the flood. This adjustment fitted the moisture retention curve, *i.e.* the ψ *vs* θ relationship, and helped to compensate for the properties of the surface clay. Fitting of K_s was done after λ and C were set. A simulation was run, and K_s adjusted, until the modelled salt fronts moved the observed distance after the flood.

The calibrated values of soil hydraulic parameters are given in Table 5.4. The calibrated values of λ and C were physically sensible, *i.e.* larger for the horizons with higher clay content. One of the more encouraging aspects of the work is the general consistency of the calibrated soil hydraulic parameters across the five sites, each with different leaf area, watertable level dynamics, and flood duration. We are therefore confident that the soil hydraulic properties are representative of the soils in the area of the observation sites.

There was good agreement in general between the measured and modelled profiles before and after the flood (Figs. 5.6 to 5.11 for sites S1, S3, S4, S5 and S6 respectively). However, the modelled salt in the 0–1 m layer in particular, was less than observed. This suggests that the leaching process in this layer is relatively inefficient and that not all the solute is readily mobile. This is not unexpected in aggregated clay soils. The assumption explicit in using Richards' equation that the soil matrix is rigid is inappropriate in the surface cracking clay, and will contribute to the enhanced modelled leaching.

Table 5.4. Calibrated values of BW parameters for each soil horizon at each site.

Depth m	Texture Code	K_s m day^{-1}	θ_s	θ_r	λ m	C
Site 1						
0.0–0.6	T3	0.006	0.36	0.1	0.5	1.05
0.6 +	T2	0.006	0.36	0.1	0.3	1.04
Site 3						
0.0–0.7	T4	0.002	0.4	0.1	1.0	1.10
0.7–1.0	T3	0.006	0.36	0.1	0.5	1.05
1.0–1.4	T2	0.006	0.36	0.1	0.3	1.01
1.4 +	T1	0.05	0.36	0.05	0.2	1.01
Site 4						
0.0–0.6	T3	0.002	0.36	0.1	0.5	1.04
0.6–0.9	T4	0.002	0.45	0.1	1.0	1.10
0.9 +	T1	0.05	0.36	0.05	0.2	1.01
Site 5						
0.0–0.6	T4	0.002	0.5	0.1	1.0	1.10
0.6–0.8	T2	0.003	0.4	0.1	0.5	1.05
0.8 +	T1	0.05	0.36	0.05	0.2	1.01
Site 6						
0.0–0.3	T3	0.002	0.45	0.1	0.6	1.10
0.3–0.75	T4	0.002	0.45	0.1	1.0	1.10
0.75–1.8	T3	0.002	0.45	0.1	0.5	1.10
1.8 +	T4	0.002	0.45	0.1	1.0	1.10

The plant growth model had two fitted parameters. The slope parameter g_1 was calibrated to give good results on measured transpiration rates and soil-water profiles. The leaf carbon partitioning factor was calibrated to give a realistic range of leaf mass consistent with that observed for the 25 year simulations. Fig. 5.12 shows measured and modelled rates of transpiration at Site 1, from October 1993 to March 1994. While we expect the magnitude of transpiration to be right, the figure shows the model feedbacks reproduces well the changes in transpiration rates due to the flood event, and changing season.

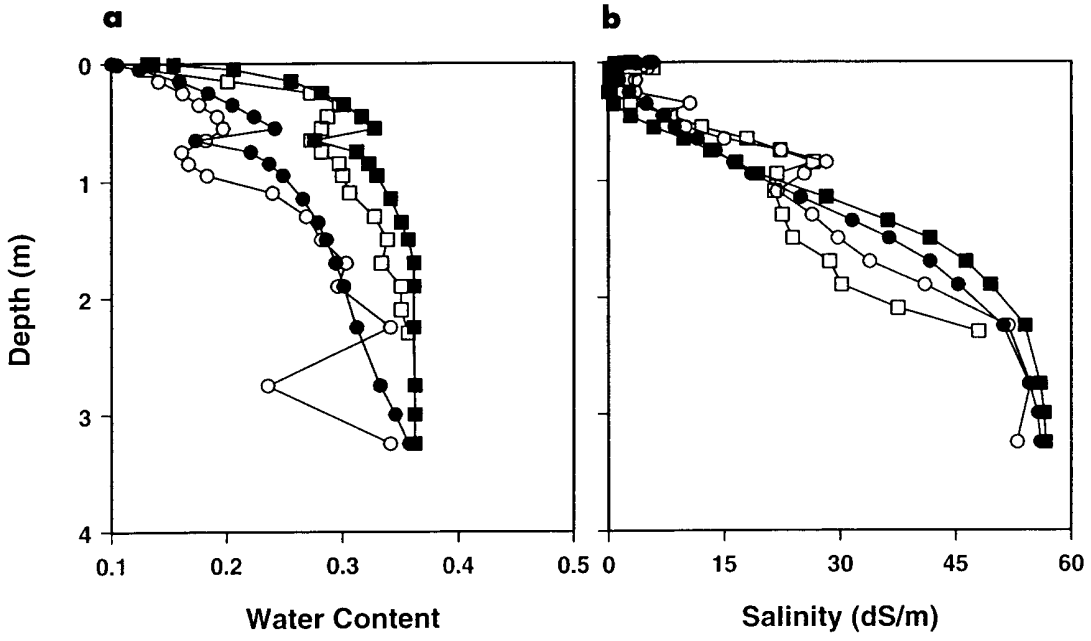

Fig. 5.7. Observed (open symbol) and predicted (filled symbol), (a) water and (b) salt profiles, from Site 1, for pre-flood (circles, January 1994) and post-flood (squares, April 1994) conditions.

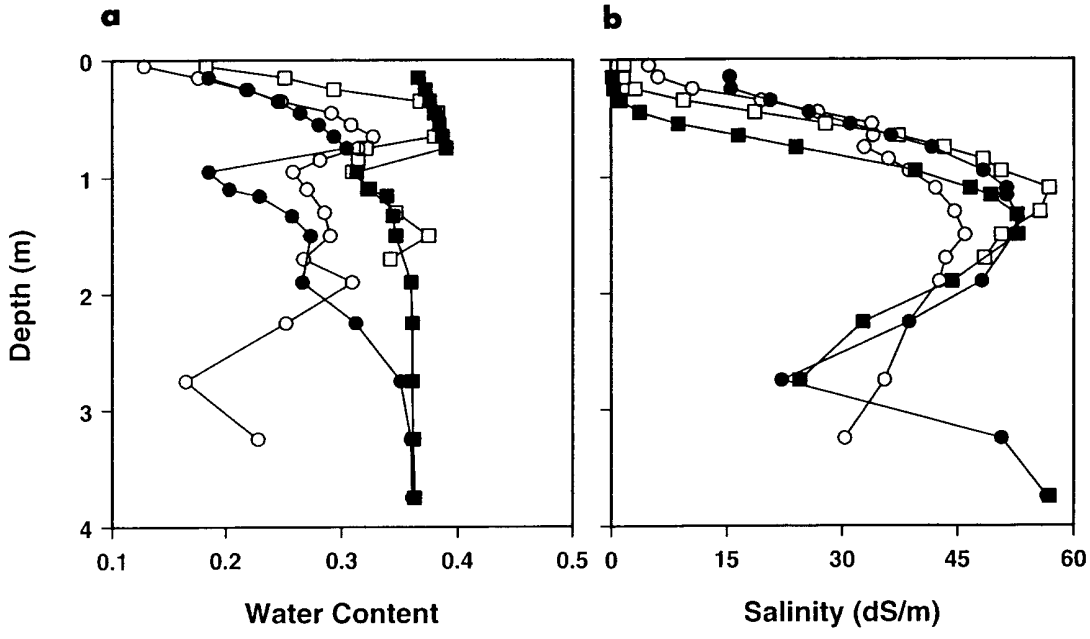

Fig. 5.8. Observed and predicted, (a) water and (b) salt profiles, from Site 3, for pre-flood (January 1994) and post-flood (April 1994) conditions.

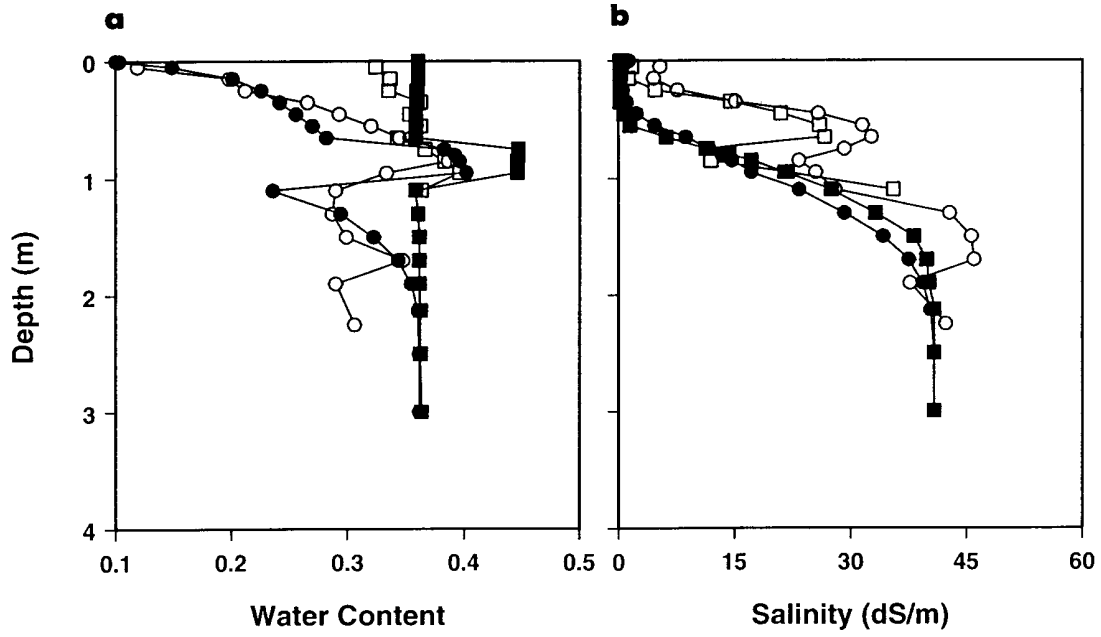

Fig. 5.9. Observed and predicted, (a) water and (b) salt profiles, from Site 4, for pre-flood (January 1994) and post-flood (April 1994) conditions.

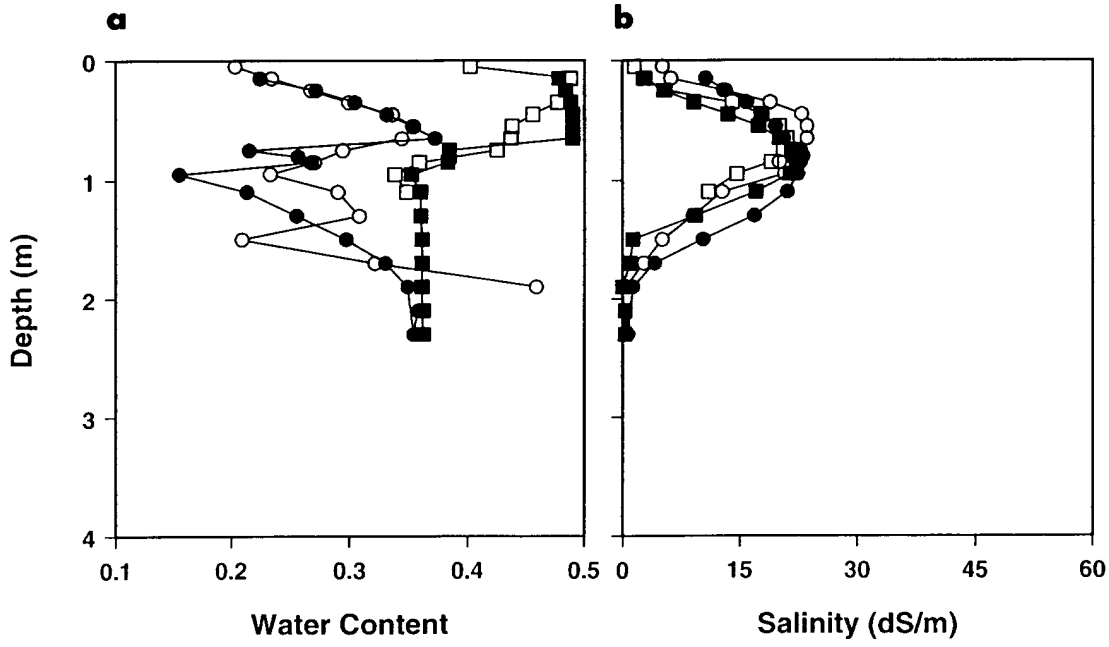

Fig. 5.10. Observed and predicted, (a) water and (b) salt profiles, from Site 5, for pre-flood (January 1994) and post-flood (April 1994) conditions.

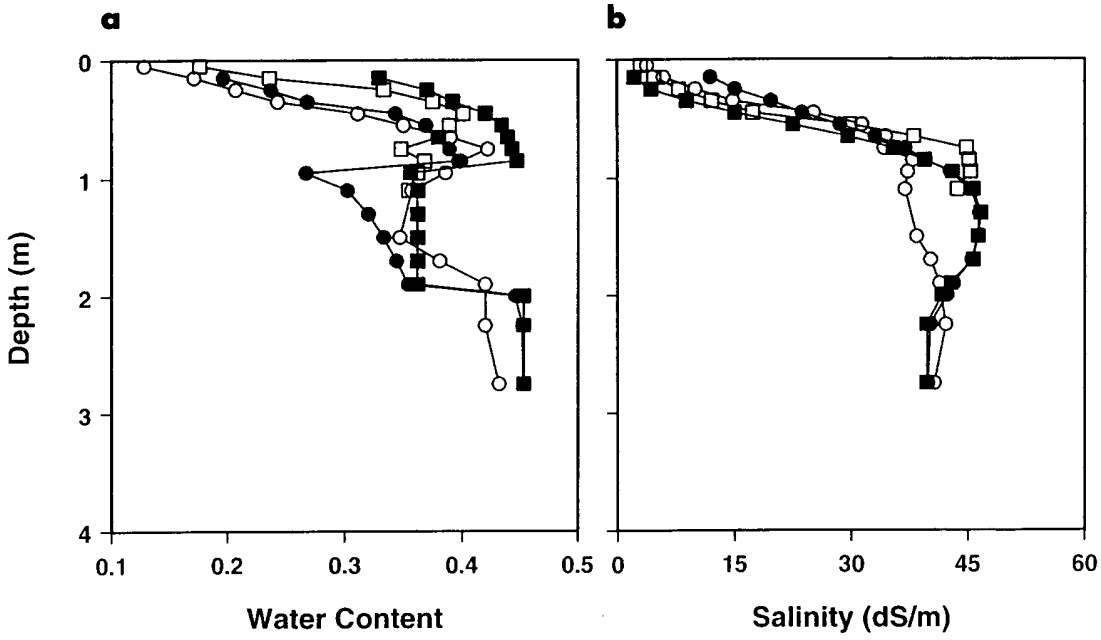

Fig. 5.11. Observed and predicted, (a) water and (b) salt profiles, from Site 6, for pre-flood (January 1994) and post-flood (April 1994) conditions.

As a further test of the calibration parameters, WAVES was run with observed groundwater and climatic data until January 1995 when the sites were monitored again. Fig. 5.13 shows the observed water and salt profiles at Site 1, and the model results using the original two soil layer description and a four soil layer model. It is apparent there is a lens of material at 0.3 m with different water holding properties to the two original layers; the water content changes but the measured matrix potential does not, indicating the profile is uniformly at residual water content. There is no better agreement with salt profiles using the four layer model because the movement of salt has been halted by the absence of water to move it.

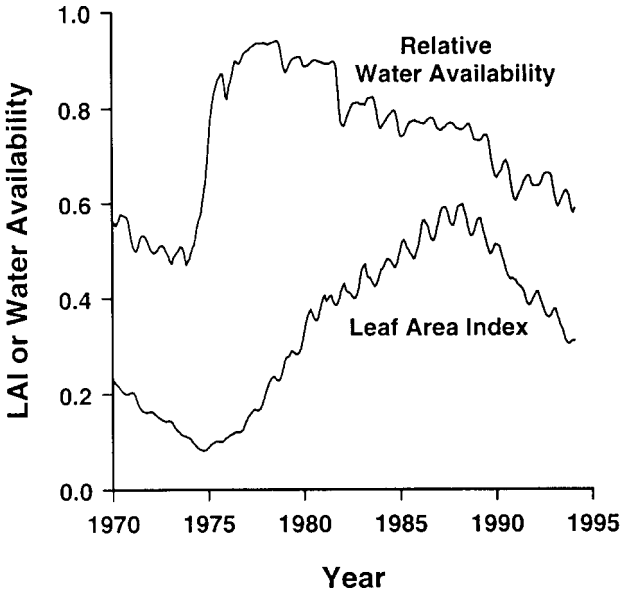

Fig. 5.12. Measured and modelled transpiration at Site 1 before and after the flood event.

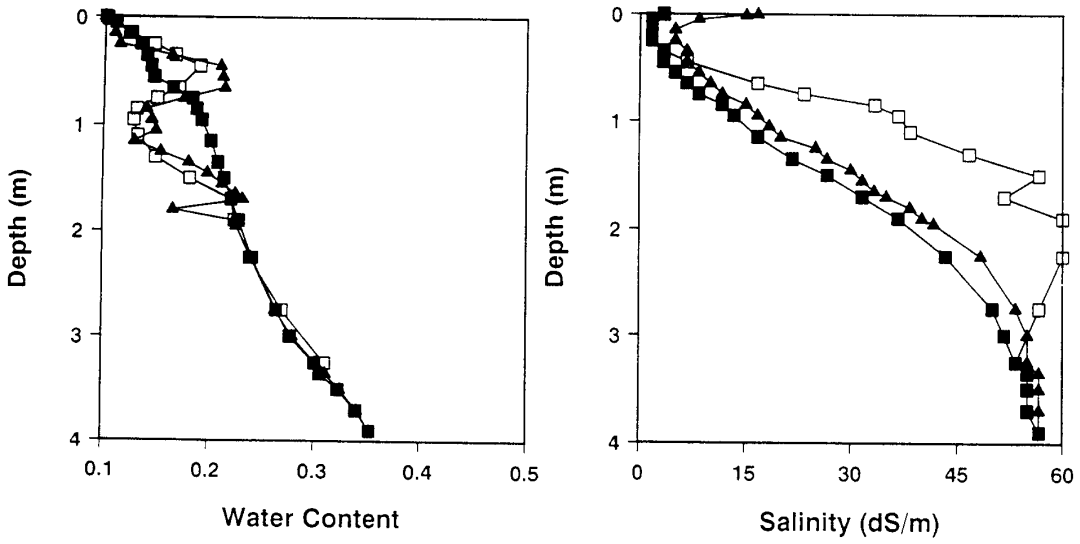

Fig. 5.13. Observed (open squares) and predicted, (a) water and (b) salt profiles, at Site 1 using two (filled squares) and four (filled triangles) soil layers for January 1995.

This does raise an important philosophical question for the modeller: what detail is required? If we are interested in short term flood dynamics to examine flood leaching events and closely matching profiles of salt and water, for example, then four layers would be appropriate. If we are interested in long term dynamics, retaining the important feedbacks and vertical detail, on longer term effects of salinisation on vegetation health, then use of two layers is adequate. We must also confront the question of the destructive nature of the sampling for salt and water profiles. The observed data approximate because of heterogeneity, so that exact matching is problematic.

5.2.6 Long Model Runs

The soil hydraulic and vegetation parameters were calibrated using a relatively short period of 180 days. The model parameters were further tested using a 25 year simulation run, from 1970 to 1995, to compare the response of the system to measured climatic and river dynamics at two sites. The long term behaviour should be consistent with field observations of vegetation decline in relation to salinity, and numerically stable. These simulations also illustrate the potential applications of the calibrated model. Sites 1 and 6 were used in the simulations, because they show strong contrast in soil type while having the same elevation and flooding extent. The main features to observe in the simulations are: (1) the development of a moving salt front from the deep watertable, which is consistent with field observation, (2) a 5 to 10 year period of vegetative decline from a shallow saline watertable; this is again consistent with field observations at shallow watertable sites, and (3) relatively long periods of consistent leaf area that drop within two years to a new level; this behaviour is consistent with Hatton and Wu (1995) who suggested that trees retain leaf area until sufficient stress has built up to necessitate a dramatic loss of leaves.

Fig. 5.14a shows the simulated leaf area and water availability scalar (used in the plant growth model) over 25 years at Site 1. Floods inundated the sites for a total of 219 days between 1974 and 1977. They are clearly shown in the water availability scalar, when much of the salt in the root zone is flushed down to the groundwater table. The water availability remains relatively high, around 80%, until 1990; this corresponds with a period of slow leaf area development. However, as salt builds up in the root zone (Fig. 5.14b), and especially in the top 2 m of soil, both water availability and leaf area show alarming decline. The only other flood of note is that in 1994 studied in this work. This site is currently rated as relatively healthy (Walker *et al.*, 1996, Ch. 10).

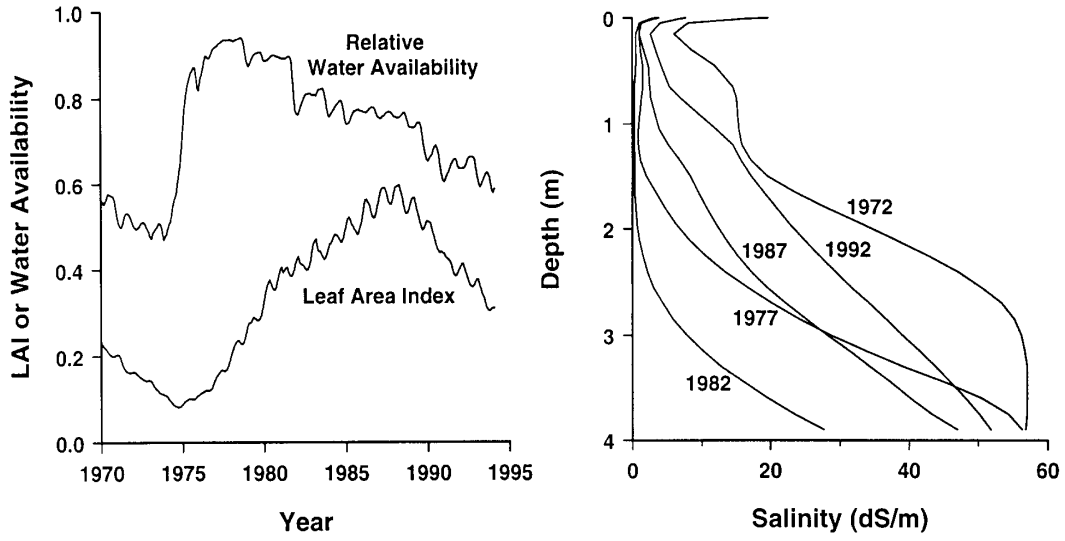

Fig. 5.14. Results of a 25 year simulation at Site 1, showing (a) water availability scalar and leaf area index, and (b) profile of soil water salinity.

Fig. 5.15a shows the simulated leaf area and water availability scalar over 25 years at Site 6. The soils at this site are heavier than Site 1, and the groundwater salinity is less. The net result is that the flood has resulted in only limited leaching of salt and only to 2 m depth. However, the consequent salt build up is mainly in the surface soil where a large bulge has developed. The leaf area and water availability graphs show little variation over the 25 years of simulation, indicating that the heavy soil acts as a buffer to both flooding and salt accumulation. Fig. 5.15b shows a salinity bulge forming in the profile between 1 and 2 m depth. This is consistent with the field observations made for the calibration exercise, and corresponds to a natural soil layer of low sorptivity at this site. Again note the steady build-up of salinity over time.

5.2.7 Comparison with other Models and Data

The hydraulic parameters shown in Table 5.4 were used to calculate maximum steady-state groundwater discharge with a watertable at 4.0m, after the method of Jolly *et al.* (1993). From Site 1, rates vary from 6.1 to 7.0 mm yr^{-1}, which compare favourably to Jolly's estimated value of

8.0 mm yr^{-1} from deuterium profiles from a bare site, and our modelled rates of 3.6 mm yr^{-1} for the vegetated site. This result is very encouraging since it was not calibrated directly: it is a result of calibrating transpiration and modelling soil-water dynamics realistically.

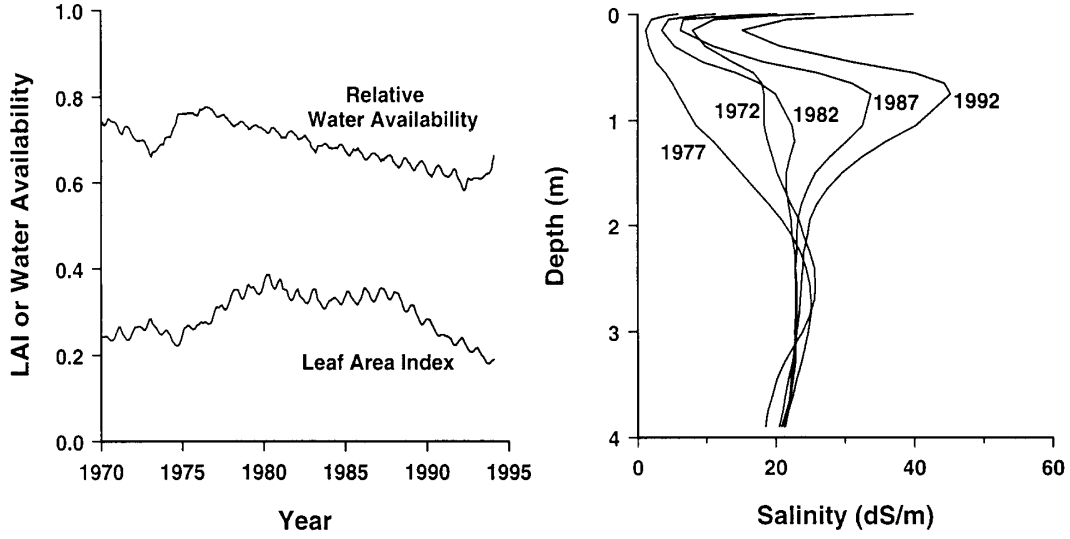

Fig. 5.15. Results of a 25 year simulation at Site 6, showing (a) water availability scalar and leaf area index, and (b) profile of soil water salinity.

The WAVES growth model requires a parameter that is the maximum proportion of gross assimilate partitioned to above-ground carbon pools, *i.e.* leaves and stems. The final actual amount is a function of this value and the water availability; less available water causes more resources to be devoted to root development. The calibrated maximum partitioning of 17% to leaves, 17% to stems, and 66% to roots is remarkably consistent with McMurtrie's (1985) partitioning of 20:20:60 for a "poor quality wooded site". Such a result shows that the internal feedbacks within WAVES reasonably represent the processes. The calibrated slope of the modified Ball *et al.* (1987) equation yielded canopy resistance of 120–4500 s m^{-1}, and averaging 330 s m^{-1}. McNaughton and Jarvis (1991) reported resistances of 50 s m^{-1} for well watered crops and pastures, around 100 s m^{-1} for forest and wild vegetation, and resistances of 250 s m^{-1} or more "in arid lands where leaf area index is very small, or the vegetation is suffering severe water stress". These reported values compare very well with those modelled with WAVES.

5.2.8 Conclusions

The parameterisation of the physically based ecohydrological model WAVES, has given good prediction of the rate of soil drying after flooding, the rate of chloride leaching during flooding, and the rate of transpiration for a 6-month monitoring period. The good performance of WAVES in fitting both water and salt profiles is encouraging. If this exercise were performed for a single site only, then these results would have less significance. However, the good performance at a

range of sites with different soil layering, flooding and vegetation covers is significant for this type of model.

Empirical models of salt and water balances generally do not give vertical distributions of water and salt at a site, and do not easily handle changing groundwater levels or floods. Further, their fitted parameters may vary greatly between sites such as these. However, if point-based SVAT models can identify critical parameters and processes of interest, in the future simpler models may be developed that only model these critical feedbacks but at the whole floodplain scale, say within a GIS framework, and may be compared to remotely sensed data (Taylor *et al.*, 1996).

The utility of the calibrated model is clear. It can be used to explore the likely impacts of flooding patterns, along with the time scale of plant response. This can aid in the definition of a critical groundwater depth, or flooding frequency, for a given level of plant health or cover. All of these results may be site dependant also, so that the mean return period required to keep vegetation at Site 6 “relatively healthy”, with water availability at 30% or greater for example, may be greater than for Site 1, which might be shown to have more rapid salinisation. The experience at Site 5 with a fresh water lower boundary condition, has also given useful insight into the processes occurring near creeks on the floodplain.

This paper is the first in a series from continuing work at Chowilla and other floodplain areas along the River Murray. Othe papers describe in detail (1) development of the new plant growth model (Slavich *et al.*, 1998), (2) alternate management scenario modelling using the calibrations established here, and (3) comparison of WAVES with a simpler lumped model of water and solute behaviour to evaluate critical processes, and how well they can be reproduced by simpler means.

Engineering for human benefits has had a dramatic negative effect on health of riparian vegetation. The decisions on river management are being made now by committees responsible for areas along the river course, such as the Chowilla Working Group. The ability to evaluate and plan management regimes for the best ecological benefits, may ultimately result in the stabilisation and conservation of these fragile and important areas.

Acknowledgements

The authors wish to thank Ian Jolly, Lisa Mensforth, Peter Taylor, and Peter Thorburn for their efforts collecting data at Chowilla for this, and other, papers.

5.3 Modelling the Growth of Irrigated Lucerne over a Shallow Saline Watertable

L. Zhang, W.R. Dawes, P.G. Slavich, W.S. Meyer, P.J. Thorburn,
D.J. Smith, G.R. Walker

Submitted to *Agricultural Water Management*

Abstract

Shallow saline watertables underlie large areas of the Riverine Plains of the Murray Basin of southern Australia. It is believed that deep-rooted perennial plants in these areas are able to reduce recharge and use shallow groundwater, thus controlling groundwater levels. Lysimeters represent the best experimental technique for investigating capillary upflow from shallow watertables and the associated processes of salt accumulation, plant water use, and growth response. Techniques involving stable isotopes of water help determine the components of upflow due to vegetation. When combined with models that simulate salt and water movement in the soil zone and the plant water use and growth, we can thoroughly test our understanding of salinity processes and the ability of plants to control watertables. Results from WAVES simulations of plant growth, evapotranspiration, groundwater uptake, salt accumulation, and the impacts on lucerne growth are compared against measurements made in lysimeters at Griffith, NSW, Australia. With minimal calibration, WAVES was able to reproduce both the daily and seasonal variation in evapotranspiration, upward flux from the groundwater table, plant growth in terms of leaf area development, soil water profiles, soil water salinity, and root water extraction patterns. There was a decline of 36% in transpiration, 42% in leaf area growth, and 67% in upward flux after the salinity of the watertable was increased from 0.1 dS/m to 16 dS/m. Although upward flux of water was large, lucerne used little of it (< 20%), preferring 'fresher' rainfall and irrigation water near the surface. Given the tests presented in this work, we think WAVES is applicable to irrigated agricultural systems.

5.3.1 Introduction

Changes in agricultural practice in Southern Australia have led to increases in groundwater recharge, which in turn have led to rising watertables and increased salinisation. However, reducing groundwater recharge is not always the best way of controlling salinity. For regional groundwater systems the extractions must be increased; it is not enough to reduce inputs. The management of these groundwater systems relies on a combination of engineering options (pumping, drainage, disposal), biological controls (tree plantations, perennials on shallow watertables), and recharge reduction (increased irrigation efficiency).

The Riverine Plains in southern Australia is an example of an area underlain by regional groundwater systems. A combination of irrigation and increased pressures in the confined groundwater systems has led to large areas of shallow water tables. Plantation forests on farms with shallow saline watertables, revegetation of saline agricultural land and reduced leaching fractions are being proposed as part of the overall management options. These would create areas where there is a net flux of water from the groundwater into the soil zone. This water would be lost from the soil either by evaporation or by transpiration and the salt would accumulate and be concentrated in the root zone. There is concern that this will affect the sustainability of these management options.

Whereas there has been a number of past studies of plant response to salinity, few have dealt with the interactions between plant water uptake, salt accumulation, groundwater salinity and plant growth. For dryland areas, lucerne has been proposed as an option to not only reduce recharge but to access shallow groundwater. In the irrigation areas of the Riverine Plains, lucerne is commonly irrigated and it has been suggested that by reducing irrigation, lucerne may be able to use shallow fresh groundwater.

Capillary upflow from groundwater and salt accumulation in the soils are difficult parameters to measure in the field. Lysimeters offer an option for measuring these and other components of the water budget simultaneously in a field-like situation. The lysimeter facilities at Griffith, N.S.W, allow accurate measurement of capillary upflow and drainage, concurrent with measurements of rainfall, irrigation, evapotranspiration, soil moisture content, plant leaf area index, soil water salinity, and isotope analyses (Smith *et al.* 1996).

While a lysimeter can be used to measure capillary upflow, it can not be used for determining how much of this upflow is being used by the plant. Stable isotopes of water have been used in a number of recent experiments to help determine sources of water used by plants and plant water use strategies. Often the main limitation to successful use of isotopes is the similarity of the stable isotope composition of the various sources. This leads to poor discrimination of the relative

importance of various sources. Within the lysimeter, it is possible to overcome this limitation by artificially enriching the isotope composition within the groundwater thus increasing the sensitivity of the technique (Thorburn *et al.* 1994).

The above processes are interlinked and complex and depend on a range of climatic, plant, soil, and groundwater factors. Physically based models can provide insights into the behaviour of this complex system provided that they are tested against measurements to check that they adequately simulate key processes. A tough test on any model is to predict the impacts of changing external conditions, particularly when these changes involve most of the key processes.

This paper describes a lysimeter, isotope and modelling study aimed at testing our understanding of lucerne grown over shallow water tables. It explores what happens to lucerne, a deep-rooted perennial, when irrigation is reduced to the extent that there is a net upward flux from the groundwater into the soil zone. During the course of a lysimeter experiment conducted at Griffith, NSW, the water table is changed in both depth and salinity and the groundwater is 'doped' with isotopically enriched water. A complex soil–vegetation–atmosphere transfer model, WAVES, is calibrated on pre-change data and only two parameters allowed to vary during this calibration. Model predictions of responses of transpiration, capillary upflow, lucerne growth and salt accumulation to changed water table conditions are compared with measured responses. If we can accurately model several different water balance responses, thus eliminating the possibility of compensating errors in other processes, we should feel confident in using WAVES to assess the suitability of lucerne, and perhaps other vegetation types, for management systems aimed at controlling groundwater levels.

5.3.2 Materials and methods

Field experiment

The field data collected has been presented in detail by Thorburn *et al.* (1994) and Smith *et al.* (1996). It was carried out during the period of 1990 to 1993 at CSIRO Land and Water, Griffith Laboratory, N.S.W., Australia (34°17′S, 146°03′E). Two weighing lysimeters each consisted of a concrete outer and steel inner box were installed. Each inner box encased an undisturbed soil core. The dimensions of the Lysimeter 1 (L1) are 1.2 m wide by 1.45 m long by 1.5 m deep, and those of Lysimeter 2 (L2) are 1.05 m wide by 1.3 m long by 1.7 m deep. The soil in L1 was Hanwood loam (Butler, 1979; Northcote, 1981), a Rhodoxeralf, and the soil in L2 was Mundiwa clay loam (van Dijk, 1961; Northcote, 1981), also a Rhodoxeralf. The Handwood loam has red-brown sandy loam (60% sand, 10% silt, and 30% clay) to 0.25 m depth and light brown clay (35% sand, 5% silt, 50% clay, and 10% calcium carbonate) from 0.25 to 1.5 m. The Mundiwa clay loam has brown sandy clay loam (60% sand, 23% silt, and 17% clay) to 0.2 m, a dark reddish

brown heavy clay (25% sand 14% silt, and 61% clay) to 0.6 m and with mottled yellow red clay to 1.7 m (Loveday *et al*., 1984). Mass changes of both lysimeters were calculated daily from load cell output and resolution of the lysimeters was equivalent to 0.05 mm water depth. Upward flux from the watertable was measured daily as the volume of water supplied by the Mariotte tank to maintain a constant watertable.

The field had been fallow following a maize crop in 1989–90. Lucerne (WL Southern Special) was sown on 10 October 1990 in rows 175 mm apart. The leaf area index was determined using *in situ* tube solarimeters on each lysimeter and converting intercepted irradiance values using a locally calibrated function (Meyer *et al.*, 1990). Lucerne in both lysimeters were routinely cut and it took approximately one month for established lucerne to exceed a leaf area index of 3. The field was irrigated using a sprinkler system to maintain a high water status. Irrigation was applied to both lysimeters and the surrounding field with the application of irrigation based on a soil water deficit of 80 mm in L1. Soil moisture contents were measured using a field-calibrated neutron probe (Smith *et al*., 1996).

A non-saline watertable (EC 0.1 dS m^{-1}) at 60 cm below the soil surface was established before sowing and was dropped to 100 cm in March 1991 using the Mariotte tanks. In March 1992, a saline watertable was introduced (EC 16 dS m^{-1}) and maintained at 100 cm until the end of the experiment. Soil water was extracted from each lysimeter at seven depths using ceramic suction cups, and the electrical conductivity (EC) was measured.

An automatic weather station was located immediately adjacent to the field on the western side. Wet and dry bulb temperature was measured using temperature sensors with a standard muslin wick. A tipping bucket rain gauge recorded rainfall amount and duration. Solar radiation was measured 1 m above the canopy using a Delta-T^6 TS81L tube solarimeter.

Stable isotope ratios of hydrogen ($^2H/^1H$) and oxygen ($^{18}O/^{16}O$) were measured in the ground-water, soil water, and plants to trace the uptake of the saline groundwater by plants. To facilitate the tracing, the saline groundwater was made isotopically distinct from rainfall and irrigation water by doping with ^2H_2O. From February 1992 soil solution samples were extracted immedi-ately after each irrigation application for isotopic analysis. Between irrigation events, samples of three plant crowns were taken on 15 occasions for isotopic measurements. The final four were taken weekly in April 1993, after irrigation ceased and the lysimeter soil was allowed to dry.

At each sampling time a section of the crown of the three plants was removed and placed in a jar containing kerosene (Thorburn and Mensforth, 1993). Water was extracted from the plant sample using azeotropic distillation (Thorburn *et al.*, 1993). Analyses for ^2H was performed by reduction of 25 μℓ of water to hydrogen gas over uranium at 800°C (Bigeleisen *et al.*, 1952). Values of ^{18}O

were determined by a modification of the Epstein and Mayeda (1953) CO_2 equilibration technique using 1 mℓ of water. All isotopic ratios were expressed as standard δ notation:

$$\delta\ (‰) = (R_i/R_s - 1) * 1000 \qquad (5.1)$$

where R is the ratio of heavy to light isotope, the subscript i indicates the isotope samples, and s the ocean water standard (V-SMOW).

Model calibration

The two WAVES vegetation parameters that dynamically allocate carbon, maximum above and below ground partition factors, were calibrated to match leaf area index over the period of 1990 to 1991. Solute concentration, upward water flux, leaf area index, evapotranspiration, and soil moisture contents for the period 1990–93 were used as a test of the model. Vegetation parameters for lucerne were initially set to those used by Zhang *et al*. (1999) in a dryland setting. The maximum assimilation rate of carbon and light extinction coefficient were taken from Whitfield *et al.* (1986). The saturated soil moisture content was set from measurements made with a neutron probe, and saturated hydraulic conductivity was estimated based on observed infiltration rates. The moisture characteristic shape parameters of the BW soil model were estimated from the texture profile description and fitted to observed capillary fringes in the soil.

Once the model was calibrated, it was run for the period 1990–93 using measured meteorological data, irrigation data, prescribed groundwater tables, and salinity data. No change was made to any parameter values after the saline groundwater table was introduced.

5.3.3 Results and Discussion

Leaf area development

During the period of the experiment, lucerne was routinely cut and the measured leaf area index varied between 0.05 and 4.0 (Fig. 5.16). Lucerne grown in L2 was less well established in the 1990–91 season with average leaf area index of 1.5 compared to 1.9 in L1. The maximum leaf area index in L2 was 2.8 compared to 3.7 in L1. The difference in leaf area index may be due to the soil conditions limiting seedling vigour and root growth (Meyer *et al*., 1996). The root length density in L2 was much lower than that in L1 due to the presence of a heavy clay layer (Smith *et al*., 1996). WAVES does not model root length density, but root carbon. There is no measured data against which to compare this.

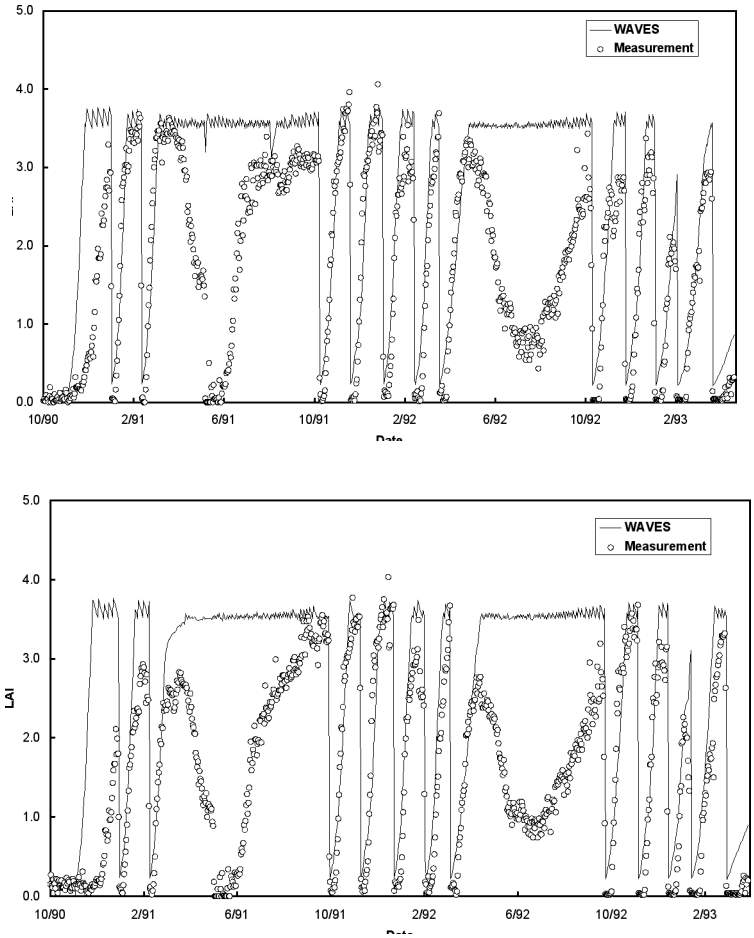

Fig.5.16. Comparison of modelled (—) and measured (○○○) leaf area index (LAI) for (a) Lysimeter 1 and (b) Lysimeter 2.

Once established as described in the previous section, lucerne exceeded a leaf area index of 3.0 by, on average, 28 days after a cut. The modelled leaf area index agreed very well with the measurements and they showed similar temporal patterns, except for the winter period (May to August) (Fig. 5.16). The large difference between modelled and measured leaf area index in winter was probably due to dormancy. If these winter periods are excluded, linear least-squares regression of modelled to observed leaf area index gives a slope of 0.91 with a zero intercept, regression coefficient (r^2) of 0.90, and root mean square error (RMSE) of 0.46. It was observed that the lucerne in the lysimeters started to lose leaves when the minimum air temperature was below 5°C. This specific dormancy behaviour is not modelled by the generic growth model in WAVES. In other models with specific modules to handle individual crop types, such as APSIM (McCown *et al.* 1996), such effects are incorporated with extra parameters in the detailed phenological descriptions. This period exhibits very low transpiration (1.2 mm day^{-1}) due to climatic controls not vegetation. Since WAVES incorporates the atmospheric demands directly, this period of low evaporation is modelled accurately in water-balance terms. Further, the fact that only allocation

parameters needed to be calibrated implies the form and feedbacks within WAVES growth model are robust and appropriate.

Evapotranspiration and upward flux

There is good agreement between modelled and measured monthly evapotranspiration for both lysimeters (Fig. 5.17). For L1, least-squares linear regression yielded a slope of 1.06 with zero intercept, r^2 of 0.86, and RMSE of 0.96 mm day^{-1}. In L2, the slope was 1.06, r^2 of 0.82, and RMSE of 0.92 mm day^{-1}. Evapotranspiration showed significant temporal variations. In the summer months, daily evapotranspiration rate exceeded 15 mm day^{-1} and dropped to less than 1 mm day^{-1} in the winter periods.

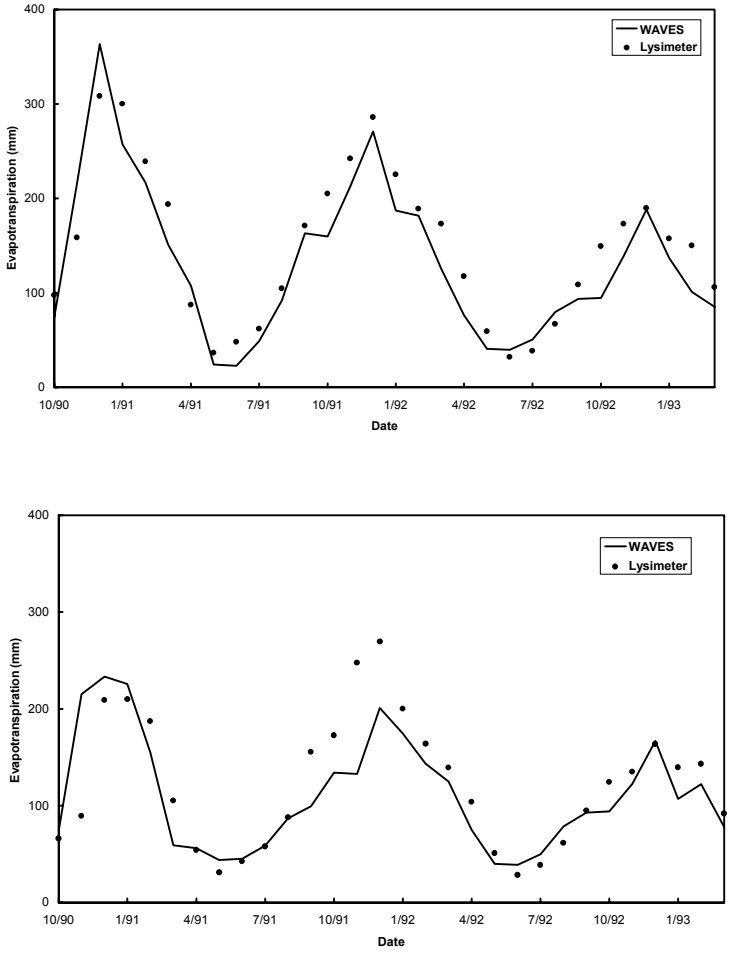

Fig. 5.17. Comparison of modelled (—) and measured (•••) monthly evapotranspiration for (a) Lysimeter 1 and (b) Lysimeter 2.

Evapotranspiration rates from L2 were consistently lower than those from L1, especially for the period of 1990–1991. For the entire period, observed evapotranspiration from L2 was 80% of that from L1. The difference between the two lysimeters may be due to the presence of the heavy clay layer in L2, which caused the lucerne to grow less vigorously than the surrounding plants (Meyer

et al., 1990). As a result, lucerne grown in L2 before saline watertable introduction had 10% less leaf area index than L1 (Fig. 5.16). Average annual irrigation for 1990–92 was 730 mm, and rainfall was 90 mm. Despite these inputs, average actual evapotranspiration rate (5 mm day^{-1}) was only half of the average potential evapotranspiration rate (10 mm day^{-1}) estimated using the Penman–Monteith equation with zero canopy resistance. Thus, evapotranspiration was supply limited and controlled by soil hydraulic properties. WAVES successfully modelled evapotranspiration from the two lysimeters with the only difference being soil profiles and properties (Table 5.5).

Table 5.5. List of Broadbridge–White soil parameters and soil layer depths used in the study

Site	Depth (m)	K_s (m/d)	θ_s	θ_d	λ_c (m)	C
Lysimeter 1	0–0.1	0.07	0.30	0.12	0.2	1.01
	0.1 – 0.3	0.05	0.35	0.20	0.3	1.05
	0.3 – 0.6	0.02	0.45	0.20	0.4	1.05
	0.6 – 1.5	0.02	0.38	0.15	0.3	1.05
Lysimeter 2	0 – 0.1	0.08	0.30	0.12	0.2	1.01
	0.1 – 0.2	0.04	0.35	0.20	0.3	1.05
	0.2 – 0.6	0.01	0.40	0.25	0.4	1.10
	0.6 – 1.7	0.001	0.40	0.25	0.4	1.10

The modelled monthly upward flux was also in good agreement with the measurements and showed similar trends to evapotranspiration (Fig. 5.18). The ratio of the upward flux to evapotranspiration varied between 25 to 65% and decreased after the saline groundwater table was introduced. These results suggest that the magnitude of upward flux was significant compared to the evapotranspiration (Table 5.6). However, it does not necessarily follow that upward flux accounted for up to 65% of the evapotranspiration.

The modelled and measured soil moisture contents at 10, 20, 60, and 100cm depths are shown in Fig. 5.19. It is clear that WAVES was able to accurately reproduce the daily and seasonal variations in soil moisture for two different soil types. The modelled soil moisture contents agree very well with the measurements with RMSE of 0.062, 0.063, 0.030, 0.008 respectively for the four soil depths shown in Fig. 5.19a. The modelled soil moisture contents for L2 showed better agreement with the measurements at 10 and 20 cm depths compared to L1, with RMSE of 0.060, 0.053, 0.035 and 0.016 at the four depths in Fig. 5.19b. The differences between modelled and measured soil moisture contents for L1 are relatively large at 10 and 20 cm depths for the period of October 1991 to February 1992 (Fig. 5.19).

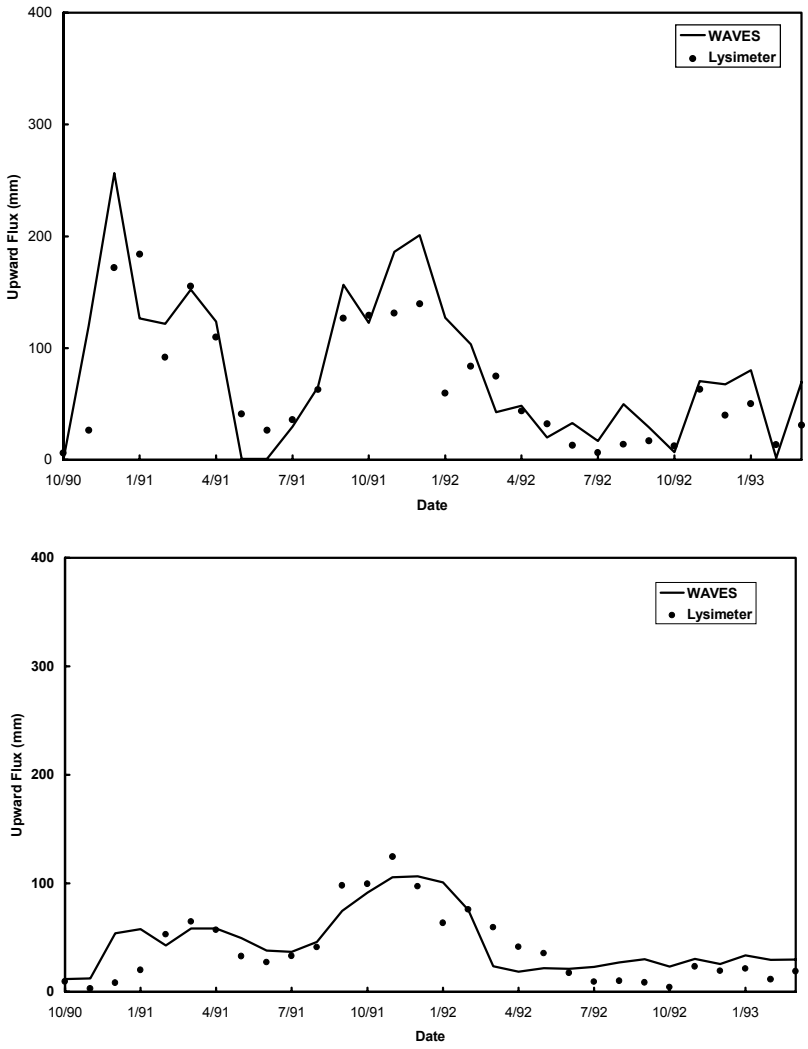

Fig. 5.18. Comparison of modelled (—) and measured (•••) upward flux for (a) Lysimeter 1 and (b) Lysimeter 2.

The distribution of root water extraction is a dynamic process influenced by soil water salinity, and root carbon distribution. Many functions have been proposed to represent water uptake by roots (Molz, 1981). The difficulty of incorporating microscopic variables such as root length and diameter into a macroscopic model is well known. Models that simplify the system, not requiring the measurement and modelling of these microscopic processes for a daily water-balance, offer the most practical tools. In WAVES, the proportion of transpiration taken from a depth node is a function of the amount of root present, and the osmotic and matric potentials at that node. Further, salinity in the root zone decreases apparent water availability, which feeds back to the plant as decreased assimilation and transpiration. WAVES assumes that matric and osmotic effects are identical to the plant in creating water stress, except that the sensitivity of the plant to salt may magnify or reduce the apparent osmotic potential. WAVES only simulates osmotic effects of salt on water availability, and not specific toxicity of high salt concentrations on roots. These approaches, and variations of them, are detailed in Meiri (1984).

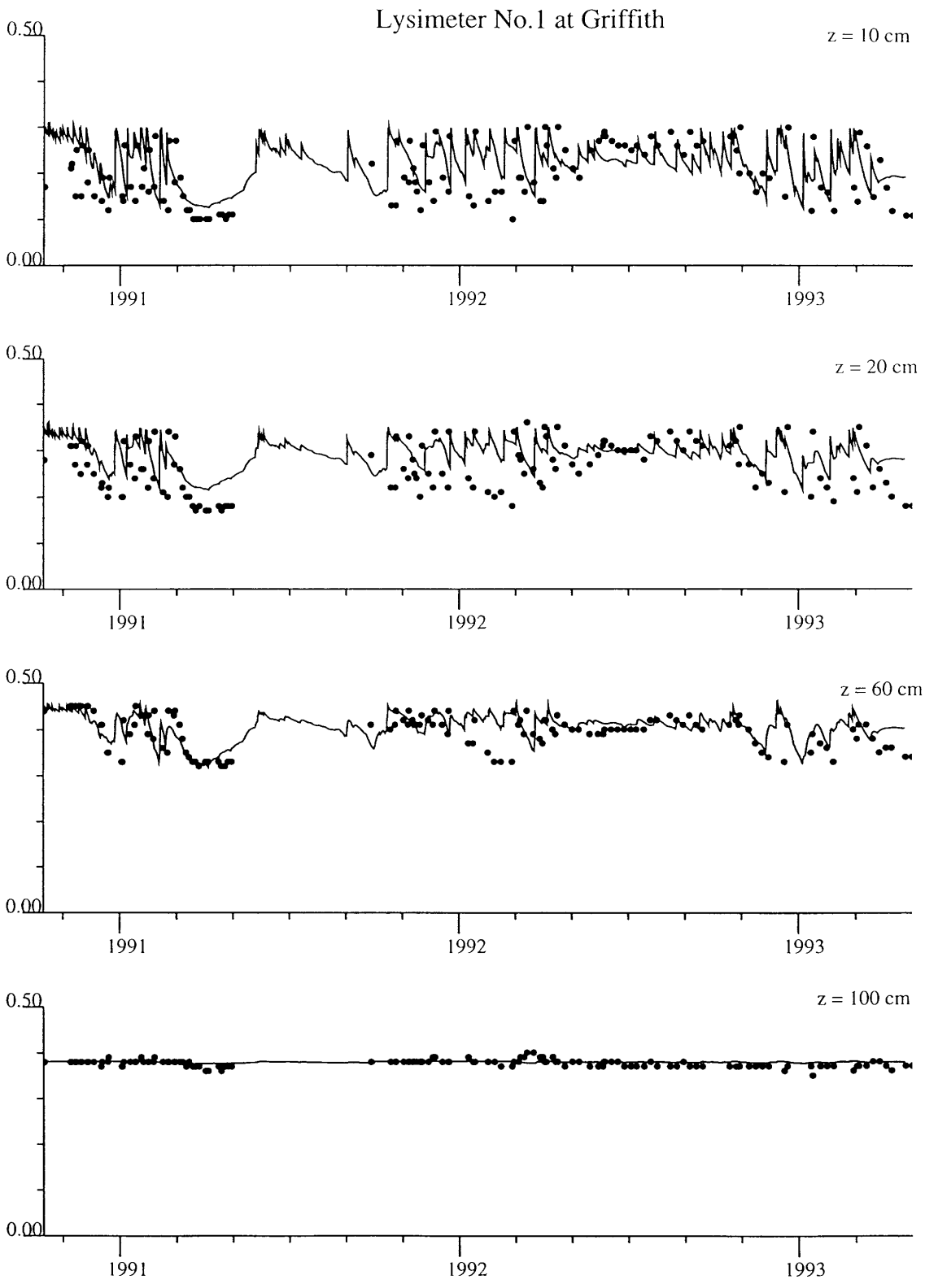

Fig. 19a. Modelled and measured soil moisture content at 10, 20, 60, and 100 cm (lysimeter 1)

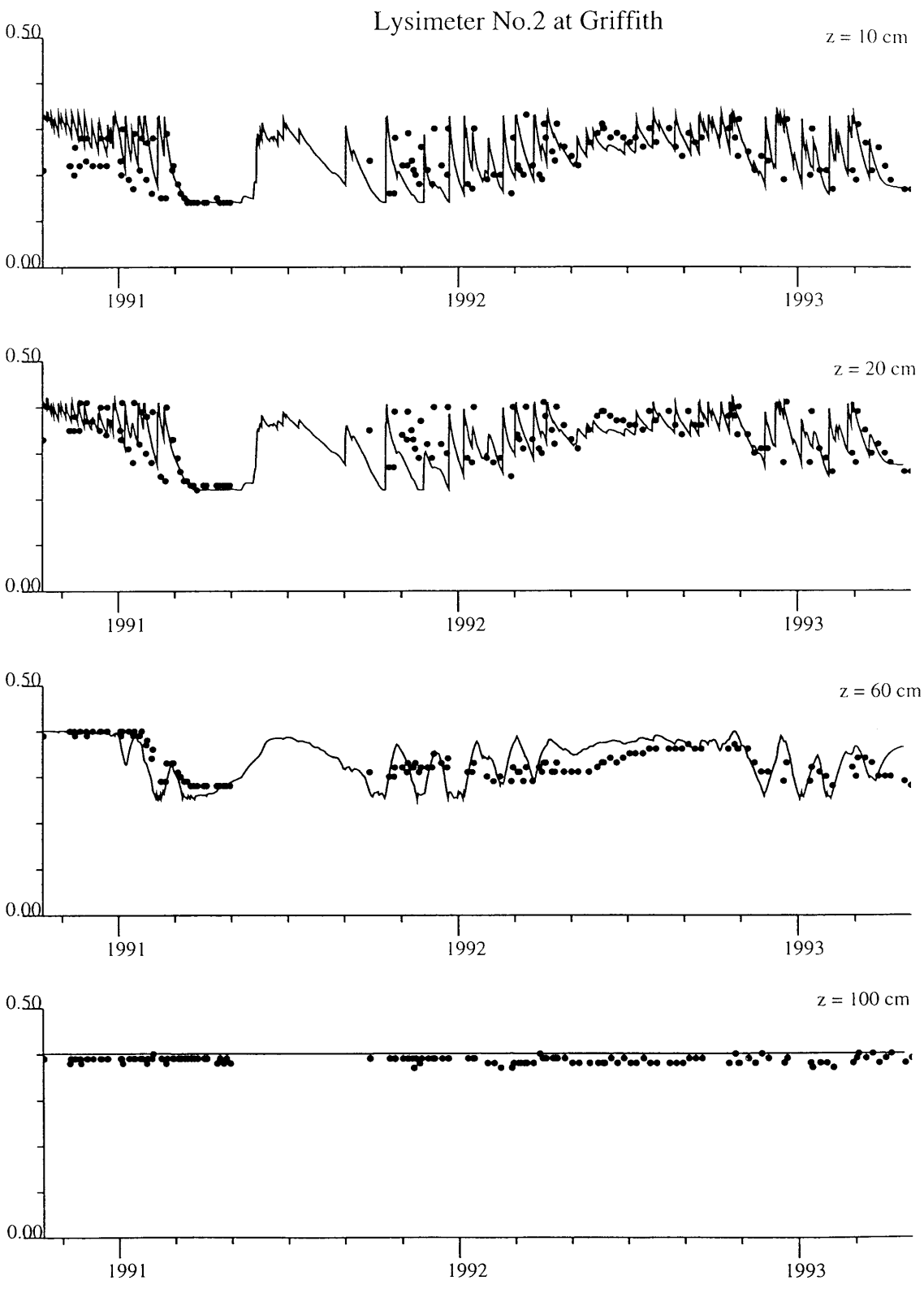

Fig. 19b. Modelled and measured soil moisture content at 10, 20, 60, and 100 cm (lysimeter 2)

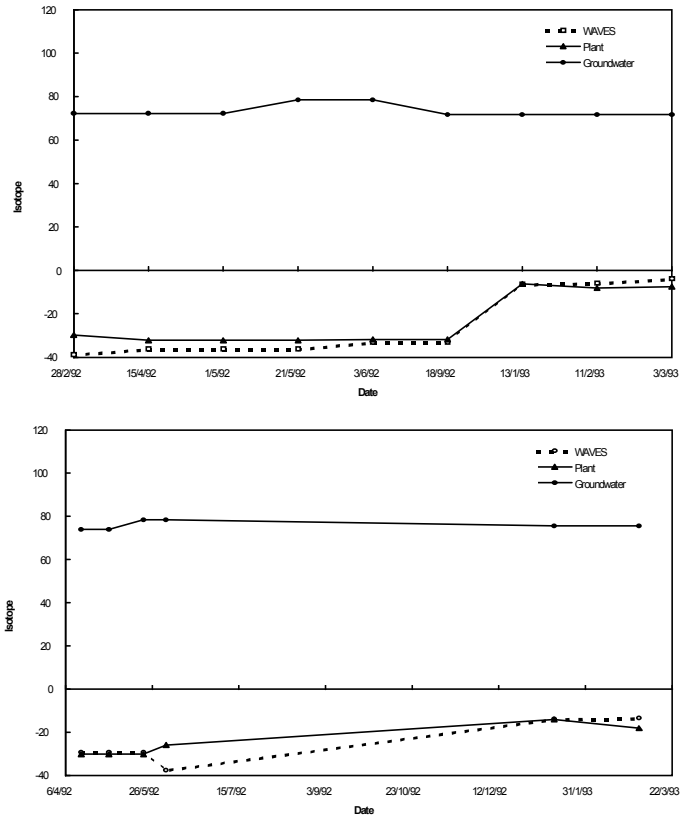

Fig. 5.20. Comparison of the δ^2H values of groundwater, water extracted from lucerne plants, and calculated from the WAVES model during the experiment for (a) Lysimeter 1 and (b) Lysimeter 2.

Root water extraction patterns

To evaluate the plant water extraction patterns in the root zone and groundwater uptake, the plant and groundwater δ^2H values were analysed. It is clear that plant δ^2H values were substantially different from those of the groundwater (Fig. 5.20) and Thorburn *et al.* (1994) concluded that only small (i.e. < 20%) proportions of saline groundwater were taken up by the plants. To compare modelled plant δ^2H values, we calculated the following:

$$\delta^2\overline{H} = \frac{\sum_{i=1}^{n} ET_i \delta^2 H_i}{\sum_{i=1}^{n} ET_i} \qquad (5.2)$$

where $\delta^2\overline{H}$ is the modelled average plant δ^2H value, ET_i is the plant water extraction at depth i simulated by WAVES, $\delta^2 H_i$ is the measured soil water values at soil depth i.

The results shown in Fig. 5.20 indicate that the modelled plant δ^2H values agree very well with the isotope measurements, and this provided an independent test for the model in terms of root

water extraction. Using the water balance terms from WAVES, and assuming that irrigation, rainfall, and stored soil water were used in preference to saline groundwater, we estimate that 19% of the upward flux was actually used by the plants for transpiration. Saline water moving from the water table would have replenished soil water deficit caused by the plant water uptake of fresh water from rainfall and irrigation. Given that the potential evaporation was very high and the lucerne did not use appreciable amounts of groundwater, actual evapotranspiration and capillary upflow would have to decline. This is supported by the fact that both evapotranspiration and upflow decreased substantially when the water table was saline (see Figs. 5.17, 5.20, and Table 5.6). These results are consistent with the conclusions of Thorburn *et al.* (1994). Fig. 5.21 shows how the modelled root water extraction pattern changed as a result of the increase in salinity of the groundwater. These results indicate that WAVES accurately simulated the upward flux of groundwater, plant water extraction patterns, and salinity feedbacks to plants.

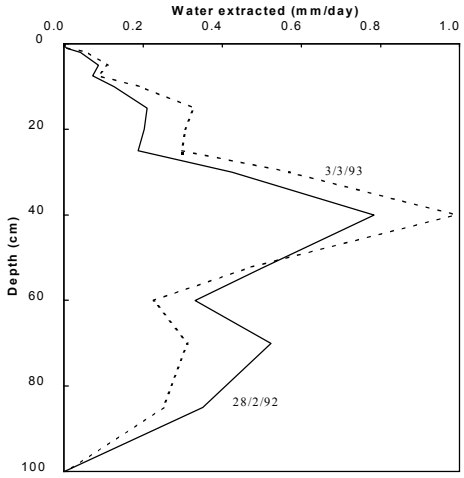

Fig. 5.21. Root water extraction patterns on 28 February 1992 (fresh water (—)) and on 3 March 1993 (saline water (- - -)) for Lysimeter 1. The saline water table was introduced on 4 March 1992 and maintained at 1.0 m until end of March 1993.

Impact of saline watertable on lucerne growth and water uptake

WAVES models coupled water and conservative solute dynamics (Dawes and Short, 1993). As described in the previous section, WAVES also models the osmotic feedback of salt in the root zone on carbon assimilation, transpiration, root growth, and root water extraction. The salinity in the root zone depends on groundwater salinity, upward water flux, root water extraction patterns, rainfall, and drainage. Fig. 5.22 shows good agreement between modelled and measured soil water salinity. While there appears to be some systematic error in the profile salinity, this could be due to collecting water samples by suction applied to ceramic cups.

The convection of solutes was the dominant process, while diffusion and mechanical dispersion played roles in reducing the solute gradients within the soil profile (Fig. 5.23). The magnitude of the errors in the modelled salt concentration due to neglecting either diffusion or dispersion was 5 dS/m. It has been suggested by Morris (pers. comm. 1997) that salt diffusion plays a significant role in the sustainability of vegetation. This measurement and modelling exercise suggests that this is not the case in this irrigated environment.

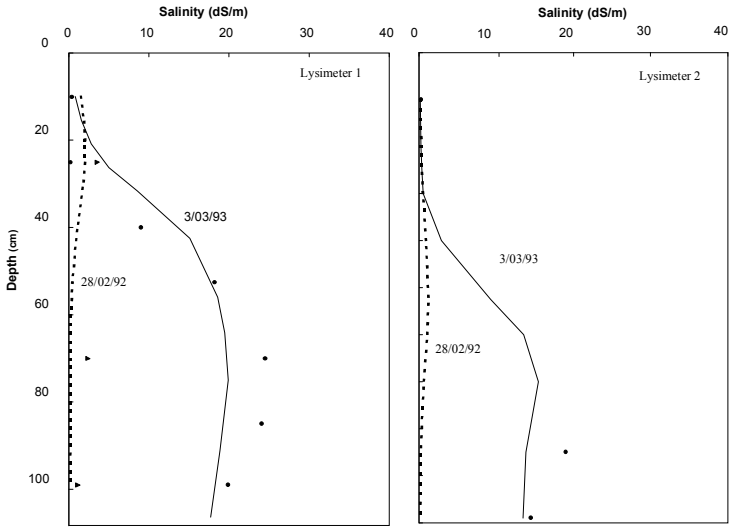

Fig. 5.22. Comparison of modelled and measured soil water salinity for (a) Lysimeter 1 and (b) Lysimeter 2.

Under drying conditions, diffusion and dispersion result in lower salt concentration around maximum root length density and higher salt concentration close to the surface (Fig. 5.22b) (Bresler, 1972). If these processes were not considered, plants would have had less uptake near the watertable, not use as much groundwater, and actual evapotranspiration rates could decline, as the surface soil store is depleted.

The introduction of a saline groundwater table in March 1992 had a noticeable impact on the leaf area index (Fig. 5.16), evapotranspiration rates (Fig. 5.17), and upward flux (Fig. 5.18). During the period of 1992–1993, average leaf area index was reduced by 41%, average evapotranspiration was reduced by 36% (potential ET dropped by 16%), and average upward flux was reduced by 67% (Table 5.6). These decreases can be attributed to an increase in salt in the root zone. Measurements showed that electrical conductivity (EC) of soil water in the root zone was very high, 25 dS/m, toward the end of the experiment (Fig. 5.22) as a result of saline groundwater movement. The high salinity of the soil water reduces the water availability to plants and hence limits plant growth (Hillel, 1980). WAVES was able to model these changes with the parameters measured and calibrated for the period 1990–1991, as outlined in section 5.2.

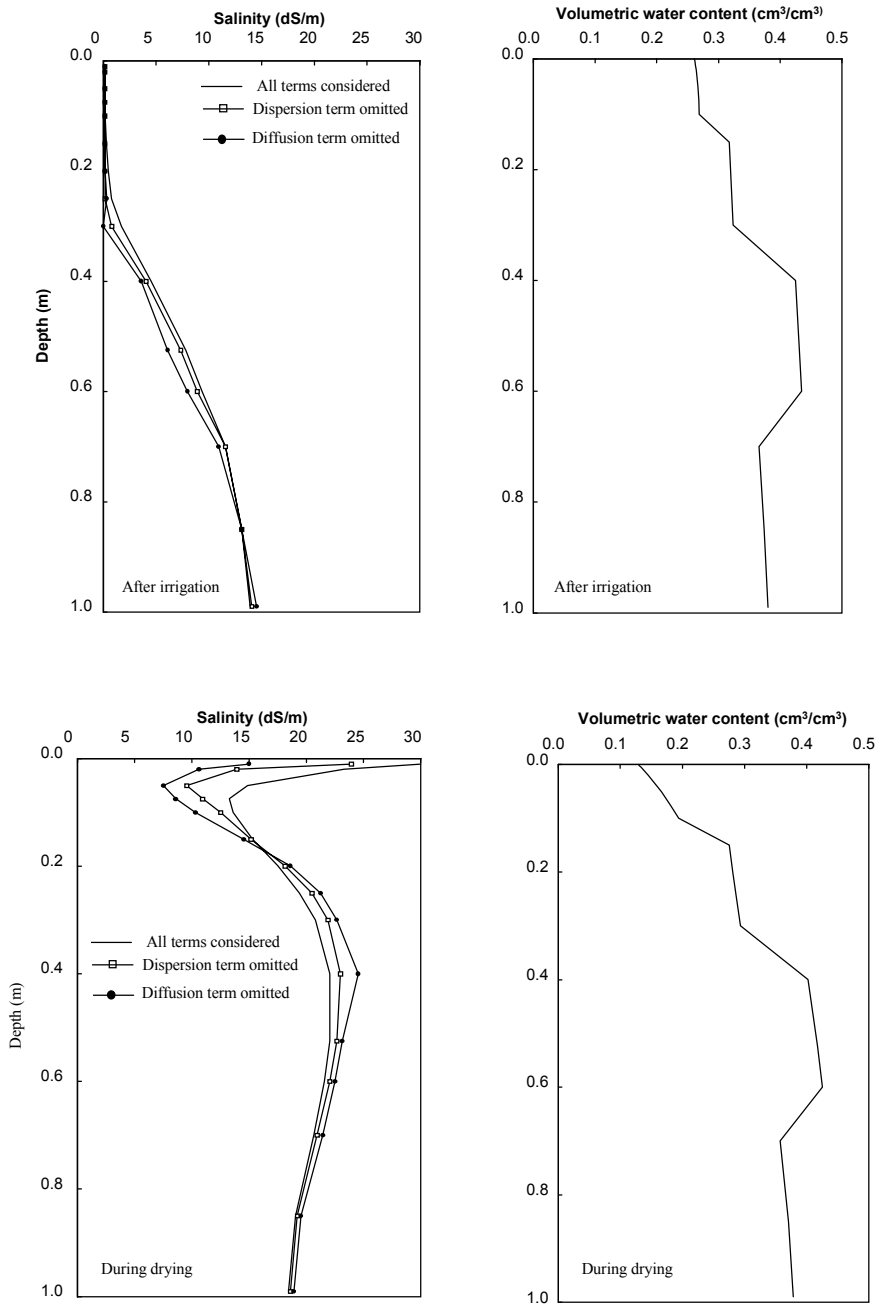

Fig. 5.23. Modelled soil water salinity and soil moisture content profiles after irrigation (a) and during drying (b). The convection, diffusion, and dispersion terms were considered (solid line), dispersion term was omitted (open square), and diffusion term was omitted (solid circle).

Table 5.6. Effect of saline groundwater table on evapotranspiration, upflow, and leaf area index.

	Before			After		
	ET	Upflow (mm/d)	LAI (mm/d)	ET	Upflow (mm/d)	LAI (mm/d)
Lysimeter No. 1	5.9	3.3	2.2	3.8	1.1	1.3
WAVES	5.3	3.7	2.4	3.7	1.3	1.7
Lysimeter No. 2	4.4	2.2	1.9	3.1	0.7	1.4
WAVES	4.1	2.3	2.3	3.0	0.8	1.8

Lysimeters are artificial environments. In the field where groundwater levels will fluctuate, we would expect a reduction in local groundwater levels to occur rather than the large fluxes of upflow as observed. This changes the short term behaviour significantly, but at some point in time, the lucerne will reach an impediment to root growth or meet the regional groundwater heads, and the salinisation of the soil will start at that level. As the deep environment becomes more prohibitive for root water extraction, water levels will start to rise again, and salinisation will creep toward the surface. This situation emphasises the need for an integrated approach to salinity mitigation, combining engineering (*e.g.* pumping), biological (e.g. deep rooted plants, perennial plants, grazing regimes, impact of grazing animals on surface soil properties), and irrigation controls (e.g. irrigation amount, and timing).

5.3.4 Conclusions

In the presence of a shallow saline groundwater table, lucerne does not appear to derive much of its water from the watertable directly, preferring to use 'fresher' water stored in the soil profile. The size and vigour of the canopy developed decreases with increased salt in the root-zone. Root water extraction patterns change as a result of an increase in salinity of the groundwater, and exaggerate drying at the surface. The process of drying out the soil water store causes upward capillary flow of groundwater, and can have a significant impact on groundwater levels in the short term. This capillary upflow causes salt to be brought into the soil and root zones, and this leads to a reduction in transpiration, plant growth, and upward flow. If this process operates without some irrigation, the lucerne crop would not be sustainable, or there would be a large reduction in leaf area.

The comparison between experimental results and those of the WAVES modelling showed that the assumptions inherent in the model capture the key processes relating to groundwater and salinity responses. Only two plant parameters were calibrated and good agreement was found for a wide range of measurements including trends in leaf area index, evapotranspiration, groundwater upflow, soil moisture and salinity profiles. The salinity impacts on water use, root water extraction patterns (from isotope data), and plant growth were fully explained by assuming only the osmotic effects of salt, and using the calibration obtained from the fresh groundwater case. WAVES also simulated the very different measured responses in a second lysimeter where the only difference was the soil profile and hydraulic properties. This gives us confidence that we understand the key processes and feedbacks and that the representations of these in WAVES is both adequate and appropriate. Thus we can use WAVES to investigate the effect of changing the irrigation or groundwater environment on lucerne. With sufficient data, we should be able to predict the long-term sustainability of lucerne under any specified management regime.

5.4 Quantifying Episodic Recharge Under Crop/Pasture/Fallow Rotations

L. Zhang, W.R. Dawes, T.J. Hatton, I.H. Hume,
M.G. O'Connell, D.C. Mitchell, P.L. Milthorpe, M. Yee

Submitted to *Agricultural Water Management*

Abstract

A field and modelling project to investigate episodic recharge in the Mallee region (Hillston and Walpeup) of Australia is described. More specifically, the project evaluates the impact of agronomic practices on recharge, and in particular episodic recharge. Episodic recharge is of concern because we anticipated that agronomic practices are not likely to affect it significantly.

Various crop and pasture rotations involving fallow, field pea, Indian mustard, wheat, oats, lucerne, and medic pastures were considered. A biophysically based model (WAVES) was calibrated with the field data and then used to simulate soil moisture content, plant growth, and recharge under these rotations.

Results showed that (1) recharge just below the root zone was episodic and that just 10 % of annual recharge events contributed over 85 % of long-term totals. Episodic recharge could therefore reduce the effectiveness of land management options in controlling recharge; (2) winter fallows can increase recharge significantly; (3) changes in land management may take a considerable period of time (> 10 years) to have any noticeable impacts on recharge; (4) recharge under lucerne was approximately 30 % of that under medic pasture.

5.4.1 Introduction

The rise of groundwater tables and associated dryland salinity have been identified as major land degradation problems in the Mallee region of southeastern Australia. This region is characterized by a semi-arid climate, and originally a low, sparse woodland of multi-stemmed individuals of the genus *Eucalyptus*. Much of the salinity problem is caused by massive clearing of native vegetation and the use of shallow-rooted annual crops and pastures (Clifton *et al.* 1995). These land use changes have significantly altered the water balance of the region and led to increased recharge to the groundwater system; recharge under native Mallee vegetation is less than 0.2 mm yr^{-1} (Allison *et al*. 1990), but following replacement by annual cropping increases by a factor of 100. It appears to be economically and sociably infeasible to restore the natural water balance/recharge rate/water table depth by replanting the native vegetation on a sufficient scale, but better management of agricultural practices may reduce the undesirable effects associated with dryland salinity.

The main emphasis of current salinity control strategies is to enhance plant water uptake to minimize groundwater recharge. For example Clifton and Taylor (1995) propose that land management include either improving the growth of existing annual crops and pastures, or replacing these with perennial vegetation. The traditional agricultural practice in the Mallee regions involves winter fallows in crop rotations and this has been shown to contribute to improved crop yield (French 1978; Fischer 1987). However, it has also been shown that winter fallows have caused increased recharge (O'Connell *et al.* 1995). It is desirable to evaluate recharge rates and their long term impact on regional water balance and salinity under different crop rotations.

A number of studies have been conducted to evaluate current rates of groundwater recharge and its relationship to environmental factors (Walker *et al.* 1991; Kennett-Smith *et al.* 1994). These have shown that a simple water balance model can be used to analyse the general factors which affect recharge in a region. However, the need for a more detailed physically based model to evaluate the effect of different agronomic practices on recharge has also been recoginsed. An important step in predicting groundwater recharge is to better understand its episodic nature, how it varies across the landscape, and how it is influenced by landuse and agricultural management. Physically based models (e.g. Dawes *et al*. 1997; Hauhs 1990) can help identify key processes and the most important factors controlling groundwater recharge, providing information that can be used to develop sustainable land management practices.

Recharge in the Mallee region is generally considered to be episodic in nature. Episodic recharge is infrequent significant recharge events. The word 'significant' refers to the relative magnitude of the recharge. While it is true that better agronomic practices can reduce mean annual recharge, it is anticipated that they are not likely to affect episodic recharge significantly. as a result of rare

but very large rainfall events. Rainfall in the Australian arid zone is marked by extreme variability and that rare, very large rainfall events are important for recharge process. It is therefore the distribution of these events that determines the patterns of recharge.

During the period of 1991 to 1995, two field experiments were conducted at Hillston (New South Wales) and Walpeup (Victoria) to study the effectiveness of changing landuse and agronomic practices in reducing groundwater recharge (Hume and Mitchell 1996). The purpose of the study was to investigate episodic recharge in the Mallee region and to evaluate the impact of agronomic practices on recharge, and in particular episodic recharge.

5.4.2 Field experiments and data

An integrated program of field experimentation was established on the Mallee Research Station, Walpeup, Victoria (35°07′ S, 141°59′ E) and on a farm property near Hillston, NSW (33° 22′ S, 145° 51′ E).

The Hillston site was located on aeolian deposits of Devonian hills in the N.E. of the Murray Basin. The soil is a calcareous red earth (Stace *et al.*, 1968) with a Northcote classification Gn 2.13 (Northcote, 1979; Isbell, 1996). The Hillston experiment was established in a field that had been cleared of trees (mallee, bulloak and western red box) in 1988. Two dryland wheat crops were grown on the site during 1989 and 1990, and it was ploughed and leveled during 1991 in preparation for experiment. The site has a predominant northeasterly aspect and a uniform slope of less than 0.3%. The climate is semi-arid with mean annual rainfall of 371mm (1890–1992), of which 56–68 % falls in the growing season (May – November). The Hillston site was irrigated prior to the commencement of field measurements.

The Walpeup site was located in a swale within an east–west oriented dune system (Newell 1961; Rowan and Downes 1963). The soil is a solonised brown soil (Stace *et al*. 1968) with a Northcote classification Gc 2.22 (Northcote 1979) and has been used for agriculture since being cleared of native Mallee vegetation in 1914. The site has a westerly aspect with a uniform slope of 1%. The climate is semi-arid with mean annual rainfall of 340 mm (1957–94), of which 65–70% falls in the growing season (May – November) but with significant variation in quantity and distribution. The mean potential evaporation is approximately 2000 mm yr^{-1}.

Experimental design

A common experimental methodology was used at both locations although the cropping treatments differed to reflect local cropping practice. Two perennial plantings; one traditional, and one modified rotational cropping treatments were established at each location. The rotational cropping treatments were established as a cyclical rotational experiment (Patterson 1963). Each phase of

each rotation is expressed in each year of the experiment providing an efficient means of replication in both time and space. The spatial variability of soil properties was assessed by electromagnetic survey (Geonics EM38). Experimental treatments were randomly allocated to account for these spatial patterns in the 'blocking' of the experiment.

Experimental layout

The Walpeup experimental site rotational treatments were allocated to 18 plots, each 21 m by 20 m, and separated from its neighbour by a 5–10 m buffer. Two PVC neutron moisture meter (NMM) access tubes were installed 5.5 m deep and 10 m apart in each plot to monitor soil water. A fallow rotation treatment (fallow/wheat/field pea) and a continuous crop rotation treatment (Indian mustard/wheat/field pea) were established in June 1993. Three years of biomass, soil moisture, and climate measurements were made, ending in December 1995.

Soil data

The relationships between volumetric water content, hydraulic conductivity, and soil water potential were described with the Broadbridge and White (1988) soil model. The parameters of the soil model were estimated by inverse modelling (Hume and Mitchell 1996). Soil water beneath each treatment was measured at intervals of two to four weeks. Measurements at Hillston started in November 1991 and continued until December 1995, while the period of measurements at Walpeup was from June 1993 to December 1995.

Meteorological data

At each site, meteorological data were recorded hourly by automatic weather stations. Wet and dry bulb temperatures were measured using temperature sensors with a standard muslin wick at Walpeup, and relative humidity measured at Hillston. A tipping bucket rain gauge recorded rainfall amount and intensity. Radiation sensors with a uniform spectral response from 500 to 1000 nm were used to record solar radiation. Missing rainfall data were taken from a manual rain gauge on site. Other missing meteorological data were interpolated using measurements from neighbouring weather stations.

Plant growth data

Plant biomass was sampled several times throughout each growing season, approximately 3 weeks apart at Walpeup, and one harvest was conducted at Hillston. At each biomass harvest, 5 × 2 m drill row above-ground samples were dried at 80°C. The date of sowing, emergence, anthesis, and grain harvest was recorded for all traditional crops. The percentage green foliage was deduced from photographs of each plot at each biomass sampling. Biomass production of

cereal crops was assessed at anthesis, by measuring the dry weight of all above ground plant material after drying at 45°C for 24 h.

To compare simulated plant growth with the measurements, we first calculated dry weight of green material based on the total dry weight and percentage green foliage. The dry weight of green material was converted into leaf area index using specific leaf area values from samples at each site or from values of Armstrong and Pate (1994) for field pea, Sharma and Kumar (1989) for Indian mustard, and Dawes *et al.* (1997) for oats and wheat.

5.4.3 Model implementation

The saturated and air-dry moisture contents for each soil horizon were estimated from soil moisture measurements (Hume *et al*. 1996). Initial estimates of saturated hydraulic conductivity were measured using disc permeameters (White *et al.* 1992). The Broadbridge–White soil parameters λ_c and C were initially estimated from an evaluation of the soil texture profiles at each plot. Finally the soil parameters were adjusted using inverse modelling (Hume and Mitchell, 1996) (Table 5.7). Four plots were selected from the two experimental sites to compare WAVES with measurements. Information on vegetation parameters appears in Table 5.8. Some of the vegetation parameters (*e.g*. maximum rooting depth) were estimated based on field measurements, while others were obtained from literature (Sharma and Kumar 1989, Whitfield *et al.* 1986; Hodges 1992; Hatton and Dawes 1993; Armstrong and Pate 1994; Dawes *et al.* 1997).

WAVES was run using daily values of maximum and minimum air temperatures, precipitation, vapour pressure deficit, and solar radiation. The simulation commenced at 1 January 1992 for Hillston, at 1 January 1993 for Walpeup, and ended on 31 December 1995 for both sites.

The ability to control recharge, especially episodic recharge, by agronomic means was evaluated in four modelling scenarios. These crop rotations are typical farming practices in NSW and Victorian Mallee. The first two scenarios compared the effectiveness of annual and perennial pastures in controlling recharge. Two crop rotations were modelled; the first was an 8-year sequence of fallow/oat/wheat/wheat/(lucerne × 4) (RT1) and the second was the same as RT1 except with four year of medic pasture (RT2). WAVES was used to simulate 32 years (1957–89) of deep drainage beneath these rotations using inputs of meteorological data measured at Hillston. The soil hydraulic properties at plot 10 and vegetation parameters listed in Table 5.8 were used in the simulations. The effect of fallowing on recharge was evaluated in two further modelling scenarios in which WAVES simulated recharge beneath a fallow rotation, medic/fallow/wheat (RT3), and one without fallow, medic/medic/wheat (RT4). These two scenarios ran for 33 years (1957–90) using meteorological data measured at Walpeup with soil hydraulic properties listed in Table 5.7 and vegetation parameters in Table 5.8. To further evaluate the impact of rooting depth on recharge,

the second two scenarios were run using deep rooting depth of 100 cm (RT3d and RT4d). In these simulations all the model parameters were kept constant, except maximum rooting depth at Walpeup, which varied from 50 to 100 cm.

Table 5.7 Broadbridge–White soil parameters for each soil layer used in WAVES simulations at Hillston and Walpeup

Plot	Soil layer	Depth (cm)	K_s (m/d)	θ_s (cm^3/cm^3)	θ_d (cm^3/cm^3)	λ_c (m)	C
			Hillston				
1	1 (sandy clay loam)	0 – 52	0.05	0.30	0.05	0.60	1.10
10	2 (sandy clay)	52 – 375	0.05	0.35	0.10	0.42	1.01
	1 (sandy clay loam)	0 – 52	0.05	0.30	0.05	0.30	1.50
	2 (sandy clay)	52 – 375	0.01	0.35	0.10	0.35	1.05
			Walpeup				
3 & 10	1 (sandy loam)	0 – 10	0.10	0.40	0.20	0.10	2.00
	2 (sandy clay loam)	10 – 18	0.10	0.40	0.05	0.10	1.07
	3 (sandy clay)	18 – 187	0.01	0.35	0.10	0.30	1.05
	4 (light clay)	187 – 487	0.001	0.35	0.10	0.40	1.10

Table 5.8. Vegetation parameters used to simulate crop and pasture growth at Hillston and Walpeup

Parameter	Oats	Wheat	Mustard	Field pea	Medic	Lucerne
IRM weighting factor for water	0.2	0.2	0.2	0.2	0.2	0.2
IRM weighting factor for nutrients	0.5	0.5	0.5	0.5	0.5	0.5
Specific leaf area (m^2 kg leaf dry weight)	12.0	12.0	7.5	10.5	12	12.0
Slope in conductance model	0.70	0.70	0.70	0.70	0.90	0.70
Maximum carbon assimilation rate (kg C m^{-2} d^{-1})	0.015	0.015	0.012	0.015	0.012	0.01
Light extinction coefficient	0.65	0.65	0.65	0.65	0.65	0.85
Temp. for optimum growth (°C)	20	25	21	25	20	20
Temp. for half optimum growth (°C)	5.0	5.0	7.0	5.0	10.0	10.0
Degree daylight hours (°C hours)	15000	15000	13000	13500	16000	—
Saturation light intensity (μmols m^{-2} s^{-1})	1000	1000	1000	1000	1200	1000
Maximum rooting depth (m)	1.0	1.5	0.3	0.3	1.0	3.0
Leaf respiration coefficient (kg kg^{-1} d^{-1})	0.0015	0.0045	0.0065	0.0025	0.0002	0.0002
Root respiration coefficient (kg kg^{-1} d^{-1})	0.00012	0.00012	0.00012	0.00008	0.0001	0.0001

5.4.4 Results and discussion

Simulated plant growth

Fig. 5.24 shows a comparison of simulated leaf area index and the measured values for six selected plant types. The model results are in good agreement with the measurements. The predicted leaf area index followed the measurements reasonably well for wheat, Indian mustard, and field pea. The model captured the peak leaf area index well in terms of timing and its magnitude. However, it slightly overestimated leaf area index during the first month of the growing season. For medic pasture, WAVES predicted the leaf area index very well. The simulated leaf area index for lucerne showed reasonable agreement with the observed values. There was only one measurement available for oats at Hillston, however it is not unreasonable to assume that the leaf area index pattern is realistic for the site given that the simulated peak leaf area index was in good agreement with the measurement.

The peak LAI of Indian mustard grown at Walpeup in 1993 was only 0.5. Wheat grown after this mustard crop in the drought in 1994 reached a maximum LAI of 1.5, while wheat grown in the same year on land fallowed during 1993 reached LAI of 2.5. There was no difference in the LAI of field peas grown during 1995 suggesting that the soil moisture at sowing was similar beneath both the fallow and non-fallow treatments. The wheat grown during the 1994 drought explored all available soil water and the effect of fallowing on crop growth was only apparent in the year immediately after the fallow. WAVES faithfully reproduced this behaviour without the need to adjust the parameters that characterise plant growth. This shows WAVES' ability to accurately model the effect of different levels of moisture availability on growth.

WAVES is primarily concerned with the responses and feedbacks of plants on water balance under different climatic conditions. It uses a generic plant growth model incorporating the integrated rate methodology (IRM) of Wu et al. (1994). It explicitly considers the effect of light, temperature, available water, and nutrients on plant growth on a daily time step. The IRM framework provides an explicit means of combining these factors into a single response function. It also provides a means of taking into account not only the relative availability of resources, but also other possible factors such as salinity. IRM retains a mechanistic representation of relative plant growth response to resources availability in the form of its enzyme kinetics origins. The treatment of plant stomatal functioning, transpiration, carbon allocation, and respiration in WAVES is based on well-established relationships with some simplification. The canopy conductance model of WAVES is adapted from Ball et al. (1987) as modified by Leuning (1995) and it provides the key linkage between the transport of water and carbon in the system. It is well understood that the amount of transpiration by a plant is directly related to its leaf area and therefore, it is important to be able to accurately simulate plant leaf area index.

WAVES uses a number of parameters to describe canopy carbon balance and plant growth (see Table 5.8). A necessary step in applying the model is to determine the values of these parameters or constants for the site under consideration. Parameter estimation may have at least as great an effect on the accuracy of the model results as the intrinsic accuracy of the model itself. In this study, most of the parameter values were obtained from literature as discussed previously, while the growing season length (degree daylight hours) and the leaf and root respiration coefficients (which are very difficult to measure) were obtained by trial and error methods for the first growing season. The results shown in Fig. 5.24 represent the following growing seasons with the fitted parameter values. It is encouraging to note that WAVES performed well in simulating leaf area index for six plant types under different rotation systems, given different soils at the two sites, and that annual rainfall was quite variable during the period of experiments.

Maximum rooting depth was found to play an important role in plant growth and soil moisture distribution. At Walpeup the maximum rooting depth was set to 30 cm for wheat and medic (Table 5.8), which is much smaller than the values reported in the literature (Gajri and Prihar, 1985). Field measurements showed that pH was 9.6 and exchangeable sodium percentage (ESP) was 18 % between 18 and 50 cm at the site. These factors indicate that the soil is highly sodic and provides very unfavourable conditions for root growth. This restriction in rooting depth allowed more accurate modelling of both leaf area development, and soil moisture profiles. Shallow rooting depth in the Victorian Mallee has serious implications for plant growth and recharge control because rooting zone acts as a buffer in reducing recharge and shallow rooting depth means little recharge control. Incerti and O'Leary (1990) suggested that one of the options is to introduce varies which are more tolerant to high pH.

The simulations presented here provided thorough tests for the plant growth component of WAVES. It was shown that the model performed well under a range of land use and climatic conditions and this suggests that WAVES is robust for simulating plant growth.

Temporal and vertical variation of soil moisture

The simulated soil water agrees very well with the measured values at both sites throughout the study period (Figs. 5.25 and 5.26). These particular depths were chosen to represent different soil layer (see Table 5.7) and root zone (Table 5.8) at the two sites. The model was able to reproduce seasonal variations in soil moisture for different soil types under various cropping rotations. These results support the findings of Dawes *et al*. (1997) and Zhang *et al*. (1999c) for two dryland catchments at Wagga Wagga, NSW.

To further evaluate the performance of the model in simulating soil water dynamics, we compared calculated and measured soil moisture profiles for different periods. At both sites, the model

agrees very well with the measurements throughout the soil profile (Figs 5.27 and 5.28). A drying front associated with maximum rooting density at approximately 1 m was observed throughout the study period at Hillston, below which the soil water remained relatively constant.

The maximum rooting depth used at Walpeup had a significant effect on modelled soil moisture. As mentioned already, soil physical and chemical measurements supported using a shallow rooting depth. Also, soil moisture measurements indicated that any drying front penetrated to a depth of only about 30 cm. When we used a rooting depth of 100 cm, WAVES was unable to reproduce the moisture profiles in the top 100 cm of soil, or the peak LAI of the crops.

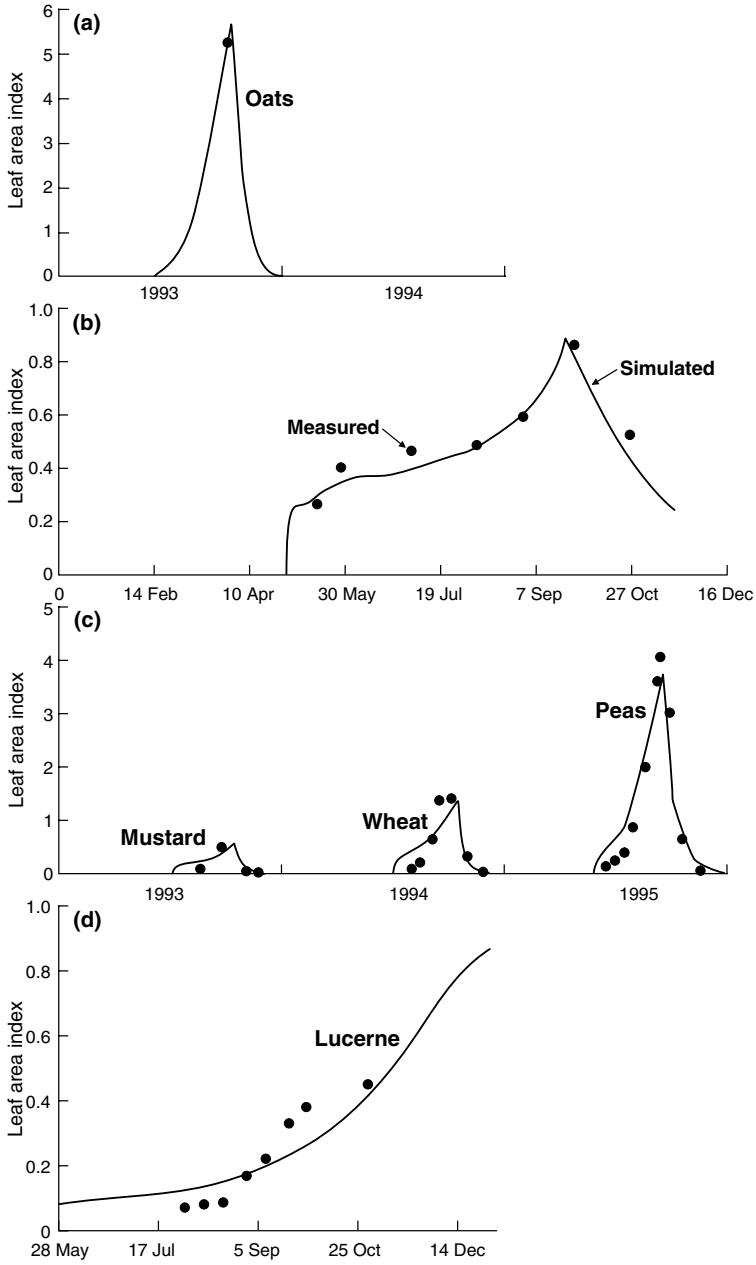

Fig. 5.24. Comparison between simulated (—) and measured (•••) leaf area index (LAI) at Hillston and Walpeup.

Table 5.9. Annual rainfall and estimates of annual recharge at 1.5 m and 4.0 m depths, using the WAVES model.

Plot	1992			1993			1994			1995		
	Rainfall (mm)	Drainage at 1.5 m (mm)	Drainage at 4.0 m (mm)	Rainfall (mm)	Drainage at 1.5 m (mm)	Drainage at 4.0 m (mm)	Rainfall (mm)	Drainage at 1.5 m (mm)	Drainage at 4.0 m (mm)	Rainfall (mm)	Drainage at 1.5 m (mm)	Drainage at 4.0 m (mm)
					Hillston							
1	471	24	13	581	10	12	212	3	13	365	0	13
10	471	23	27	581	6	33	212	0	29	365	0	25
					Walpeup							
3	—	—	—	348	18	10	153	11	10	382	30	10
10	—	—	—	348	21	10	153	5	10	382	40	10

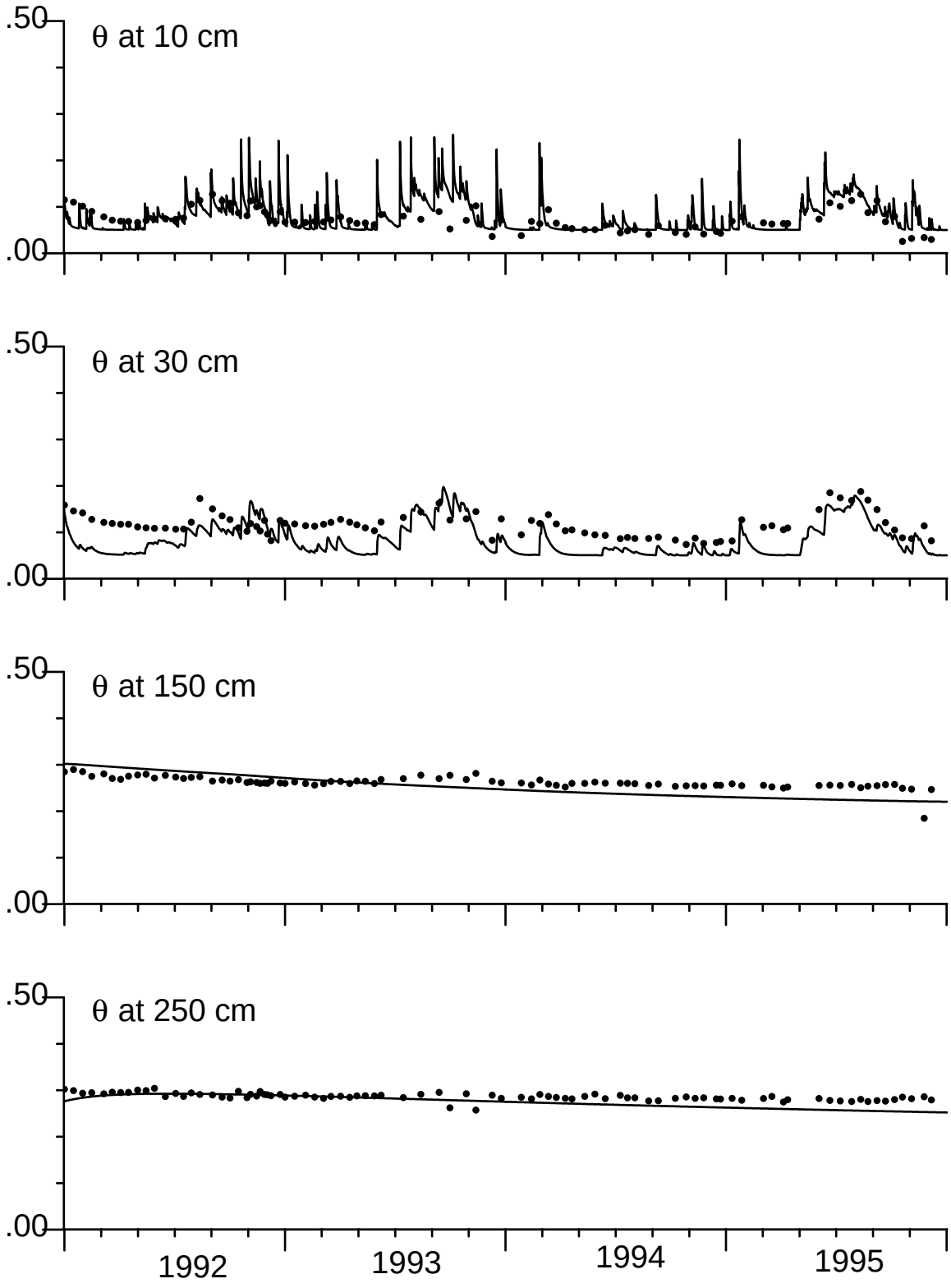

Fig. 5.25. Comparison between predicted (—) and measured soil water content (•••) at Hillston (plot 10).

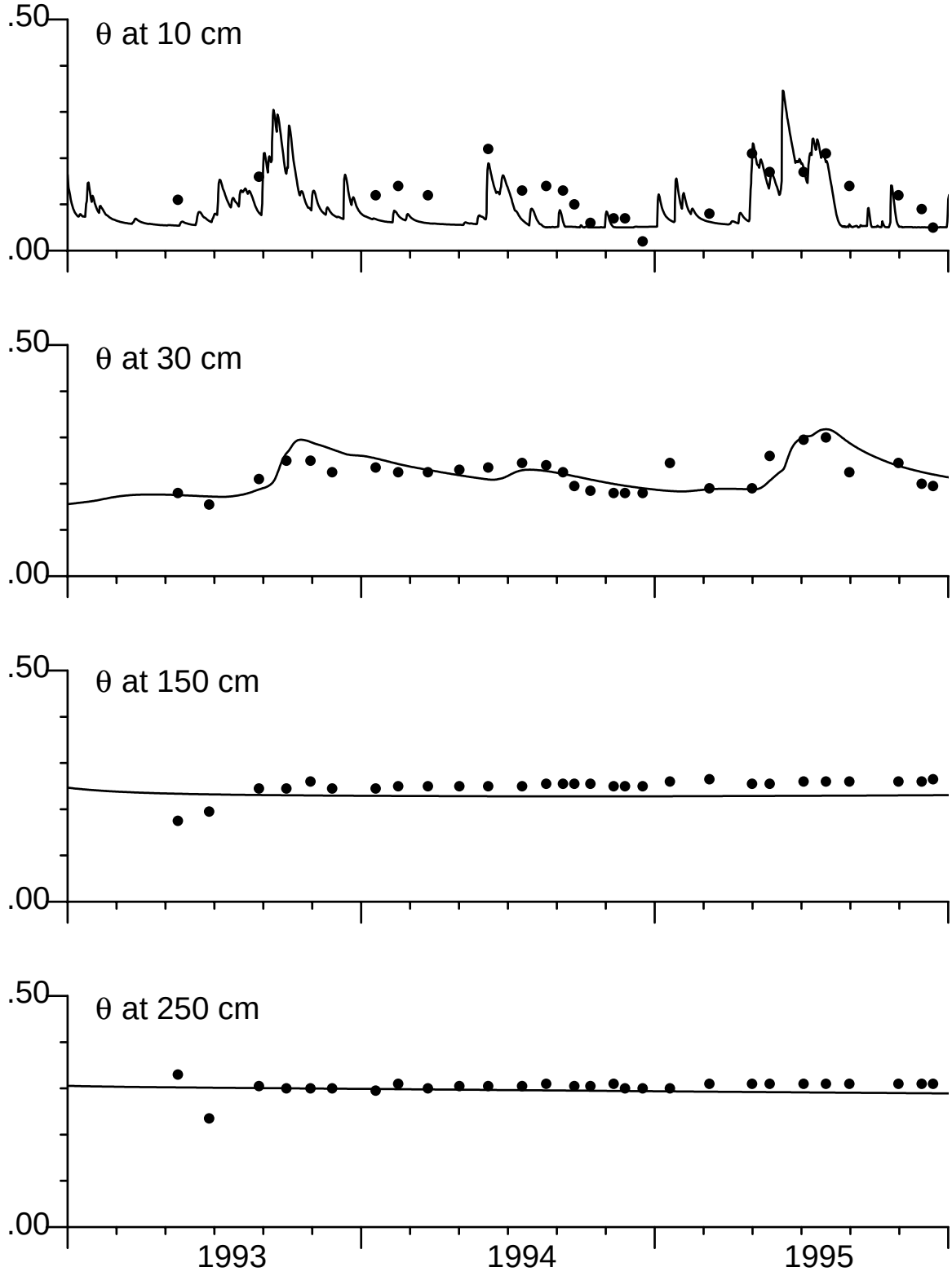

Fig. 5.26. Comparison between predicted (—) and measured soil moisture content (•••) at Walpeup.

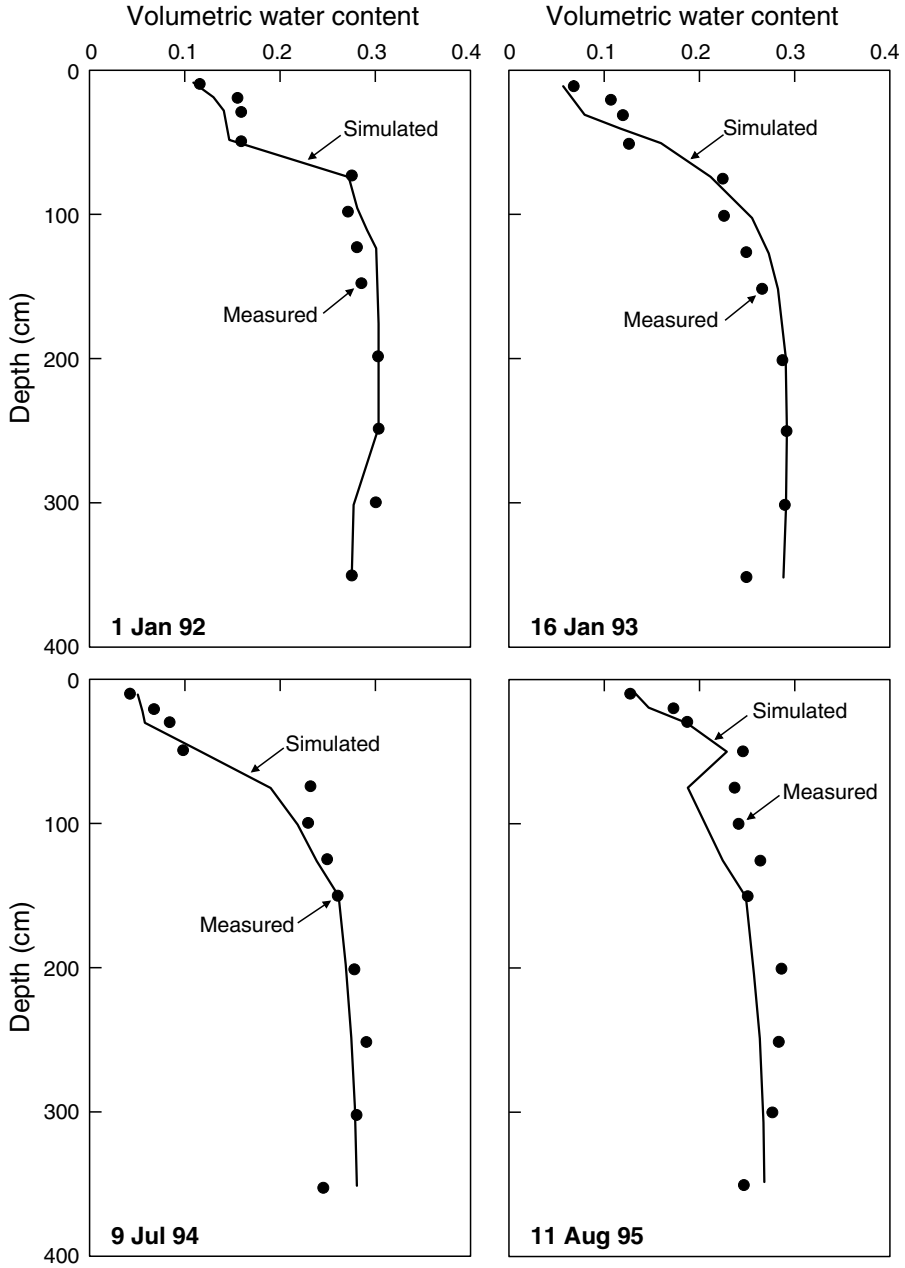

Fig. 5.27. Simulated (—) and measured (•) soil moisture profiles at Hillston for the selected dates.

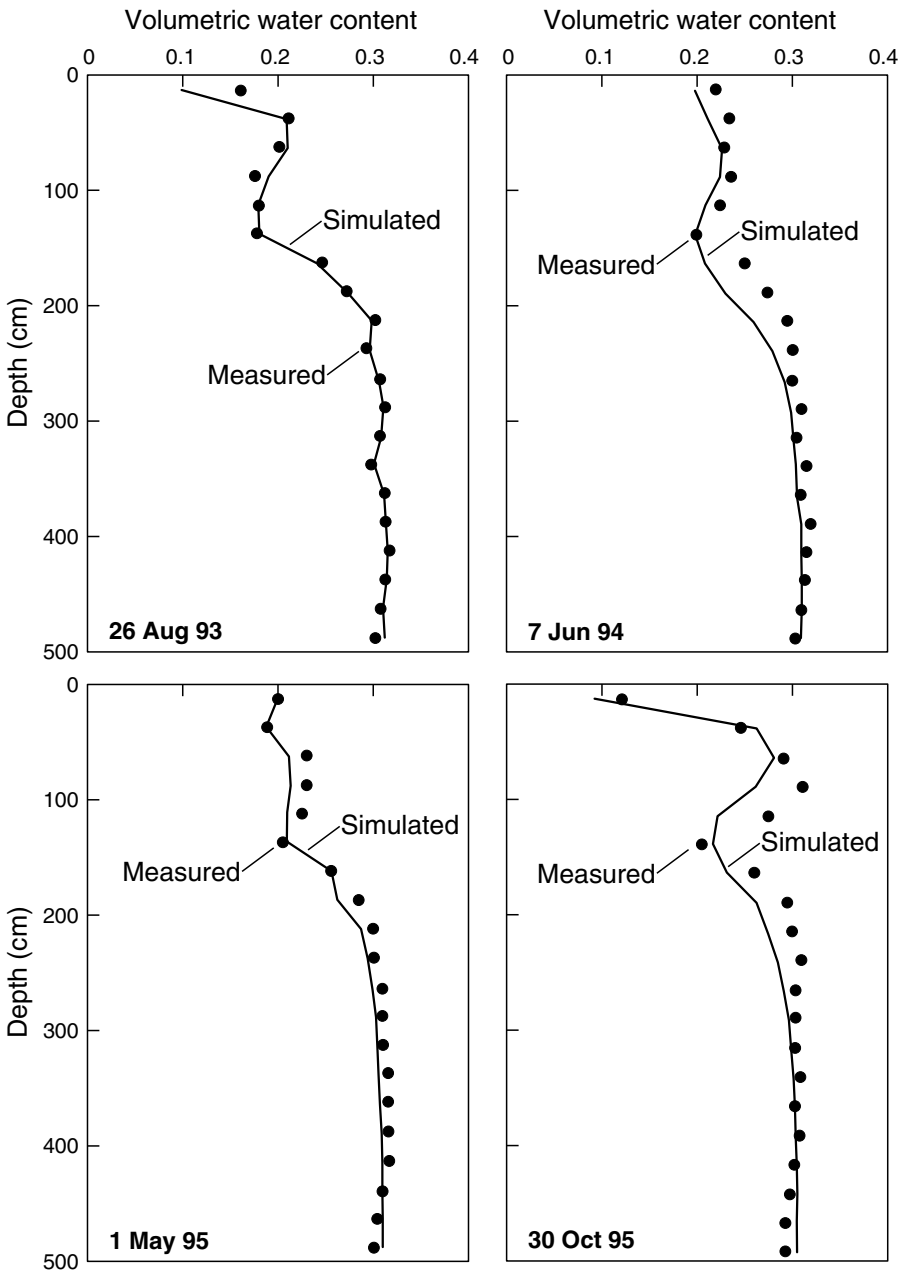

Fig. 5.28. Simulated (—) and measured (•) soil moisture profiles at Walpeup for the selected dates (plot 3).

Groundwater recharge

Modelled groundwater recharge (deep drainage) rates range from 9 to 33 mm per year (Table 5.9). The highest recharge occurred under plot 10 at Hillston, while the two cropping systems at Walpeup showed consistently lower recharge rates. The high recharge rate under plot 10 at Hillston may well be attributed to the fact that the bottom soil layer of the plot 10 was about 15% wetter than the other plots at the site.

As a result, the unsaturated hydraulic conductivity for plot 10 was twice that of plot 1, despite the lower saturated hydraulic conductivity. Given that the Hillston site was flood irrigated before the experiment started and the deep soil layer of plot 10 was always above field capacity, the cropping rotations had little impact on recharge to groundwater. These results are consistent with our understanding of the processes controlling recharge, and the measured soil moisture data.

Deep drainage is affected by a number of factors, such as rainfall, soil hydraulic properties, and vegetation. The annual recharge simulated at 4 m depth for the both sites showed no obvious relationship to the annual rainfall (Table 5.9). We have included the net flux modelled passing 1.5 m depth, this depth being the common maximum rooting depth of wheat (Incerti and O'Leary, 1990). The Hillston results show the impact of the first year irrigation, then subsequent cropping water use accounted for stored water and eliminating any deep drainage passing 1.5 m. The Walpeup data, with a much shallower rooting depth, deep drainage followed, generally, the annual rainfall, with actual crop rotation having little effect.

During the period of the study, the deep soil layers were relatively wet and deep drainage occurred mainly as a result of antecedent soil moisture content. Therefore, potential groundwater recharge showed little response to annual rainfall or crop rotations. It can be argued that for deep soil layers with low hydraulic conductivity it takes a long time for surface management to have noticeable impacts on recharge. However, over a long enough period of time the effects of vegetation changes may then be quite significant in terms of rising groundwater tables. The unsaturated hydraulic conductivity of the soil at the base of plot 10 was estimated to be 0.8 mm/d based on the Broadbridge–White soil model. At that rate, it would take nearly 13 years for water from the surface to reach the bottom of the soil column. This estimate is likely to be an upper limit, but places the time scale of recharge control in context.

Fallow soil water storage

At Walpeup in June 1993 the soil water storage was similar between fallow and continuous cropping systems (Fig. 5.29). By sowing in 1994 an additional 44 mm of water was stored in the upper 1.5 m soil profile due to fallowing. The additional soil water content at sowing due to fallowing (Fig. 5.29) resulted in the higher leaf area index of fallow wheat in the 1994 drought. At Hillston in 1992 similar soil water profiles occurred under each cropping system (Fig. 5.29). By sowing 1993, fallowing had stored an additional 25 mm of soil water.

On average, an additional 22 to 37 mm of soil water is stored in Mallee environments due to fallowing (French 1978; Incerti *et al.* 1993; O'Leary and Connor, 1997) and the stored water can be used to increase crop yield (French, 1978). However, the effect of fallowing, especially long fallowing, should not be overlooked because only part of increases in crop yield after fallowing

could be ascribed to additional water supply (French, 1978). Furthermore, the distribution of additional soil water from fallowing has been observed in the lower portion of the root zone or below the root zone, potentially leading to deep drainage (Incerti *et al.* 1993; O'Leary and Connor 1997). This has implications for recharge control under dryland conditions as highlighted by O'Connell *et al.* 1995. Incerti *et al.* (1993) argued that the use of long fallows to increase soil water supply for crop yield can not be justified. This was because it is likely to increase drainage below the root zone, and crops could only use a fraction of the stored water due to relative shallow rooting depth and sandy soil texture in the Mallee.

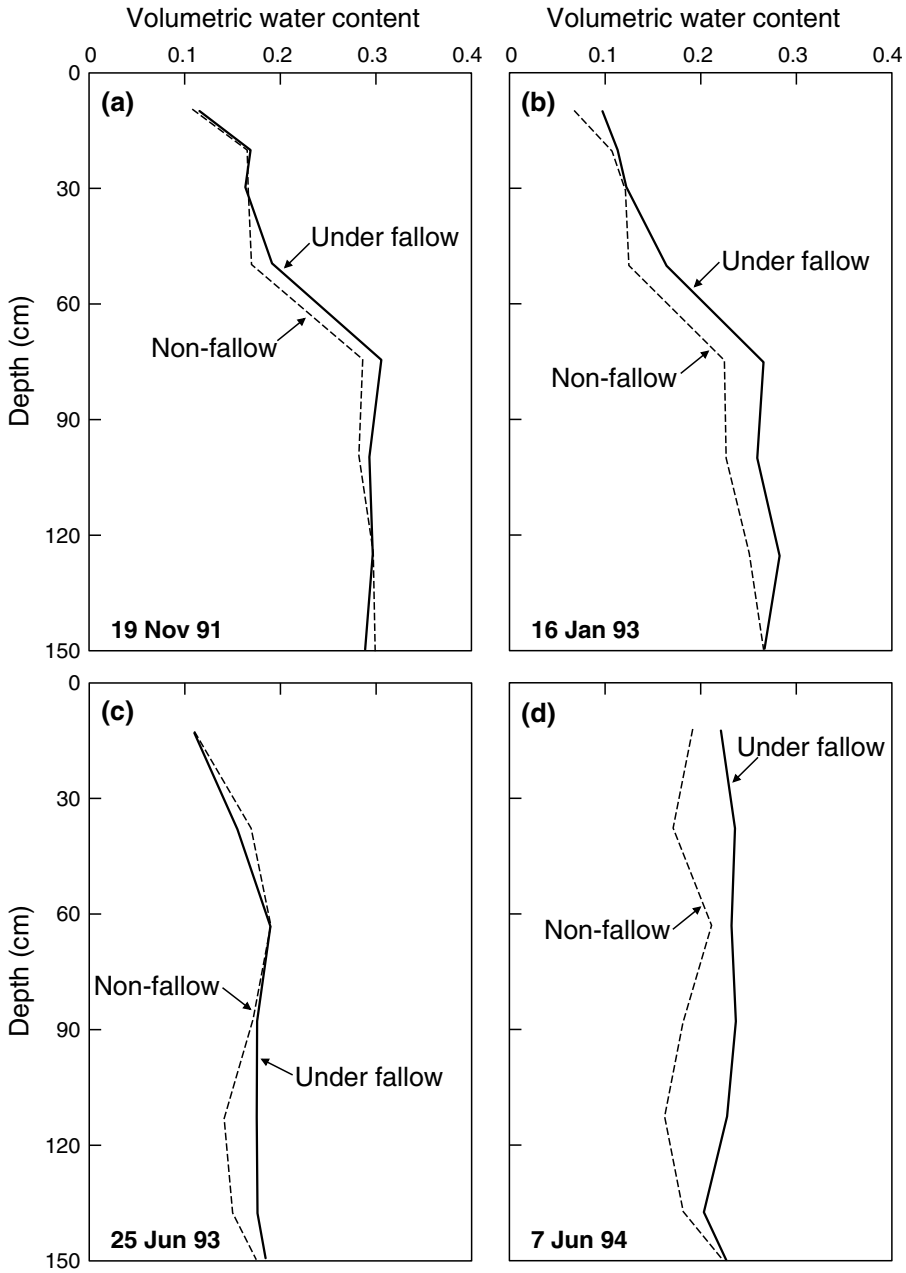

Fig. 5.29. Measured soil moisture profiles prior to (a) and after (b) fallowing at Hillston and Walpeup under fallow (—) and non-fallow (•••) crop rotations.

Long-term modelling

Recharge in the Mallee region is generally considered to be episodic as a result of infrequent large rainfall events. Rainfall at the two study sites showed extreme variability, especially at Hillston (Fig. 5.30). More than 20% of total rainfall occurred in less than 5% of total time (Fig. 5.30). Because these rainfall events are infrequent in time and significant in magnitude, they can cause large episodic recharge. As a result, it is anticipated that any agronomic practices are not likely to affect episodic recharge significantly.

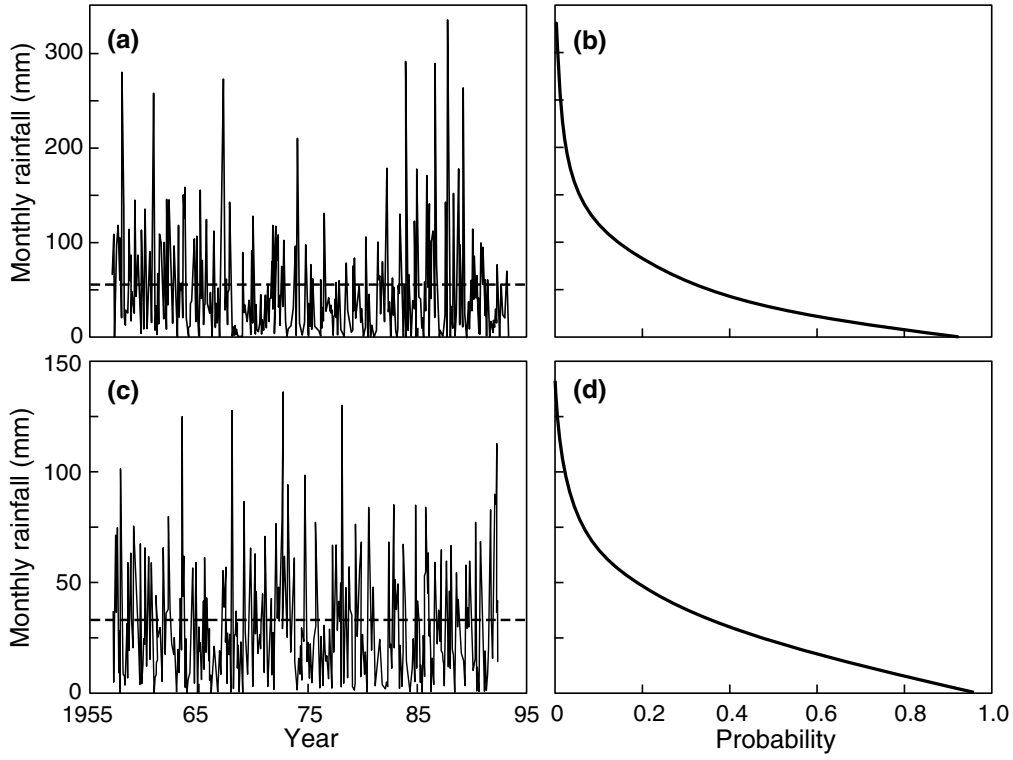

Fig. 5.30. Monthly rainfall and frequency distribution at Hillston (a,b), and at Waleup (c,d) during the period of 1957 to 1992. The horizontal lines indicate the mean rainfall.

The long-term scenario modelling at both Hillston and Walpeup is summarised in Table 5.10. Average recharge at 4 m under the lucerne rotation (RT1) was approximately 30% of that under medic rotation (RT2) and this suggests that on average lucerne has better control on recharge than medic pasture. For shallow rooted plants (*i.e.* 0.5 m rooting depth), average recharge at 4 m under the fallow rotation was 26 mm year^{-1} compared to 19 mm year^{-1} from the non-fallow rotation. This difference in recharge due to fallowing is 7 mm year^{-1} which equates to 35% extra deep drainage. The difference in average recharge between fallow and non-fallow rotations is 9 mm year^{-1} with rooting depth of 1 m (Table 5.10). Fallowing was found to cause similar deep drainage increases at Walpeup by O'Connell *et al.* (1995) using chloride profile analysis.

Table 5. 10. Summary of long-term scenario simulations

Site	Hillston				Walpeup	
Rotation[a]	RT1	RT2	RT3	RT4	RT3d	RT4d
Average rainfall (mm)	564			351	351	
Rooting depth (m)	1.5	1.5	0.5	0.5	1.0	1.0
Min. recharge (mm/yr)	0	4	8	8	5	7
Max. recharge (mm/yr)	15	34	37	37	10	25
Average recharge (mm/yr)	4	13	19	26	7	12

a:

RT1: fallow/oat/wheat/wheat/(lucerne × 4)
RT2: fallow/oat/wheat/wheat/(medic × 4)
RT3: medic/medic/wheat
RT4: medic/fallow/wheat
RT3d: medic/medic/wheat (deep roots)
RT4d: medic/fallow/wheat (deep roots).

The impact of fallowing on recharge depends on soil hydraulic properties and maximum rooting depth of successive crops. The impact, and risk of recharge, is much greater on sandy soils than on clay soils because they are inherently more conductive, have lower water holding capacity, and higher infiltration rates. Rooting depth and total soil depth play important roles in controlling recharge. The deep-rooted crops can utilize more soil water and hence offer greater control on recharge. It is generally understood that the soil volume acts as a buffer zone in reducing recharge, the deeper the rooting system, the greater the recharge control.

The annual recharge just below the root zone (*i.e.* 100 cm depth) was episodic and showed significant temporal variations (Fig. 5.31). At Hillston, 10% of annual recharge events accounted for 50 to 75% of the totals; this ratio was increased from 20 to 85% for Walpeup conditions by changing the rooting depth from 50 to 100 cm and the magnitude of these annual recharge events was as high as 130 mm year^{-1}; it is clear that the rooting depth has significant impact on episodic recharge because it determines the size of the buffer zone.

The episodicity of the recharge events can be described by the cumulative distribution function shown in Fig. 5.32. It is clear that the use of the lucerne and non-fallow rotations could reduce average recharge, but it also makes recharge more episodic in the sense that recharge occurs much less frequently but its magnitude can still be significant (see Fig. 5.31). As a result, better agronomic practices are not likely to control episodic recharge significantly. For example, annual rainfall in 1973 was 538 mm (*i.e*. 58% higher than the long-term average) and the annual recharge at 1.0 m depth under the non-fallow rotation (RT4) even exceed that under the fallow rotation (RT3). This was because the soil profile under RT4 was wetter than that under RT3, which lad to substantial more surface runoff and hence less infiltration. However, this was only observed to occur under wet years and the fallow rotations generally produced more recharge at 1.0 m depth.

The recharge rate at 4.0 m was much less variable compared to drainage rate at 1.5 m (Fig. 5.33). At Hillston, the recharge rate at 4.0 m depth increased dramatically after 10 years for the medic rotation (RT2) but not for the lucerne rotation (RT1), which continues to decrease. The recharge under RT2 appears to respond to the cumulative rainfall anomaly. At Walpeup, a similar trend was observed for the fallow rotation with shallow rooting depth (RT4). However, an increase in recharge occurred after 20 years with deep-rooted plants (RT4d) (Fig. 5.33).

It is interesting to note that the fallow rotation (RT4d) was insensitive to the cumulative rainfall anomaly. These results suggest that changes in land management (e.g. fallowing, crop rotation) may take a considerable period of time (>10 years) to have any noticeable impacts on recharge; the difference in recharge under fallow and non-fallow rotations is significant (Table 5.10).

Annual recharge at 4 m depth under the fallow rotations responded to cumulative rainfall anomaly (Fig. 5.33). It is also shown that deep-rooted plants have better control on recharge, but the degree of control is modified by soil characteristics and the prevailing weather conditions.

Results from this study showed that the recharge just below the root zone is episodic in the sense that it occurs infrequently and its magnitude is significant. Given the fact that plants can only use water in root zone, the effect of current agronomic practices on episodic recharge is limited. During these events, the root zone, generally considered as a buffer zone, became saturated and significant recharge occurred. As a result, episodic recharge can substantially reduce the effectiveness of land management options in controlling recharge. This is more so for sandy soils than for clay soils because of low water holding capacity and high infiltration rates.

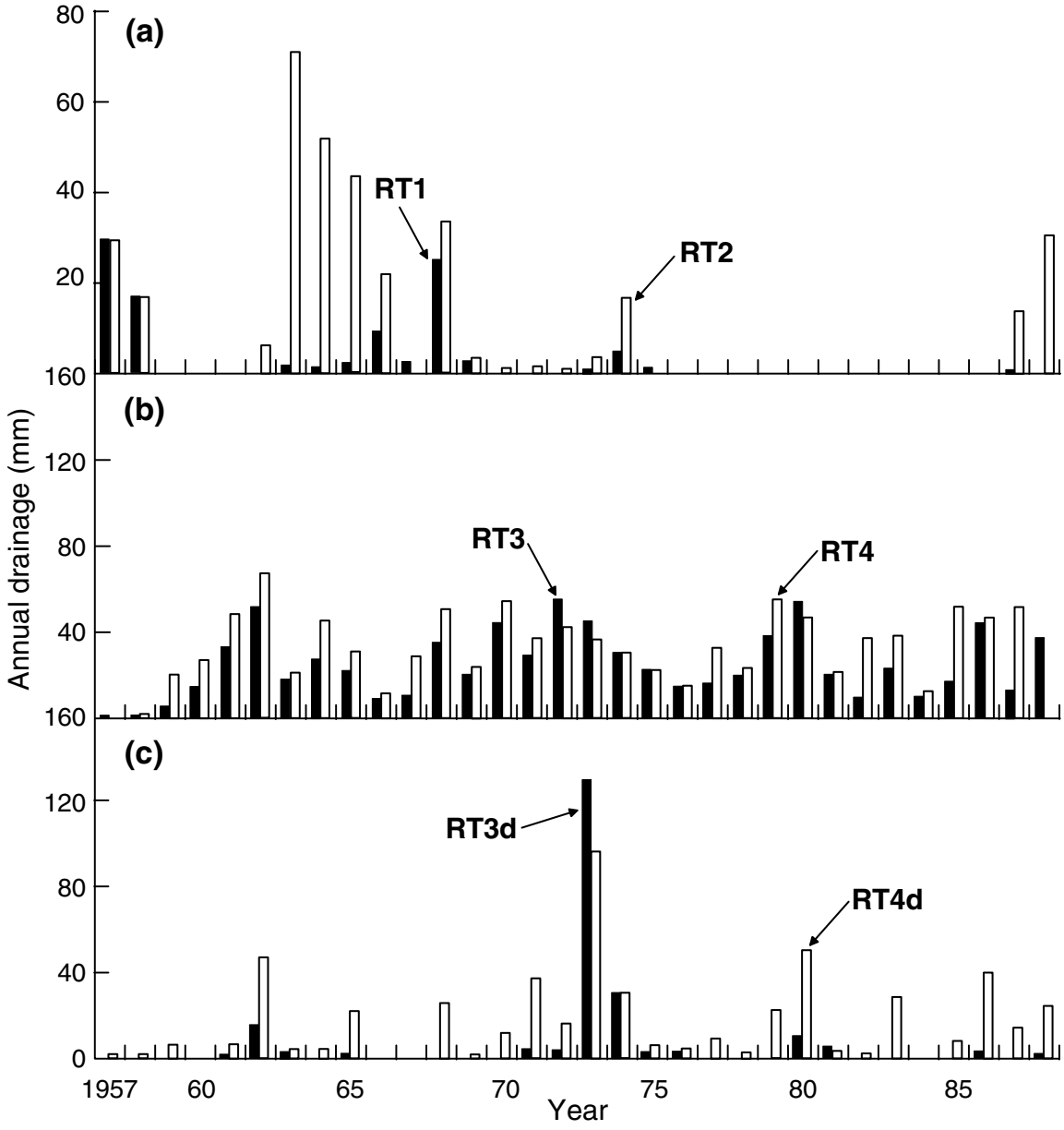

Fig. 5.31. Simulated recharge rates at 1.0 m depth for (a) Hillston under lucerne rotation (RT1) (▮) and medic rotation (RT2) (□), (b) Waleup under non-fallow (RT3) (▮) and fallow rotation (RT4) (□) with rooting depth of 0.5 m, and (c) Waleup under non-fallow (RT3d) (▮) and fallow rotation (RT4d) (□) with rooting depth of 1.0 m.

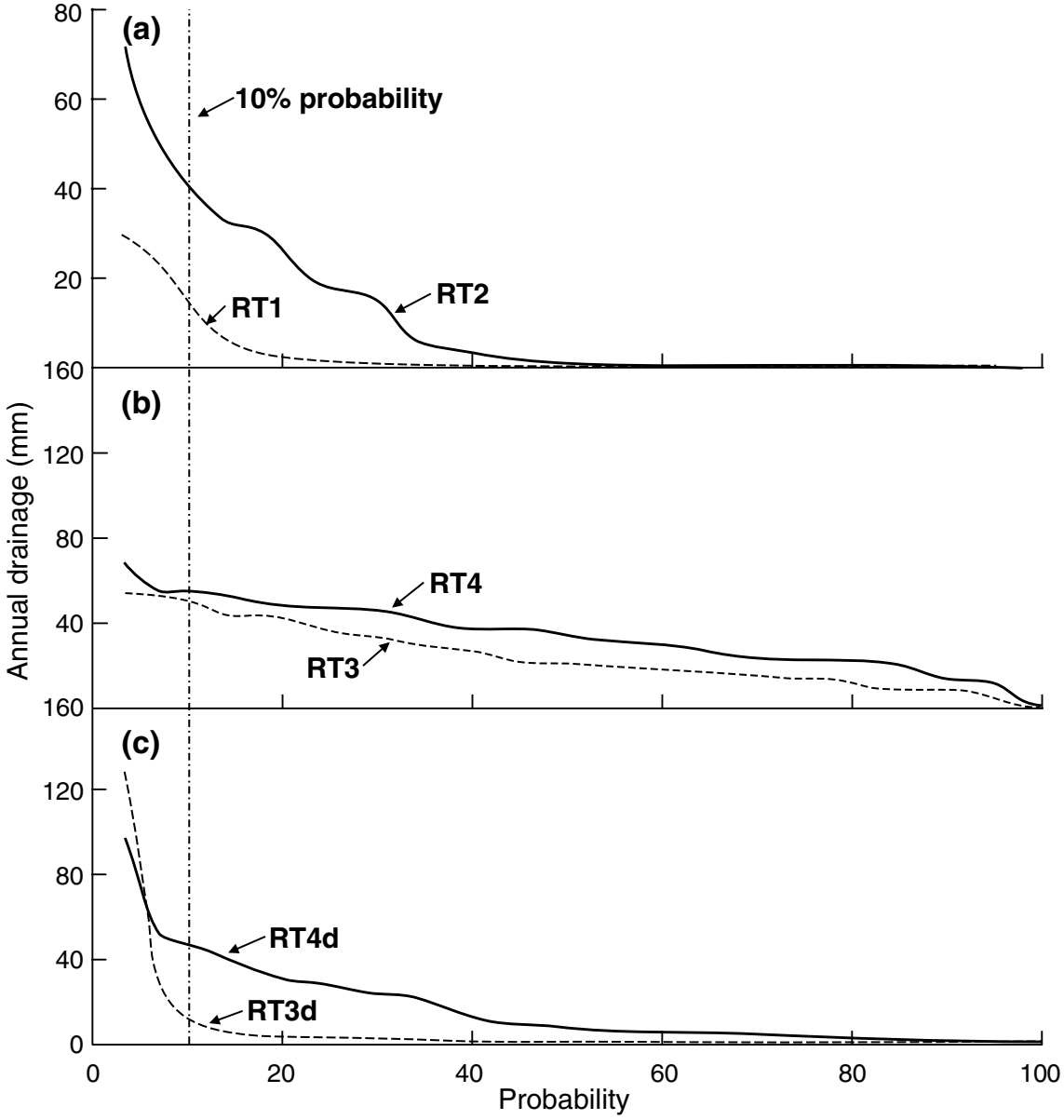

Fig. 5.32. Frequency distribution of annual recharge at 1.0 m depth for (a) Hillston under lucerne rotation (RT1) and medic rotation (RT2), (b) Waleup under non-fallow (RT3) and fallow rotation (RT4) with rooting depth of 50 cm, (c) Walpeup under non-fallow (RT3d) and fallow rotation (RT4d) with rooting depth of 100 cm. The vertical line indicates 10% probability.

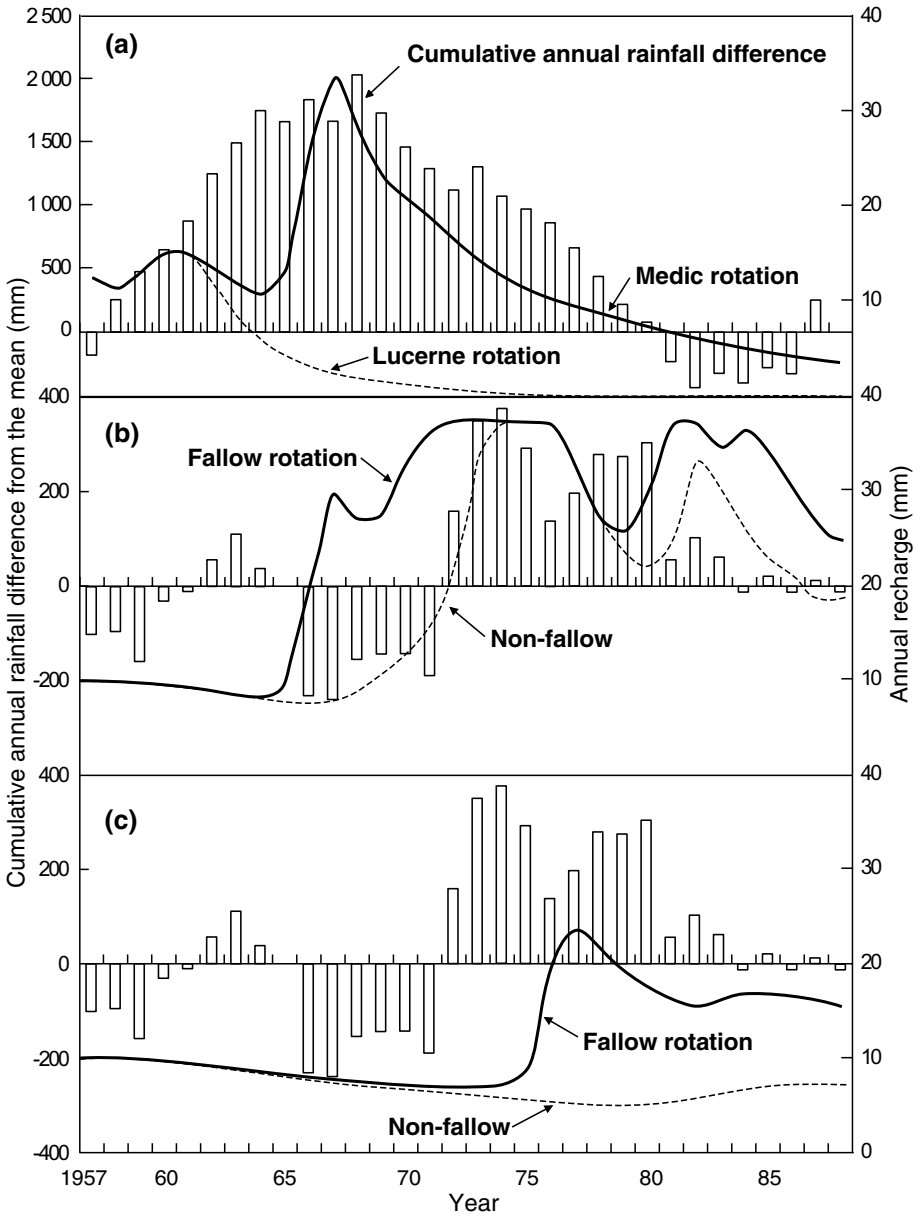

Fig. 5.33. Cumulative annual rainfall differences from the mean (□) and annual recharge rates at 400 cm depth for (a) Hillston under lucerne rotation and medic rotation, (b) Waleup with rooting depth of 50 cm, and (c) Waleup with rooting depth of 100 cm under non-fallow and fallow rotation.

Conclusions

Recharge just below the root zone is episodic and 10% of the annual recharge events accounted for 25 to 85% of the long-term totals under the Mallee conditions. The magnitude of these annual recharge events can be up to 130 mm year^{-1} and it is these events that contribute largely to groundwater recharge. Given the episodic nature of recharge in the Mallee region, better agronomic practice is not likely to affect episodic recharge significantly although it can reduce mean annual recharge.

Changes in surface management (*e.g.* fallowing, crop rotation) may take a considerable period of time (>10 years) to have any noticeable impacts on recharge as observed in the above scenario modelling. It is important to recognize the long term impacts of any agronomic practices on recharge because the effects of these changes may not be apparent for a short period of time, but may then be devastating in terms of rising groundwater table. Lucerne appeared to have better control on recharge than medic pasture and average recharge under lucerne was only 30% of that under medic pasture.

One of the advantages of physical models such as WAVES is the ability to simulate the hydrological effects of various land management options and to identify key factors controlling the processes. An attempt was made in this study to evaluate the effects of winter fallowing in crop rotations on groundwater recharge. The results showed clearly the long term benefit of non-fallowing in reducing recharge and this has implications for dryland salinity control. The traditional practice of winter fallow significantly increased soil moisture storage, groundwater recharge, and the risk of salinity. We argue that winter fallowing has contributed to dryland salinity in the Mallee regions, and more areas could be affected in the future unless improved agronomic practices are implemented. O'Connell *et al.* (1995) suggest that fallowing may be eliminated, provided its alternative encourages vigorous vegetative growth (e.g. replacement with grass-free pasture, grain legume, oilseed phase) as reported by Griffiths and Walsgott (1987) and Incerti *et al.* (1993).

Acknowledgements

This work was partially funded by the Murray–Darling Basin Commission through its Natural Resources Management Strategy Investigation and Education Program (Grant No. M4025). Technical assistance in site maintenance and data collection was provided by S.D. Blandthorn, A.J. Corbett, S. Wisneske, M.C. Brown, M.J. Ferguson, J.L. Latta, M.W. Ferguson. We are grateful to Mr. W. Milthorpe for the use of his farm at Hillston. We are grateful to V. Snow and F. Lewis for comments on a draft of this paper.

5.5 Improving Water Use Efficiency of Irrigated Crops in the North China Plain – Measurements and Modelling

H.X. Wang, L. Zhang, W.R. Dawes, C.M. Liu

Abstract

High crop productivity in the North China Plain relies on irrigation. However, as a result of rapid regional development in the last two decades, the competition for water has become very high. This presents a serious problem for sustaining agriculture in the region. This work examines relationships between irrigation, evapotranspiration, crop growth, and water use efficiency of a corn–wheat rotation common in the region. During the period of 1984 to 1996, field experiments were conducted at Luancheng Agricultural Ecosystem Station in the North China Plain to measure water and energy balance components and crop growth of corn and wheat. A process-based model (WAVES) was used to analyse the measurements and to simulate the effect of irrigation management on crop growth. The summer dominant rainfall of the region means that irrigation is required during the winter wheat growing season, when the difference between rainfall and evapotranspiration is large. While corn grows during summer, some irrigation is still required. Soil evaporation (E_s) is a significant proportion of total evapotranspiration (E_t) especially when leaf area index (L) is low, and on average E_s under a wheat canopy accounted for 30 % of E_t. Mulching reduced soil evaporation by up to 50% and saved 80 mm of water during a wheat growing season. Current irrigation schemes in the area can be improved by reducing irrigation frequency and amount.

5.5.1 Introduction

The North China Plain (NCP) is a major agricultural area in China. The region covers an area of 3×10^5 km^2, supports a population of over 300 million people, and produces 19% of the nation's food and 42% of the cotton (Huang, 1989). Traditional agriculture is well developed in the area. However, due to limited summer dominant precipitation and annual variability, agricultural productivity is low without irrigation. As a result of rapid regional development in the last two decades, the competition for water has become very high. There are no reliable surface water resources for irrigation, so groundwater has been used causing the regional groundwater table to drop significantly (Zhang and You 1996). On the other hand, the demand for high crop yield has led to irrigation water for winter wheat to increase from 100 mm/ha in the 50s to 300mm/ha in the 1980s (Zhang and You, 1996). This presents a serious problem for sustainable agricultural development in the region.

It is known that shortage of water restricts crop productivity and the purpose of irrigation is to minimise crop water stress and to achieve maximum yield. However, maximising yield should not be the sole objective and other constraints (e.g. water availability, irrigation cost, etc.) should be considered, especially in the arid regions. The response of crop yield to irrigation has been studied extensively (Skogerboe *et al.* 1979). Through proper irrigation management, it should be possible to provide only the water that matches the crop evapotranspiration. An important issue in sustainable agriculture is to optimise productivity with respect to resource inputs such as water.

It is believed that substantial improvement can be made to the current agricultural and irrigation practices in the North China Plain. A key area under investigation is the development of strategies for water-saving agriculture and to identify water management problems. In order to study this area, it is essential to understand the exchange processes between soil–plant–atmosphere in terms of water and carbon, dry matter accumulation and yield, and to improve partitioning of total evapotranspiration into soil evaporation and plant transpiration. This will provide considerable insight into efficient water use and better management.

In the last decade, a number of process-based models have been developed to simulate crop growth and water balance (Ritchie and Otter-Nacke 1985, Zhang *et al*. 1996). It is believed that these models can help us to better understand the processes and feedbacks in these systems and to identify key factors controlling plant growth and water use. During the period of 1984 to 1996, several field experiments were carried out at Luancheng Agricultural Ecosystem Station in the North China Plain to measure water balance components, crop yield, and physiological parameters. The purpose of this report is to investigate relationships between soil evaporation, transpiration, crop growth, and irrigation for corn and winter wheat in the North China Plain. This report also examines the effects of mulching on soil evaporation to reduce unnecessary loss of water.

The WAVES model (Zhang *et al.,* 1996, Dawes *et al.,* 1997) is used to assist in analysing the field data and to simulate the effects of irrigation scheduling on crop growth. This work is part of a larger study on water-saving agriculture in the North China Plain.

5.5.2 *Field measurements*

Experimental site

The experiments were conducted at Luancheng Agricultural Ecosystem Station in the North China Plain (37°53′N, 114°41′E) with an elevation of 50 m above the sea level (Fig. 5.34). The annual precipitation is about 480 mm, concentrated in the period of July to September. The dominant soil type is loam with average bulk density of 1.53 g/cm^3. Cropping practice in the region is corn followed by winter wheat and Table 5.11 shows growth stages for the two crops. The groundwater table is about 28 m below the ground surface with mineral content less than 0.5 g/ℓ.

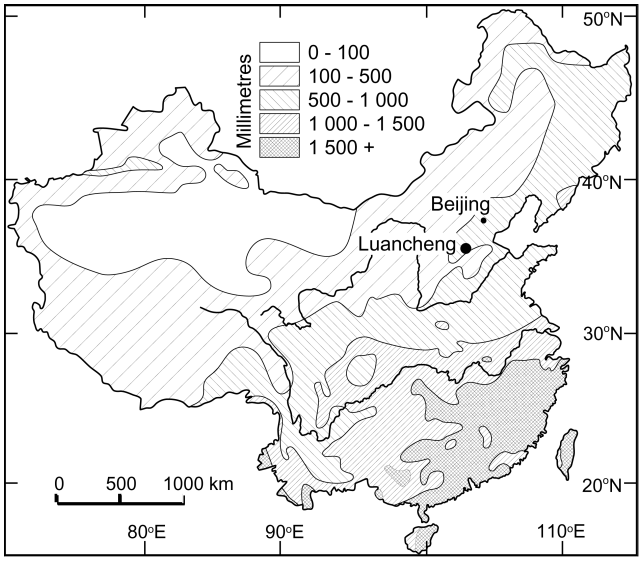

Fig.5.34. Location of study site in the North China Plain

Evapotranspiration and soil evaporation measurement

One large weighing lysimeter was installed at the station in 1985. It has a surface area of 3 m^2, and is 2.5 m deep, containing approximately 11.5 tonnes of soil. A mechanical scale allowed readings to 0.02 mm of water. A data-logger recorded changes in weight every 5 minutes and these were aggregated to daily total evapotranspiration. Inside the lysimeter, neutron access tubes were installed to monitor soil water content. Evapotranspiration was also measured using the Bowen Ratio method in an adjacent field.

Soil evaporation under the crop canopy was measured directly using micro-lysimetry. The micro-lysimeters were made of 12 cm I.D. PVC tubing 20cm long. The micro-lysimeters were weighed

once per day at 8:00 am and daily soil evaporation could be inferred. For this size of lysimeter, 1 g weight change in the soil core equals 0.09 mm of water evaporated. The soil core within the lysimeter was changed every two or three days to keep the same water status as the surrounding fields.

Table 5.11. Cropping practice and date of growth stage of corn and winter wheat in the North China Plain

Growth stage	Sowing	emergence	over-wintering	turn-green	jointing	heading	flowering	grain filling	grain harvest
wheat	1 Oct	7 Oct	15 Nov	1 Mar	10 Apr	1 May	5 May	20 May	20 Aug
corn	12 Jun	15 Jun			18 Jul		10 Aug	10 Jun	29 Sep

Soil water content measurement

Soil water content was measured using neutron probes at 20 cm intervals down to 200 cm. The measurements were taken once a week or according to the crop growth stage. The soil water content of the surface 0–20 cm interval was measured gravimetrically because neutron probes could not get an accurate readings near the surface.

Leaf area index measurement

At each crop growth stage, samples of thirty plants were randomly harvested and the length and width of each leaf was measured manually. The leaf areas of the samples were averaged to give a single value for each plot.

Meteorological data

Meteorological data were recorded hourly at the experimental site. Wet and dry bulb temperatures were measured using temperature sensors with a standard muslin wick. A tipping bucket rain gauge recorded rainfall amount and intensity. Sunshine hours and wind speed were also measured. Any missing meteorological data were filled in from neighbouring weather stations.

5.5.3 Calibration

WAVES was run from January 1984 to June 1996 using daily values of maximum and minimum air temperatures, precipitation, vapour pressure deficit, and solar radiation. The initial vegetation parameters for corn and wheat were set from previous studies (Hodges 1992; Hatton and Dawes 1993; Dawes *et al.* 1997; Zhang *et al*. 1999*a,b*). The length of growing season, and bulk respira-

tion coefficient were fitted to match leaf area development over the first three years; previous studies have been mainly concerned with C3 plants in the southern hemisphere.

The soil profile was based on soil texture profile data. The BW parameters were estimated from measured soil moisture, and soil texture (Table 5.12). Short *et al.* (1995) have shown the large dimensionless region where Richards' equation is guaranteed to work with the BW soil parameters, and the soil parameters were kept within their ranges.

Table 5.12. List of Broadbridge–White soil parameters and soil layer depths at Luancheng Station used in the study

Layer	Texture	Depth (cm)	K_s (m/d)	θ_s (cm^3/cm^3)	θ_r (cm^3/cm^3)	λ_c (m)	C
1	sandy-loam	0–35	1.0	0.40	0.05	0.05	1.02
2	loam	35–90	0.1	0.40	0.10	0.10	1.50
3	clay-loam	90–200	0.001	0.45	0.10	0.50	1.50

5.5.4 Results and discussion

Simulated crop growth and evapotranspiration

Fig. 5.35 shows a comparison of simulated and measured leaf area index for corn and winter wheat. The simulated leaf area index followed the measurements very well and the model captured the peak leaf area index in terms of timing and magnitude. Winter wheat in the North China Plain has a much longer growing season than to corn. During the winter period, wheat is usually covered by snow and its leaf area index stays constant, then starts to grow in spring; the model was able to simulate these changes. For the period 1984 to 1996, simulated peak leaf area index varied from 4.5 to 6.1 for winter wheat and 5.0 to 6.3 for corn (not shown in Fig. 5.35).

Estimates of evapotranspiration from WAVES are plotted against the lysimeter measurements in Fig. 5.36. The best fit slope through the origin is 0.98, with a correlation coefficient of 0.94. During the period of the measurements, leaf area index changed from less than 1 to above 5 and evapotranspiration rates varied between 0.5 to 7.0 mm per day. The model was able to reproduce this range and variation in evapotranspiration.

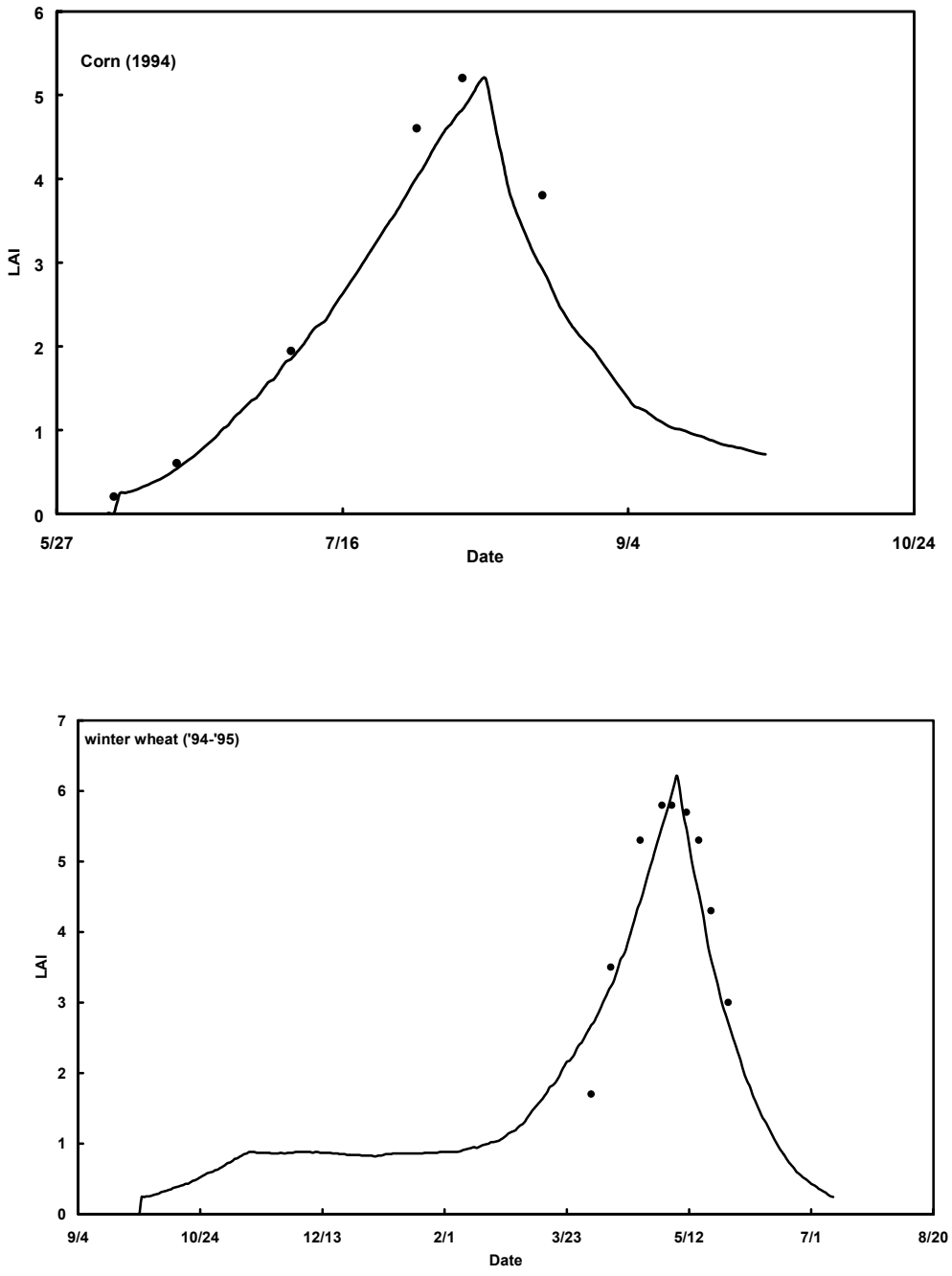

Fig.5.35. Comparison between modelled and measured leaf area index (LAI) for (a) corn and (b) winter wheat.

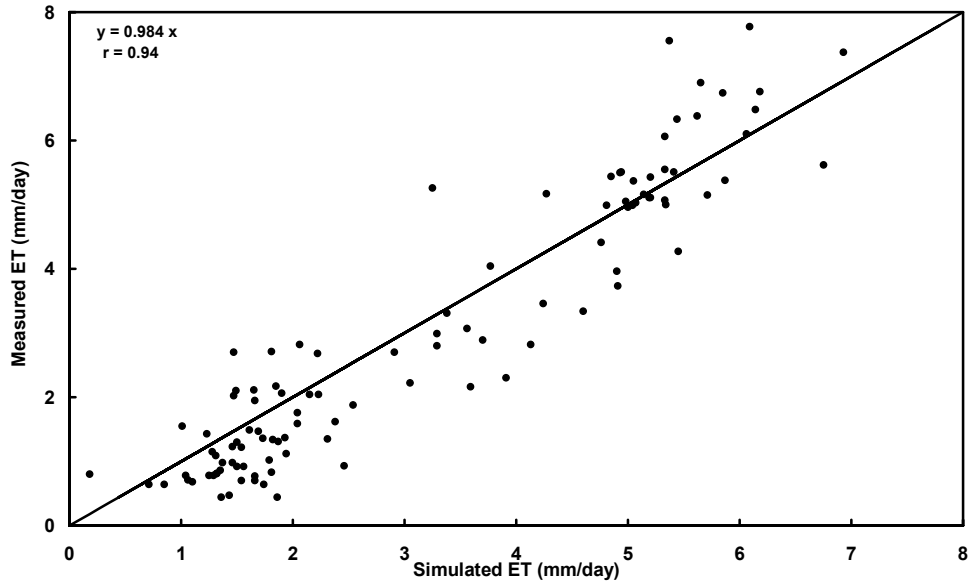

Fig.5.36. Comparison between evapotranspiration modelled by WAVES and evapotranspiration measured by lysimeter.

Soil evaporation and leaf area index

The partitioning of the total evapotranspiration (E_t) into plant transpiration (E_v) and soil evaporation (E_s) was evaluated using WAVES. Denmead (1973) proposed that the ratio E_s/E_t should decrease monotonically as leaf area index increases. Villalobos and Fereres (1990) and Wallace *et al*. (1991) confirmed the relationship by measuring E_s under corn, sunflower, and sugar cane canopies. The results from WAVES showed a similar relationship between E_s/E_t and leaf area index (L) (Fig. 5.37). The best-fit exponential relationship to the data is $E_s/E_t = exp(–0.61L)$. This conformed to the relationship obtained by Denmead *et al*. (1997).

This relationship resembles Beer's law for radiation partitioning. It can be argued that this relationship is valid for relatively wet soil where available energy is the controlling factor and this suggests that available energy at the ground surface is a good indicator of stage one soil evaporation (Villalobos and Fereres, 1990).

As shown in Fig. 5.37, calculated soil evaporation was lower than the values obtained from the theoretical curve for low leaf area index. This can be attributed to the fact that the soil moisture content of the top 10 cm of soil was only 10%. As a result, soil evaporation was limited by the available water, or stage two evaporation. A relevant issue in irrigated agriculture is the relative importance of soil evaporation and transpiration. Fig. 5.37 suggests that before canopy closure (LAI < 1) soil evaporation accounted for 50% to 90% of the total evapotranspiration. There appears to be scope to improve irrigation efficiency by altering the balance between these two fluxes. One strategy is to reduce soil evaporation by mulching. Covering the surface with plant

residues can reduce radiation and wind at the surface and hence reduce evaporation. Reduction of soil evaporation during the first stage can provide the crops with a greater opportunity to use the moisture of the top soil layers. During the second stage of drying, the rate of evaporation is usually much lower than during the first stage and the effect of mulching is likely to be small. Measured values from this study showed that mulching reduced soil evaporation by 50% under winter wheat (Fig. 5.38) and this is equivalent to 80 mm of water. In terms of irrigation efficiency, it means that we can reduce irrigation water by 25%.

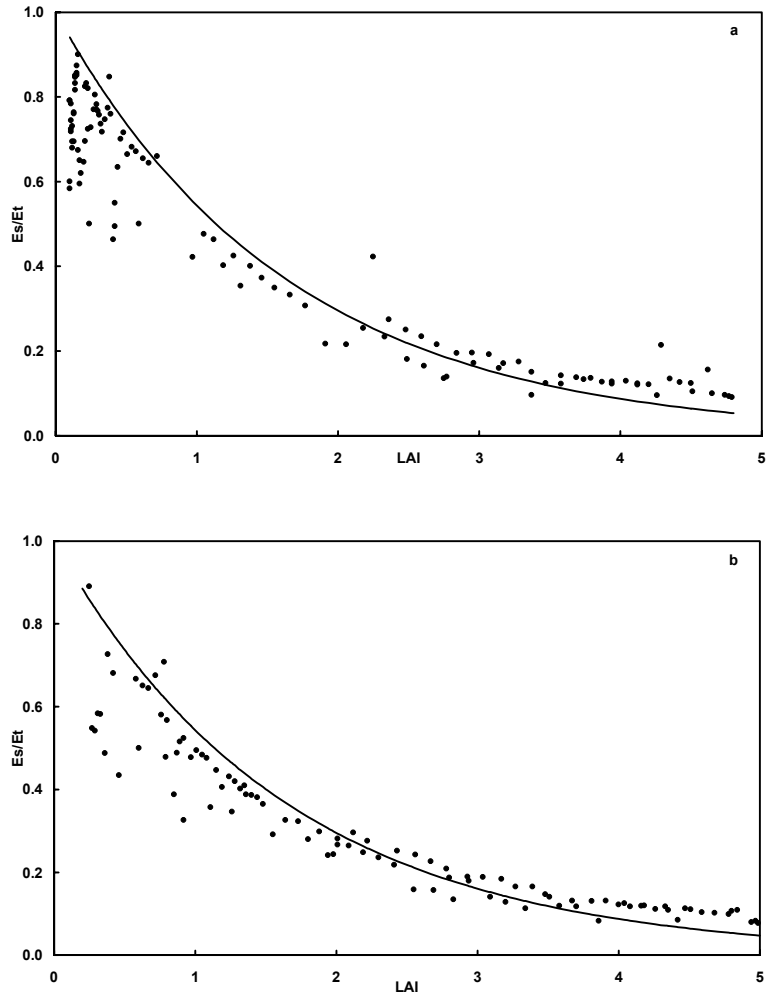

Fig.5.37. Variation of E_s/E_t with LAI for (a) corn and (b) winter wheat as simulated by WAVES. Fitted curve is for $E_s/E_t = \exp(-0.61LAI)$. E_s is soil evaporation and E_t is evapotranspiration.

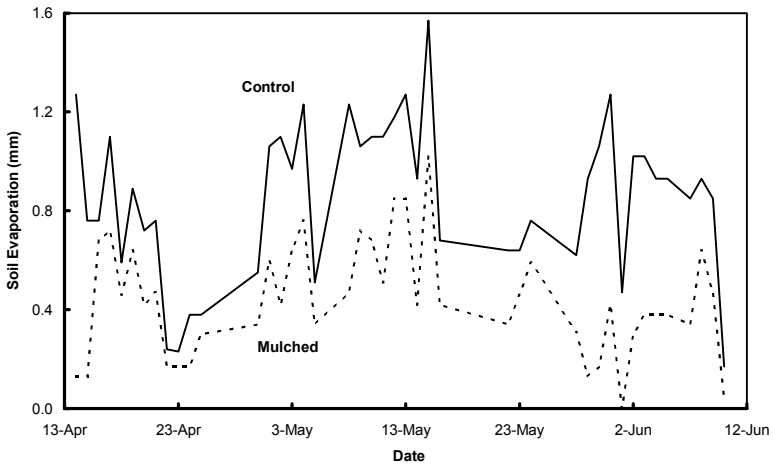

Fig.5.38. Effect of mulching on soil evaporation under winter wheat.

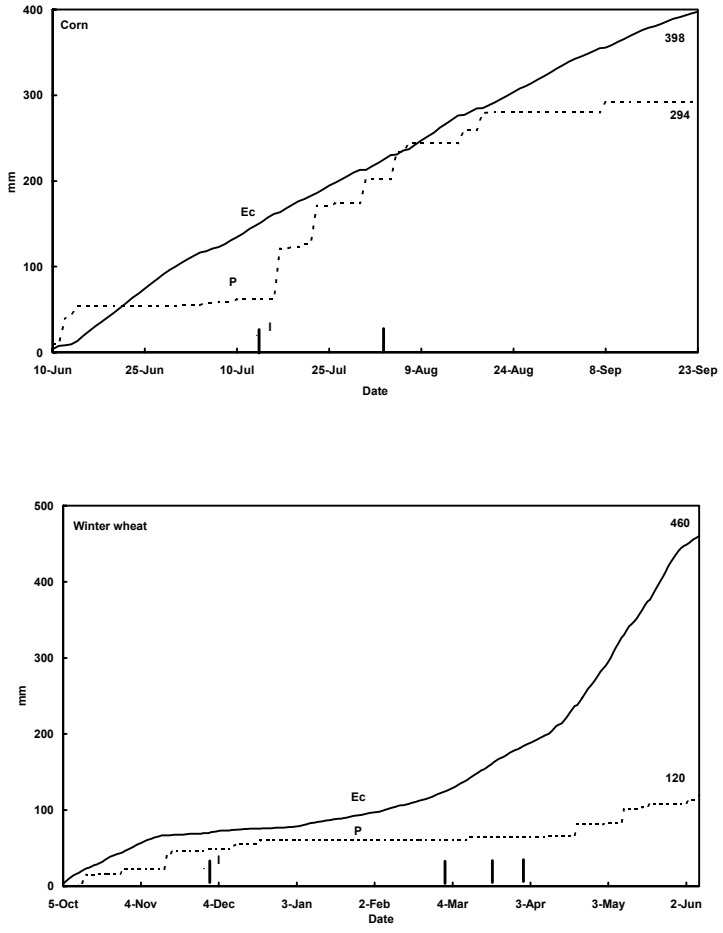

Fig.5.39. Cumulative rainfall and evapotranspiration for (a) corn and (b) winter wheat.

Effects of irrigation on crop growth

Annual precipitation in the North China Plain is extremely variable ranging from 300 to 1000 mm, with an average of 480 mm (Zhang and You, 1996). During the corn growing season (June to September), average rainfall is 350 mm (73% of annual precipitation), while for the winter wheat growing season, average precipitation is only 130 mm (27% of annual precipitation). As shown in Fig. 5.39 for 1989, total evapotranspiration during the corn growing season was 398 mm and rainfall was 294 mm. The difference was supplemented by 160 mm of irrigation water. For winter wheat, the difference between precipitation and evapotranspiration was 320 mm. These results suggest that during the corn growing season rainfall is nearly enough for evapotranspiration and irrigation can be kept to a minimum. For winter wheat however, a significant amount of water has to be supplied by irrigation to maintain high yield.

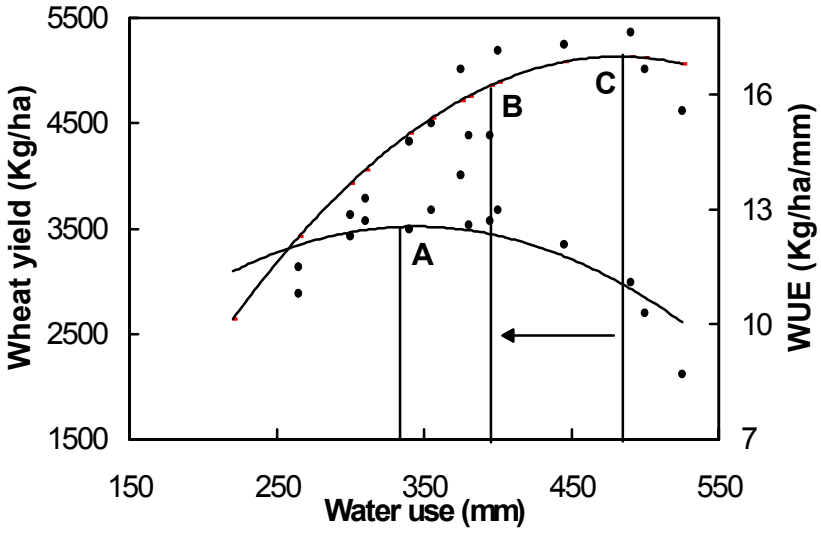

Fig.5.40. Relationship between yield, water use efficiency (WUE), and water use for winter wheat.

Water balance estimates in Fig. 5.39 show that precipitation in the North China Plain can not meet evapotranspiration demands. However, the relationship between crop yield and water use is non-linear (Fig. 5.40). Successive applications of irrigation water increase the yield until there is sufficient water in the soil for crop to meet evapotranspiration demands. It is interesting to note that the rate of increase in crop yield decreases as water use increases. In economic terms, yield response to applied irrigation is a diminishing-return function. The point marked 'A' represents maximum water-use efficiency with 200 mm of irrigation water added and a yield of 4.3 t/ha. The point marked 'C' represents maximum yield of 5.2 t/ha but this requires 350 mm of irrigation water. The point marked 'B' represents the maximum value of the 'sum' of the two curves. This point has a yield only 7% less than 'C' but uses 21% less irrigation water.

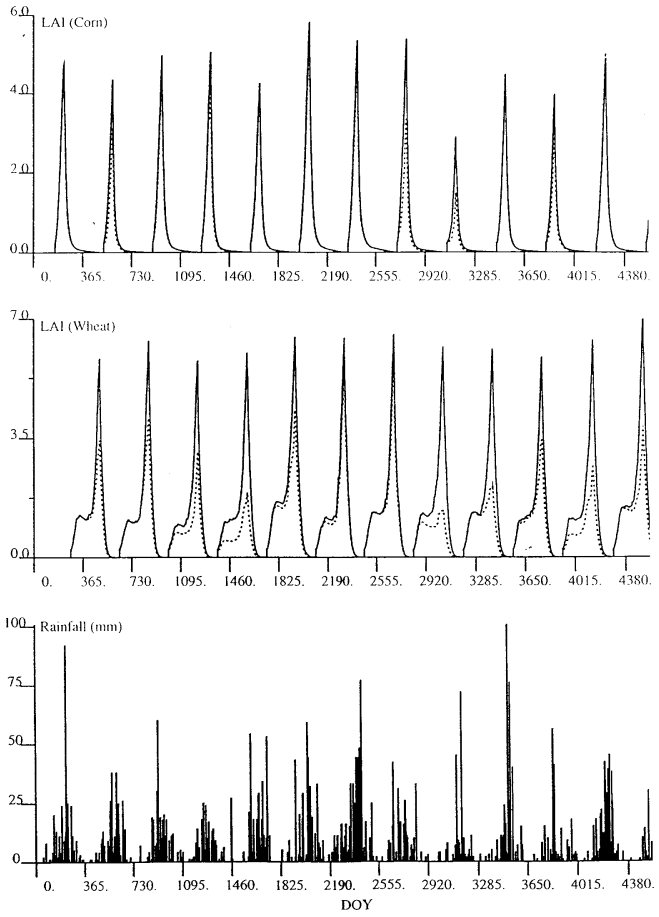

Fig.5.41. Leaf area development under different irrigation regimes. Solid line represents 80 mm of irrigation

To further investigate the effect of irrigation on crop yield (growth), several scenario simulations were conducted using WAVES. The amount of water applied in each irrigation varied from 0 mm to 80 mm and the resulting leaf areas developed are shown in Fig. 5.41. It should be noted that irrigation had no impact on crop growth in wet years, while in dry years it enhanced crop growth significantly. However, the benefit became less obvious as irrigation water supply increased. The results suggest that current irrigation practices in the area tend to over-irrigate crops. Given the water available for irrigation in the region is limited, it is not sustainable to maintain irrigation at current levels.

5.5.5 Conclusions

Precipitation in the North China Plain showed significant temporal variation. The difference between precipitation and evapotranspiration during the corn growing season is much smaller than during the winter wheat growing season. As a result, different irrigation schemes should be applied. Water balance estimates indicate that soil evaporation on average is about 30% of total evapotranspiration and the ratio is significant higher before crop canopy closure. There appears to

be scope to improve water use efficiency by altering the water balance and one strategy is to reduce soil evaporation by mulching. The effect of mulching is larger during the first stage of drying than the second stage. Results from this study showed that mulching can reduce soil evaporation by 50%, which is equivalent of 80 mm of water for winter wheat growing season. An irrigation scheme having high irrigation frequency can cause the first stage soil evaporation to persist much longer and result in more water loss than ones with low irrigation frequency. Current irrigation schemes in the North China Plain can be improved by reducing both irrigation frequency and amount, especially during corn growing season.

REFERENCES

Allen, M. B., and Murphy, C. L., 1985. A finite element collocation method for variably saturated flows in porous media. *Numerical Methods for Partial Differential Equations*, 3, 229-239.

Allen, M. B., and Murphy, C. L., 1986. A finite-element collocation method for variably saturated flow in two space dimensions. *Water Resour. Res.*, 22, 1537-1542.

Allison, G.B., Cook, P., Barnett, S.B., Walker, G.R., Jolly, I.D. and Hughes, M.W., 1990. Land clearing and river salinisation in the western Murray Basin. *J. Hydrol*., 119, 1-20.

André, J.C. et al., 1988. HAPEX-MOBILHY: first results from the Special Observing Period. *Ann. Geophys.*, 6, 477-492.

Armstrong, E.L., and Pate, J.S., 1994. The field pea crop in S.W. Australia. I. Patterns of growth, biomass production and photosynthetic performance in genotypes of contrasting morphology. *Aust. J. Agric. Res.,* 45, 1347-1362.

Armstrong, E.L., and Pate, J.S., 1994. The field pea crop in S.W. Australia. II. Effects of contrasting morphology and environment on reproductive performance. *Aust. J. Agric. Res*., 45, 1363-1378.

Ball, J. T., Woodrow, I. E. and Berry, J. A., 1987. A model predicting stomatal conductances and its contribution to the control of photosynthesis under different environmental conditions. In: Progress in Photosynthesis Research Vol IV. (ed J. Biggins*)*, Martinus Nijhoff, Dordrecht, 221-224.

Barnes, C.J., 1993. The art of catchment modeling: what is a good model? In: Proceedings of the International Congress on Modelling and Simulation (M. McAleer and A.J. Jakeman, eds.), December 6-10, University of Western Australia, Perth, pp. 19-24.

Barry, D. A., J.-Y. Parlange, G. C. Sander, and Sivapalan, M., 1993. A class of exact solutions for Richards' equation. *J. Hydrol.*, 142, 29-46.

Ben Mehrez, M., Taconet, O., Vidal-Madjar, D. and Valencogne, C., 1992. Estimation of stomatal resistance and canopy evaporation during the HAPEX-MOBILHY experiment. *Agric. For. Meteorol*., 58, 285-313.

Beven, K., 1989. Changing ideas in hydrology – the case of physically-based models. *J. Hydrol.,* 105, 157-172.

Beven, K., 1993. Prophecy, reality and uncertainty in distributed hydrological modelling. *Advances in Water Resources*, 16, 41-51.

Bigeleisen, J., Perlan, M. L., and Prosser, H. C., 1952. Conversion of hydrogenic materials to hydrogen for isotopic analysis. *Anal. Chem*., 24,1356-1357.

Black, T.A., Gardner, W.R. and Thurtell, G.W., 1969. The prediction of evaporation, drainage, and soil water storage for a bare soil. *Soil Sci. Soc. Amer. Proc*., 33, 655-660.

Bresler, E., 1972. Control of salinity. In: "Optimizing the Soil Physical Environment Toward Greater Crop Yields" (D. Hillel, ed.), pp 102-132, Academic Press, New York.

Bresler, E., 1973. Simultaneous transport of solutes and water under transient unsaturated flow conditions. *Water Resour. Res.*, 9, 975-986.

Broadbridge, P., 1990. Moving boundary problems with nonlinear diffusion. Mathematics Research Paper No. 90-18, La Trobe University, Bundoora 3083, Australia.

Broadbridge, P., and White, I., 1988. Constant rate rainfall infiltration: a versatile nonlinear model 1. Analytic solution, *Water Resour. Res.*, 24, 145-154.

Broadbridge, P., J. H. Knight, and Rogers, C., 1988. Constant rate rainfall in a bounded profile: solutions of a nonlinear model, *Soil Sci. Soc. Am. J.*, 52, 1526-1533.

Brunt, D., 1932. Notes on radiation in the atmosphere: I. *Q. J. R. Meteorol. Soc*., 58, 389-420.

Brutsaert, W., 1971. A functional iteration technique for solving the Richards equation applied to two-dimensional infiltration problems. *Water Resour. Res.,* 7, 1583-1596.

Brutsaert, W., 1982. Evaporation into the atmosphere. D. Reidel Publishing Company, Dordrecht, Holland.

Buckingham, E, 1907. Studies on the movement of soil moisture, *USDA Bur. Soils Bull.*, 38, 61 pp.

Butler, B. E., 1979. A soil survey of the horticultural soils in the Murrumbidgee Irrigation Area of New South Wales. CSIRO Aust. Bull. No. 289 – revised edition of Bull. No. 118 (1983) by Taylor, J. K. and Hooper, P. D., CSIRO Aust, Melbourne, Australia.

Campbell, G. S., 1974. A simple method for determining unsaturated conductivity from moisture retention data. *Soil Sci.*, 117, 311-314.

Campbell, G. S., 1985. Soil Physics With Basic, pp. 73-97, Elsevier, New York.

Canadell, J. Jackson, R.B., J. Ehleringer, J.R., Mooney, H.A., Sala, O.E., and Schulze, E.D., 1996. Maximum rooting depth of vegetation types at the global scale. *Oecologia*, 108, 583-595.

Celia, M. A., E. T. Bouloutas, and Zarba, R. L., 1990. A general mass-conservative numerical solution for the unsaturated flow equation. *Water Resour. Res.*, 26, 1483-1496.

Charles-Edwards, D.A., 1982. Physiological Determinants of Crop Growth. Academic Press.

Chaudhari, N. M., 1971. An improved numerical technique for solving multidimensional miscible displacement equations. *Soc. of Petrol. Eng. J.*, 11, 277-284.

Childs, E. C., and Collis-George, N., 1950. The permeability of porous materials. *Proc. Royal Soc. Series A*, 201, 392-405.

Choudhury, B.J. and Monteith, J.L., 1988. A four-layer model for the heat budget of homogeneous land surfaces. *Q. J. R. Meteorol. Soc.,* 114, 373-398.

Clapp, R. and Hornberger, G., 1978. Empirical equations for some soil hydraulic properties. *Water Resour. Res.*, 14, 601-604.

Clifton, C.A. and Taylor, J.M., 1995. Improving pasture management for control of dryland salinity. Research Note No. 8, Centre For Land Protection Research.

Clifton, C.A., Taylor, J.M. and Schroder, P.M., 1995. Pasture management, the water balance and dryland salinity management. Paper presented at Workshop on the Role of Perennial Pasture in Recharge Control, Centre For Land Protection Research, Bendigo, Vic.

Collatz, G.J., Ball, J.T., Grivet, C., and Berry, J.A., 1991. Physiological and environmental regulation of stomatal conductance, photosynthesis and transpiration: A model that includes a laminar boundary layer. *Agric. For. Meteorol*., 54, 107-136.

Collatz, G.J., Ribas-Carbo, M. and Berry, J.A., 1992. Coupled photosynthesis-stomatal conducatnce model for leaves of C_4 plants. *Aus. J. Plant Physiol*. 19, 519-538.

Cooley, R. L., 1983. Some new procedures for numerical solution of variably saturated flow problems. *Water Resour. Res.*, 19, 1271-1285.

Cosby, B.J., Hornberger, G.M., Clapp, R.B., and Ginn, T.R., 1984. A statistical exploration of the ralationships of the soil moisture characteristics to the physical properties of soils. *Water Resour. Res.* 20, 682-690.

Cresswell, H.P. and Paydar, Z., 1996. Water retention in Australian soils. I. Description and prediction using parametric functions. *Aust. J. Soil Res*., 34, 195-212.

Dawes, W. R. and Short, D. L., 1993. The efficient numerical solution of differential equations for coupled water and solute dynamics: the WAVES model. CSIRO Division of Water Resources Technical Memorandum 93/18, Canberra, ACT.

Dawes, W. R., and Hatton, T. J., 1993. TOPOG_IRM: Model Description. CSIRO *Division of Water Resources Technical Memorandum 93/5*, Canberra.

Dawes, W.R., Zhang, L., Hatton, T.J., Reece, P.H., Beale, G, and Packer, I., 1997. Evaluation of a distributed parameter ecohydrological model (TOPOG_IRM) on a small cropping rotation catchment. J. *Hydrol.,* 191, 64-86.

De Wit, C.T., 1958. Transpiration and crop yields. Versl. Landbouwk. Onderz. 64.6 Inst. of Biol. And Chem. Res. On Field Crops and Berbage, Wageningen, The Netherlands.

Denmead, O.T., 1973. Relative significance of soil and plant evaporation in estimating evapotranspiration. In: Plant Response to Climatic Factors. Proc. Uppsala Symp. UNESCO, Paris, pp. 505-511.

Denmead, O.T., Dunin, F.X., Leuning, R., and Raupach, M.R., 1997. Measuring and modelling soil evaporation in wheat crops. *Physics and Chemistry of the Earth*, 21, 97-100.

Dickinson, R.E., Henderson-Sellers, A., Kenndy, P.J., and Wilson, M.F., 1986. Biosphere-atmosphere transfer scheme (BATS) for the NCAR community climate model. NCAR Tech. Note/TN-275+STR, 69pp., Natl. Cent. for Atmos. Res., Boulder, Colo.

Dunin. F.X., O'Loughlin, E.M. and Reyenga, W., 1988. Interception loss from Eucalypt forest: Lysimeter determination of hourly rates for long term evaulation. *Hydrol. Proc*., 2, 315-329.

Eldrige, S. R., Thorburn, P. J., McEwan, K. L. and Hatton, T. J., 1993. Health and structure of *Eucalyptus* communities on Chowilla and Monoman Islands of the River Murray flood-plain, South Australia. CSIRO Division of Water Resources Divisional Report 93/3, Adelaide, SA.

El-Kadi, A. I., and Ling, G., 1993. The Courant and Peclet number criteria for the numerical solution of the Richards equation, *Water Resour. Res.*, 29, 3485-3494.

Epstein, S. and Mayeda, T., 1953. Variations of ^{18}O content of water from natural sources. *Geochim. Cosmochim. Acta*, 42, 213-224.

Farquhar, F.D., von Caemmerer, S., and Berry, J.A., 1980. A biochemical model of photosynthesic CO_2 assimilation in leaves of C_3 species. *Planta*, 149, 78-90.

Fischer, R.A., 1987. Responses of soil and crop water relations to tillage. In: P.E. Cornish and J.E. Pratley (Eds.), Tillage: New Directions in Agriculture. Inkata Press, Melbourne/ Sydney, pp. 194-221.

Fogarty, P., 1992. The soils of the Tambera experimental catchment. N.S.W. Department of Conservation and Land Management, unpublished report, Queanbeyan, N.S.W., 18 pp.

Forrest, J.A., Beatty, J., Hignett, C.T., Pickering, J. and Williams, R.G.P., 1985. A survey of the physical properties of wheatbelt soils in eastern Australia. CSIRO Division of Soils, Divisional Rep. 78, Canberra, ACT.

French, R.J., 1978. The effect of fallowing on the yield of wheat. I. The effect on soil water storage and nitrate supply. *Aust. J. Agric. Res*. 29, 653-68.

Fujita, H., 1952. The exact pattern of a concentration-dependent diffusion in a semi-infinite medium. *Textile Res. J.*, 22, 823-827.

Gardner, W. R., 1919. The movement of moisture in soil by capillarity. *Soil Sci.*, 7, 313-317.

Gardner, W. R., 1920. A capillary transmission constant and methods of determining it experimentally. *Soil Sci.*, 10, 103-126.

Gardner, W. R., 1958. Some steady-state solutions of the unsaturated moisture flow equation with application to evaporation from a water table. *Soil Sci.*, 85, 228-232.

Gardner, W. R., and Widtsoe, J. A. , 1921. The movement of soil moisture. *Soil Sci.*, 11, 215-232.

Goutorbe, J.P., 1991. A critical assessment of the SAMER network accuracy. In: Schumugge, T.J. and André, J.C. (eds.), Land Surface Evaporation. Springer-Verlag, pp. 171-182.

Grayson, R.B. and Chiew, F.F.S., 1994. An approach to model selection. Proceedings of the Joint Congress of the International Association of Hydrogeologists and International Hydrology and Water Resources Symposium, Adelaide, 21-25 November 1994.

Greacen, E.L., 1981. Soil water assessment by the neutron method. CSIRO, Melbourne.

Green, S. R. and Clothier, B. E., 1988. Water use by kiwi fruit vines and apple trees by the heat pulse technique. *J. Exp. Bot*., 39, 115-123.

Green, T.R., Bates, B.C., Fleming, P.M., and Charles, S.P., 1997a. Simulated impacts of climate change on groundwater recharge in the subtropics of Queensland, Australia. In: Subsurface Hydrological Responses to Land Cover and Land Changes, M. Taniguchi, Ed., Kluwer Academic, pp. 187-204.

Green, T.R., Charles, S.P., Bates, B.C., and Fleming, P.M., 1997b. Simulated effects of climate change on groundwater recharge: Gnangara Mound, Western Australia. In: 24th Hydrology and Water Resources Symposium Proceedings, Auckland, N.Z., Nov. 1997.

Griffiths, J.B., and Walsgott, D.N., 1987. Water use of wheat in the Victorian Mallee. In: 'Proceedings of the 4th Australian Agronomy Conference'. p. 296 (Australian Society of Agronomy, Parkville, Vic.).

Hatton T.J. and Dawes, W.R., 1993. TOPOG_IRM 2. Example Simulations. CSIRO Division of Water Resources Technical Memorandum 93/6.

Hatton, T. J. and Wu, H., 1995. Scaling theory to extrapolate individual tree water use to stand water use. *Hydrological Processes*, 9, 527-540.

Hatton, T., Dawes, W.R. and Walker, J., 1994. Predicting the impact of land change on salinity – the role of spatial models. In: Proceedings of Resource Technology '94, pp. 556-568. Melbourne, Australia, September 26-30, 1994.

Hatton, T., Dyce, P., Zhang, L., and Dawes, W.R., 1995. WAVES – an ecohydrological model of the surface energy and water balance: sensitivity analysis. CSIRO Division of Water Resources Technical Memorandum 95/2.

Hatton, T.J., Walker, J., Dawes, W.R. and Dunin, F., 1992. Simulation of hydroecological responses to elevated CO_2 at the catchment scale. *Aust. J. Bot*., 40, 679-696.

Hauhs, M., 1990. Ecosystem modelling: science or technology? *J. Hydrol*., 116, 25-33.

Haverkamp, R., and Vauclin, M., 1981. A comparative study of three forms of the Richard equation used for predicting one-dimensional infiltration in unsaturated soil, *Soil Sci. Soc. Am. J.*, 45, 13-20.

Haverkamp, R., M. Vauclin, J. Touma, P. J. Wierenga, and Vachaud, G., 1977. A comparison of numerical simulation models for one-dimensional infiltration, *Soil Sci. Soc. Am. J.*, 41, 285-294.

Hillel, D., 1971. Soil Physics. Academic Press, New York.

Hillel, D., 1980. Fundamentals of Soil Physics. Academic Press, New York.

Hodges, V., 1992. References, vegetation type and parameters used in developing and applying the TOPOG_IRM model. CSIRO Division of Water Resources Technical Memorandum 92/4, Canberra, ACT.

Hollingsworth, I. D., Meissner, A. P. and Davies, G., 1990. A reconnaissance soil survey of the Chowilla Anabranch System of the River Murray in South Australia and New South Wales, South Australian Department of Agriculture Report to the Murray-Darling Basin Commission, Canberra, ACT.

Hornung, U., and Messing, W., 1981. Simulation of two-dimensional saturated/unsaturated flows with an exact water balance. Flow and Transport in Porous Media, ed. A. Verruijt and F. B. J. Barends, pp 91-96, Balkema, Rotterdam, Netherlands.

Huang B.W., 1989. Agriculture and river conservancy of the North China Plain in relation to the potential productivity of the terrain (in Chinese). In: Study on Agro-ecological Environment, pp. 3-16.

Huang, K., R. Zhang, and van Genuchten, M. T , 1994. An Eulerian-Lagrangian approach with an adaptively corrected method of characteristics to simulate variably saturated water flow. *Water Resour. Res.*, 30, 499-507.

Hume, I.H. and Mitchell, D.C., 1996. Estimating Soil Hydraulic Properties by inverse modelling. Proc. ASSI and NZSSS, National Soils Conference, Vol. 3, pp. 109-110.

Hunt, R., 1982. Plant Growth Curves: The Functional Approach to Plant Growth Analysis. University Park Press, Baltimore, 248 pp.

Huyakorn, P. S., S. D. Thomas, and Thompson, B. M., 1984. Techniques for making finite elements competitive in modelling flow in variably saturated porous media. *Water Resour. Res.*, 20, 1099-1115.

Incerti, M., and O'Leary, G.J., 1990. The rooting depth of wheat in the Victorian Mallee. *Aust. J. Exp. Agric.*, 30, 817-824.

Incerti, M., Sale, P.W.G., and O'Leary, G.J., 1993. Cropping practices in the Victorian Mallee. 2. Effect of long fallows on the water economy and yield of wheat. *Aust. J. Exp. Agric*. 33, 885-894.

Isbell, R.A.F., 1996. The Australian soil classification. In: Australia Soil and Land Survey Handbook Series No. 4, CSIRO, Melbourne.

Jackson, R.B., Canadell, J. Ehleringer, J.R., Mooney, H.A., Sala, O.E., and Schulze, E.D., 1996. A global analysis of root distribution for terrestrial biomes. *Oecologia*, 108, 389-411.

Jarvis, P.G. and McNaughton, K.G., 1986. Stomatal control of transpiration: scaling up from leaf to region. *Adv. Ecol. Res*., 15, 1-49.

Jolly, I. D. and Walker, G. R., 1995. A sketch of salt and water movement in the Chowilla floodplain. CSIRO Division of Water Resources, Adelaide, South Australia, 42 pp.

Jolly, I. D., Walker, G. R. and Thorburn, P. J., 1993. Salt accumulation in semi-arid floodplain soils with implications for forest health. *J. Hydrol.,* 150, 589-614.

Kennett-Smith, A. Cook, P.G., Walker, G.R., 1994. Factors affecting groundwater recharge following clearing in the south western Murray Basin. *J. Hydrol*., 154, 85-105.

Kirkland, M. R., R. G. Hills, and Wierenga, P. J., 1992. Algorithms for solving Richards' equation for variably saturated soils. *Water Resour. Res.*, 28, 2049-2058.

Klute, A., 1952. Some theoretical aspects of the flow of water in unsaturated soils. *Soil Sci. Soc. Am. Proc.*, 16, 144-148.

Landsberg, J.J. and Wring R.H., 1997. A generalised model of forest productivity using simplified concepts of radiation-use efficiency, carbon balance and partitioning. *For. Eco. Manage*., 95, 209-228.

Larcher, W., 1980. Physiological Plant Ecology. Springer-Verlag, Berlin.

LaRue, M.E., Nielsen, D.R., and Hagan, R.M., 1968. Soil water flux below a ryegrass root zone. *Agron. J*., 60, 625-629.

Leuning, R. 1995. A critical appraisal of combined stomatal-photosynthesis model for C_3 plants. *Plant Celll and Environment*, 18, 339-355.

Leuning, R., Condon, A. G., Dunin, F. X., Zegelin, S. and Denmead, O. T., 1994. Rainfall interception and evaporation from below a wheat canopy. *Agric. For. Meteorol.*, 67, 221-238.

Li, C. W., 1993. A simplified Newton iteration method with linear finite elements for transient unsaturated flow. *Water Resour. Res.*, 29, 965-971.

Loveday, J. Greacen, E. L., Forest, J., Beatty, H. J., 1984. Soil data from a preliminary sampling of the Whitton common experimental site, NSW. Technical Memorandum No. 16, CSIRO Division of Soils, Glen Osmond, SA, Australia.

Margules and Partners, P., Smith, J., and Dept. Conservation, Forests and Lands, 1990. Riparian Vegetation of the River Murray. Murray-Darling Basin Commission, Canberra.

Markar, M. S., and Mein, R. G., 1987. Modeling of evapotranspiration from homogeneous soils. *Water Resour. Res.*, 23, 2001-2007.

Marshall, T.J. Holmes, J.W. and Rose C.W., 1996. Soil Physics (3rd edition). Cambridge University Press.

McCown, R.L., Hammer, G.L., Hargreaves, J.N.G. Holzworth, D.P. and Freebairn, D.M. 1996. APSIM: a novel software system for model development, model testing and simulation in agricultural systems research. *Agricultural Systems*, 50, 255-271.

McEwan, K. L., Richter, M. and Jolly, I. D., 1995. Compilation of soil, groundwater, and transpiration measurements of Eucalyptus largiflorens on the Chowilla Floodplain around the 1993/94 flood. CSIRO Division of Water Resources Technical Memorandum 95/11, Adelaide, S.A.

McMurtrie, R. E., 1985. Forest productivity in relation to carbon partitioning and nutrient cycling: a mathematical model. In: Attributes of Trees as Crop Plants, Ed. M. G. R. Cannell and J. E. Jackson, Institute of Terrestrial Ecology, pp. 194-207.

McNaughton, K. G. and Jarvis, P. G., 1991. Effects of spatial scale on stomatal control of transpiration. *Agric. For. Metorol.*, 54, 279-301.

Meiri, A., 1984. Plant response to salinity: Experimental methodology and application to the field. In: “Soil Salinity under Irrigation: Processes and Management” (Shainberg, I. and Shalhevet, J. eds.), pp. 284-297, Springer-Verlag, Berlin.

Metten, U., 1966. Desalination by Reverse Osmosis. MIT Press, Cambridge, MA.

Meyer, W. S., Dugas, W. A., Barrs, H. D., Smith, R. C. G. and Fleetwood, R. J. 1990. Effects of soil type on soybean crop water use in weighing lysimeters. I. Evaporation. *Irrig. Sci.* 11, 69-75.

Meyer, W.S., White, B. and Smith, D. 1996. Water use of lucerne over shallow watertables in Australia. In: Proceedings of ASCE Irrigation and Drainage Division, San Antonio, Texas.

Miller, R. D., and Bresler, E., 1977. A quick method for estimating soil water diffusivity functions. *Soil Sci. Soc. Am. Proc.*, 41, 1021-1022.

Milly, P. C. D., 1985. A mass conservative procedure for time-stepping in models of unsaturated flow. *Adv. Water Resources*, 8, 32-36.

Mitchell, A. R., 1969. Computational Methods in Partial Differential Equations. John Wiley and Sons, London.

Molz, F. J., 1981. Models of water transport in the soil-plant system: a review. *Water Resour. Res.*, 17, 1245-1260.

Monteith, J. L., 1977. Climate and efficiency of crop production in Britain. *Phil. Trans. R. Soc.,* 281B, 277-294.

Monteith, J.L. 1981. Evaporation and surface temperature. *Q. J. R. Meteorol. Soc.,* 107, 1-27.

Monteith, J.L. and Unsworth, M.H., 1990. Principles of Environmental Physics, 2nd edn. Routledge, Chapman and Hall, New York, 291 pp.

Monteith, J.L., 1965. Evaporation and the environment. In: G.E. Fogg (Ed.), The State and Movement of Water Living Organisms. *Sym. Soc. Exp. Biol*, 19, 205-234.

Monteith, J.L., 1979. Does light limit crop production? In: Physiological Processes Limiting Plant Productivity. Edited by Johnson, C.B. London, Butterworths.

Narasimhan, T. N., and Witherspoon, P. A., 1976. An integrated finite difference method for analyzing fluid flow in porous media. *Water Resour. Res.*, 12, 57-64.

NEC, 1988. Chowilla Salinity Mitigation Scheme – Draft Environmental Impact Statement, Report prepared by National Environmental Consultancy for the Engineering and Water Supply Department of South Australia.

Newell, J.W., 1961. Soil of the Mallee Research Station, Walpeup, Victoria. Department of Agriculture Victoria, Technical Bulletin No. 13, 56 pp.

Northcote, K. H. 1981. Morphology, distribution and classification. In: Pades, J. M., Lewis D. G. and Norrish, K. (eds) Red-brown Earths of Australia. Waite Agric. Res. Instit. and CSIRO Div. of Soils, Adelaide.

Northcote, K.H., 1979. A Factual Key for the Recognition of Australian Soils. CSIRO and Rellim Technical Publications, Adelaide, Australia.

Noye, B. J, 1990. A new third-order finite-difference method for transient one-dimensional advection-diffusion. *Communications in Applied Numerical Methods*, 6, 279-288.

O'Connell, M.G. and O'Leary, G.J., 1997. A dryland drainage lysimeter experiment: design and installation. Technical report (unpublished).

O'Connell, M.G. O'Leary, G.J., Incerti, M., 1995. Potential groundwater recharge from fallowing in north-west Victoria, Australia. *Agric. Water Manage*., 29, 37-52.

O'Leary, G.J. and Connor, D.J., 1997. Stubble retention and tillage in a semiarid environment: 1. Soil water accumulation during fallow. *Field Crops Research*, 52, 209-219.

O'Malley, C., 1990. Floodplain vegetation. In: Chowilla Floodplain Biological Study (C. O'Malley and F. Sheldon, editors), Nature Conservation Society of South Australia, Adelaide, South Australia, 224 pp.

Overton, I. C., Taylor, P. J., Hodgson, G., Correll, R. L., Hatton, T. J. and Walker, G. R.,1994. The evaluation of a geographical information system for assessing the health of vegetation on a River Murray floodplain. In: Proceedings (Vol. 1) of Water Down Under 94, Institute of Engineers, Australian National Conference Publication No. 94/10, 605-608.

Paniconi, C., Aldama, A. A., and Wood, E. F., 1991. Numerical evaluation of iterative and noniterative methods for the solution of the nonlinear Richards equation. *Water Resour. Res.*, 27, 1147-1163.

Patterson, H.D., 1963. The theory and design of rotational experiments. Proc. Statistical Soc. read at a research methods meeting of the Royal Statistical Society, 13th November 1963.

Penman, H.L., 1948. Natural evaporation from open water, bare soil and grass. *Proc. R. Soc. London, Ser. A.*, 193, 120-146.

Philip, J. R., 1957a. The theory of infiltration: 1. The infiltration equation and its solution. *Soil Sci.*, 83, 345-357.

Philip, J. R., 1957b. The theory of infiltration: 3. Moisture profiles and relation to experiment. *Soil Sci.*, 84, 163-178.

Philip, J. R., 1958. The theory of infiltration: 6. Effect of water depth over soil. *Soil Sci.*, 85, 278-286.

Philip, J. R., 1992. Exact solutions for redistribution by nonlinear convection-diffusion. *J. Austral. Math. Soc. Ser. B*, 33, 363-383.

Philip, J. R., 1993. Approximate analysis of falling-head lined borehole permeameter. *Water Resour. Res.*, 29, 3763-3768.

Philip, J. R., and Knight, J. H., 1991. Redistribution of soil water from plane, line, and point sources. *Irrig. Sci.*, 12, 169-180.

Poss, R., Smith, C.J., Dunin, F.X., and Angus, J.F., 1995. Rate of soil acidification under wheat in a semi-arid environment. *Plant Soil*, 177, 85-100.

Press, W. H., B. P. Flannery, S. A. Teukolsky, and Vetterling, W. T., 1986. Numerical Recipes in C. Cambridge University Press, New York.

Raats, P. A. C., and Gardner, W. R., 1971. Comparison of empirical relationships between pressure head and hydraulic conductivity and some observations on radially symmetric flow. *Water Resour. Res.*, 7, 921-928.

Raison, R.J., Myers, B.J., Benson, M.L., 1992. Dynamics of Pinus radiata foliage in relation to water and nitrogen stress: I. Needle production and properties. *Forest Ecology and Management,* 52, 1-4.

Raupach, M.R. and Thom, A.S., 1981. Turbulence in and above plant canopies. *Annual Review of Fluid Mechanics,* 13, 97-129.

Read, J. and Bushby, JR., 1990. Comparative response to temperature of the major canopy species of Tasmanian cool temperate rainforest and their ecological significance. II. Net photosynthesis and climate analysis. *Australian Journal of Botany,* 38, 185-205.

Redinger, G. J., G. S. Campbell, K. E. Saxton, and Papendick, R. I., 1984. Infiltration rate of slot mulches: measurement and numerical simulation. *Soil Sci. Soc. Am. J.*, 48, 982-986.

Richards, L. A., 1931. Capillary conduction of liquids through porous media, *Physics*, 1, 318-333.

Ritchie, J.T., 1972. Model for predicting evaporation from a row crop with incomplete cover. *Water Resour. Res.,* 8, 1204-1213.

Ritchie, J.T., Otter-Nacke, S. 1985. Testing and validating the CERES-Wheat model in diverse environments. AgRISTART Publ. No. YM-15-00407. NTIS, Springfield, VA.

Roache, P. J., 1976. Computational Fluid Dynamics. Hermosa Publishers, Alberquerque, N. M..

Ross, J., 1981. The Radiation Regime and Architechture of Plant Stands. Dr. W. Junk Publisher, The Hague, The Netherlands

Ross, P. J., 1990. Efficient numerical methods for infiltration using Richards' equation. *Water Resour. Res.*, 26, 279-290.

Ross, P. J., and Bristow, K. L., 1990. Simulating water movement in layered and gradational soils using the Kirchhoff transform. *Soil Sci. Soc. Am. J.*, 54, 1519-1524.

Ross, P.J., 1993. A method of deriving soil hydraulic properties from field water contents for application in water balance studies. *J. Hydrol*., 144, 143-153.

Rowan, J.N. and Downes, R.G., 1963. A study of the land in north-western Victoria (Soil Conservation Authority, Victoria).

Running, S.W. and Coughlan, J. C., 1988. A general model of forest ecosystem processes for regional applications. 1. Hydrological balance, canopy gas exchange and primary production processes. *Ecological Modelling*, 42, 125-154.

Running, S.W., Nemani, R.R., and Hungerford, R.D., 1987. Extrapolation of synoptic meteorological data in mountainous terrain, and its use for simulating forest evapotranspiration and photosynthesis. *Can. J. For. Res*., 174, 472-483.

Salama, R., Hatton, T.J., Zhang, L., and Dawes, W.R., 1999. Predicting land use impacts on regional scale groundwater recharge and drainage. *J. Env. Qual*., 28, 446-460.

Sander, G. C., J.-Y. Parlange, V. Kühnel, W. L. Hogarth, D. Lockington, and O'Kane, J. P. J., 1988. Exact nonlinear solution for constant flux infiltration. *J. Hydrol*., 97, 341-346.

Sellers, P.J., F.G. Hall, G. Asrar, D.E. Strebel., and Murphy, R.E., 1988. The first ISLSCP field experiment (FIFE). *Bull. Am. Meteorol. Soc*., 69, 22-27.

Sellers, P.J., Hall, F.G., Strebel, D.E. and Murphy, R.E., 1992b. An overview of the first international satellite land surface climatology project (ISLSCP) field experiment (FIFE). *J. Geophys. Res*., 97(D17), 1934-1837.

Sellers, P.J., J.A. Berry, G.L. Collatz, C.B. Field, and Hall, F.G., 1992a. Canopy reflectance, photosynthesis and transpiration. Part III: A reanalysis using enzyme kinetics – electron transport models of leaf physiology. *Remote Sens. Environ*., 42, 187-216.

Sellers, P.J., Y. Mintz, Y.C. Sud and Dalcher, A., 1986. The design of a simple biosphere model (SiB) for use within General Circulation Models. *J. Atmos. Sci.,* 43, 505-531.

Shao, Y., Leslie, L., Munro, R. K., Irannejad, P., Lyons, W. F., Morison, R., Short, D. L. and Wood, M. S., 1997. Soil moisture prediction over the Australian continent. *Meteorology and Atmospheric Physics,* 63, 195-215.

Sharma, D.K. and Kumar, A., 1989. Effect of irrigation on growth analysis, yield and water use in Indian mustard (Brassica juncea subsp juncea). *Indian Journal of Agricultural Sciences,* 59, 162-165.

Shoop, T. E., 1979. A Practical Guide to Computer Methods for Engineers. Prentice-Hall, Englewood Cliffs, NJ.

Short, D. L. and Dawes, W. R. and White, I., 1995. The practicability of using Richards' equation for general purpose soil-water dynamics models. *Environment International*, 21, 723-730.

Shuttleworth, W.J. and Wallace, J.S., 1985. Evaporation from sparse crops – an energy combination theory. *Q. J. R. Meteorol. Soc*., 111, 839-855.

Shuttleworth, W.J., 1979. Evaporation. Report No. 56, Institute of Hydrology, Wallingford, U.K.

Shuttleworth, W.J., 1991. Insight from large-scale observational studies of land/atmosphere interactions. In: Land surface atmosphere interactions: parameterization and analysis for climate modelling (ed. E.F. Wood), 3-30, D. Reidel, New York.

Skogerboe, G.V., Hugh, J.W., Treat, B.J., and McWhorter, D.B., 1979. Potential effects of irrigation practices on crop yields in Grand Valley. U.S. Environ. Proc. Agency Tech. Ser. Pap. No. EPA600/2-79-149. U.S. Government Printing Office, Washington, D.C.

Slavich, P. G., Hatton, T. J. and Dawes, W. R., 1998. The canopy growth and transpiration model of WAVES: Technical description and evaluation. CSIRO Land and Water Technical Report. No. 3/98.

Smith, D. J., Meyer, W. S., Barrs, H. D., and Schwamberger, E. C., 1996. Lucerne daily water use and capillary upflow using weighing lysimeters: effects of soil type and groundwater salinity. CSIRO Division of Water Resources Technical Memorandum, 96/6.

Smith, E. A., Harry, J.C., W.L. Crosson, and Weng, E.Y., 1993. Estimation of surface heat and moisture fluxes over a prairie grassland. 3. Design of a hybrid physical/remote sensing biosphere model. *J. Geophys. Res*., 98, 4951-4978.

Stace, H.C.T., Hubble, G.D., Brewer, R., Northcote, K.H., Sleeman, J.R., Mulcahy, M.J. and Hallsworth, E.G., 1968. A Handbook of Australian Soils. Rellim Technical Publications, Glenside, South Australia.

Swanson, R. H. and Whitfield, D. W. A., 1981. A numerical analysis of the heat-pulse velocity theory and practice. *J. Exp. Bot*., 32, 221-239.

Taylor, P. J., Walker, G. R., Hodgson, G., Hatton, T. J. and Correll, R. L., 1996. Testing of a GIS Model of *Eucalyptus largiflorens* health on a semi-arid, saline floodplain. *Environmental Management* 20, 553-564.

Taylor, P.J., 1993. An assessment of the applicability of an existing G.I.S and aerial photography for predicting the health of black box (*Eucalyptus largiflorens* F. Muell.) on the Chowilla floodplain. Honours Thesis, Department of Environmental Science and Rangeland Management, The University of Adelaide.

Thom, A.S., 1975. Momentum, mass and heat exchange of plant communities. In: Vegetation and the atmosphere. Ed. J.L. Monteith, Academic Press, New York, pp. 57-109.

Thorburn, P. J. and Mensforth, L. J., 1993. Extraction of water from *Medicago sativa* for analysis of stable isotopes of water. *Comm. Soil Sci. Plant Anal.*, 24, 549-557.

Thorburn, P. J., Walker, G. R. and Brunel, J. P., 1993. Extraction of water from Eucalyptus trees for analysis of deuterium and oxygen-18: Laboratory and field techniques. *Plant, Cell and Env*., 16, 269-277.

Thorburn, P.J., McEwan, K.L., Smith, D.J., Schwamberger, E.C. and Meyer, W.S. 1994. Uptake of saline groundwater by irrigated lucerne. In: Proceedings of the Third National Workshop on the Productive Use of Saline Lands, Echuca, Victoria, Australia, March 1994.

Van De Griend, A.A. and Van Boxel, J.H., 1989. Water and surface energy balance model with a multilayer canopy representation for remote sensing purposes. *Water Resour. Res*., 25, 949-971.

Van Dijk, D. C., 1961. Soils of the southern portion of the Murrumbidgee Irrigation Areas. Soils Land Use Series. CSIRO Australia, No. 40, 40 pp.

van Genuchten, M. T., 1980. A closed-form equation for predicting the hydraulic conductivity of usaturated soils, *Soil Sci. Soc. Am. J.*, 44, 892-898.

Versteeg, M.N. and van Keulen, H., 1986. Potential crop production prediction by some simple calculation methods as compared with computer simulations. *Agricultural Systems*, 19, 249-272.

Vertessy, R.A., Hatton, T.J., Benyon, R.G., and Dawes, W.R., 1996. Long-term growth and water balance predictions for a mountain ash (*Eucalyptus regnans*) forest catchment subject to clear-felling and regeneration. *Tree Physiology*, 16, 221-232.

Vertessy, R.A., T.J. Hatton, P.J. O'Shaughnessy and Jayasuriya, M.D.A., 1993. Predicting water yield from a mountain ash forest catchment using a terrain analysis based catchment model. *J. Hydrol.,* 150, 665-700.

Villalobos, F.J., and Ferres, E., 1990. Evaporation measurements beneath corn, cotton and sun-flower canopies. *Agron. J*., 82, 1153-1159.

Walker, G. R., Jolly, I. D. and Jarwal, S. D., 1996. Salt and water movement in the Chowilla floodplain. CSIRO Division of Water Resources, Water Resources Series No. 15, Canberra, ACT.

Walker, G.R., Jolly, I.D. and Cook, P.G., 1991. A new chloride leaching approach to the estimation of diffuse recharge following a change in land use. *J. Hydrol.*, 128, 49-67.

Wallace, J.S., Batchelor, C.H., Dabeesing, D.N., Teeluck, M. And Soopramanien, G.C., 1991. A comparison of the light interception and water use of plant and first ratoon sugar cane inter cropped with maize. *Agric. For. Meteorol*., 57, 85-105.

Wallach, R., and Shabtai, R., 1992. Surface runoff contamination by soil chemicals: Simulations for equilibrium and first-order kinetics. *Water Resour. Res.*, 28, 167-173.

Wang, H.X., Zhang, L., Dawes, W.R., Liu, C.M., 1997. Efficient water use in agricultural system in North China Plain (draft paper for *Agricultural Water Management*).

Warrick, A. W., 1991. Numerical approximations of Darcian flow through unsaturated soil, *Water Resour. Res.*, 27, 1215-1222.

Wheater, H.S. and A.J. Jakeman, 1993. Progress and directions in rainfall-runoff modelling. In: Modelling Change in Environmental Systems (A.J. Jakeman, M.B. Beck and A.J. McAleer, eds.), John Wiley & Sons Ltd.

Whisler, F. D., and Klute, A., 1967. Rainfall infiltration into a vertical soil column. *Trans. Am. Soc. Agric. Eng.*, 10, 391-395.

White, I. and Broadbridge, P., 1988. Constant rate rainfall infiltration: A versatile nonlinear model. 2. Applications of solutions. *Water Resour. Res.*, 24, 155-162.

White, I., and Sully, M. J.,1988. Macroscopic and microscopic length and time scales from field infiltration. *Water. Resour. Res.*, 23, 1514-1522.

White, I., Sulley, M.J., and Perroux, K.M., 1992. Measurement of soil surface properties: Disc permeameters, tension infiltrometers and other techniques. *Soil Science Society of America Journal*, 3, 69-103.

Whitfield, D. M., Wright, G. C., Gyles, O. A., and Taylor, A. J., 1986. Growth of lucerne in response to frequency of irrigation and soil amelioration on a heavy clay soil. *Irrig. Sci.,* 7, 1-37.

Wu, H., E.J. Rykiel., Jr. T. Hatton and J. Walker., 1994. An integrated rate methodology (IRM) for multi-factor growth rate modelling. *Ecological Modelling*, 73, 97-116.

Zhang, L. and Dawes, W.R., 1995. Influence of atmospheric stability upon evapotranspiration estimates – tests using HAPEX-MOBILHY data and the WAVES model. CSIRO Division of Water Resources Technical Memorandum, 95/1.

Zhang, L. Dawes, W.R., Hatton, T.J., 1996. Modelling hydrologic processes using a biophysically based model – application of WAVES to FIFE and HAPEX-MOBILHY. *J. Hydrol.*, 185. 147-169.

Zhang, L., Dawes, W. R., Hatton, T. J., Hume, I. H., O'Connell, M. G., Mitchell, D. C., Milthorpe, P. L. and Yee, M., 1999a. Estimating episodic recharge under different crop/pasture rotations in the Mallee region. Part 1. Experiments and model calibration. *Agric. Water Manage.,* 42, 219-235.

Zhang, L., Dawes, W.R., Slavich, P.G., Meyer, W.S., Thorburn, P.J.,Smith, D.J., Walker, G.R., 1999b. Growth and groundwater uptake responses of lucerne to changes in groundwater levels and salinity: lysimeter, isotope and modelling studies. *Agric. Water Manage*., 39, 265-282.

Zhang, L., Dawes, W. R., Hatton, T. J., Reece, P. H., Beale, G., and Packer, I., 1999c. Estimation of soil moisture and groundwater recharge using the TOPOG_IRM model. *Water Resources Research*, 35, 149-161.

Zhang, X. and You, M, 1996. Dynamics of soil water content and potentials of water-saving in the farmland of Taihand Piremont. *Eco-agriculture Research*, 4, 63-68. (in Chinese)

Appendix A. Longwave radiation in a canopy stand

The longwave radiation transfer equations can be written as (Ross, 1981):

$$\frac{di_{ld}(L,r)}{dL}\cos\theta = -G(L,r)i_{ld}(L,r) + \eta(L,r) \tag{A.1}$$

$$\frac{di_{lu}(L,r)}{dL}\cos\phi = G(L,r)i_{lu}(L,r) - \eta(L,r) \tag{A.2}$$

where $i_{ld}(L,r)$, $i_{lu}(L,r)$ are the longwave downward and upward radiation intensities inside a plant stand, r is the direction in space, θ is the inclination angle and ϕ is equal to ($\pi-\theta$), $G(L,r)$ is the foliage area orientation function, $\eta(L,r)$ is the leaf emission coefficient.

The boundary conditions are given as:

$$\begin{aligned} i_{ld}(0) &= \varepsilon_A \\ i_{lu}(L_0) &= \varepsilon_B + \frac{A_{BJ}}{\pi}\int_{\Omega_1} i_d(L_0, r')\cos\theta' \, d\,\Omega' \end{aligned} \tag{A.3}$$

where ε_A is the intensity of longwave radiation of the atmosphere, ε_B is that emitted from the ground surface below the stand, A_{BJ} is the albedo of the ground surface for longwave radiation.

By assuming the leaf temperature is the same in a horizontal layer, one can obtain the following expressions:

$$\begin{aligned} R_{ld}(L) = 2\pi\int_0^{\pi/2}\varepsilon_A(\theta)\exp\left[-\frac{LG(\theta)}{\cos\theta}\right]\cos\theta\sin\theta\, d\theta + \\ \int_0^L R_{lc}(L')\left\{2\int_0^{\pi/2} G(\theta)\exp\left[-(L-L')\frac{G(\theta)}{\cos\theta}\right]\sin\theta\, d\theta\right\} dL' \end{aligned} \tag{A.4}$$

$$
\begin{aligned}
R_{lu}(L) = {} & 2R_{lg}\int_0^{\pi/2} exp\left[-(L_0 - L)\frac{G(\phi)}{\cos\phi}\right]\cos\phi\sin\phi d\phi + \\
& \int_L^{L_0} R_{lc}(L')\left\{2\int_0^{\pi/2} G(\phi)exp\left[-(L_0 - L)\frac{G(\phi)}{\cos\phi}\right]\cos\phi\sin\phi d\phi\right\}dL' + \\
& 2\pi(1-\delta_B)\int_0^{\pi/2} exp\left[-(L_0 - L)\frac{G(\phi)}{\cos\phi}\right]\cos\phi\sin\phi d\phi \times \\
& 2\pi\int_0^{\pi/2}\varepsilon_A(\theta)exp\left[-L_0\frac{G(\theta)}{\cos\theta}\right]\cos\theta\sin\theta d\theta + \\
& 2\pi(1-\delta_B)\int_0^{\pi/2} exp\left[-(L_0 - L)\frac{G(\phi)}{\cos\phi}\right]\cos\phi\sin\phi d\phi \times \\
& \int_0^{L_0} E_L(L)\left\{2\int_0^{\pi/2} G(\theta)exp\left[-(L_0 - L)\frac{G(\theta)}{\cos\theta}\right]\sin\theta d\theta\right\}dL'
\end{aligned}
\qquad \text{(A.5)}
$$

where $R_{ld}(L)$ and $R_{lu}(L)$ are the longwave downward and upward irradiances.

The first term in equation (A.4) defines that part of longave radiation of the atmosphere which penetrates the layer (0, L) of the stand and reaches the level L, the second term defines the downward flux of the longwave radiation of leaves in the layer (0, L), which reaches the level L. In equation (A.5), the first term defines that part of longwave radiation of the ground which penetrates the layer (L, L_0) and reaches the level L, the second term describes the upward flux of longwave radiation of leaves in the layer (L, L_0) which reaches the level L, and the third term defines that part of longwave radiation of the atmosphere which penetrates the whole layer of the stand, is reflected from the ground and, penetrating through the layer (L, L_0), reaches the level L. The last term represents that part of the downward flux of radiation of the leaves off the whole stand which reaches the ground, is reflected from it, penetrates the layer (L, L_0) and reaches the level L.

Since $(1-\delta_B) \approx 0.05$, the last two terms in expression (A.5) can be neglected as a first approximation and in the case of isotropic longwave radiation of the atmosphere, we can obtain the following expressions from equations (A.4) and (A.5):

$$R_{ld}(L) = R_{lc} - (R_{lc} - R_{la})a_D(L) \qquad \text{(A.6)}$$

$$R_{lu}(L) = R_{lc} - (R_{lc} - R_{lg})a_D(L) \qquad \text{(A.7)}$$

where R_{lc} is the longwave radiation emitted from the stand, R_{la} is the longwave radiation from the atmosphere, R_{lc} is the longwave radiation from ground surface, $a_D(L)$ is the penetration function

$$a_D(L) = 2\int_0^{\pi/2} exp(-\tfrac{LG(\theta)}{\cos\theta})\cos\theta\sin\theta\, d\theta \qquad \text{(A.8)}$$

The net longwave radiation can be written as:

$$R_{ln}(L) = -(R_{lc} - R_{la})a_D(L) - (R_{lg} - R_{lc})a_D(L_0 - L) \quad \text{(A.9)}$$

For relatively dense stand, $R_{lg} \approx R_{lc}$, $R_{lu} = R_{lc}$ and one obtains:

$$R_{ln} = (R_{la} - R_{lc})a_D(L) \quad \text{(A.10)}$$

The penetration function for longwave radiation can be defined as:

$$a_D(L) = 2\int_0^{\pi/2} exp(-\frac{LG(\theta)}{\cos\theta})\cos\theta \sin\theta \, d\theta \quad \text{(A.11)}$$

where L is the leaf area index, $G(\theta)$ is the so-called G-function which is a complicated double integral of inclination (θ) and azimuth orientation. This equation can be equally applied to diffuse radiation in a plant canopy.

The penetration function for shortwave radiation in a canopy with uniform orientation (spherical orientation) can be expressed as:

$$a_s(L) = exp(\frac{-L}{2\sin\beta}) \quad \text{(A.12)}$$

where β is the solar elevation.

It is clear that both penetration functions are exponential. Data from Ross (1981, Table II.5.1) presented in Figure A1 shows that both shortwave and longwave radiation can be approximated by the same function (Beer's law) with the same parameter value (bulk extinction coefficient).

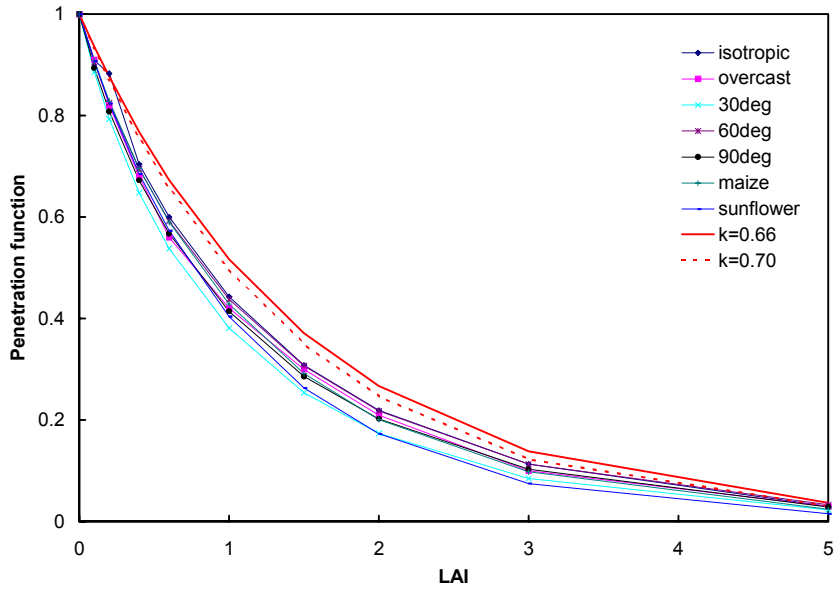

Figure A1. Penetration function for shortwave and longwave radiation in a spherical canopy under various sky conditions.

Appendix B: Details of Analytical Solutions

We here formulate u and u' (i.e. $\partial u/\partial\zeta$) for the analytical solutions presented in section 4.9.4, equations (4.13) and (4.14). The most general formulation (*Broadbridge*, 1990) has not been given succinctly, or in a form that permits exact evaluation.

We express u as:

$$u = u_0 + u_{s1} + u_{s2} \tag{B.1}$$

where u_0 is required regardless of initial and lower boundary conditions, u_{s1} and u_{s2} are non-zero summations when there is a finite-depth profile, and u_{s2} is non-zero only for a finite-depth profile with non-zero initial soil-water content.

To represent the effect of non-zero initial soil-water content $\Theta_i^\ddagger$, we define:

$$Q = \rho + 0.5\frac{\Theta_i^\ddagger}{1-\Theta_i^\ddagger} \tag{B.2}$$

With a completely dry initial condition $\Theta_i^\ddagger = 0$, equation (B.2) yields $Q = \rho$.

Expressions for u_0 and u'_0/u_0

$$u_0 = 0.5\exp\left(-\zeta^2/\tau\right)(a+b-c+d-e) \tag{B.3}$$

where:

$$a = 2\exp\left(\left(\zeta - Q\tau\right)/\sqrt{\tau}\right)^2 \tag{B.4}$$

$$b = f\left(\left(\zeta - g\tau\right)/\sqrt{\tau}\right) \tag{B.5}$$

$$c = f\left(\left(\zeta - Q\tau\right)/\sqrt{\tau}\right) \tag{B.6}$$

$$d = f\left(\left(\zeta + g\tau\right)/\sqrt{\tau}\right) \tag{B.7}$$

$$e = f\left(\left(\zeta + Q\tau\right)/\sqrt{\tau}\right) \tag{B.8}$$

$$g = \rho\sqrt{1 + 1/\rho} \tag{B.9}$$

$$f(x) = \exp(x^2)\operatorname{erfc}(x) \tag{B.10}$$

Differentiating (B.3) with respect to ζ yields:

$$u'_0 = exp\left(-\zeta^2/\tau\right)\left(Q(a+c-e)-g(b-d)\right) \tag{B.11}$$

Equation (4.13) requires u'_0/u_0. Because b, in (B.5), is some orders of magnitude larger than the other terms in (B.3) and (B.11), Θ-values computed directly from these equations may slightly exceed the theoretical maximum at the trailing edge of the wetting front, using 64-bit arithmetic. By taking the quotient of (B.3) and (B.11) and rearranging the algebra, b may be eliminated from the numerator, and the numerical error is minimised. The resulting expression is:

$$u'_0/u_0 = 2\left(\frac{Q(a+c-d)+gd}{a+b-c+d-e}\right) - 2g\left(1-\frac{a-c+d-e}{a+b-c+d-e}\right) \tag{B.12}$$

Equations (B.3) and (B.12) can be used to solve (4.13) and (4.14).

Expressions for summation terms of u and u'

$$u_{s1} = \frac{1}{2}\sum_{n=1}^{\infty}\sum_{j=1}^{4} S_j\left(exp(c_1)f(c_2) - exp(c_3)f(c_4)\right) \tag{B.13}$$

$$u_{s2} = \sum_{n=0}^{\infty}\sum_{j=1}^{3}\omega_j\left(exp(c_5)f(c_6) - exp(c_7)f(c_8)\right) \tag{B.14}$$

where:

$$c_1 = 4n^2\left(1-\Theta_i^{\ddagger}\right)^{\ddagger}\rho - \left(2n\left(1-\Theta_i^{\ddagger}\right)^{\ddagger}+\zeta\right)^2/\tau \tag{B.15}$$

$$c_2 = \left(2n\left(1-\Theta_i^{\ddagger}\right)^{\ddagger}+\zeta\right)/\sqrt{\tau} - \left(2n\rho+b_j\right)\sqrt{\tau} \tag{B.16}$$

$$c_3 = 4n^2\left(1-\Theta_i^{\ddagger}\right)^{\ddagger}\rho - \left(2n\left(1-\Theta_i^{\ddagger}\right)^{\ddagger}-\zeta\right)^2/\tau \tag{B.17}$$

$$c_4 = \left(2n\left(1-\Theta_i^{\ddagger}\right)^{\ddagger}-\zeta\right)/\sqrt{\tau} - \left(2n\rho-b_j\right)\sqrt{\tau} \tag{B.18}$$

$$c_5 = \left(4n^2+4n\right)\left(1-\Theta_i^{\ddagger}\right)^{\ddagger}\rho - \left((2n+1)\left(1-\Theta_i^{\ddagger}\right)^{\ddagger}+\zeta\right)^2/\tau \tag{B.19}$$

$$c_6 = \left((2n+1)\left(1-\Theta_i^{\ddagger}\right)^{\ddagger}+\zeta\right)/\sqrt{\tau} - \left(2n\rho+a_j\right)\sqrt{\tau} \tag{B.20}$$

$$c_7 = \left(4n^2+4n\right)\left(1-\Theta_i^{\ddagger}\right)^{\ddagger}\rho - \left((2n+1)\left(1-\Theta_i^{\ddagger}\right)^{\ddagger}-\zeta\right)^2/\tau \tag{B.21}$$

$$c_8 = \left((2n+1)\left(1-\Theta_i^\ddagger\right)l^\ddagger - \zeta\right)/\sqrt{\tau} - \left(2n\rho + a_j\right)\sqrt{\tau} \tag{B.22}$$

$$\omega_j = \left[-exp\left(2\left(1-\Theta_i^\ddagger\right)l^\ddagger Q\right), -\omega_1/2, -\omega_1/2\right] \tag{B.23}$$

$$S_j = [+1, +1, -1, -1] \tag{B.24}$$

$$a_j = [\rho, 2\rho, -Q, Q] \tag{B.25}$$

$$b_j = \left[\sqrt{\rho(\rho+1)}, -\sqrt{\rho(\rho+1)}, Q, -Q\right] \tag{B.26}$$

The derivatives of the summation terms with respect to ζ are:

$$u'_{s1} = \sum_{n=1}^{\infty}\sum_{j=1}^{4} -S_j\left(2n\rho + b_j\right)\left(exp(c_1)f(c_2) + exp(c_3)f(c_4)\right) \tag{B.27}$$

$$u'_{s2} = \sum_{n=0}^{\infty}\sum_{j=1}^{3} -2\omega_j\left(2n\rho + a_j\right)\left(exp(c_5)f(c_6) + exp(c_7)f(c_8)\right) \tag{B.28}$$

For a finite-depth profile, a test of computational roundoff error at the critical lower boundary may be made by checking the deviation of $z^\ddagger(\zeta_{max})$ from depth $l^\ddagger$, where $\zeta_{max} = (1-\Theta_i^\ddagger)l^\ddagger - \rho\tau$ represents the lower boundary at any point in time. Analytic solutions are valid in principle for $\zeta_{max} > 0$. However this test is required because summation terms in the expressions for $\partial u/\partial\zeta$ and u may be too large for accurate computation, even with 64-bit arithmetic, because the greatest number that can be represented is $10^{\pm 308}$. This problem occurs if ρ is too large in relation to $l^\ddagger$ and soil-water content is large at the lower boundary. It cannot be solved simply by rearranging the algebra (*Broadbridge*, 1990). The test provides a good direct check on the accuracy of $z^\ddagger$ as computed by (4.14), and an indirect check on the accuracy of $\Theta^\ddagger$ as computed by (4.13).

For a semi-infinite profile, no fixed value of ζ_{max} will correspond to an arbitrary scaled depth $l^\ddagger$. For computation to that depth, ζ_{max} lies in the range of $(1-\Theta_i^\ddagger)l^\ddagger - \rho\tau \le \zeta_{max} \le l^\ddagger$. In general, the ζ-range must be searched to obtain a solution for a given value of $z^\ddagger$.